Oil &Gas Application Issues for Gas Turbines & Centrifugal Compressors

Edited by Geoff Sheard

Sigel Press

Sigel Press
51A Victoria Road
Cambridge CB4 3BW
England

4403 Belmont Court
Medina, Ohio 44256
USA

Visit us on the World Wide Web at: www.sigelpress.com

Internal Design: Professional Book Compositors, Lorain, Ohio, USA
Cover Design: Harp Mando
Cover Images: Klaus Brun, South West Research Institute and Rainer Kurz, Solar Turbines

ISBN 10: 1-905941-18-8
ISBN 13: 978-1-905941-18-6

A catalogue record for this book is available from the British Library.
Typeset in Times Roman

The publisher's policy is to use paper manufactured from sustainable forests.

Permissions Acknowledgements

Chapter 1, *Compressors in High-pressure Pipeline Applications*, was originally published in the Proceedings of the 55th American Society of Mechanical Engineers Gas Turbine and Aeroengine Congress, paper number GT2010-22018. Reprinted with the permission of The American Society of Mechanical Engineers. Permission to publish received April 2, 2012.

Chapter 2, *Measurement Uncertainties Encountered during Gas Turbine Driven Compressor Field Testing,* was originally published in the Proceedings of the 43rd American Society of Mechanical Engineers Gas Turbine and Aeroengine Congress, paper number 98-GT-001 and subsequently in *Transactions of the American Society of Mechanical Engineers, Journal of Engineering for Gas Turbines and Power*, volume 123. Reprinted with the permission of The American Society of Mechanical Engineers. Permission to publish received April 2, 2012.

Chapter 3, *Surge Avoidance in Gas Compression Systems*, was originally published in the Proceedings of the 49th American Society of Mechanical Engineers Gas Turbine and Aeroengine Congress, paper number GT2004-53066 and subsequently in *Transactions of the American Society of Mechanical Engineers, Journal of Turbomachinery*, volume 126. Reprinted with the permission of The American Society of Mechanical Engineers. Permission to publish received April 2, 2012.

Chapter 4, *Compression Systems during Emergency Shutdowns*, was originally published in the Proceedings of the 54th American Society of Mechanical Engineers Gas Turbine and Aeroengine Congress, paper number GT2009-59064 and subsequently in *Transactions of the American Society of Mechanical Engineers, Journal of Engineering for Gas Turbines and Power*, volume 132. Reprinted with the permission of The American Society of Mechanical Engineers. Permission to publish received April 2, 2012.

Chapter 5, *Effects of Pulsations on the Stability of Compressors in Mixed Reciprocating and Centrifugal Compressor Stations*, was originally published in the Proceedings of the 53rd American Society of Mechanical Engineers Gas Turbine and Aeroengine Congress, paper number GT2008-50540 and subsequently in *Transactions of the American Society of Mechanical Engineers, Journal of Engineering for Gas Turbines and Power*, volume 132. Reprinted with the permission of The American Society of Mechanical Engineers. Permission to publish received April 2, 2012.

Chapter 6, *Aerodynamic Instability and Life Limiting Effects of Inlet and Inter-stage Water Injection into Gas Turbines,* was originally published in the Proceedings of the 50th American Society of Mechanical Engineers Gas Turbine and Aeroengine Congress, paper number GT2005-68007. Reprinted with the permission of The American Society of Mechanical Engineers. Permission to publish received April 2, 2012.

Chapter 7, *Transient Pressure Loss in Compressor Station Piping Systems*, was originally published in the Proceedings of the 55th American Society of Mechanical Engineers Turbine and Aeroengine Congress, paper number GT2010-22017. Reprinted with the permission of The American Society of Mechanical Engineers. Permission to publish received April 2, 2012.

Chapter 8, *Degradation in Gas Turbine Compression Systems*, was originally published in the Proceedings of the 45th American Society of Mechanical Engineers Gas Turbine and Aeroengine Congress, paper number 2000-GT-0345 and subsequently published in *Transactions of the American Society of Mechanical Engineers, Journal of Engineering for Gas Turbines and Power*, volume 123. Reprinted with the permission of The American Society of Mechanical Engineers. Permission to publish received April 2, 2012.

Chapter 9, *Fouling Mechanisms in Axial Compressors*, was originally published in the Proceedings of the 56th American Society of Mechanical Engineers Gas Turbine and Aeroengine Congress, paper number GT2011-45012 and subsequently published in *Transactions of the American Society of Mechanical Engineers, Journal of Engineering for Gas Turbines and Power*, volume 134. Reprinted with the permission of The American Society of Mechanical Engineers. Permission to publish received April 2, 2012.

Chapter 10, *Solid Particle Surface Impact Behavior in Turbomachines to Asses Blade Erosion*, was originally published in the Proceedings of the 41st Turbomachinery Symposium. Reprinted with the permission of the Turbomachinery Laboratory, Texas A&M University. Permission to publish received March 14, 2012.

Chapter 11, *Industrial Gas Turbine Performance Degradation*, was originally published in the Proceedings of the 53rd American Society of Mechanical Engineers Turbine and Aeroengine Congress, paper number GT2008-50020 and subsequently published in *Transactions of the American Society of Mechanical Engineers, Journal of Engineering for Gas Turbines and Power*, volume 131. Reprinted with the permission of The American Society of Mechanical Engineers. Permission to publish received April 2, 2012.

Contents

List of Figures

List of Tables

Preface

Design-related errors in gas turbine driven centrifugal compressor based compression systems remain regrettably common. Those involved in the design process must ask, "Do we learn from our mistakes?" Undoubtedly, where there are humans there will be human error. Some errors are both unforeseeable and unavoidable. When we encounter a new physical limit and inadvertently pass over it, there is little that we can do. However, we should be able to forsee the majority of design errors. We can develop appropriate tools and techniques, with systematic development serving as the practical process of "learning from our mistakes". New tools and techniques that capture experience allow engineers to work differently, and thus avoid repeating past mistakes.

The design of gas turbine driven centrifugal compressor based compression systems is challenging, made more so by some of the environments in which the compression systems operate. There have been many in-service problems associated with applications issues that we can trace back to design errors during the compression system conceptual and detailed design. When we study these application issues, they fall into one of 11 categories, each associated with a specific design error, and each addressable during the design process, if appropriate tools and techniques are available to guide the engineers involved.

The collection of papers that forms the chapters of this edited volume is intended for engineers undertaking the conceptual and detailed design of gas turbine driven centrifugal compressor based compression systems. Each presents a model that addresses one design-related problem that has resulted in an application issue in the past. Collectively they provide engineers with a suite of models that enables them to work through the design process, with the final design then avoiding the design-based application issues that have resulted in past in-service problems.

The collection of models constitutes a way to capture an accumulation of knowledge, and provide new insight into the design challenge. These papers provide engineers with the necessary raw material for them to think and perceive differently, and change what they do to avoid repeating the past mistakes of others. Although intended primarily for design engineers, all those working within the oil and gas industry will have an interest in the application issues that they may face, making this volume of interest to a wide audience within the oil and gas community.

Geoff Sheard
Fläkt Woods Group
January 1, 2013

Acknowledgements

Many individuals have helped in writing the academic papers upon which this volume is based and it is my pleasure to acknowledge this. Foremost among these are the authors, Klaus Brun, Augusto Garcia-Hernandez, Rainer Kurz, Jeffrey Moore, Marybeth Nored, Sebouh Ohanian, Harold Simmons, Dennis Tweten, Robert White and Meron Wollie.

I also wish to thank Thomas Sigel, first for his tremendous contribution in turning around extensive scripts into succinct and easily readable text, and second for his assistance with the process of converting the final text into this published volume.

Last, I would like to acknowledge the contribution of Kirsten Greenzweig, who converted the original academic papers upon which this volume is based into electronic files that could then be edited and typeset. Kirsten also recreated the original figures in electronic form, an undertaking that proved to be far more time consuming than either of us imagined.

Geoff Sheard
Fläkt Woods Group

About the Authors

The chapters of this volume comprise revised and extended versions of previously published papers. I, the Editor, selected the papers from Klaus Brun and Rainer Kurz's collected published work. These scholars have worked together for over a decade, studying compression system in-service failures, developing tools and techniques to avoid design-related errors in future systems. I selected the papers as they constitute Klaus and Rainer's key contributions to the identification of design-related errors in compression systems.

The International Gas Turbine Institute's oil and gas application technical committee has recognized the significance of this research. In 1998, 2000, 2003, 2005, 2009, 2010 and 2012 these esteemed researchers presented technical papers at the annual ASME Turbo Expo conference that went on to receive the oil and gas application technical committee best paper award. Five of these papers form the basis of chapters in this volume. Many academics and industrialists spend a lifetime publishing without winning a single best paper prize. To do so seven times is unprecedented, a point that illustrates the regard with which the oil and gas community holds the reported research..

Klaus Brun is the Director of the Machinery Program at the Southwest Research Institute in San Antonio, Texas. Previously he held positions in engineering, project management and management at Solar Turbines, General Electric and Alstom. Klaus has a doctorate and master's degree from the University of Virginia, plus a bachelor's degree from the University of Florida. He has won a research and development 100 award and the *San Antonio Business Journal* selected him as one of the "40 under 40". Klaus is a past chairman of the International Gas Turbine Institute Board of Directors, a member of the API 616 and 692 Task Forces, the Fan Conference Advisory Committee and the Latin American Turbomachinery Conference Advisory Committee. Having published over 100 technical papers and authored a gas turbine textbook, Klaus has published widely. He is the Executive Correspondent of Turbomachinery International Magazine and an Associate Editor of the *Journal of Engineering for Gas Turbines and Power*.

Rainer Kurz is the Manager, Systems Analysis at Solar Turbines Incorporated, in San Diego, California. His organization is responsible for predicting compressor and gas turbine performance, for conducting application studies and for field performance testing. Rainer has a doctorate and engineer diploma, a master's level degree, from the Universitaet der Bundeswehr in Hamburg, Germany. He is a member of the Gas Machinery Research Council Project Supervisory Committee, the Texas A&M

Turbomachinery Symposium Advisory Committee and the San Diego State University Aerospace Engineering Advisory Committee. Rainer is a Fellow of the American Society of Mechanical Engineers, has published over 120 technical papers and 30 practitioner journal articles. In additional to his International Gas Turbine Institute best paper awards he has also won two best tutorial awards and the 2013 Industrial Gas Turbine Technology award.

Geoff Sheard
Fläkt Woods Group

About the Editor

Wearing many hats, Geoff Sheard is the Fläkt Woods Group Vice President of Fan Technology, a leading global supplier of energy-efficient solutions operating in both the air climate for buildings and air movement for the infrastructure and industry markets. He is a director of Fläkt Woods Limited, Solyvent Fläkt Woods Limited and Fläkt Woods Fans (Australia) Pty Limited.

Geoff is an Honorary Professor at the Aston University Department of Engineering and Applied Science, a Visiting Professor at *Sapienza* University of Rome *Dipartimento di Ingegneria Meccanica e Aerospaziale* and a Visiting Professor at the University of Northampton Business School.

Geoff is a director of the Air Movement & Control Association (AMCA), member of the AMCA Executive Board and Chairman of the European Air Movement & Control Association Board of Directors. He is also a member of the International Gas Turbine Institute (IGTI) Board of Directors and Vice Chairman of the Institution of Mechanical Engineers (IMechE) Fluid Machinery Group.

Geoff has doctorate degrees from the University of Oxford in turbomachinery aerodynamics and from the University of Northampton in leadership and team development. He also holds a masters degree in business administration from Cranfield University and a bachelor's degree in mechanical engineering from Liverpool University.

A chartered engineer, a Liveryman of the Worshipful Company of Engineers, a fellow of the Institution of Mechanical Engineers, a fellow of the Royal Aeronautical Society, a fellow of the American Society of Mechanical Engineers and a fellow of the Chartered Institute of Building Service Engineers, Geoff has published widely in both technical and management areas. He has published four books, two monographs, over 150 articles and is a member of the *Journal of Power and Energy* editorial board, the *Journal of Management Development* editorial advisory board and the *Leadership and Organisational Development Journal* editorial review board.

Introduction: Application Issues in Pipelines

Geoff Sheard

> "*Just as Art consists not simply of works of art but of an attitude, the artistic spirit, so does Science consist not in the accumulation of knowledge but in the creation of fresh modes of perception. The ability to perceive or think differently is more important than the knowledge gained.*"
>
> David Bohm, quantum physicist

This volume of collected papers documents research undertaken in response to a need: to provide engineers with the tools and techniques required to design gas turbine driven centrifugal compressor based compression systems. The volume arises from discussions around 11 papers that collectively comprise the chapters. Each documents a single model that engineers can utilize to avoid a specific design error that has historically resulted in a compression system application issue. Collectively the chapters provide a suite of models that, if applied systematically, enable an engineer to avoid those design-related application issues that have occurred in the past.

The book arises from discussions around four conference papers and seven journal papers, which collectively comprise the 11 chapters. The chapters broadly relate to one of three separate but complementary themes that impact on the in-service performance of compression systems and hence are of interest within the oil and gas community:

1. basic issues in compressors and pipelines;
2. surge and instability; and
3. degradation and fouling.

The design of compression systems begins with the pipeline conceptual design. How will engineers operate and maintain the compression stations in unpopulated areas? What is the cost of the different piping that is available? How valuable is the transported gas and the gas used as fuel? These questions drive the compression system's conceptual design. Once an engineer has developed a compression system specification, he or she must then define the accuracy with which one can assess the specification in an imperfect working environment. Only once one has developed the conceptual design, a detailed specification and an agreement on the field assessment of performance should compression system detail design commence.

A compression system's detailed design has a fundamental impact on the compressors' stability and their propensity to surge. The piping design upstream and

downstream of the compressor is of particular importance during an emergency shutdown. The current practice of mixing gas turbine driven and reciprocating compressors introduces pressure pulses that also have a significant impact on compressor stability. The current practice of applying power augmentation devices to the gas turbines' compressor compounds the problem of driven compressor instability by reducing the gas turbine compressors' stability. Fluid and structural resonances may further exacerbate the above stability issues, introducing unforeseen dynamic pressure losses that result in both the gas turbine and compressor working at an unplanned off-design point.

Compression systems are frequently installed in unforgiving environments. Sand and dust enter the gas turbine compressor, resulting in degradation and fouling. Predicting the effects of degradation and fouling on a gas turbine's compressor is important for design engineers. Assessing a gas turbine's susceptibility to fouling, and the associated selection of air filtration systems, is an important aspect of the design process. Insight into the susceptibility to fouling and the effectiveness of air filtration systems provides a basis for assessing a gas turbine's rate of wear, and hence the determination of time between major overhaul.

Chapter 1 & 2: Basic Issues in Compressors and Pipelines

The conceptual design of a compression system is intrinsically linked to the location of the associated pipeline and the gas transported by the pipeline. Environmental rather than technical considerations frequently drive the process of determining the pipeline's route and the number and location of compression stations. Despite the above caveat, there is a significant technical aspect associated with a compression system's conceptual design. A fundamental technical aspect of the conceptual design process is pipeline operating pressure selection. There is no correct operating pressure for a pipeline, with the optimum dependent on externally imposed factors that the design engineer takes into account when optimising the conceptual design. Once a compression system specification is finalized, the engineer must define and verify the method that the manufacturer will use to verify that specification has been achieved during commissioning.

The models which the authors present in Chapters 1 and 2 clarify the externally imposed factors that impact on the optimum compression system operating pressure. The authors present a process that a design engineer may work through to identify the optimum pipeline pressure and discuss a method for assessing the relative merits of high- and low-pressure compression systems. The authors then consider the process by which engineers validate that chosen compression system specification and present a model to enable design engineers to identify the accuracy with which they can measure key parameters.

Chapter 1 considers the first of the above basic issues in compression systems. A typical pipeline operates at pressures up to about 100 Bar; however, it is possible for pipelines to operate at significantly higher pressure. There is no single correct operating pressure for a pipeline, with the optimum economic choice dependent on the

cost of operating compression stations, cost of the pipeline itself, value of the transported gas and value of gas used as fuel. Each pipeline project will impose different constraints on the design engineer, with the optimum choice of operating pressure dependent on each project's unique requirement. This chapter assists design engineers by providing a method for assessing the optimum pipeline operating pressure, while taking into account each project's specific requirement.

Chapter 2 considers the second of the above basic issues in compression systems. Engineers typically test gas turbine driven compressor based compression systems after installation to verify the manufacturer's performance claims. Field testing requires accurate performance determination in an imperfect working environment. Engineers may establish the uncertainty associated with field testing using experience-adapted uncertainty physical equations that govern turbomachinery performance. This chapter assists design engineers by providing an experience-adapted analytical method that enables determination of the overall accuracy with which they may measure performance during a field test.

Chapter 3, 4, 5, 6 & 7: Surge and Instability

Aerodynamic instability generally and surge specifically are primary considerations during compression system design. Gas turbine driven compressors and the gas turbine's compressor itself become aerodynamically unstable as they approach their respective surge lines. Selecting a compressor and a gas turbine to drive it at a specific duty point is a routine design exercise. However, in practice compression systems seldom operate at their intended design point. Although we may conceptualize routine operation as a series of steady-state operating points, transient operation requires more detailed analysis. We may associate transient conditions with a compression system's emergency shutdown, the effects of pulsating flow, the impact of gas turbine power augmentation devices and the transient pressure loss in compression station piping systems. Each introduces its own stability issues, and engineers must consider all during a compression system's detailed design.

The models which the authors present in Chapters 3, 4, 5, 6 and 7 identify five separate aspects of the compression system detail design that impact on compression system aerodynamic stability. Collectively the models provide a design engineer with a suite of tools that enable him or her to analyse and develop a preliminary compression system design during the detail design process. This enables the design engineer to refine the design such that it is inherently aerodynamically stable and will avoid surge under both steady state and transient operating condition.

Chapter 3 considers the first of the issues associated with surge and instability. Traditional methods of surge avoidance consist of a fast-acting valve that opens to reduce pressure across the compressor as it approaches its surge limit. Such systems work well during routine operation; however, during unplanned emergency shutdowns they are unable to respond quickly enough to avoid surge. This chapter assists design engineers by presenting guidelines that help with the sizing of upstream and downstream compressor piping systems. The guidelines constitute a model that en-

ables a design engineer to develop the upstream and downstream compression station pipe layout that will reduce the probability of compression system surge during an emergency shutdown.

Chapter 4 continues the theme of Chapter 3, considering the second of the issues associated with surge and instability. Surge is an intrinsically transient phenomenon, therefore there is a need to model the compression system's transient behavior during an emergency shutdown. This chapter assists design engineers by presenting a surge model that will predict the compression system's transient behavior during an emergency shutdown. This enables design engineers to evaluate a compression station design and establish if the upstream and downstream compressor piping system constitutes a design that avoids compressor surge during emergency shutdown.

Chapter 5 considers the third of the issues associated with surge and instability. Engineers frequently apply centrifugal and reciprocating compressors into mixed operation in a single compression system. The reciprocating compressors can impose pressure variations up to 25 percent of the overall pressure rise. The pressure variations can result in the centrifugal compressor transiently driving to its surge line. This chapter assists design engineers by presenting a model for centrifugal to reciprocating compressor piping design that assists them in avoiding acoustic resonance condition and to introduce attenuation of the reciprocating compressor pressure pulses. This enables the design engineer to produce an inherently more stable compression system design.

Chapter 6 considers the fourth issue associated with surge and instability. Gas turbine power enhancement technologies are becoming increasingly common place. However, these devices may have a negative effect on the gas turbine's operational integrity. The combination of power enhancement technology and off-design operation can reduce the gas turbine's compressor surge margin, which we may link to compressor blades' high cycle fatigue failure. This chapter assists design engineers by presenting a method that they can use to evaluate the impact of power augmentation devices on gas turbine compressor aerodynamic stability. This enables a design engineer to evaluate the gas turbine compressor's aerodynamic stability, assisting in mitigating the risk of catastrophic compressor blade failure.

Chapter 7 considers the fifth of the issues associated with surge and instability. The flow through a compression system's piping is frequently transient as a consequence of acoustic resonances. When these resonances coincide with piping acoustic resonance lengths, the piping system produces a significant dynamic pressure loss. This chapter assists design engineers by presenting a piping system model that predicts the pressure losses associated with piping–structure interactions. Design engineers may use the model to predict the dynamic pressure losses through a compression system, and then tune the piping system to minimize dynamic pressure loses.

Chapter 8, 9, 10 & 11: Degradation and Fouling

Degradation and fouling are primary considerations during compression system design. Over time the gas turbine that drives a compression system's compressor will wear. That wear occurs as a consequence of fouling, hot corrosion, corrosion due to contaminants, erosion, abrasion and foreign object damage. All degradation mechanisms are important, and consequently the engineer must establish their effects during the design process. The final design must result in a compression system that can operate for its full service interval between major overhauls.

The models which the authors present in Chapters 8, 9, 10 and 11 identify four separate analytical techniques that collectively provide a design engineer with the tools that enable him or her to assess the impact of gas turbine degradation. This enables the design engineer to check a detailed design, verifying that it will remain aerodynamically stable for the planned service interval.

Chapter 8 examines the first of the issues associated with degradation and fouling. The authors consider the gas turbine package as a system, with the objective of establishing the degradation impact on the matching of components within that system. This chapter assists design engineers by presenting a methodology that simulates gas turbine degradation effects that in turn facilitate an assessment of the degradation's impact on compression system performance. A design engineer can use the model to evaluate degradation effects on gas turbine components and assist in the gas turbine's control system optimisation and definition of its preventative maintenance schedule.

Chapter 9 considers the second of the issues associated with degradation and fouling. Compressor blade fouling is a particular problem in some compression system applications, leading to the gas turbine's performance degradation. This chapter assists design engineers by presenting a set of factors that characterize a gas turbine's susceptibility to fouling. These factors constitute a model design that engineers can use to ensure that an air filtration system matches to a specific gas turbine and its application. This enables a design engineer to minimize fouling and its associated gas turbine performance degradation.

Chapter 10 continues the theme of Chapter 9, considering the third issue associated with degradation and fouling. Determining the optimum air filter material for a gas turbine requires knowledge of the solid particle's size, type and weight that enters the gas turbine. This chapter assists design engineers by presenting a probabilistic analysis of solid particles' behavior. The analysis enables a design engineer to predict the probability of a solid particle's given size and weight that impacts on a gas turbine's compressor components. The analysis enables a design engineer to assess the effectiveness of a given air filtration system, and optimize air filtration capability and a compressor's maintenance schedule.

Chapter 11 considers the fourth issue associated with degradation and fouling. Gas turbines operate as a set of matched components. By considering the gas turbine as a system, it is possible to characterize the effect of component degradation not only on component performance, but also on system matching and consequently, on system performance. This chapter assists design engineers by providing a basis for evaluating the component degradation impact on gas turbine system degradation. The provided insight highlights the relative importance of changes in gas turbine parameters that engineers classically use in condition monitoring systems. This assists in the specification of condition monitoring systems generally, and specifically in the selection of fuel treatment systems that can reduce the performance degradation rate.

Summary of Chapters

Geoff Sheard

This summary of technical contributions provides a detailed description of the work in each chapter. It clarifies the content and summarizes its contribution to compression system design. The goal is to clarify the relevance of the reported work to those design engineers responsible for compression system design. Each chapter addresses an application issue associated with gas turbine and compressor based compression systems. By presenting models and analytical techniques, this edited volume provides design engineers with a tool kit that will assist them in avoiding design-related in-service problems.

The papers comprising each chapter constitute the lead authors Klaus Brun and Rainer Kurz's published scholarly work that relates to application issues for gas turbines and centrifugal compressor based compression systems. The editor selected them based on the degree to which the content contributed towards the creation of a coherent body of knowledge.

Chapter 1 Compressors in High-pressure Pipeline Applications

This chapter considers the first of two basic issues that design engineers associate with pipeline operation. While typical gas transmission pipelines operate at pressures up to about 100 Bar, there are applications in North America and Australia that use pipelines that operate at significantly higher pressures. In this chapter, the authors clarify the underlying reasons that make a high-pressure pipeline economically attractive, and emphasize the trade-offs that occur when design engineers use high-pressure pipelines versus traditional lower pressure pipelines.

To assist design engineers during the conceptual design of a new pipeline, the authors present a parametric study to evaluate the impact of higher operating pressures on a pipeline's economic viability. The authors specifically discuss economic consequences which occur with compressing the pipeline gas to a higher pressure.

In this study, the authors did not find a clear advantage of high-pressure pipelines compared to pipelines at traditional pressure levels. The relative advantage of the former, when compared to the latter, is dependent on four externally imposed factors:

- cost of operating compression stations in unpopulated areas;
- cost of different quality piping for pipeline manufacture;
- value of the transported gas in the pipeline; and
- value of the gas used as fuel.

The authors concluded that either high-pressure pipelines or low-pressure pipelines may provide the best economic solution, with the optimum project specification dependent on the combination of externally imposed factors. This chapter provides a method for assessing the relative merits of high- and low-pressure pipeline operation, and constitutes a basis for establishing the most economic project specification for each unique set of externally imposed factors.

Chapter 2 Measurement Uncertainties Encountered during Gas Turbine Driven Compressor Field Testing

This chapter considers the second of two basic issues that design engineers associate with the operation of gas turbine driven centrifugal compressors in pipeline applications. Operators frequently test gas turbine driven compression packages after installation in the field to verify the manufacturer's performance claims. Failure to meet the claimed performance typically results in financial penalties for the manufacturer, as well as operator discontent. Therefore, compressor and gas turbine manufacturers, as well as the operator, require an accurate determination of field performance.

Compression package field testing requires the accurate determination of efficiency, capacity, head, power consumption and fuel flow in an imperfect working environment. In this chapter the authors present an analytical method that design engineers can use to define an allowable measurement uncertainty range, acceptable to the manufacturer and operator, prior to a field test. The authors derive a set of uncertainty equations from the physical equations of state governing turbomachinery performance. They present typical field test measurements and their associated errors for different sets of instrumentation and sensors.

By introducing these experience-derived errors into the uncertainty equations, design engineers can predict the total efficiency, power and compressor discharge pressure uncertainty for a compression package prior to the field test for a given operating condition. The authors use two actual field test examples to demonstrate the method's viability. They also include a parametric study to provide insight into uncertainty trends. The authors identify parameters that most significantly affect the total package uncertainty to highlight each field test instrument's relative importance. This drives home the relative importance of instrumentation accuracy. The analytical method therefore provides design engineers with a tool to determine field test measurement errors prior to a field test, and second, a method to assess the impact that higher specification instrumentation will have on the overall package measurement uncertainty.

Chapter 3 Surge Avoidance in Gas Compression Systems

This chapter considers the first of five issues associated with surge and instability. An aspect of surge avoidance lies in the compressor station design and, in

particular, the piping upstream and downstream of the compressor. The traditional method for surge avoidance consists of a recycle loop that a fast acting anti-surge valve activates when the control system detects that the compressor approaches its surge limit.

Typical control systems use suction and discharge pressure and temperature, together with the compressor inlet flow as input, to calculate the present operating point's relative distance (the surge margin) to the compressor's predicted or measured surge line. If the compressors operating point approaches the compressor surge line, the anti-surge valve starts to open, thereby reducing the compressor's pressure ratio and increasing the flow through the compressor.

A critical situation arises upon emergency shutdown. Here, the fuel supply to the gas turbine driving the compressor is cut off instantly and consequently, the power turbine and the driven compressor coast down on their own inertia. Anti-surge systems are typically capable of avoiding surge during normal operation. However, unplanned emergency shutdowns present a significant challenge, and surge avoidance in these cases depends largely on the compression system layout.

This chapter presents data from a compressor that surged during an emergency shutdown. The authors present a model to simulate shutdown events and develop guidelines that help design engineers with the appropriate sizing of upstream and downstream compressor piping systems, as well as the necessary control elements. The authors analyze the compression system, thus validating the model. The model correlates well with the field data, particularly with regards to surge event prediction. The model provides design engineers with a tool to determine whether a compression system will surge during emergency shutdown.

Chapter 4 Compression Systems during Emergency Shutdowns

This chapter considers the second of five issues associated with surge and instability, continuing the theme in Chapter 3. Although there are steps that design engineers can take to design a compression system to avoid surge during normal operation, it is challenging to design the compression system to avoid surge during emergency shutdown. Despite the caveat that it is difficult to avoid surge during emergency shutdown, one must avoid surge to protect the compressor.

Surge is a system phenomenon that depends on the compressor, its driver, the piping system and the anti-surge valve behavior. Further, these compression systems behave differently under steady state and transient load. While compression systems do not always operate at fully steady-state conditions, routine operating condition changes are typically slow enough to serve as a succession of steady-state operating points. However, during an emergency shutdown a steady state assumption is no longer valid.

Different compression system behavior under steady and transient load makes the compressor systems' transient behavior of interest to design engineers. Predicted transient behavior is an important input during the compression system design that assists design engineers in optimizing the design to avoid damage during emergency

shutdowns. Academics and industrialists alike have developed simulations and modeling approaches to predict the compressor systems' transient behavior. However, the available experimental data is not of sufficient quality or resolution to facilitate comparison with analytical results. Necessary information about the compressor, driver, valves and piping system geometry is generally not available, making transient behavior prediction using a model difficult.

This chapter presents the development of an experimental facility that can reproduce a compression system's transient behavior during emergency shutdowns, and thus generate transient performance data sets that facilitate verification of the authors' transient surge model. Furthermore, design engineers can use the data as a reference to test other transient surge models. The chapter describes facility setup, instrumentation and test procedures. To facilitate test data comparisons with different compression systems sized for a range of operating conditions, the authors developed and validated relevant dimensionless parameters utilizing the test data.

Overall, the authors' transient compression system model predicted the experimentally observed compression system's transient shutdown behavior reasonably accurately without tuning the model. Design engineers can improve the model accuracy if they gather and use steady-state test data to refine pressure drops and pipe friction factors. They can achieve further improvement by using actual, as opposed to predicted, valve opening times. Consequently, the authors are able to make recommendations to optimize their model. This enables design engineers to maximize its accuracy and therefore its usefulness when optimizing compression system design.

Chapter 5 Effects of Pulsations on the Stability of Compressors in Mixed Reciprocating and Centrifugal Compressor Stations

This chapter considers the third of five issues associated with surge and instability. Centrifugal and reciprocating compressor mixed operation in a single compression plant has become common design practice. This arrangement provides benefits when the process profile is highly cyclical. In these particular compression systems, design engineers place the compressors in parallel or series, such that large gas turbine driven centrifugal compressors provide the base-load compression while smaller reciprocating compressors follow cyclical or peak compression demands.

Design engineers may place a centrifugal compressor upstream or downstream of a reciprocating compressor, with the choice dependent on the application. Irrespective of the application, both arrangements lead to significantly higher pressure pulses on the centrifugal compressor than parallel operation. These pressure pulses may affect the compressor's operational stability. Typically, a centrifugal compressor operating with a suction pressure of 40 Bar and discharge pressure of 70 Bar may experience pressure pulsations from a reciprocating compressor exceeding 10 Bar peak-to-peak.

These pressure variations of up to 25 percent present a challenge for any centrifugal compressor's aerodynamic stability, especially if the compressor's operating

point is near its surge line. Thus, design engineers must accurately analyze the piping arrangement between reciprocating and centrifugal compressors to avoid acoustic resonance conditions and attenuate the pressure pulsations from the reciprocating compressor.

This chapter presents a fully transient one-dimensional Navier-Stokes equation solver for complex systems of interconnected pipes. Design engineers may use the developed model when predicting flow, pulsation amplitudes and frequencies in mixed compression systems. The model serves as a tool to assist design engineers during compression system piping design. The model enables design engineers to identify piping configurations that attenuate the predicted pressure pulses and produce an inherently more aerodynamically stable compression system design that is intrinsically less likely to surge.

Chapter 6 Aerodynamic Instability and Life Limiting Effects of Inlet and Inter-stage Water Injection into Gas Turbines

This chapter considers the fourth of five issues associated with surge and instability. Operators employ gas turbine power enhancement technologies such as inlet fogging, inter-stage water injection, saturation cooling, inlet chillers and combustor injection without necessarily evaluating the potentially negative effects that these devices may have on the gas turbine's operational integrity. As the widespread introduction of inlet cooling and water injection technologies for gas turbines is a relatively recent development, only limited historical field operating data on the effect on parts life is available.

Design engineers often overlook the effect of power augmentation technologies in combination with off-design operating conditions on the gas turbine's compressor surge margin. Despite this lack of consideration, we can link directly operation at off-design conditions with compressor blade high-cycle fatigue and subsequent catastrophic gas turbine failure. Consequently, the prudent design engineer should conduct an analysis before applying power augmentation devices. Analysis is particularly important if the design engineer is aware that the operator intends to operate the gas turbine in an extreme environment.

This chapter discusses a method that design engineers can use to evaluate the principal factors associated with power augmentation technologies that affect the aerodynamic stability of a single-shaft gas turbine's axial compressor. As an example, the authors apply the method to a frame-type gas turbine. The results show that inlet cooling alone will not cause gas turbine aerodynamic instabilities, but that it can contribute to instability if the gas turbine's surge margin is already reduced for other reasons. Design engineers can employ the method to evaluate the gas turbine compressor's aerodynamic stability to identify high-risk applications and a gas turbine's operating limit. This enables design engineers to minimize the risk of aerodynamic instability and its associated potential for the gas turbine's catastrophic failure.

Chapter 7 Transient Pressure Loss in Compressor Station Piping Systems

This chapter considers the fifth of five issues associated with surge and instability. The fluid flow in compression system piping is frequently highly transient due to pipe length acoustic resonances coupled with flow excitation. These periodically transient flows pulsate at discrete frequencies and may correspond to forced excitation frequencies if they coincide with a piping acoustic resonance length. Furthermore, if these pipe flow pulsation frequencies align with any structural resonances, vibrations will result at the compressor, piping or support structures.

Aside from causing undesirable life-limiting vibrations, fluid–structure resonance represents a direct transfer of energy from the fluid in the pipeline to the structure and, thus, a transient flow "dynamic" pressure loss. Conventionally, design engineers determine dynamic pressure losses by assuming a periodically pulsating one-dimensional flow profile and calculating the transient pipe friction losses by multiplying a friction factor by the average flow dynamic pressure component. In reality, the dynamic pressure loss is more complex and is not a single component, but rather comprises pressure losses that occur with different physical effects. The pressure losses due to fluid–structure interactions represent one of these physical loss mechanisms and are presently the least well understood loss term.

This chapter presents an experimental program utilizing an instrumented piping system in a closed loop compressor facility to determine dynamic pressure loss. The authors utilized steady and dynamic pressure transducers and mounted on-pipe accelerometers to study the dynamic pressure loss. The purpose of the experiments was to quantitatively assess the individual pressure loss components which contribute to the overall dynamic pressure loss for a typical centrifugal or reciprocating compressor piping system.

The authors compared the experimental results to steady-state and dynamic pressure loss predictions from a three-dimensional fluid model. They utilized both steady and transient flow conditions to quantify the associated loss terms. The comparison between model and experimental results indicated that pressure losses associated with the piping fluid–structure interactions can be both significant and underestimated by a three-dimensional fluid model.

Design engineers may use the comparison between model and experimental results to provide model correction factors that assist in the correction of predicted dynamic pressure losses in compression systems. Therefore, design engineers are better able to model and optimize the compression system to avoid surge.

Chapter 8 Degradation in Gas Turbine Compression Systems

This chapter considers the first of four issues associated with degradation and fouling. Treating the gas turbine package as a system facilitates the study of degradation effects on the match of components within a compression system. Six primary mechanisms cause gas turbine degradation:

1. particle adherence to aerofoils and annulus surfaces cause fouling;
2. chemical reactions between the component and contaminants cause hot corrosion, the loss or deterioration of material from components exposed to hot combustion gases;
3. corrosion caused by both inlet air contaminants and combustion-derived contaminants;
4. erosion caused by particles impinging on flow surfaces resulting in the abrasive removal of material;
5. abrasion caused by a rotating surface rubbing on a stationary surface; and
6. foreign object damage caused by objects striking the flow path components.

While cleaning or washing a gas turbine can reverse the effects of fouling, the other degradation effects require the adjustment, repair or replacement of components. These degradation mechanisms lead to changes in blade profiles, affecting the blade aerodynamic performance. They can also lead to changes in seal geometries and clearances, affecting parasitic and secondary flows.

This chapter presents a methodology that design engineers may use to simulate the effects of gas turbine and compressor degradation, providing them with a tool for assessing the impact of degradation on compression system performance. Using a relatively simple set of equations that describe gas turbine behavior, and linear deviation factors derived from gas turbine test data, the methodology models compression system behavior for varying degrees of degradation. Using the model, design engineers are equipped with a tool to evaluate the degradation effects on gas turbine components, as well as the effect of water washing the gas turbine, plus the impact of changes to the gas turbine's control system.

Chapter 9 Fouling Mechanisms in Axial Compressors

This chapter considers the second of four issues associated with degradation and fouling. It focuses on compressor blade fouling as a mechanism leading to performance deterioration in gas turbines. Adherence of small particles (typically smaller than 10 μm) to aerofoils and annulus surfaces causes fouling. Smoke, oil mists, carbon and sea salts are common examples of fouling particles.

When observing fouled compressors, the authors noticed evidence of contamination of both the compressor blade's suction and pressure sides. The authors cite numerical simulations indicating that suction side fouling has a greater impact on performance than fouling on the pressure side. Any prediction methodology based on inertial impact of particles would predict that fouling would occur on the pressure side only, and consequently, the authors concluded that an inertial impact-based prediction methodology does not describe the physics of fouling. The authors concluded that a mechanism that explains the process by which particles become attached to the blades' suction side requires very small particles.

This chapter presents a set of factors that rate the gas turbines' fouling susceptibility, based on the probability of different sized particles impacting the blade

surface. The authors evaluated fouling mechanisms based on observed data, and present a discussion on fouling susceptibility. The chapter concludes with practical advice for design engineers on appropriate air filtration system selection. This provides design engineers with insight into the importance of matching air filtration system specification to the application to minimize gas turbine fouling and therefore the associated degradation in gas turbine performance.

Chapter 10 Solid Particle Surface Impact Behavior in Turbomachines to Assess Blade Erosion

This chapter considers the third of four issues associated with degradation and fouling. In recent years, there has been renewed interest in the prediction of solid particle behavior when ingested into a gas turbine compressor, because of practical limits of filter material efficiency, size and cost. Specifically, to determine an optimum filter material and design for a ground-based gas turbine in a compression system, the design engineer must predict the size, type and weight of solid particles which would cause the gas turbine operational damage as a consequence of erosion.

Solid particle admission is one of the principal gas turbine compressor damage mechanisms and drivers of compressor failure. Design engineers therefore have an interest in better predicting the durability of gas turbines that operate in environments where one cannot avoid the ingestion of sand, dust and dirt.

This chapter presents a mixed computational fluid dynamics–empirical model that performs a probabilistic analysis of solid particulates' impact behavior. The authors' method in the mixed computational fluid dynamics–empirical model incorporates a commercially available computational fluid dynamic solver to calculate the gas turbine or compressor's steady-state flow field. The authors utilize the output to determine a series of non-dimensional coefficients via a set of empirical functions to predict the statistical probability of a given weight and size or distribution of solid particles impacting on a specified rotating or stationary surface.

Based on this model's output, design engineers can assess the need for improved inlet air filtering techniques and optimize gas turbine and compressor maintenance practices. To determine the empirical coefficients and to validate the model, the authors utilized a particle image velocimetry measurement technique with an aerofoil in a wind tunnel. They continued the experimental work with particle injection into a full-scale centrifugal compressor test rig. Test results facilitated model optimization to better reflect rotating machinery particle impact behavior.

Chapter 11 Industrial Gas Turbine Performance Degradation

This chapter considers the fourth of four issues associated with degradation and fouling. Any gas turbine exhibits the effects of wear over time. Because the gas turbine operates as a result of the matched operation of many components, the authors focus on the gas turbine as a system, rather than on isolated component performance.

Treating the gas turbine as a system assists in characterizing the effects of degradation on component match.

The authors clarify the impact of component interaction, as component interaction plays an important role in understanding degradation effects. This facilitates insight into the relevance of other published studies on degradation that typically address individual component performance. The authors are able to provide the design engineer with a basis for evaluating the apparent change in a component's efficiency due to component deterioration, as well as change in component matching. Specifically, the authors highlight the compressor operating point's change as a result of the compressor and turbine section's degradation.

By treating the gas turbine as a system, this chapter provides the design engineer with a method that clarifies the impact of a given component degradation on gas turbine performance and how performance varies for different operating conditions. This insight will shed light on the relative importance of changes in gas turbine parameters that design engineers classically use in condition monitoring systems. Therefore, design engineers have a basis for inlet system design and selection of fuel treatment systems that can significantly reduce the performance degradation and time between gas turbine overhaul.

Chapter 1

Compressors in High-pressure Pipeline Applications

R. Kurz, S. Ohanian and K. Brun

ABSTRACT

While typical gas transmission pipelines operate at pressures up to about 100 Bar, a number of applications in North America and Australia use or are planning pipelines that operate at significantly higher pressures. Often, we refer to these pipelines as "dense phase". This chapter describes and analyzes existing dense phase pipeline installations.

In this chapter we explain the underlying reasons why the industry is considering dense phase pipelines, as well as the trade-offs compared to traditional, lower pressure pipelines. The chapter presents a parametric study to evaluate the impact of higher operating pressures on the pipelines' net present value. We discuss the impact of the necessary effort to bring the gas to the higher pressure. Since engineers design some of the pipelines to transport carbon dioxide, we highlight the particular issues that occur with high-pressure carbon dioxide transport. We also consider the impact on compressor and driver selections, in particular the impact of the centrifugal compressors' higher power density at higher pressures.

This chapter is a revised and extended version of Kurz, R., Ohanian, S., and Brun, K. (2010), "Compressors in High Pressure Pipeline Applications", *Proceedings of the 55th American Society of Mechanical Engineers Gas Turbine and Aeroengine Congress*, Glasgow, Scotland, 14–18 June, Paper No. GT2010-22018.

NOMENCLATURE

C'	constant
D	diameter
f	friction factor
L	length
MAOP	maximum allowable operating pressure
p	pressure
Q_{std}	standard flow
SG	specific gravity
T	temperature
WT	wall thickness
Z	compressibility factor
ς	loss coefficient
$	arbitrary monetary unit

PIPELINE ECONOMICS AND PRESSURE RATIO

We begin by revisiting the reasons why engineers design pipeline compressors with relatively low pressure ratios. We will start by calculating the parameters that control the pressure drop in a transmission pipeline (Fozi, 2008). Figure 1.1 shows a control volume with gas entering from the left with known flow rate, pressure and velocity. Friction forces that are proportional to the square of velocity act on the control volume's surface and gas exits the control volume with changes to its pressure and velocity.

The control volume yields the universal flow equation:

$$p_1^2 - p_2^2 = Q_{std}^2 \frac{f \cdot Z_{ave} T \cdot SG \cdot L}{C'^2 D^5} \tag{1}$$

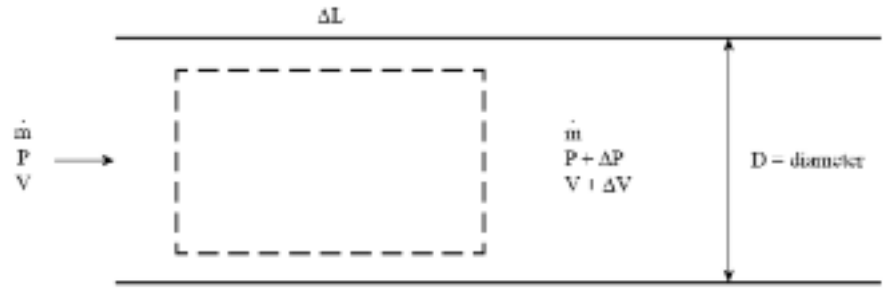

FIGURE 1.1. Balance of forces in a straight pipeline.

Equation 1 applies to any type of pipeline, but it does not directly address the question, "What are the benefits of higher pressure operation?" Axelby (2008) states that we can find the most dramatic improvement in a pipeline's gas carrying capability by installing high capacity ANSI Class 900 pipelines which have operating pressures up to 155 Bar. There are few land-based pipeline designs that operate at or close to this pressure range; however, Figure 1.2 shows a high-pressure pipeline compression station from one of the few that has been built.

With the exception of subsea pipelines, in North America only the Alliance Pipeline system operates at an elevated pressure (120 Bar). There are some proposed, much longer, pipelines in Canada (Mackenzie Gas Pipeline, 180 Bar, and TCPL's Alaska Pipeline, 172 Bar) that would also operate at an elevated pressure. Notably, the Canadian proposals exceed the ANSI Class 900 pressure rating. This is a significant point as valves and flanges at a rating higher than ANSI 900 significantly increase both cost and the availability of potential replacement components during both planned and unplanned maintenance.

Concerns relating to dense phase pipelines include apprehension over the larger gas volumes that would require release if there is a need to isolate pipeline parts for repairs, together with higher regulatory attention and community concerns (Botros *et al*., 2004; Axelby, 2008). Operating at elevated pressures not only increases engineering difficulties that can occur when designing, manufacturing and maintaining the pipeline itself, but also with compression station and valve design.

GENERALIZED PIPELINE CHARACTERISTICS

When a compressor operates in a system with pipe length L_u upstream and a pipe length L_d downstream, and further when the pressure at the beginning of the upstream pipe p_u and the end of the downstream pipe p_e are known and constant, we may utilize a simple compressor station pipeline system model. The pressure gradient in the pipeline, which is a function of gas density, gas velocity, friction factor and

FIGURE 1.2. An Australian high-pressure pipeline compressor station control room (left) and view of the overall installation (right).

pipe diameter, can be integrated if we assume isothermal behavior, to yield the pressure drop for a pipeline segment (Mohitpour *et al.*, 2007). If we assume that the friction factor f is constant, and a constant flow capacity Q_{std}, the pipeline will then impose a pressure p_s at the suction and p_d at the compressor's discharge side:

$$\frac{p_d}{p_s} = \sqrt{\frac{p_e^2 + \varsigma_e Q_{std}^2}{p_u^2 - \varsigma_u Q_{std}^2}} \tag{2}$$

with a pressure loss coefficient ς that incorporates the friction losses. The pressure loss coefficient ς depends on pipe length, diameter, gas composition, temperature profile, pressure profile, surface roughness and flow velocity profile in the respective pipe sections. The pressure loss coefficient ς is proportional to the pipeline's length L (Mohitpour *et al.*, 2007). We may also calculate the suction side pressure p_s and discharge side pressure p_d using more elaborate pipeline hydraulic simulations (Ohanian and Kurz, 2002). Figure 1.3 outlines the results for $p_u = p_d$, $p_e = p_s$ and $\varsigma_u = \varsigma_e = \varsigma$, which is typical for a compressor station in the middle of a pipeline and which simplifies Equation 2 to Equation 3:

$$\frac{p_d}{p_s} = \sqrt{\frac{\varsigma Q_{std}^2}{p_s^2} + 1} \tag{3}$$

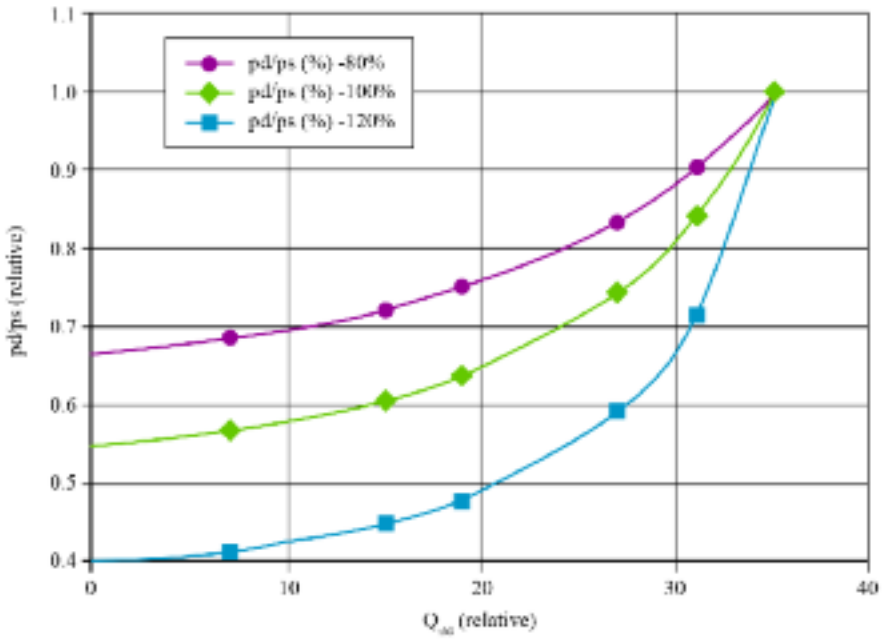

FIGURE 1.3. Pipeline characteristics for different pipeline resistance (Equation 3), for nominal loss coefficient, 80 percent of nominal loss coefficient and 120 percent of nominal loss coefficient.

Lightly loaded pipelines, for example pipelines with a relatively short distance between stations, tend to have a flatter pipeline characteristic, and will show a smaller increase in required station pressure ratio for a given increase in flow. Pipelines where stations are further apart have a steeper characteristic, where even small changes in flow cause large changes in station pressure ratio. This is an important consideration when making a compressor selection, as the compressor map has to cover the entire pipeline characteristic.

An additional consideration when selecting a compressor is that the compressor station pressure ratio reduces at a higher operating pressure (higher p_s). The loss factor ς contains specific gravity and the compressibility factor in a roughly linear relationship (Equation 1); however, for natural gas at pressures up to about 150 Bar, the compressibility factor reduces when the pressure increases if temperature stays constant. For lower temperatures, and heavier gases, the point where the compressibility factor minimizes the volume moves to lower pressures (Gas Processors Suppliers Association, 2012). Thus, pipelines transporting natural gas with a larger amount of components heavier than methane can take advantage of the reduction in compressibility factors at lower operating pressures.

DENSE PHASE COMPRESSION

Under moderate pressures, most gases will form liquids if the temperature reduces sufficiently. Above a critical pressure, no phase change occurs with temperature reduction. In this high-pressure region, the distinction between liquid and gas is no longer significant within the context of pipeline and compressor station design. There is a large region at pressures above the critical pressure and at temperatures roughly around the critical temperature where one can use rotating equipment derived from either pumps or compressors as the basis for a compression station.

Natural gas mixtures have very low critical temperatures resulting in the compression station compressor operating far from the critical point. In contrast, carbon dioxide has a critical point close to compressor operating points. The result is that carbon dioxide requires transportation in its dense phase, otherwise even moderate changes in ambient air temperature or soil temperature in a buried pipeline can lead to a two-phase mixture in the pipeline. A two-phase mixture in the pipeline would damage compression station compressors.

The volume reduction for the compression of carbon dioxide rich gases at a given pressure ratio is sensitive to the gas composition (Figure 1.4). This sensitivity impacts the selection of the compressor's aerodynamic components. Despite a much larger change in compressibility factor for the pure carbon dioxide gas, the density increase (and thus the volume reduction) is smaller than for the carbon dioxide–methane mixtures. The relatively smaller change in density for the pure carbon dioxide gas occurs because the change in compressibility counteracts the volume reduction. Because the compressibility factor depends both on temperature and pressure, the lighter mixtures of carbon dioxide and methane which yield a higher discharge

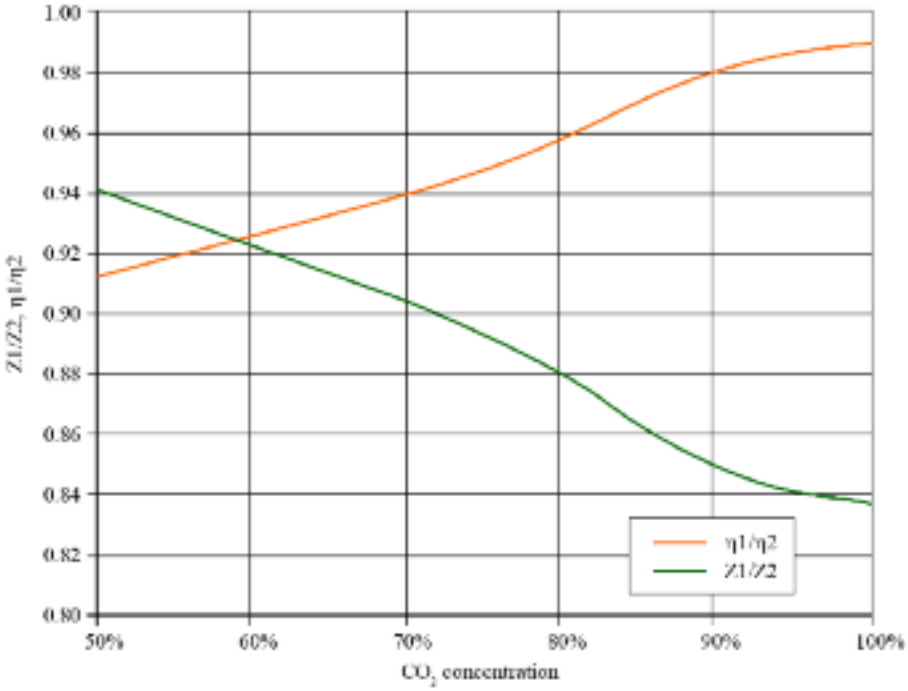

FIGURE 1.4. Change in compressibility factor and change in density for compression of CO_2–CH_4 mixtures. Suction conditions are 26.7°C and 124 Bar, discharge conditions are 152 Bar and a discharge temperature yielding 80.5 percent isentropic efficiency.

temperature than the pure carbon dioxide cause a smaller change in compressibility factor from suction to discharge conditions (Figure 1.4).

IMPACT ON COMPRESSOR DESIGN

A higher gas density impacts compressor design. Since the forces that gas imposes on the compressor are proportional to the gas density, destabilizing aerodynamic forces on the compressor rotor increase. This increase in aerodynamic destabilizing forces will generally result in designers favoring beam style compressors over overhung designs.

A further issue with dense phase pipelines is that the compressor's power density increases. The higher gas compression density results in a smaller compressor absorbing more power. We may illustrate the increase in power density by considering an 80 Bar natural gas pipeline. A compressor with 760 mm flanges and 635 mm impellers will absorb 11 MW for an 80 Bar natural gas pipeline. In contrast, a compressor in a 170 Bar pipeline that absorbs the same power would require a compressor with 406 mm flanges and 380 mm impellers. An additional consideration

when selecting a compressor is to achieve the same pressure ratio at the same power turbine speed. Note that the smaller compressor would require more impellers because for a given speed, the compressor discharge pressure per impeller depends on its diameter.

CARBON DIOXIDE PIPELINES

Carbon dioxide is transported in pipelines in its dense phase above about 69 Bar. In its dense phase the distinction between liquid and gaseous carbon dioxide diminishes. Transportation of carbon dioxide in its gaseous phase, below the critical pressure, is not economic (Mohitpour *et al.*, 2007) because small changes in temperature can cause a two-phase pipeline flow, resulting in high pressure losses and possible damage to the compression station compressors. A further concern is the potential presence of water in the gas. Water and carbon dioxide form carbonic acid, which can be extremely corrosive.

The density of carbon dioxide at a given pressure is sensitive to changes in the gas temperature, which in turn depends on the ambient temperature, or the temperature of the surrounding soil. A 10°C change in ambient temperature results in a 10 percent change in volumetric flow at typical pipeline conditions (Table 1.1). In contrast, the same change in ambient temperature would result in only a 6 percent change in the natural gases' volumetric flow.

The relatively low speed of sound in carbon dioxide (about 260 m/s) compared to natural gas (about 420 m/s) also presents compressor designers with a challenge. The low speed of sound results in a higher relative Mach number which, in turn, reduces a compressor's operating range in comparison to the same compressor operating with natural gas. This operating range reduction is partly offset as the isentropic head required for a given pressure ratio is significantly lower for carbon dioxide than for natural gas (Table 1.1). This reduction in required isentropic head, for the same nominal flow and pressure ratio, results in a physically smaller carbon dioxide compressor.

Table 1.1. *Compression of 600,000 Nm3/h of carbon dioxide or natural gas at 100 Bar, pressure ratio = 1.47.*

	CO_2 (T_1 = 30°C)	CO_2 (T_1 = 20°C)	Natural gas (T_1 = 30°C)	Natural gas (T_1 = 20°C)
Head (kJ/kg)	6.0	5.4	49.7	46.8
Actual flow (m^3/s)	0.42	0.38	1.56	1.47

HIGH-PRESSURE PIPELINE ECONOMICS

In their study, Tobin and Labrujere (2005) outlined key findings for a 1000 kilometer, 2900 million standard cubic feet per day standard pipeline for fixed outlet conditions similar to the analysis above. They found a reduction in capital expenditure and power requirements with increased design pressure up to a pressure of about 100 Bar. Above 100 Bar, capital expenditure increases again (Figure 1.5). Tobin and Labrujere (2005) also studied the cost impact of using higher steel grades for the pipeline, and concluded that despite the increased material cost with higher steel grades, the higher the steel grade, the lower the overall pipeline cost (Figure 1.6). This assumes that higher grades of steel are available in sufficient quantities, which often is a limiting factor for pipeline projects.

Subsea pipelines require thick walled pipes as a consequence of the method used to lay them on the seafloor. Therefore, one can meet the high-pressure requirement at a small incremental cost. Higher gas pressures, above the critical pressure, also help avoid "liquid dropout" as a result of the low-temperature environment subsea. Similar considerations apply to carbon dioxide pipelines, where one can avoid liquid dropout by operating at sufficiently high pressures.

ASSUMPTIONS FOR THE PRESENT STUDY

We can illustrate the issues that impact high-pressure pipeline economics by examining three pipelines with maximum allowable operating pressures of 69 Bar, 103 Bar and 152 Bar. We set the pipeline capacity, expressed as the required flow at the pipeline outline, to 500 million standard cubic feet per day for all cases. This study will illustrate that costs are similar for the three considered pressure levels. We as-

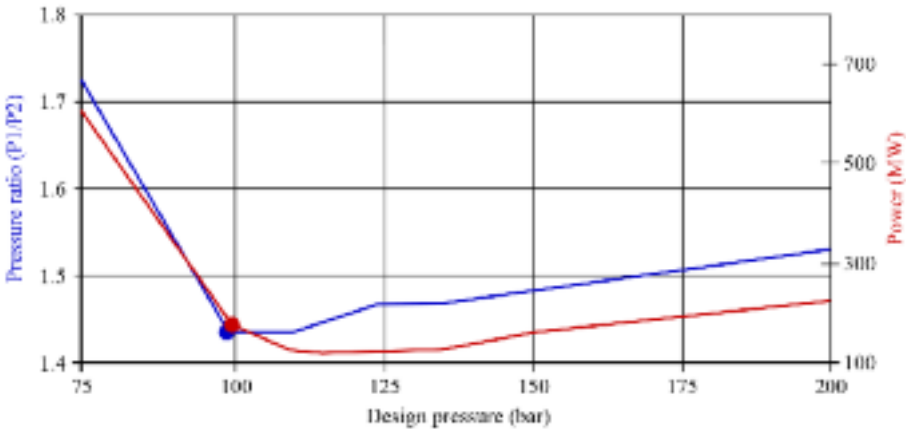

FIGURE 1.5. Effect of design pressure on capital expenditure and installed power (Tobin and Labrujere, 2005).

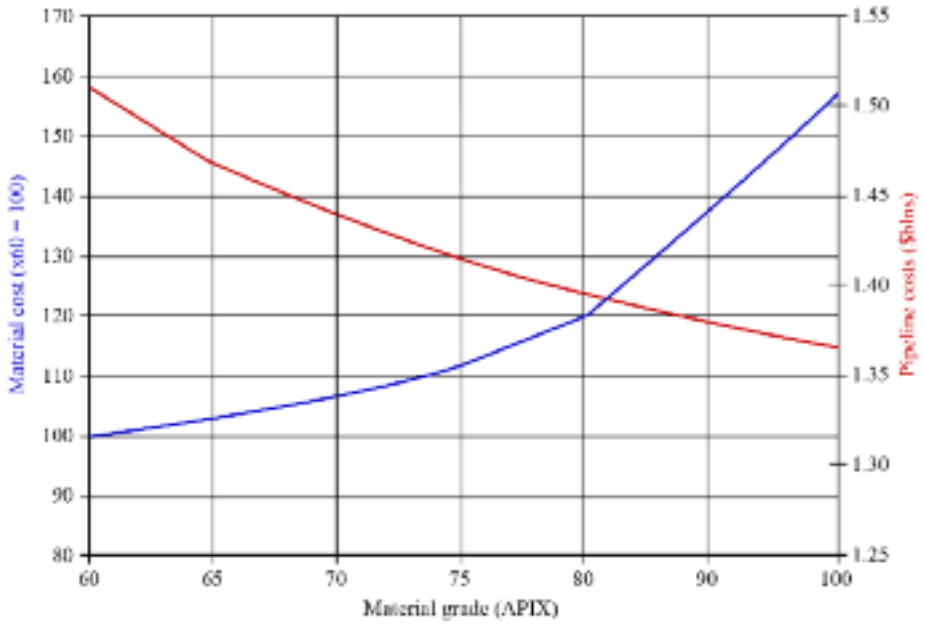

FIGURE 1.6. Effect of pipe material grade on material and construction cost (Tobin and Labrujere, 2005).

sumed a 3220 kilometer onshore buried gas transmission pipeline for transporting natural gas with a specific gravity of 0.6 (Table 1.2).

When attempting to optimize a gas transportation pipeline diameter and compression station spacing, engineers may consider a wide range of primary variables which include right of way costs, permit costs, freight rates, onshore or offshore construction costs, availability of material and quality of labor. The pipeline route and compression station locations also have an impact on cost as pipelines frequently pass through remote, harsh, mountainous regions and require lake and river crossings. In some cases the construction crew, pipeline and compression station operators also require housing simply as a consequence of the remote location.

Many companies initially operate pipeline systems at reduced capacity, but size them to allow for future growth. When companies tap additional gas reservoirs, they add more gas consumers. This potential capacity increase results in engineers designing the pipeline with a larger than optimum diameter for the initial capacity. An alternative strategy is to build only a portion of the ultimately required compression stations, with a provision for adding more at a future date as capacity increases. The effect of designing for some future increased capacity effectively increases the pipeline system's cost for the initial capacity.

Availability of pipe fittings, valves and flanges also constitutes a factor in the pipeline design. In the present study, we assume that ANSI Class 900 flanges and valves will be readily available with material group 1.2, capable of operation at 156

Table 1.2. *Assumptions for pipeline simulation.*

Required flow at pipeline outlet	500 million standard cubic feet per day
Off takes along the pipeline	None
Pipeline maximum allowable operating pressure	152, 103, 69 Bar
Pipe material grade	API 51X70
Steel density	7900 kilograms per cubic meter
Pipe internal roughness	0.0018 mm
Pipeline profile	Flat
Pipeline inlet/outlet pressure	Same as maximum allowable operating pressure
Pipeline flowing temperature	15°C
Pipeline flow regime	Isothermal and steady
Flow equation	(Fundamental) general
Gas lower heating value	37,000 kJ/Nm^3
Station suction piping loss	0.35 Bar
Station discharge piping loss	0.35 Bar, 0.7 Bar with discharge cooler
Compressor isentropic efficiency	83%
Compressor mechanical efficiency	98%
Gas turbine driver heat rate:	
Above 5500 kW	11,090 kJ/kWh
Below 5500 kW	[17,090.5 – 1.091*kW] kJ/kWh
Station construction cost*	24,050*(kW/0.745)$^{-0.2866}$, $ per kW
Annual station operation cost*	$33.56/kW
Pipe material cost*	$1000 per ton
Pipeline construction cost*	$155,000 per kilometer
Fuel gas	$1.9 per GJ
Project life	20 years
Escalation factor for fuel and operation cost	3.5% per year
Depreciation	Not considered
Driver power	Site rated

* The monetary units are arbitrary, and do not reflect 2009 US$.

Bar pressure and moderate temperatures. The present study also uses the *Oil and Gas Journal* (1996) and *Oil and Gas Journal* (2009) construction cost data for compression stations. The compression station cost estimate is approximate as it does not consider extremely high or low station costs. For this study, we used a simplified approach for pipeline construction cost by assuming $1000 per ton of steel plus $156,250 per kilometer of pipe. With these assumptions, the cost per kilometer for the 610 mm pipe with 13.3 mm wall thickness is approximately $374,000.

Although the pipeline itself is amenable to simplifying assumptions, it is more difficult to simplify the compression station cost estimates. One approach would be to assume that the cost per unit of power for a given compression station would decrease as compressor size increases. Although an apparently reasonable assumption, no reliable data was available in the open literature to support the assumption. The available data provides figures that range from $9.00 per kilowatt to $60.00 per

kilowatt. A wide range of factors drives these cost variations: primary logistics, spare parts inventory, equipment durability, overhaul interval, full or part load operation, fired hours, number of starts and stops, annual survey and testing costs of compression station equipment and pipeline pigging operations. Despite the difficulty of generalizing compression station costs, we chose in this study a cost of $33.56 per kilowatt, regardless of the compressor's size. Finally, we also assumed that the driving gas turbine heat rate was 17,090.5 kilojoules per kilowatt hour at zero power, and then reduced linearly with power increasing to 5500 kW. Above 5500 kW, we assumed the heat rate to remain constant at 11,090 kilojoules per kilowatt hour.

Given the above assumptions, for a compression ratio of 2.2 and 15.8 megawatts per compression station, this study shows that the most economical pipe diameter is 560 mm, with ten compression stations 3200 kilometers apart. However, when we considered fuel costs, operation and maintenance over 20 years, assuming a 3.5 percent annual cost escalation and a 10 percent capital cost, the least costly pipe diameter is 620 mm with six compression stations 536 kilometers apart.

We continued the study with life-cycle cost for three alternate pipe design pressures of 69 Bar, 103 Bar and 152 Bar (Figures 1.4, 1.5 and 1.6). For this study, we assumed the use of internally coated pipe which resulted in 0.0018 mm roughness. Internal coating reduces friction losses through the pipeline. The authors did not consider the effect of gas expansion (the Joule-Thomson effect). Also, the study is a steady-state study, with no attempt to perform a transient flow analysis that we normally associate with daily, weekly and seasonal load variations. We further assumed that the average compressibility factor Z is constant in each pipe element.

DISCUSSION OF THE RESULTS

Small diameter pipelines require more compression stations for a fixed pipeline length. The result is an increase in compression station capital cost, operating costs and maintenance costs. These cost increases offset the lower pipe cost. In contrast, large diameter pipelines will require fewer compression stations for a fixed pipeline length. The decrease in compressor station capital cost, operating costs and maintenance costs offset the higher pipe cost. Figures 1.7, 1.8 and 1.9 illustrate the optimum pipeline diameter and number of compression stations for each of the three considered pipeline pressures.

We undertook the analysis that we presented in Figures 1.7, 1.8 and 1.9 as follows. We calculated the pressure drop along the pipeline utilizing the general flow equation (Equation 1). We considered pipeline diameter and compression station spacing at compression ratios of 1.2, 1.3, 1.4, 1.6, 1.8, 2.0 and 2.2. We then calculated the pipeline wall thickness, following which it was possible to calculate the pipeline weight which facilitated us in calculating the pipeline construction cost. Next, we calculated the required shaft power at each compression station, assuming 83 percent compressor isentropic efficiency. We used power to determine the compression station cost and the gas turbine heat rate. This helped us to calculate the annual operating and maintenance costs for an assumed 20-year project life.

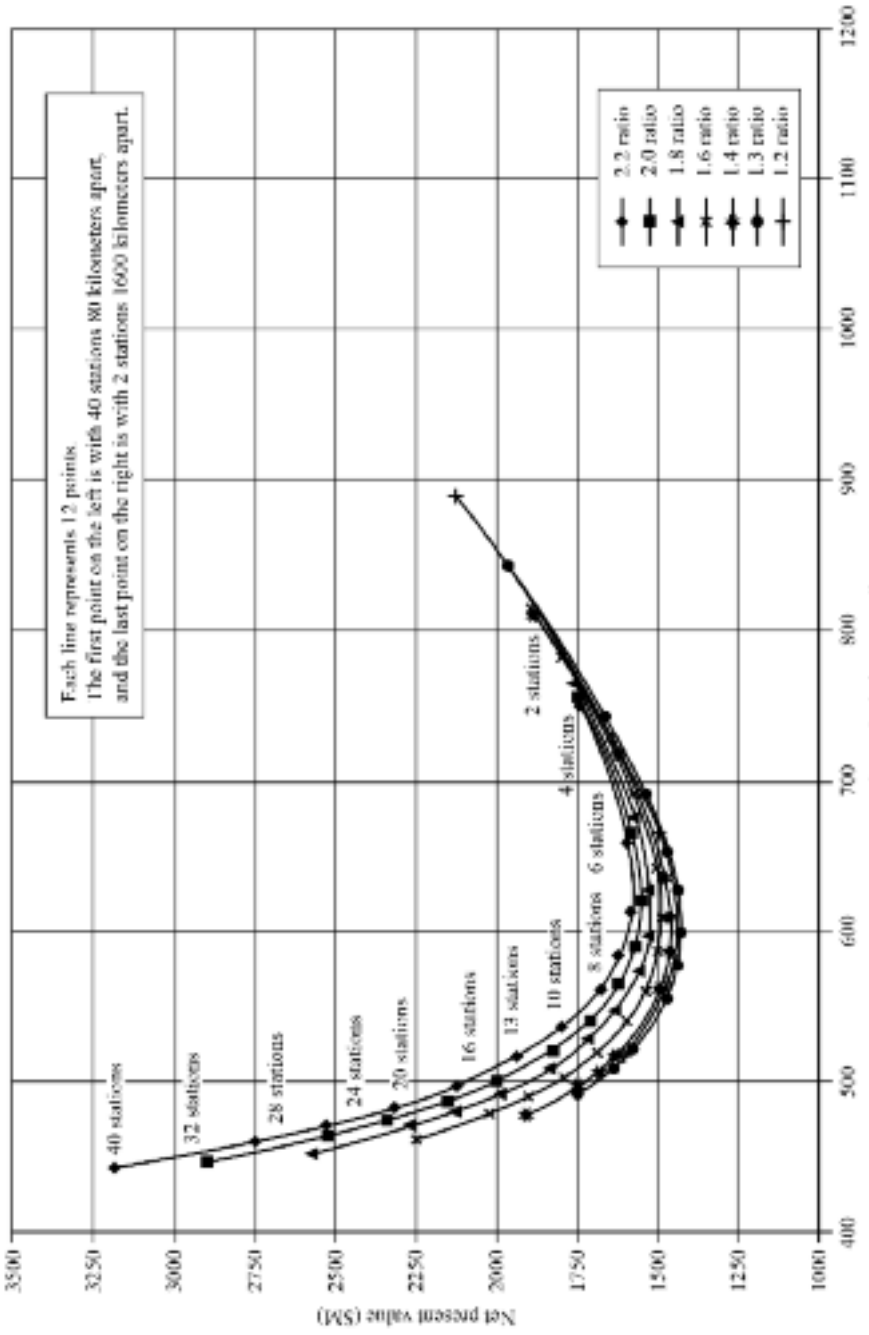

FIGURE 1.7. Net present value for 152 Bar pipeline for different numbers of stations and station pressure ratios.

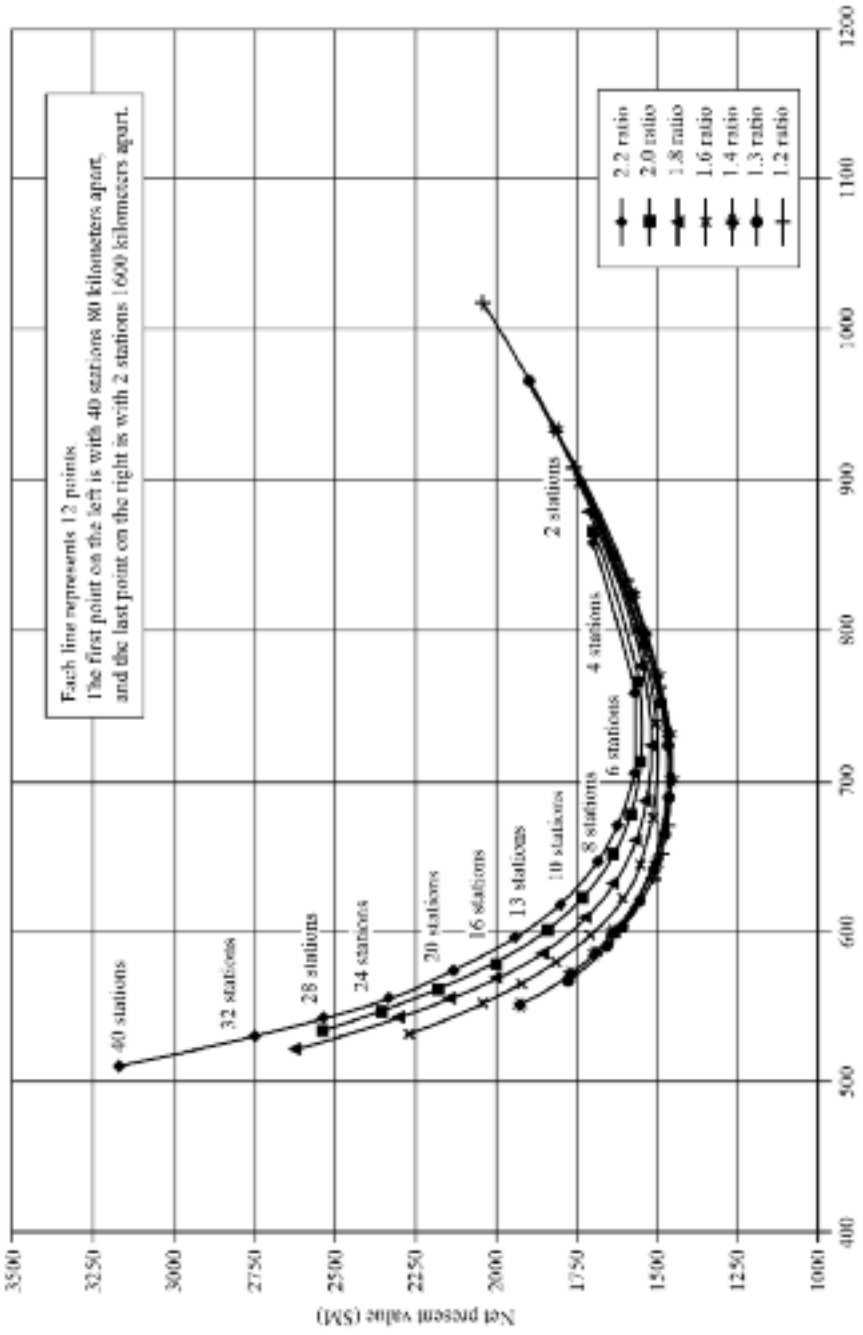

FIGURE 1.8. Net present value for 103 Bar pipeline for different numbers of stations and station pressure ratios.

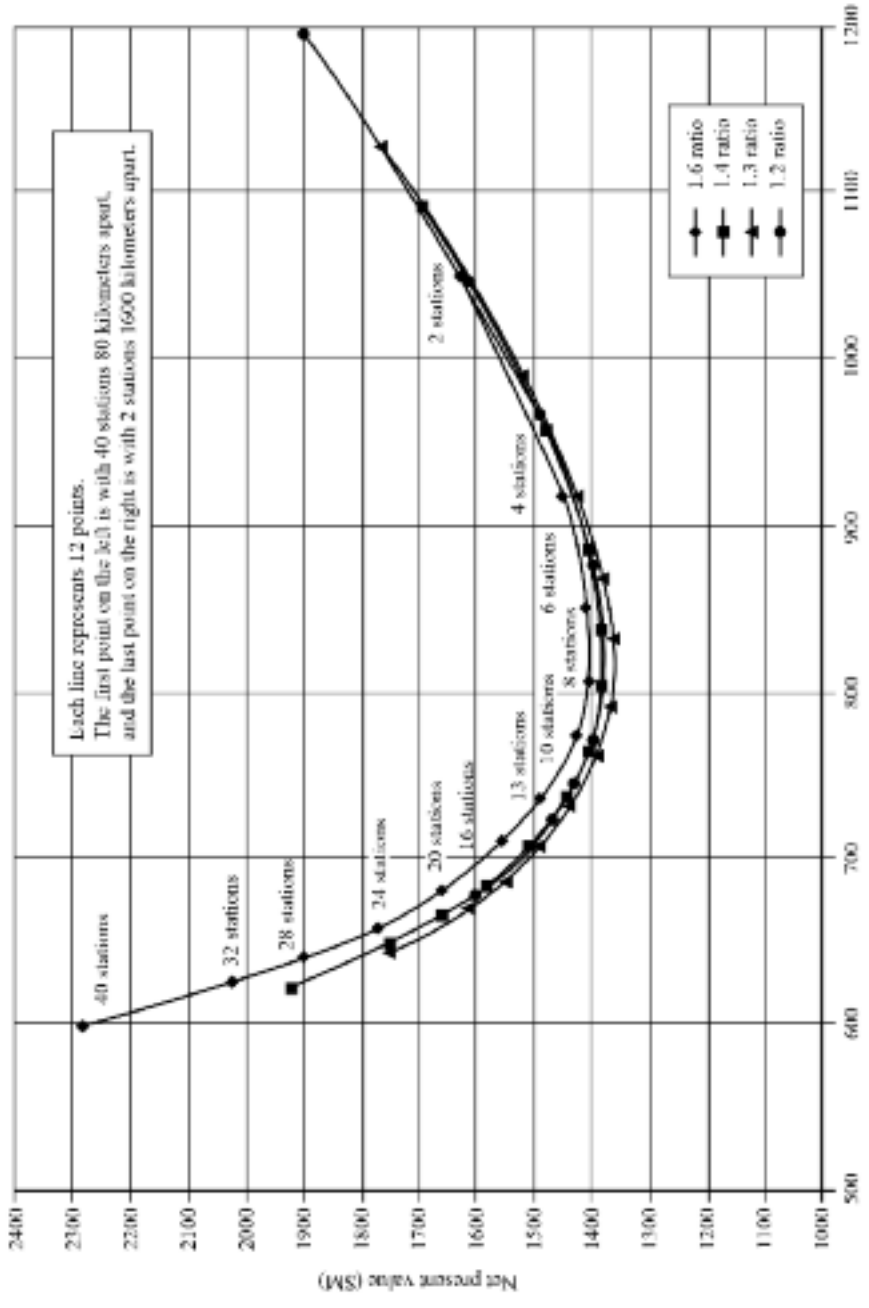

FIGURE 1.9. Net present value for 69 Bar pipeline for different numbers of stations and station pressure ratios.

The minima of each curve in Figures 1.7, 1.8 and 1.9 represent the economic pipeline diameter and compression station spacing for the respective compression ratio. The study indicates that for all three considered pipeline pressures, the optimum pipeline diameter and minimum operating cost is similar for compression ratios of 1.2, 1.3 and 1.4. For a compression ratio of 1.3, Table 1.3 presents a summary of each of the three considered pressure levels based on fractional pipe size and without flow adjustment for fuel takeoff. A net present value calculation for each of the considered pipeline pressures indicates that the 69 Bar pipeline has the lowest net present value and consequently, the lowest ownership cost over the assumed 20-year project life. Because the flow capacity remains the same for all calculations, the lowest cost of ownership also represents the lowest transportation cost per unit of flow.

We continued our study, assuming that pipes are available in 50 mm diameter increments, and selected the nearest even increment to the pipeline diameter that we calculated during the study. The pipeline diameters that we selected were 610 mm, 710 mm and 860 mm for the 152 Bar, 103 Bar and 69 Bar pressure pipelines. For this step, we considered the fuel gas consumption along the pipe, and its effect on the actual flow through the pipe. Consequently, the flow into the pipe is higher than the flow out of the pipe due to the compression station gas turbines' fuel usage. Having refined the calculation using available pipeline diameters, we present the results in Figure 1.10. Table 1.4 presents a summary of each of the three considered pressure levels with flow adjustment for fuel takeoff. Once again, the 69 Bar pipeline has the lowest net present value and consequently, the lowest cost of ownership over the assumed 20-year project life.

In practice, engineers design compression stations with a common driver and compressor size for installation along the pipeline's entire length. Making each compression station identical minimizes required spares and standardizes operation and maintenance. A standard compression station design results in a fixed compression station power and consequently, engineers must adjust the compression station spacing to account for topological effects along the pipeline route, as well as for the flow reduction that occurs as a consequence of compression station gas turbine fuel usage. This results in subsequent compression stations having to compress slightly less gas than each previous compression station. In the present study, the predicted required compression station power for the 69 Bar pipeline ranged from 5750 kilowatts at the start of the pipeline to 5320 kilowatts at the end. By dividing the total power for all compression stations by the number of compression stations, we calculated the average power per compression station at 5510 kilowatts.

Table 1.3. *Net present value calculations before refinement.*

MAOP, Bar	No. of stations	Distance, km	Comp. ratio	Total kW	Heat rate, kJ/kWh	Theory OD, mm	Theory WT, mm	Present value, $M
152	13	250	1.3	59,000	12,000	606	13.3	1456
103	13	250	1.3	62,500	12,000	700	10.4	1412
69	10	320	1.3	51,000	11,500	870	8.6	1375

Table 1.4. *Net present value calculations after refinement.*

MAOP, Bar	No. of stations	Distance, km	Comp. ratio	Average kW/station	Total kW	Fuel, m_N^3/h	Pipe OD, mm	Pipe WT, mm	Present value, $M
152	13	250	1.0293–1.320	4582	59,570	19,552	610	13.3	1464
103	12	265	1.313–1.341	5096	61,150	19,061	710	10.4	1417
69	10	320	1.328–1.352	5514	55,137	16,527	860	8.6	1376

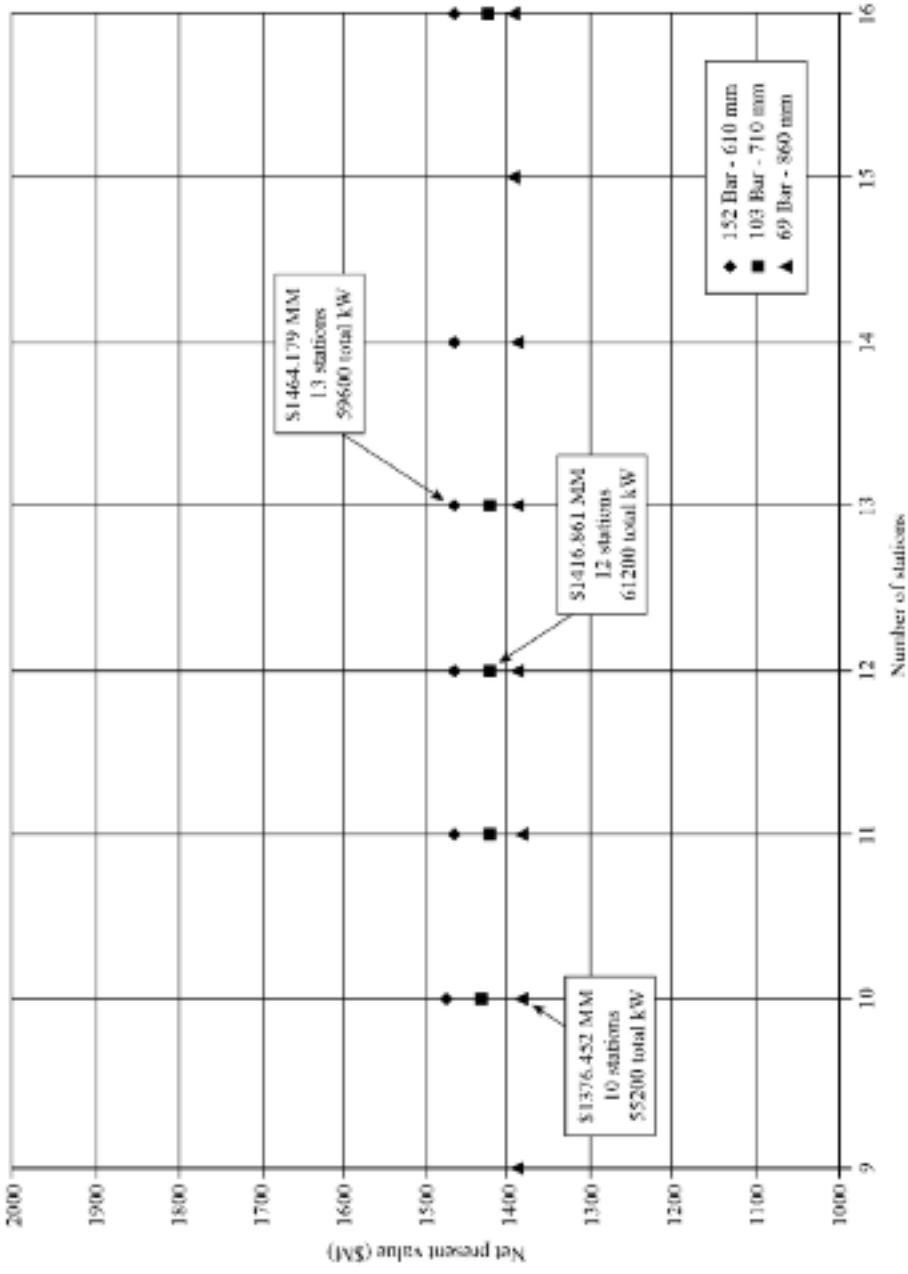

FIGURE 1.10. Optimum number of stations and optimum maximum allowable operating pressure for the 3220 km, 560,000 m_N^3/h sample pipeline. The lowest cost configurations for each maximum allowable operating pressure solution are marked.

COST SENSITIVITY ANALYSIS

Because the results are sensitive to relative cost assumptions, the study continued with an analysis of each cost to determine the pipeline system's net present value sensitivity to variation in cost (Figure 1.11). We calculated the sensitivity to variation in compressor station, pipeline and operation and maintenance costs by using the 69 Bar pipeline with 1.3 compression ratio costs as a base line. Doubling the compression station cost shifts the curve up and to the right, indicating that with a higher station cost, the net present value is higher and consequently, larger diameter pipelines are preferable.

We assessed the sensitivity to pipeline cost by flexing the pipeline construction cost with pipeline diameter, using an assumed cost of $10,000 per mm-kilometer. This assumption of construction cost per mm-kilometer results in a pipeline cost of $150,000 per kilometer for a 610 mm diameter pipeline pipe and $260,000 per kilometer for a 1000 mm pipeline. When compared to our original assumptions about pipeline cost, the curve shifts up and to the left, signifying that when the pipeline cost increases more rapidly, smaller diameter pipelines are preferable.

Finally, increasing the 69 Bar pipeline annual operation cost from $20 per kilowatt to $50 per kilowatt shifts the curve slightly up. This relatively small change is a consequence of the fuel cost, representing a relatively small proportion of the pipeline system's net present value. We also see the same relatively small effect for the 103 and 152 Bar pipelines.

The results of the sensitivity analysis indicate that the 69 Bar pipeline with a compression ratio of between 1.328 and 1.352 is the most economical solution for the assumed conditions and cost data. However, when we studied the data in Table 1.4 and Figure 1.10, the 69 Bar pipeline net present value is within +/–3 percent of the 103 Bar pipeline cost. Therefore, we concluded that the net present value is virtually the same for the three considered pipeline pressures, within the uncertainty of the assumptions. Consequently, one must decide on optimum pipeline pressure based on project-specific costs given the local conditions along the pipeline route. The compression ratios, which define optimum station spacing, are from 1.293 to 1.352.

A final consideration when contemplating a higher pressure pipeline is the relative cost of bringing the transported gas to the higher operating pressure. We can illustrate the significance of bringing the transported gas to a higher operating pressure by considering an 800 kilometer and a 400 kilometer pipeline where the operating pressure varies between 74 Bar and 98 Bar. We assume that all compression stations use multiple drivers of the same type and rating. For the 800 kilometer pipeline:

- With the lowest maximum allowable operating pressure of 74 Bar, the number of required compression stations is six. The distance between compressor stations is 160 kilometers and the average compressor station pressure ratio is 1.38.

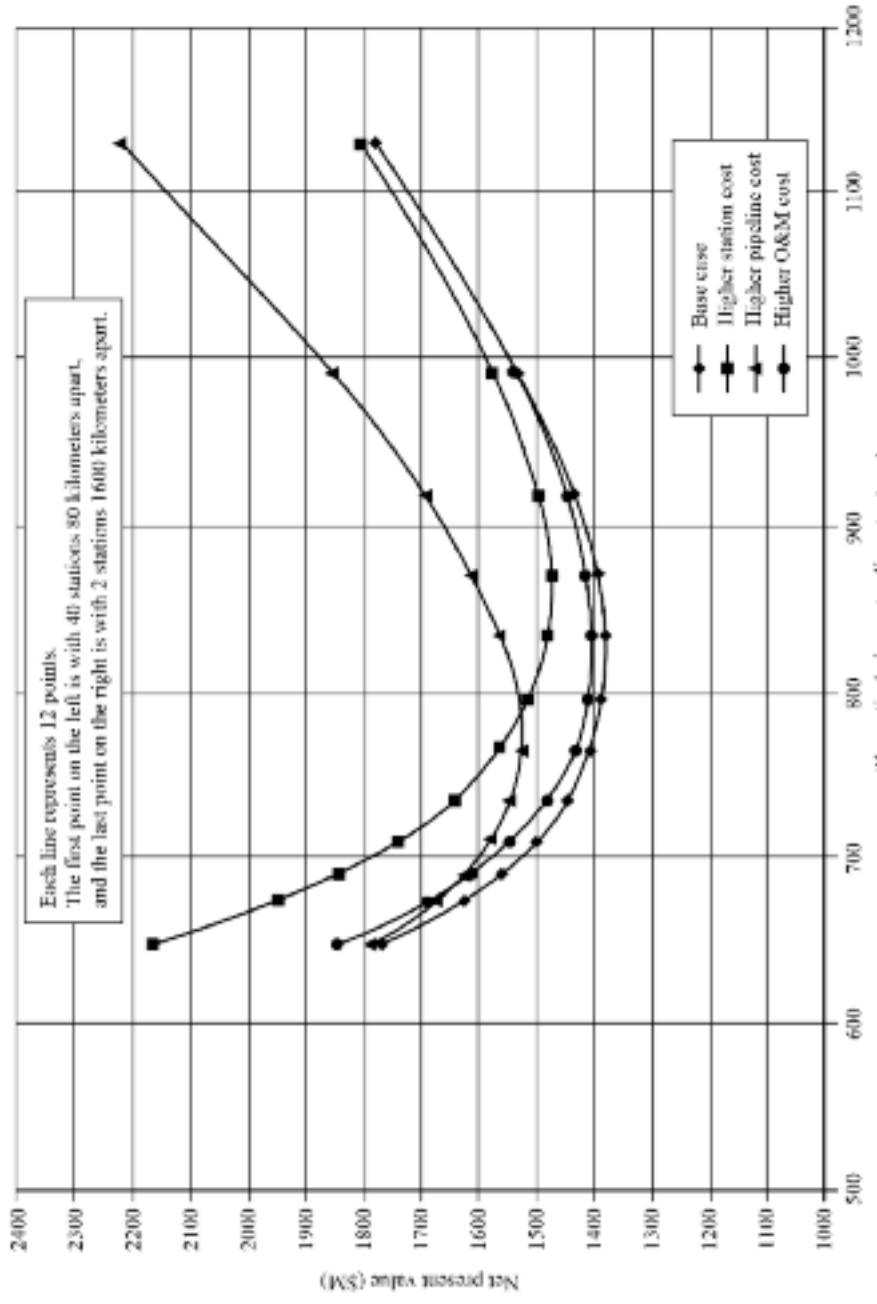

FIGURE 1.11. Sensitivity analysis.

- With a maximum allowable operating pressure of 84 Bar, the number of required compression stations is five. The distance between stations is 200 kilometers and the average compression station pressure ratio is 1.37.
- With the highest maximum allowable operating pressure of 98 Bar, the number of required compression stations is four. The distance between compression stations is 265 kilometers and the average compression station pressure ratio is 1.35. The 400 kilometer pipeline would require proportionally fewer compression stations.

The first compression station in all three cases is a "head station" that brings the gas from gas supply pressure (which we assumed was the same for all three cases) to the pipeline maximum allowable operating pressure. For higher maximum allowable operating pressure, the pipeline consumes more power in the head station, and less in the line compressor stations (Figure 1.12). While the 800 kilometer pipeline minimum power consumption is at the highest maximum allowable operating pressure of 98 Bar, the 400 kilometer pipeline minimum power consumption is at the intermediate maximum allowable operating pressure of 84 Bar. The 400 kilometer pipeline has a lower power requirement at a lower maximum allowable operating pressure because the "line stations" no longer compensate for the additional power requirement at the head station. Consequently, it is not economic to run shorter pipelines at higher pressures.

SUMMARY

The study in this chapter does not clearly demonstrate the universal advantage of high-pressure pipelines. The relative advantages of different pipeline pressures are a function of individual project specifications. High-pressure pipelines, therefore, have their place; however, they do not automatically result in the lowest installation and operating costs over a project's lifetime.

High-pressure pipelines are generally preferable for offshore application where platform costs for intermediate stations could be prohibitively high. In situations where the building costs are high, operating and maintaining compression stations is expensive and high-pressure pipelines are unlikely to result in the lowest installation and operating costs over a project's lifetime. However, when the pipeline is long and where liquid formation is an issue, high-pressure pipelines may result in the lowest installation and operating costs over a project's lifetime.

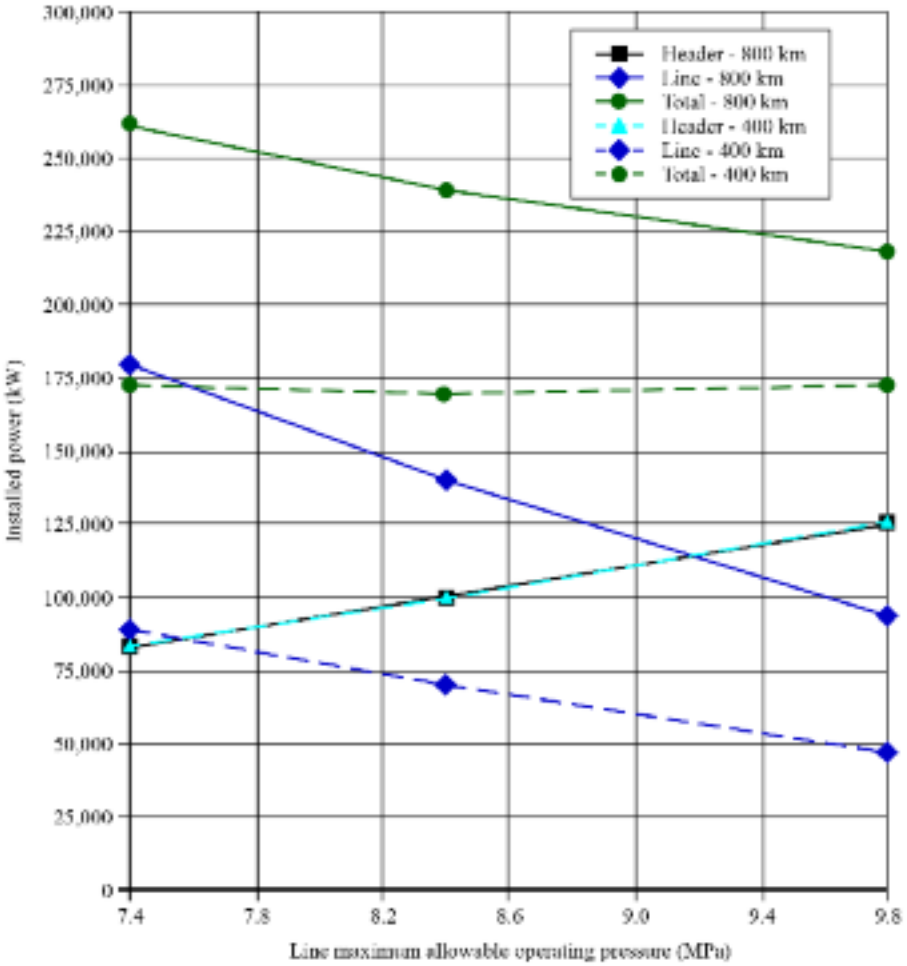

FIGURE 1.12. Power consumption for a 400 kilometer and an 800 kilometer pipeline with different maximum operating pressures.

REFERENCES

Axelby, M. (2008), "Operating Practices Change in the High-Pressure World of Class 900 Pipelines", *Pipeline and Gas Journal*, vol. 235, p. 68.

Botros, K.K., Geerligs, J., and Given, R. (2004), "Gas Pipeline Response under Rupture or Blowdown Conditions", PRCI Report.

Fozi, A.A. (2008), *Pipeline Compressor Design*, Indopipe, Jakarta.

Gas Processors Suppliers Association (2012), *Engineering Data Book*, 13th edn, Gas Processors Suppliers Association, Tulsa, Oklahoma.

Mohitpour, M., Golshan, H., and Murray, A. (2007), *Pipeline Design and Construction*, 3rd edn, ASME Press, New York, USA.

Ohanian, S., and Kurz, R. (2002), "Series or Parallel Arrangement in a Two-Unit Compressor Station", *Transactions of the ASME, Journal of Engineering for Gas Turbines and Power*, vol. 124, pp. 936–41.

Oil and Gas Journal (1996), "Pipeline Economics", November.

Oil and Gas Journal (2009), "Special Report: Pipeline Economics", September.

Tobin, M., and Labrujere, J. (2005), "High Pressure Pipelines, A Review of Basic Design Parameters", GTS, Moscow.

Chapter 2

Measurement Uncertainties Encountered during Gas Turbine Driven Compressor Field Testing

K. Brun and R. Kurz

ABSTRACT

Field testing of gas turbine compressor packages requires the accurate determination of efficiency, capacity, compressor discharge pressure, power and fuel-flow in sometimes less than ideal working environments. Nonetheless, field test results have significant implications for compressor and gas turbine manufacturers and their customers. Economic considerations demand that operators verify the performance and efficiency of the installed equipment to assure a project's return on investment. Thus, for the compressor and gas turbine manufacturers, as well as for the end-user, an accurate determination of the field performance is of vital interest. This chapter describes an analytic method to predict the measurement uncertainty and, thus, the accuracy of field test results for gas turbine driven compressors. Namely, the chapter presents a method which one can employ to verify the validity of field test performance results.

We have derived the equations governing the compressor and gas turbine performance uncertainties and compared the results to actual field test data. We present typical field test measurement uncertainties for different sets of instrumentation. Next, we identify test parameters that correlate to the most significant influence on the performance uncertainties and provide suggestions on how to minimize their measurement errors. We also discuss the effect of different equations of state on the calculated performance. Results show that compressor efficiency uncertainties can be unacceptably high when one violates basic rules for accurate testing. However, by following some simple measurement rules the overall compressor package performance measurement uncertainty can be minimized.

This chapter is a revised and extended version of Brun, K., and Kurz, R. (2001), "Measurement Uncertainties Encountered during Gas Turbine Driven Compressor Field Testing", *Transactions of the ASME, Journal of Engineering for Gas Turbines and Power*, vol. 123, pp. 62–9. This paper won the International Gas Turbine Institute Pipelines and Applications Committee 1998 best paper award.

NOMENCLATURE

c_p	specific heat at constant pressure
γ	ratio of specific heats
h	enthalpy
MW	molecular weight
p	pressure
P	power
Q	volumetric flow
R	gas constant
ρ	density
T	temperature
W	mass flow
Z	compressibility factor
η	efficiency
H	head
BWRS	Benedict-Webb-Rubin-Starling
L	$(\gamma-1)/\gamma$
LDP	Lee-Kesler-Ploecker
SRK	Soave-Redlich-Kwong

Subscripts

d	discharge
M	mechanical
p	package
s	suction
TH	thermal
*	isentropic

INTRODUCTION

Operators frequently test gas turbine compressors after their installation in the field to verify the manufacturer's performance predictions. Failure to meet claimed performance may result in financial penalties for the manufacturer as well as significant discontent on the end-user side. However, due to the non-ideal measurement conditions that one typically encounters during the field testing, uncertainties can be so significant that it may be impossible to define a simple single performance guarantee point. It is therefore important to define an allowable measurement uncertainty range acceptable to both manufacturer and end-user prior to the field test. To maintain impartiality, one should not base this uncertainty band on empirical experience, but rather on uncertainty equations derived from a mathematical expression for the gas turbine compressor performance and from the basic instrument and sensor device inaccuracies.

Limited information is available in the public domain describing actual gas turbine field test measurement uncertainties. The primary source of information which manufacturers and end-users employ are test codes which the American Society of Mechanical Engineers (ASME), the International Organization for Standardization (ISO) and the Verein Deutscher Ingenieure (VDI) provide. These specifications cover thermodynamic calculation methods, instruments, site preparation and turbomachinery test results in various degrees of detail. ASME Power Test Codes (PTC) 10 (ASME, 1979), 19.1 (ASME, 1985a) and 22 (ASME, 1985b), ISO 2314 (ISO, 1989), VDI 2048 (VDI, 1978) and 2045 (VDI, 1993) are typical examples of these standards.

A number of researchers from both academia and industry have to a limited degree discussed field testing errors and uncertainties. For example, Fozi (1995) discussed practical challenges of field performance tests. He showed that steady-state measurement conditions were critical for obtaining accurate field test results. Schmitt and Thomas (1995) compared achievable field to factory test accuracies. Results indicated that if design engineers adopt a technically rigorous field test procedure, they could achieve comparable accuracies between field and factory tests. Meier and Rhea (1982) performed compressor tests and discussed good test practices and procedures. They defined and discussed instrumentation specification requirements for reasonable accuracy in field testing. McRoberts (1984) reported on compressor performance tests which he conducted in the challenging environment of an offshore platform. Finally, Klein and Draughton (1991) undertook field performance tests of a gas reinjection compressor-turbine train. They compared PTC 10 Class I and PTC 10 Class III factory test results to field performance tests.

This chapter aims to provide information on gas turbine driven compressor field testing uncertainties. It describes an analytic method to determine compressor and gas turbine measurement uncertainties. For this method, we derived a set of uncertainty equations from the physical turbomachinery performance relations. We present typical field test measurement errors for different sets of instrumentation and sensors. By introducing these experience errors into the uncertainty equations, one can predict the total efficiency, power and compressor discharge pressure uncertainty for a gas turbine compressor prior to the field test for a given operating condition. We employed two actual field test examples to demonstrate the viability of this method. We also included a number of parametric studies which characterize uncertainty trends. We identified parameters that most significantly affect the overall compression station uncertainty, and in so doing help the user to optimize his/her field test instrumentation selection. Finally, the chapter discusses the effect of different equations of state on the calculated performance.

METHODOLOGY

For the uncertainty analysis we assume that all measurement parameters are independent and that parameters have associated statistical bounds rather than absolute

limits of errors. We also assume that all parameters have Gaussian normal distributions around their respective mean values such that we can combine the uncertainties using the root-square sum method (Doeblin, 1966). However, we add an uncertainty correction for parameters which have sample sizes smaller than 30. For example, the uncertainty widens for individual parameters to account for a Student t-type distribution (Brun, 1996). Thus, we determine the total uncertainty, ΔF, for a given function, $F = f(u_1,u_2,..u_n)$, from Scarborough (1955):

$$\Delta F = \sqrt{\left(\Delta u_1 \frac{\partial f}{\partial u_1}\right)^2 + \left(\Delta u_2 \frac{\partial f}{\partial u_2}\right)^2 + ... \left(\Delta u_n \frac{\partial f}{\partial u_n}\right)^2} \tag{1}$$

For the above method, the overall uncertainty ΔF has the same statistical meaning as the individual uncertainties Δu. Namely, if Δu represents a 95 percent confidence then the result for the total uncertainty ΔF is also a 95 percent confidence interval. Note that since it is not possible to distinguish between bias errors and data scatter in a field test environment, we do not treat them independently.

Compressor performance equations

We measured the following parameters:

1. the compressor inlet and outlet stagnation temperature, T_s and T_d;
2. the compressor inlet and outlet static pressure, p_s and p_d; and
3. the actual inlet volume flow rate, Q, during a centrifugal compressor field test (Figure 2.1).

Furthermore, we require knowledge of the gas composition to determine, based on the equations of state (Soave-Redlich-Kwong (SRK), Lee-Kesler-Ploecker (LDP) and Benedict-Webb-Rubin-Starling (BWRS)), the gas molecular weight and the specific heat ratio as a function of static temperature, $\gamma(t)$, and the gas compressibility factor as a function of static pressure and temperature $Z_{(p,t)}$. Using this information, we sequentially used the following simplified Equations 2 through 9 to determine compressor discharge pressure, commonly referred to as head, H, efficiency, η, and required driver power, P.

Gas constant:

$$R = \frac{R_{Universal}}{MW} \tag{2}$$

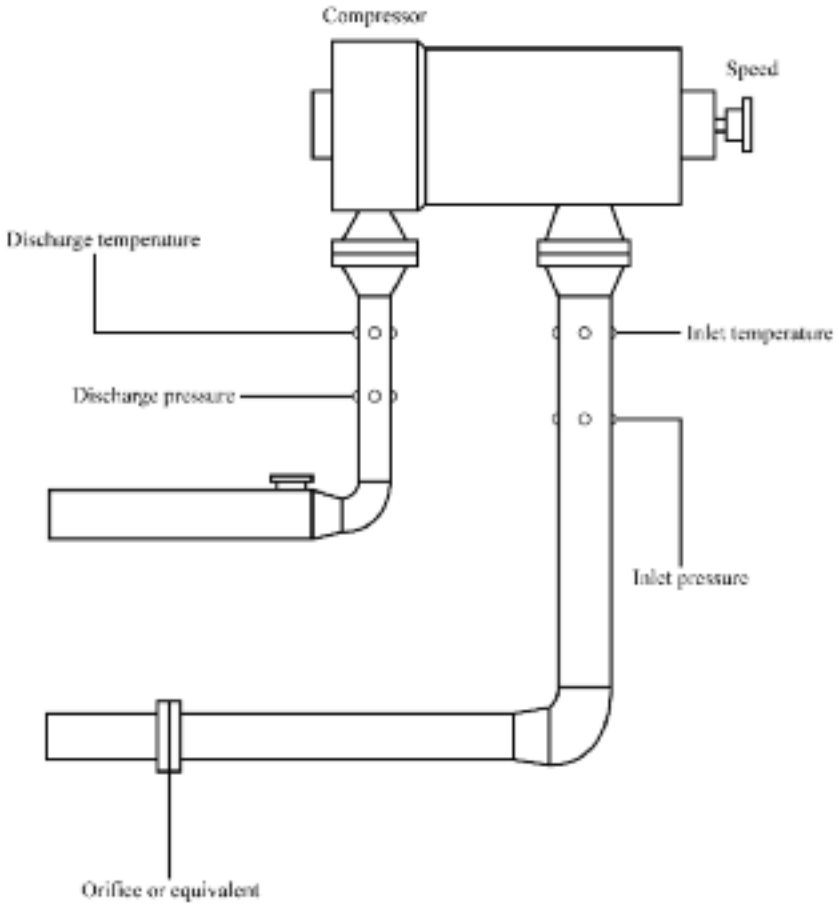

FIGURE 2.1. Test instrumentation for a gas compressor.

Density:

$$\rho = \frac{p}{R \cdot Z \cdot T} \tag{3}$$

Specific heat:

$$c_p = Z \cdot R \cdot \left(\frac{\gamma}{\gamma - 1} \right) \tag{4}$$

Head = actual enthalpy difference:

$$H = c_p(T_d)T_d c_p(T_s)T_s \tag{5}$$

Isentropic outlet temperature:

$$T_d^* = T_s \cdot \left(\frac{P_d}{p_s}\right)^{\frac{\gamma-1}{\gamma}} \tag{6}$$

Isentropic enthalpy difference:

$$h^* = c_p(T_d^*)T_d^* c_p(T_s)T_s \tag{7}$$

Isentropic efficiency:

$$\eta^* = \frac{h^*}{H} \tag{8}$$

Driver power:

$$P = \frac{H \cdot Q \cdot \rho}{\eta_M} = \frac{H \cdot Q \cdot p_s \cdot MW}{\eta_M \cdot R_{Universal} \cdot T_s} \tag{9}$$

In reality, one does not use the above simplified equations in this form to determine compressor performance, but rather they represent a close functional description of the actual physical equations. Nonetheless, since we primarily based the total uncertainty on the product of the individual uncertainty value and the governing equation's gradient (*df/du*), the simplified functional form is adequate to perform an accurate uncertainty analysis.

Also, the simplified equations do not fully model the behavior of real gases. We have neglected the heat capacity's pressure dependency effect. Also, in Equation 6, the real gas behavior would require the isentropic coefficient rather than the ratio of specific heats. Both effects, while important for the calculation of the absolute values, have little influence on the functional form, and thus on the results of the uncertainty equations.

Note that for centrifugal compressor field tests one often assumes that stagnation and static values for pressure and temperature are very close so that one can neglect their difference for the performance calculation. One should take care with this assumption. This is only a valid assumption as long as compressor local inlet and outlet local flow Mach numbers are below approximately 0.1. For example, if in a pipeline compressor the local outlet flow Mach number reaches 0.1, it leads to a stagnation-static pressure difference of 0.6 percent and temperature difference of

0.15 percent. Based on the uncertainty equations derived below, one can show that these deviations lead to a negligible compressor isentropic efficiency uncertainty of 0.12 percent. In contrast, if the Mach number approaches 0.3, a flow velocity of about 125 meters per second in a natural gas pipeline, typical pressure and temperature errors are 7.0 percent and 1.6 percent, respectively.

While the calculation of the total pressure from the static pressure is routine, once one knows the flow velocity, calculation of the difference between stagnation and static temperature is more challenging. The temperature measuring device in a thermowell will show a temperature that is somewhere between the stagnation and the static temperature. We therefore define the potential temperature error by the difference between stagnation and total temperature. For the sake of brevity, we assume herein that stagnation and static values are identical.

Compressor uncertainty equations

By substituting Equations 2, 3 and 4 into Equation 1 and simplifying the equations by representing $(\gamma-1)/\gamma$ using the letter L as a mathematical operator, we obtain the following relation for the specific heat uncertainty Δc_p:

$$\Delta c_p = \sqrt{\left(\Delta Z \cdot \frac{R_{Universal}}{L \cdot MW}\right)^2 + \left(\Delta L \cdot \frac{R_{Universal} \cdot Z}{L^2 \cdot MW}\right)^2 + \left(\Delta MW \cdot \frac{R_{Universal} \cdot Z}{L \cdot MW^2}\right)^2} \tag{10}$$

The above Equation 10 is valid if we directly determine that the physical gas properties, specific heat ratio, compressibility factor and molecular weight are from laboratory experiments. However, if we calculate these physical properties from a given gas composition via an equation of state, we cannot consider them to be independent.

For the above case, we must modify Equation 10 by accounting for the absolute value sum of the individual uncertainty terms instead of the root-square sum for their functional dependency:

$$\Delta F = \left|\Delta u_1 \frac{\partial f}{\partial u_1}\right| + \left|\Delta u_2 \frac{\partial f}{\partial u_2}\right| + \ldots \left|\Delta u_n \frac{\partial f}{\partial u_n}\right| \tag{11}$$

This leads to a more conservative estimate of the uncertainty (Doeblin, 1966). Furthermore, it is necessary to include a physical property uncertainty, due to the effect of applying uncertainties in temperature and pressure to the non-ideal gas state equation. The measurement error in temperature and pressure adds an error in determining c_p from the gas equation. We can conveniently obtain this physical property uncertainty numerically by varying temperatures and pressures parametrically in the gas equation and, thus, determine the gradients $d\gamma/dT$, $d\gamma/dp$, dZ/dT and dZ/dp indirectly. Recognizing that $d\gamma/dT = dL/dT$ and $d\gamma/dp = dL/dp$, one can determine

corrections for ΔZ and ΔL:

$$\Delta L = \sqrt{\left(\Delta T \cdot \frac{\partial \gamma}{\partial T}\right)^2 + \left(\Delta p \cdot \frac{\partial \gamma}{partialp}\right)^2} \tag{12a}$$

$$\Delta Z = \sqrt{\left(\Delta T \cdot \frac{\partial Z}{\partial T}\right)^2 + \left(\Delta p \cdot \frac{\partial Z}{\partial p}\right)^2} \tag{12b}$$

The gas properties' variation during the test's duration also affects the uncertainty in c_p. The uncertainty in c_p is mathematically difficult to describe, but one may do so numerically using a procedure similar to the one above for the variations in temperature and pressure. It is beyond the scope of this chapter to list all possible gas composition variations. However, it is important to realize that gas composition variations can affect compressibility factor, Z, and molecular weight, MW. For example, if a simple gas mixture of 90 percent methane and 10 percent ethane has a constituency uncertainty of 1 percent, then the resulting uncertainties ΔZ, ΔL and ΔMW are 0.9 percent, 0.05 percent and 0.07 percent, respectively.

The consistent application of the gas state equations is important as for identical gas compositions one finds significant physical property differences between the commonly employed gas equations of state (SRK, BWRS and LDP). Beinecke and Luedtke (1983) noted typical differences in compressibility factor values of 0.5 percent to 1.5 percent when comparing the output from SRK, BWRS and LDP for a standard pipeline application. Thus, if one compressor manufacturer employs the SRK equation and another the BWRS gas equation, predictions for identical compressors may vary significantly. Also, if one employs the compressor measurements to verify a compression system's gas turbine performance, gas equation output deviation from actual physical values will lead to incorrect results when calculating power.

By substituting Equation 10 into Equation 5, we can determine the overall compressor discharge pressure uncertainty. However, since the compressor discharge pressure uncertainty is not dependent on the absolute temperatures, but rather on the temperature difference (T_d–T_s), and since the specific heats (c_p) for the discharge and suction are functionally related, one should employ the temperature difference (T_d–T_s) for the derivation rather than the absolute temperature values (T_d, T_s).

$$\Delta H = \sqrt{(\Delta c_p \cdot (T_d - T_s))^2 + (\Delta T_d \cdot c_{pTd})^2 + (\Delta T_s \cdot c_{pTs})^2} \tag{13}$$

Uncertainties in temperature originate from the five following sources of error:

1. location: incorrect position of the thermal sensor in the gas stream;
2. installation: wall conduction heat transfer to and from the sensor due to inadequate insulation;

3. calibration: instrument drift, non-linearities, cold junction and reference temperature errors;
4. device: inherent accuracy limitations of the sensor;
5. acquisition: amplifier, transmission, noise and analog to digital conversion errors.

One can minimize the first three errors in production or laboratory test facilities. However, for field testing minimizing these errors is more difficult. Time and cost constraints can result in the test engineer accepting field test arrangements with improperly located, installed and calibrated instruments. For example, one should employ a minimum of four circumferentially spaced pressure taps to accurately measure gas pressures behind a pipe elbow. Due to the above mentioned constraints, engineers typically employ only one tap in field testing. While it is often impossible to correct these problems during a field test, it is still important to recognize them and to advise the operator of consequential measurement accuracy limitations. The ASME PTC 10 (ASME, 1979) code specifies the required installation technique and location of temperature sensors and, thus, serves as a guideline and reference when defining field test procedures. Table 2.1 shows some typical values for the above five primary sources of temperature measurement error that one encounters during field tests.

To obtain the total temperature uncertainty, ΔT, one must add the individual uncertainties using the root-square sum method. Table 2.1 illustrates that the location,

Table 2.1. *Typical magnitudes of temperature measurement errors (K)*[1, 2].

Sensor	Location error	Installation error	Calibration error	Device error	Acquisition error
Hg thermometer	0.1 K	0.1%	0.0%	0.03%	0.10%
Thermistor	0.1 K	0.1%	0.2%	0.02%	0.05%
Thermocouple	0.1 K	0.1%	0.2%	0.01%	0.05%
RTD	0.1 K	0.1%	0.2%	0.01%	0.05%
Infrared sensor	0.3 K	0.0%	0.3%	0.05%	0.05%

[1]Aust (1988) achieved under laboratory conditions ± 0.2 K with shielded NiCrNi thermocouple probes. He mentioned deviations which depended on the flow velocity. Since the flow velocities in gas compressor nozzles are clearly subsonic, inaccuracies due to recovery factors should be negligible. One will not easily achieve the high accuracy in the field, since Aust used compensation elements which he kept in an oil bath of 0.0 ± 0.1K. This procedure is not practical in the field. In any case, he found the calibration curves given in DIN43710 to describe precisely the thermocouple behavior. In the field, a total inaccuracy of ± 0.5 K seems achievable. Cleveland (1982) shows instrument accuracies for thermometers as 0.25–1.0 K, thermocouples 0.25–1.0 K and RTDs 0.0025–2.5 K. Schmitt and Thomas (1995) report 0.5 K for RTDs. VDI 2045 (1943) assumes a tolerance of ± 1.0 K for thermocouples and RTDs.

[2]The location error is based on using two probes. One can achieve lower errors by using four circumferentially distributed probes. Higher location errors occur if one takes measurements close to elbows and other flow obstructions. Also, on the compressors' discharge side, especially of those with volutes, the flow field can have significant temperature gradients. In all these cases, four probes are necessary to maintain the location error margins of Table 2.1. As a rule of thumb, the location error decreases by a multiplier of about 11M with M as the number of probes evenly distributed in the measurement plane.

installation and calibration errors are the dominant factors, while the device and acquisition errors are a smaller contribution to the overall temperature error. Also note that field test device and acquisition errors are significantly larger than values which instrument manufacturers quote. At least in part the significantly larger measurement errors may be as a consequence of poor handling of sensitive instrumentation.

Isentropic temperature

When substituting Equation 6 for Equation 1, we can obtain the uncertainty for the isentropic compressor outlet temperature:

$$\Delta T_d^* = \sqrt{\left(\Delta T_s \cdot \left(\frac{P_d}{P_s}\right)^L\right)^2 + \left(\Delta p_d \cdot \frac{LT_s p_s^{L-1}}{p_s^L}\right)^2 + \left(\Delta p_s \cdot \frac{LT_s p_d^L}{p_s^{L+1}}\right)^2} \tag{14}$$

We can once again categorize uncertainties in pressure into the following five major error groups:

1. location: incorrect position or alignment of the pressure probe in the gas stream;
2. installation: piping vibration transmission to the pressure pick-up due to inadequate damping;
2. calibration: instrument drift, non-linearities, hysteresis and reference pressure errors;
4. device: inherent accuracy limitations of the sensor;
5. acquisition: amplifier, transmission, noise, and analog to digital conversion errors.

Again, error sources 1, 2 and 3 are significantly larger in field tests than in production or laboratory tests. Although the ASME PTC 10 code (ASME, 1979) provides clear guidelines for the correct installation and location of pressure probes, one frequently finds poorly installed and located pressure probes to be the primary sources of pressure measurement errors. Table 2.2 shows some typical values for the five sources of pressure measurement errors that we encountered during field tests.

Isentropic enthalpy

We determined the uncertainty of the compressor efficiency, η^*, by substituting Equations 7 and 8 with Equation 1. Similar to Equation 13, one should use the temperature difference rather than the absolute temperature values for the derivation of the isentropic enthalpy (Equation 15).

$$\Delta h^* = \sqrt{(\Delta c_p \cdot (T_d^* - T_s))^2 + (\Delta T_d^* \cdot c_{pTd^*})^2 + (\Delta T_s \cdot c_{pTs})^2} \tag{15}$$

Table 2.2. *Typical magnitudes of pressure measurement errors (percent full scale)* [3].

Sensor	Location[4] error	Installation error	Calibration error	Device[5] error	Acquisition error
Simple static	2.0%	0.05%	0.3%	0.1%	0.01%
2 static	1.0%	0.05%	0.3%	–	–
4 static	0.5%	0.05%	0.3%	–	–
Pitot	1.0%	0.10%	0.3%	0.1%	0.01%
Kiel	0.2%	0.10%	0.3%	0.1%	0.01%

[3]Aust (1988) achieved 0.1 percent of maximum value for a calibrated system for wall static pressures, not including location. The location should not cause an error larger than 1 percent of dynamic pressure. Boelcs and Suter (1986) show wall static error dependency on wall shear stress. Wall taps need to be exactly perpendicular and flush to the surface — no burrs or slag are acceptable. On a compressor where a cutting torch blew in the pressure taps, the resulting four pressure transducer spread was almost 2 percent of the static pressure. Preferably, a larger diameter hole should follow the wall tap (Boelcs and Suter, 1986). The ratio of dynamic to static pressure for most applications will be below 1 percent, since one should select the pipe diameters (and the compressor nozzle diameters) to avoid high flow velocities. Also, the impeller distortion reduces because the flow normally accelerates considerably between the nozzle and the impeller eye.

VDI 2045 (1993) assumes 0.2 percent of full scale for transducers and gauges. One should emphasize that one selects the instruments so that most measured values are in the upper 25 percent of full scale. Liquid columns can be more precise, but the precision depends largely on the accuracy of reading the scales.

[4]This error will depend largely on the uniformity of the flow at the measuring location.

[5]Also reported by Schmitt and Thomas (1995) and by various transmitter/instrumentation manufacturers.

Isentropic efficiency

$$\Delta\eta^* = \sqrt{\left(\frac{\Delta h^*}{H}\right)^2 + \left(\Delta H \cdot \frac{h^*}{H^2}\right)^2} \tag{16}$$

Finally, we obtained the mass flow power uncertainty by combining Equations 9 and 1 to get the following:

Mass flow:

$$\begin{aligned}\Delta \cdot W^2 = &\left(\Delta p_s \cdot \frac{MW \cdot Q}{R_{Universal} Z T_s}\right)^2 + \left(\Delta MW \cdot \frac{p_s Q}{R_{Universal} Z T_s}\right)^2 \\ &+ \left(\Delta Q \cdot \frac{p_s \cdot MW}{R_{Universal} Z T_s}\right)^2 + \left(\Delta Z \cdot \frac{p_s \cdot MW \cdot Q}{R_{Universal} Z^2 T_s^2}\right)^2 \\ &+ \left(\Delta T_s \cdot \frac{p_s \cdot MW \cdot Q}{R_{Universal} Z T_s^2}\right)^2\end{aligned} \tag{17}$$

Power:

$$\Delta P = \sqrt{\left(\Delta H \cdot \frac{W}{\eta_M}\right)^2 + \left(\Delta W \cdot \frac{H}{\eta_M}\right)^2 + \left(\Delta \eta_M \cdot \frac{H \cdot W}{\eta_M^2}\right)^2} \tag{18}$$

The flow rate uncertainty, ΔQ, depends strongly on the device type that one employs for the measurements. ASME PTC 19.1 (ASME, 1985a) provides a detailed discussion of flow measurement uncertainty, so we do not discuss this further. Table 2.3 provides some typical values of ΔQ from field testing experience.

By evaluating Equations 10 through 18, we can obtain estimates of the total measurement uncertainties for the compressor efficiency, compressor discharge pressure and required driver power. If we use a torque meter, we can measure the gas turbine power with a total uncertainty as low as 1 percent, (Schmitt and Thomas, 1995). However, one source of measurement uncertainty that engineers often overlook is the uncertainty associated with a finite sample size. The above uncertainty statistics, particularly Equation 1, are valid only for mean parameters with an assumed Gaussian normal distribution. This is a good assumption for measurements where sample sizes are larger than 30. However, for field tests it is sometimes difficult to

Table 2.3. *Typical magnitudes of volume flow rate measurement errors (percent full scale)*[6] *(values obtained with quality calibrated devices in laboratory conditions are in parentheses).*

	Measurement error	Sensitivity to location	Pressure loss
Orifice	1.5% (0.5%)	Medium to low	High
Venturi	1.5% (0.5%)	Medium	Moderate
Ultrasound	0.5% (0.2%)	Medium to high	Low
Vortex	1.0% (0.3%)	—	—
Flow meter	1.0–2.0% (0.5%)	Medium	High
Annubar	1.0–1.5% (0.5%)	Medium to low	Moderate

[6]ISO 2314 (1989) assumes 0.5 percent accuracy for orifice flow measurements. This seems to be unrealistically low for field tests. Schmitt and Thomas (1995) report an uncertainty for an orifice metering run per IS05167 of 1.4 percent. Even for pipeline applications, flow measurement error margins are 1 percent or larger (Meier and Rhea, 1982). Particularly cumbersome is the analysis if one takes the gas samples far away from the compressor or upstream of a separator or knock-out vessel (McRoberts, 1984). A properly selected and calibrated fuel flow measuring device may be suitable to achieve measurement accuracies of ±0.5 percent of the measured quantity (ISO 2314, 1989). However, we cannot always justify the additional effort to get from 1 percent accuracy to 0.5 percent accuracy when one uses the driven compressor for the power measurement. For example, with a 3 percent power measurement accuracy, the gas turbine heat rate will have a tolerance of 3.16 percent and 3.04 percent, respectively, i.e., the relative gain is only 0.1 percent in accuracy. According to Valenti's publication (1997) on the efforts at the Southwest Research Institute to evaluate gas flow measuring methods, measurement errors for an orifice's flow meters were 1 percent (mainly depending on piping configuration and the orifice's diameter ratio) and measurement errors for turbine flow meters were above 1 percent (mainly due to flow pulsations). This publication emphasises the wide flow range and the very low pressure losses of ultrasonic flow meters. Ongoing research is trying to quantify the sensibility of this device to the flow profile's distortions

maintain a steady-state system operating condition for a time period long enough to collect 30 or more samples.

For small sample sizes it is more appropriate to assume a Student t-distribution instead of a Gaussian normal. Thus, one should introduce an additional uncertainty due to a finite number of samples into the total performance parameter uncertainty. We quantify this uncertainty by conservatively assuming that all individual uncertainty bands are within their 95 percent confidence intervals and then determining the percent difference between Gaussian and Student t-distribution limits. Table 2.4 shows some typical values of the added uncertainty that are associated with a limited number of samples for the compressor discharge pressure, efficiency and power. Note that the values in Table 2.4 are dependent on inlet and outlet temperatures, inlet and outlet pressures and gas composition. One should add the limited sample size uncertainty to the total parameter uncertainty using the root-square sum method.

Turbocompressor package uncertainty

To complete the above field test measurement uncertainty evaluation one also needs to consider the combined compression system gas turbine and centrifugal compressor efficiency. The gas turbine shaft output power has to equal the compressor required power ($P_{GT} = P$). Thus, we can use the following two equations to define the gas turbine thermal efficiency, η_{TH}, and the total package efficiency, η_P:

Thermal efficiency:

$$\eta_{TH} = \frac{P}{W_{fuel} \cdot q} \tag{19}$$

Package efficiency:

$$\eta_p = \eta^* \cdot \eta_M \cdot \eta_{TH} \tag{20}$$

Table 2.4. *Parameter uncertainty due to limited sample size (percent).*

Number of samples	Head uncertainty	Efficiency uncertainty	Power uncertainty
20	0.043%	0.058%	0.082%
22	0.038%	0.052%	0.072%
24	0.033%	0.046%	0.062%
26	0.028%	0.040%	0.052%
28	0.023%	0.034%	0.042%
30	0.018%	0.028%	0.032%

Here W_{fuel} is the fuel flow into the gas turbine and q is the fuel heating value. Engineers typically measure the fuel flow using an orifice plate in a metering run and they determine the heating value from the fuel's chemical composition (often one uses the centrifugal compressor discharge gas as the fuel gas). Based on the above equations, the corresponding gas turbine uncertainty, η_{TH}, and package uncertainty, η_P, are given by:

Thermal efficiency:

$$\Delta\eta_{TH} = \sqrt{\left(\Delta P \frac{1}{w_{fuel} q}\right)^2 + \left(\Delta W_{fuel} \frac{p}{w_{fuel}^2 q}\right)^2 + \left(\Delta q \frac{P}{W_{fuel} q^2}\right)^2} \tag{21}$$

Package efficiency:

$$\Delta\eta_p = \sqrt{(\Delta\eta * \eta_M \eta_{TH})^2 + (\Delta\eta_M \eta * \eta_{TH})^2 + (\Delta\eta_{TH} \eta_M \eta^*)^2} \tag{22}$$

To complete the above Equations 21 and 22, the only additional information that we need is the fuel flow uncertainty and the fuel heating value uncertainty. Since we measure the fuel flow in the same way as the flow through the gas compressor, we can use uncertainty values in Table 2.3. Also, since we obtain the heating value directly from gas composition, we can use approximately the same percent uncertainty that we obtained for the specific heat (Equation 10), namely:

$$\frac{\Delta q}{q} = \frac{\Delta c_p}{c_p} \tag{23}$$

By introducing the uncertainty experience values from Tables 2.1 through 2.4 into Equations 10 through 23, we can predict the measurement uncertainty for a field test prior to the test. Consequently, the above method allows the gas turbine manufacturers, compressor manufacturers and compression system operators to determine reasonable test uncertainties as well as necessary requirements for the test instrumentation prior to the test. One can also employ the above method to resolve observed variations of field test performance results from theoretically predicted or factory test results.

Uncertainty calculation examples and comparisons to field test results

The two examples below illustrate how one obtains the total measurement uncertainty for actual field tests. Examples 1 and 2 present comparisons to factory test results. Figure 2.2 shows a typical gas turbine driven compressor during a field performance test.

FIGURE 2.2. Typical gas turbine driven compressor during a field performance test.

Example 1

During a multistage compression system gas turbine and centrifugal compressor field test, we encountered the following conditions:

Compressor application: gas reinjection

Instrumentation: single RTD and single pressure tap on each suction and discharge; orifice flow meter for compressor flow and turbine flow meter for gas turbine fuel flow

Test conditions: p_s = 65 Bar, p_d = 226 Bar, T_s = 303 K, T_d = 448.5 K (η^* = 62.0 percent), Q = 18.4 meters cubed per minute

Gas composition: fluctuating by 5 percent in constituency composition; during test 93.1 percent methane, 5.8 percent ethane, 0.4 percent propane, 0.15 percent i-butane, 0.25 percent n-butane, 0.3 percent nitrogen

We predicted the compressor field test uncertainty by evaluating Equations 10 through 23 with assumed measurement uncertainties as Tables 2.1 through 2.3 suggest ($\Delta t_{s,d}$ = 0.4l K, $\Delta p_{1,2}$ =2.31 percent, ΔQ = 1.5 percent, η_M = 0.1 percent). We accounted for the influence of the gas constituency fluctuation on the total uncertainty by using the method in Equation 12, which yields ΔZ = 0.68 percent, γ = 0.72 percent and ΔMW = 0.08 percent for this case. From the resulting absolute uncertainty values for the specific heat, the actual compressor discharge pressure, the isentropic efficiency and the required power (Δc_p, ΔH_A, $\Delta\eta_I$, ΔW), we determined the percent total field test uncertainties, namely: $\Delta c_p/c_p$ = 2.46 percent, $\Delta H/H$ = 2.49 percent, $\Delta\eta^*$ = 3.24 percent and $\Delta P/P$ = 3.79 percent.

Thus, we see total efficiency uncertainty of above 3 percent for this set of field test measurements. The primary reason for this large uncertainty is the inadequate number of installed pressure taps at the centrifugal compressor's suction and discharge. Increasing the number of pressure taps from one to four at the suction and discharge would reduce the predicted compressor efficiency and power uncertainties to $\Delta\eta^*/\eta = 1.84$ percent, $\Delta P/P = 1.95$ percent, respectively, a significant improvement. For the above example, we performed a factory closed loop test on the centrifugal compressor in which we achieved an efficiency of 64.1 percent for a similar operating point. Accounting for the test uncertainty range, the efficiency which we measured during the field test (62 percent) confirms the factory test results.

Example 2

During a field test on a gas turbine driving a single-stage pipeline compressor, we encountered the following compression conditions:

Compressor application: pipeline

Instrumentation: four thermocouples and four pressure taps on each suction and discharge; annular flow meters for the compressor flow; orifice flow meters for gas turbine fuel flow

Test conditions: $p_s = 45.36$ Bar, $p_d = 55.1$ Bar, $T_s = 25.8°C$, $T_d = 41.9°C$ ($\eta^* = 88.1$ percent), $Q = 6.64$ meters cubed per second, $W_{fuel} = 0.47$kg/s, $\eta_{TH} = 29.6$ percent, $\eta_p = 26.0$ percent

Gas composition: 96.1 percent methane, 1.8 percent ethane, 0.3 percent propane, 0.3 percent i-butane, 0.1 percent n-butane, 0.6 percent carbon dioxide, 0.8 percent nitrogen

As a comparison, when applying the above test conditions to Equations 10 through 23 and assuming measurement uncertainties as Tables 2.1 through 2.3 show ($\Delta T_{s,d} = 0.3$ K, $\Delta p_{s,d} = 0.5$ percent, $\Delta Q = 1.5$ percent, $\Delta\eta_M = 0.1$ percent), we obtained the following percent uncertainties: $\Delta c_p/c_p = 2.40$ percent, $\Delta H/H = 3.6$ percent, $\Delta\eta^* = 5.5$ percent and $\Delta P/P = 4.0$ percent. Similarly, evaluating Equations 21 and 23 for the overall compression system and gas turbine total uncertainties with $\Delta Q_{fuel} = 1.0$ percent yields $\Delta\eta_{TH} = 4.5$ percent and $\Delta\eta^*_p = 4.3$ percent, respectively.

Note that despite a generally higher accuracy than in the first example, the uncertainties for Example 2 are higher. This is typical for applications with low pressure ratios, which are sensitive to uncertainty in measured pressure. Also note that an improvement of the flow uncertainties would increase the overall accuracy only marginally.

In Example 2, the accuracy for the power measurement is higher than the accuracy for the efficiency measurement. This is because the uncertainties for the actual compressor discharge pressure H are lower than for the isentropic compressor dis-

charge pressure H^*. Because the isentropic compressor discharge pressure calculation requires the isentropic discharge temperature T_d^* (Equation 14), the associated uncertainties for T_d^* are usually higher than the uncertainties for the directly measured T_d. Thus, we can evaluate the power more accurately than the efficiency in many cases, as long as the flow measurement accuracy is sufficiently high.

As in the previous example, one should remember that the theoretical uncertainties as determined from Equations 10 through 23 yield results for the total possible performance parameter uncertainty range which is a conservative estimate, while the deviation is just a comparison between two different measurements. Thus, one would anticipate the significantly larger theoretical uncertainty values.

Overall, the uncertainty equations predict measurement fluctuations well. However, the general experience with this method is that the uncertainty method conservatively over predicts errors by a small margin.

Parametric studies and trends

We undertook a number of parametric studies to determine the effect of varying individual measurement variables on the total performance uncertainty. These studies also help to identify parameters which have the most significant effect on the total uncertainty. Hence, we can evaluate the effect of varying a number of field test measurement parameters on the efficiency and power uncertainty. We used the compressor operating conditions presented in Example 1 as a basis for the studies below.

Figures 2.3 and 2.4 show the results of varying the compressor discharge pressure and suction temperature while keeping all other conditions, including isentropic efficiency, constant on the efficiency and power uncertainty. As the compressor discharge pressure increases, the efficiency and power uncertainties decrease. The uncertainty rate of decrease is a direct function of the increasing compressor discharge pressure. Also, the uncertainties are lower for increased compressor suction temperatures. Both of these results are expected and we can explain them as follows: the larger the pressure or temperature suction-discharge differential, the smaller the relative influence of the individual measurement errors on the total performance uncertainties.

A limitation of the results presented in Figures 2.3 and 2.4 is that they do not provide any insight into which uncertainty most significantly affects the overall performance parameter uncertainties. Thus, we derived Tables 2.5 and 2.6 to provide a quantitative comparison of the individual measurement uncertainties' effects on the compressor isentropic efficiency uncertainty. For the above parametric studies we varied only one measurement uncertainty parameter while leaving all others at the values which Example 1 above describes.

Results in Table 2.5 show that the influence of the suction and discharge pressure uncertainties on the total isentropic efficiency uncertainty is identical. This is consistent with Equation 16. The influence on the isentropic enthalpy and efficiency uncertainty due to the gas composition uncertainty is negligible when we compare it to the influence due to the compressor discharge pressure uncertainty. Table 2.6

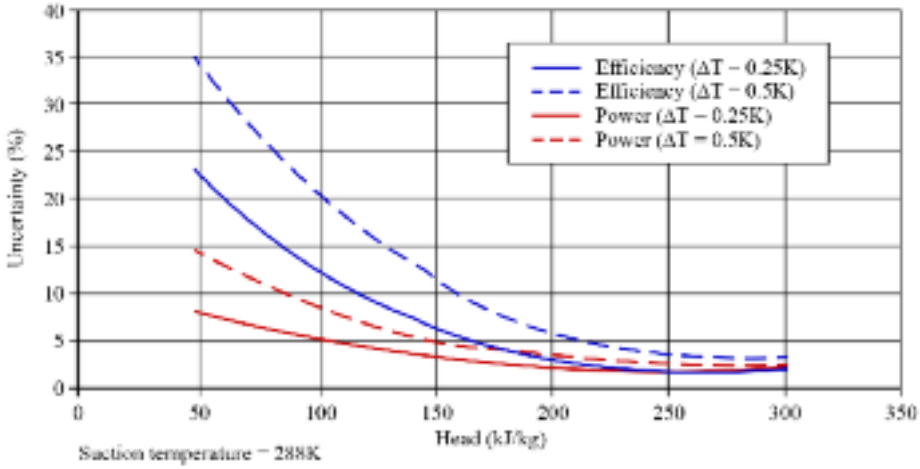

FIGURE 2.3. Power and efficiency uncertainty versus compressor discharge pressure (head) at 288 K.

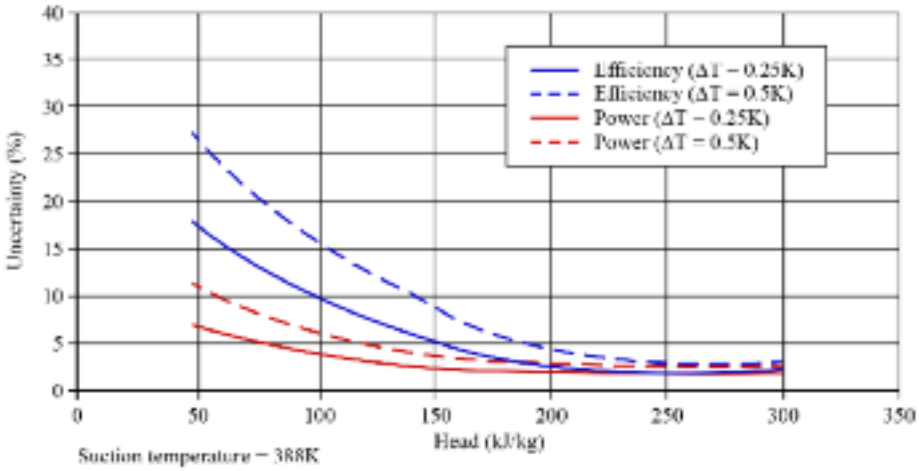

FIGURE 2.4. Power and efficiency uncertainty versus compressor discharge pressure (head) at 388 K.

shows that the suction temperature uncertainty has a stronger influence on the total isentropic efficiency uncertainty than the discharge temperature uncertainty, a trend that is more pronounced at higher temperature uncertainty levels.

Similarly, Tables 2.7 and 2.8 show a quantitative comparison of the individual measurement uncertainties' effects on the compressor's required power uncertainty. Again, for this study, we varied only one measurement uncertainty parameter while leaving all others at the values utilized in Example 1.

Table 2.5. *Compressor isentropic efficiency uncertainties (percent).*

Error, %	Δp_s uncertainty	Δp_d uncertainty
1.0%	2.95%	2.95%
2.0%	3.15%	3.15%
3.0%	3.46%	3.46%
4.0%	3.86%	3.86%

Table 2.6. *Compressor isentropic efficiency uncertainties (percent).*

Error	ΔT_s uncertainty	ΔT_d uncertainty
0.25 K	3.21%	3.23%
0.50 K	3.27%	3.25%
1.00 K	3.46%	3.30%
2.00 K	4.12%	3.46%
4.00 K	6.04%	4.00%

Table 2.7. *Compressor required power uncertainties (percent).*

Error	Δp_s uncertainty	Δp_d uncertainty	ΔQ uncertainty
1.0%	3.17%	3.79%	3.62%
2.0%	3.61%	3.79%	4.02%
3.0%	4.25%	3.79%	4.60%
4.0%	5.00%	3.79%	5.30%

Table 2.8. *Compressor required power uncertainties (percent).*

Error	ΔT_s uncertainty	ΔT_d uncertainty
0.25 K	3.77%	3.77%
0.50 K	3.81%	3.81%
1.00 K	3.90%	3.90%
2.00 K	4.22%	4.17%
4.00 K	5.20%	5.02%

Table 2.7 shows that the power uncertainty is strongly affected by the suction pressure uncertainty, but not at all affected by the discharge pressure. Equations 17 and 18 characterise the pressure influence on the power uncertainty, but only include the suction and not the discharge pressure. Also, Table 2.8 shows that the power uncertainty was almost identically affected by the suction and discharge temperature uncertainty. Only at higher temperature uncertainty levels does the influence of the suction temperature uncertainty become more pronounced. The reason for the trend

in Table 2.8 is that the required power uncertainty is primarily dependent on the temperature difference that in turn is a consequence of the equal influence of T_s and T_d in Equation 13 and not on the absolute temperature values. The power uncertainty deviation at higher temperature uncertainty levels is because the suction temperature also affects the power uncertainty through the mass flow Equation 17.

The results in Tables 2.5 through 2.8 illustrate that temperature and flow rate measurement uncertainties have a stronger effect on the overall performance uncertainties than the pressure measurement uncertainties. However, due to the added complexity of pressure measurements, the field test pressure measurement uncertainties are often significantly larger than temperature measurement uncertainties and, thus, we should not discount pressure measurement uncertainties.

SUMMARY

We derived the equations governing centrifugal compressor and gas turbine performance uncertainties and numerically compared the results of two actual field tests. We presented typical field test measurement uncertainties for different sets of instrumentation and sensors. By introducing the uncertainty experience values into the uncertainty equations, one can predict the performance measurement uncertainty for a field test prior to the test. This allows the gas turbine manufacturer, centrifugal compressor manufacturer and compression system operator to agree on an allowable performance range rather than setting a single guarantee point. One can also employ the above method to resolve observed variations between field test, theoretically predicted or factory test results.

The chapter includes a number of parametric studies which characterize uncertainty trends. We identified test parameters that have the most significant influence on uncertainty and provided suggestions on how to minimize their measurement errors. Results showed that compressor efficiency uncertainties can be unacceptably high. However, by following some basic measurement rules and maintaining commonality of the gas equations of state, the overall compression system performance measurement uncertainty can be minimized and one can achieve results accurate enough to consider meaningful.

REFERENCES

ASME PTC 10 (1979), “Compressors and Exhausters”.

ASME PTC 19.1 (1985a), “Measurement Uncertainties”.

ASME PTC 22 (1985b), “Gas Turbine Power Plants”.

Aust, N. (1988), “Ein Verfahren zur Digitalen Simulation Instationarer Vorgange in Verdichteranlagen”, Ph.D. Thesis, University of the Federal Armed Forces, Hamburg, Germany.

Beinecke, D., and Luedtke, K. (1983), "Die Auslegung von Turboverdichtem unter Berucksichtigung des Realen Gasverhaltens", VDI Berichte Number 487, pp. 271–9.

Boelcs, A., and Suter, P. (1986), *Transsonische Turbomaschinen*, G. Braun, Karlsruhe, Germany.

Brun, K. (1996), "Analysis of the Automotive Torque Converter Internal Flow Field", Ph.D. Thesis, University of Virginia, USA.

Cleveland, A. (1982), "Performance Testing of Gas Turbine Compressor Sets", *Proceedings of the 27th American Society of Mechanical Engineers Gas Turbine and Aeroengine Congress*, London, England, 18–22 March, Paper No. 82-GT-199.

Doeblin, E.O. (1966), *Measurement Systems*, McGraw-Hill, New York, USA.

Fozi, A.A. (1995), "Field Testing of Compressor Packages", Solar Turbomachinery Technology Seminar, Paper No. 98.

ISO 2314 (1989), "Gas Turbines-Acceptance Tests", Geneva, Switzerland.

Klein, J.M., and Draughton, P.A. (1991), "Field Performance Testing of an Uprated Gas Reinjection Compressor/Turbine Train", *Proceedings of the 36th American Society of Mechanical Engineers Gas Turbine and Aeroengine Congress*, Orlando, USA, 3–6 June, Paper No. 91-GT-48.

McRoberts, I.W. (1984), "Performance Trials of Two Centrifugal Compressor Trains on an Offshore Platform", *Proceedings of the Second European Congress on Fluid Machinery for the Oil, Petrochemical and Related Industries*, The Hague, Netherlands, 18–20 May, Paper Number C48/84, pp. 139–48.

Meier, R.H., and Rhea, C.S. (1982), "Centrifugal Compressor Testing Experience and Practice", *Proceedings of the 27th American Society of Mechanical Engineers Gas Turbine and Aeroengine Congress*, London, England, 18–22 March, Paper No. 82-GT-320.

Scarborough, J.B. (1955), "Numerical Mathematical Analysis", Johns Hopkins University, Baltimore, USA.

Schmitt, W., and Thomas, V. (1995), "Comparison of Test Measurements Taken on a Pipeline Compressor/Gas Turbine Unit in the Workshop and at Site", *Proceedings of the 40th American Society of Mechanical Engineers Gas Turbine and Aeroengine Congress,* Houston, USA, 5–8 June, Paper No. 95-GT-125.

Valenti, M. (1997), "Determining Gas Meter Accuracy", *Mechanical Engineering,* vol. 3, no. 119, pp. 102–6.

VDI 2048 (1978), "Inaccuracies in Acceptance Test Measurements", Düsseldorf, Germany.

VDI 2045 (1993), "Acceptance and Performance Tests on Turbo Compressors and Displacement Compressors", Düsseldorf, Germany.

Chapter 3

Surge Avoidance in Gas Compression Systems

R. Kurz and R.C. White

ABSTRACT

Academics and practitioners alike have studied extensively the physics of compressor surge and how we may prevent it. The majority of those studies available in the literature focus on the compressor itself. However, the overall compression system design influences a compressor's stability, specifically the compressor's upstream and downstream piping. The compressor's upstream and downstream piping design is particularly important during an unplanned compression system emergency shutdown. During normal operation it is relatively easy to design an effective anti-surge system. In an unplanned emergency shutdown the anti-surge system's effectiveness is dependent on the compression system layout generally, and the upstream and downstream compressor piping specifically. This chapter presents data from a compressor that surged during an emergency shutdown with an analysis of the data to determine the effects of surge. We have developed and used a model to simulate shutdown events to define rules that provide design engineers with a method to correctly size compression systems' upstream and downstream piping systems.

This chapter is a revised and extended version of Kurz, R., and White, R.C. (2004), "Surge Avoidance in Gas Compression Systems", *Transactions of the ASME, Journal of Turbomachinery*, vol. 126, pp. 501–6.

NOMENCLATURE

A	flow area
c_v	flow coefficient
C	compressible valve coefficient
F_p	piping geometry factor
h	head
H_{cooler}	gas cooler heat transfer (W)
J	inertia
k	isentropic exponent
k	constant
K_v	valve coefficient
L	pipe length
N	speed (Hz)
p	pressure
Q	volumetric flow
R	gas constant
SG	specific gravity
SM	surge margin (percent)
T	temperature
t	time
V	volume
Y	coefficient
Z	compressibility factor
α, β, γ	constants

Subscripts

avail	available
compr	compressor
op	operating point
surge	at surge
std	at standard conditions
ss	steady state
v	valve
0	condition at time of an emergency shutdown
1	compressor inlet
2	compressor discharge

INTRODUCTION

One may increase a compressor's stability by active means (Epstein *et al*., 1994; Blanchini *et al*., 2002), passive means (Arnulfi *et al*., 2000) or by increasing the accuracy with which the surge margin is determined (McKee and Deffenbaugh, 2003). A fourth option for increasing compressor stability is through a better under-

standing of the interaction between the compressor, anti-surge devices and the compression system piping layout linking coolers, scrubbers and check valves. The study in this chapter focuses on compression systems that incorporate two-shaft gas turbines. Available space (Figure 3.1) can constrain piping that occurs with compression systems that incorporate two-shaft gas turbines. This results in a complex piping system.

The compressor's maximum and minimum operating speed, maximum available power, choke flow and stability limit (Figure 3.2) limit a centrifugal compressor's operating point. When a compressor reaches its stability limit it surges, a phenomenon where flow reverses within the compressor which results in a significant increase in the aerodynamic loads on compressor blades which then results in a significant increase in fluctuating mechanical loads on compressor blades and bearings. Compressors are classically fitted with "anti-surge control" systems that comprise a recycle loop that activates in the event of compressor surge by opening a fast acting "anti-surge valve". The compressor control system calculates the compressor's operating point on its performance map using real-time measurements of compressor suction pressure, discharge pressure and temperature in combination with inlet flow rate measurements into the compressor. Calculating the compressor operating point on its performance map enables us to determine "surge margin", which is the relative distance of the compressor operating point to the predicted or measured compressor surge line (Figure 3.2). We define the surge margin by:

$$SM = \left. \frac{Q_{op} - Q_{surge}}{Q_{op}} \right|_{N=const} \tag{1}$$

Engineers classically program compressor control systems to react as a compressor approaches surge. If a compressor's surge margin falls below 10 percent, typically it triggers an alarm, and at 5 percent the control system would open the anti-surge valve. Opening the anti-surge valve reduces the compressor's pressure ratio and increases the flow through the compressor. Reducing pressure and increasing flow moves the compressor's operating point away from its surge line and protects the compressor from the detrimental effects that occur with a surge.

During normal operation a compressor classically approaches its stability limit relatively slowly, allowing the control system and associated anti-surge valve time to react before the compressor actually surges. However, an emergency shutdown cuts the compression system's gas turbine fuel supply. This results in the power turbine and compressor coasting down under their own inertia. Some installations maintain fuel flow to the turbine for between 1 and 2 seconds while the anti-surge valve opens. However, engineers do not favor this practice because it is a safety hazard.

A compressor's pressure developing capability reduces with the square of speed, and thus if compressor speed falls by half its pressure developing capability falls by three-quarters. The conditions within the upstream and downstream piping fix the pressure ratio across the compressor. Consequently, as compressor speed reduces during an emergency shutdown, the compressor will surge if the anti-surge

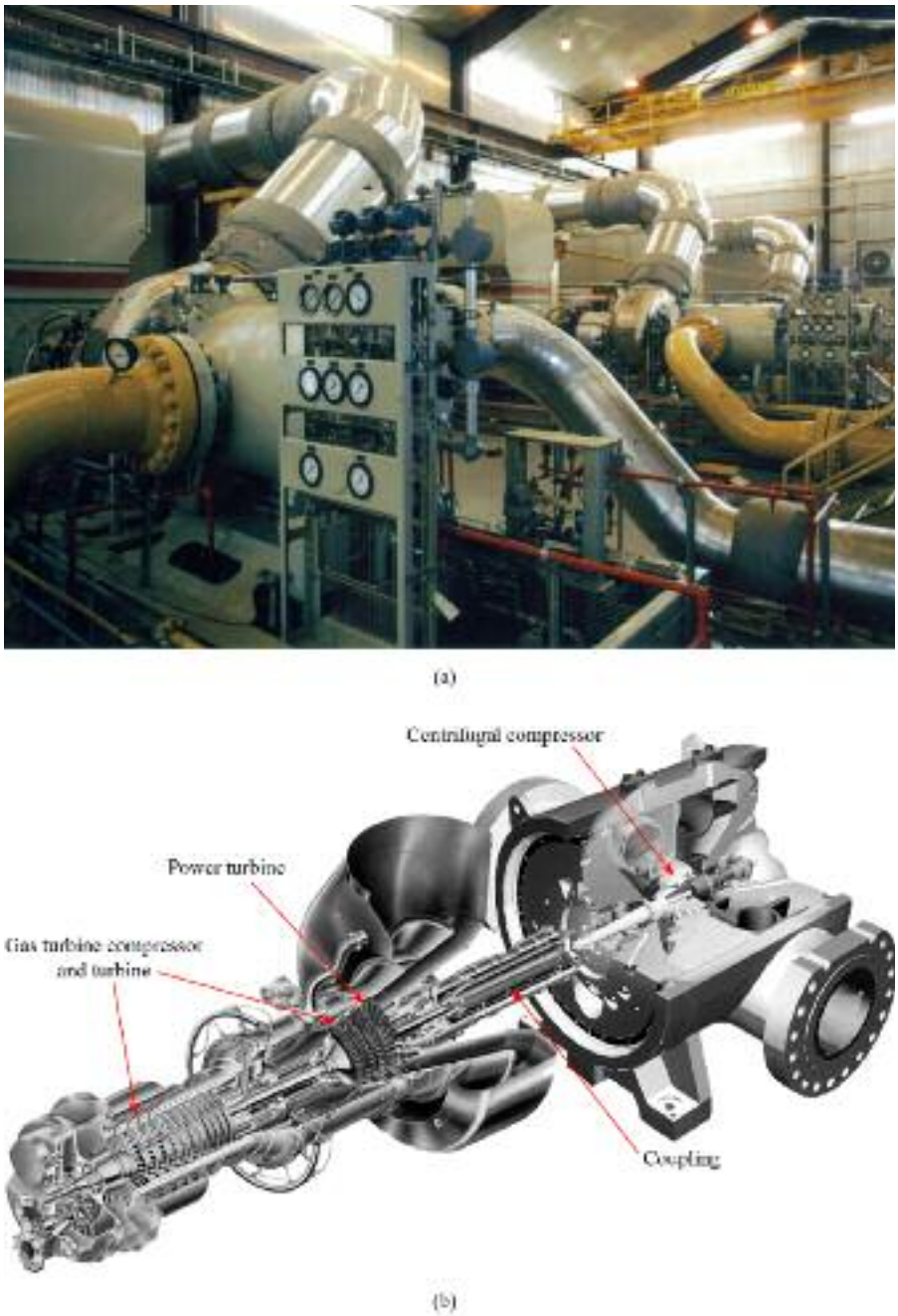

FIGURE 3.1. Gas turbine driven compressor based compression systems (a) as installed and (b) in section illustrating the gas turbine's compressor, turbine, power turbine, coupling and centrifugal compressor.

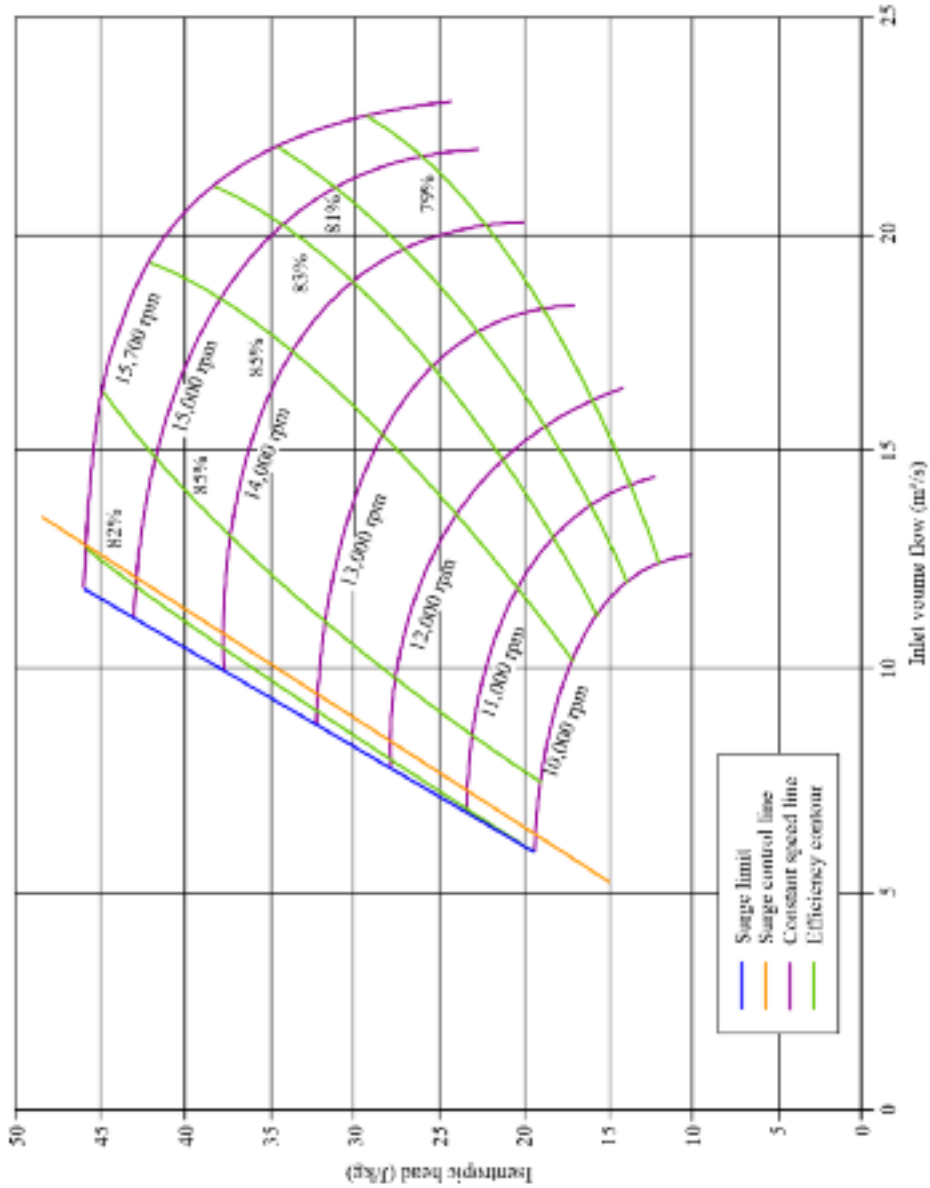

FIGURE 3.2. Typical compressor performance map.

valve does not open. The speed at which an anti-surge system can reduce the pressure across a compressor depends on the anti-surge valve's reaction time plus the upstream and downstream piping time constants. The transient behavior of upstream and downstream compressor piping depends on the enclosed gas volumes within the components and the piping system. The downstream system boundary which we adopted in the study is the first downstream check valve. The upstream boundary is either a check valve or an infinite constant pressure plenum (Figure 3.3). These upstream and downstream system boundaries result in modeling a sufficient proportion of the piping to enable one to calculate the compressor's transient behavior for a defined arrangement of upstream and downstream piping.

The control system requirements for an anti-surge system during an emergency shutdown are different from the requirements during normal operation. During an

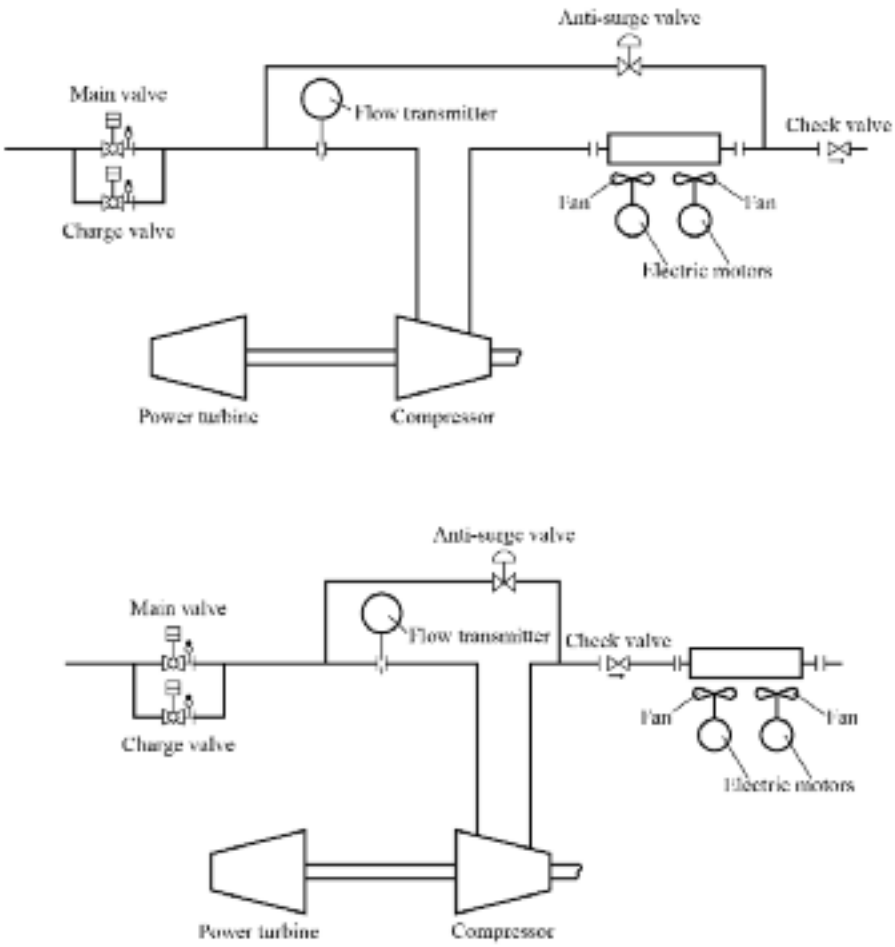

FIGURE 3.3. Anti-surge and recycle system: (top) cooled recycle, (bottom) hot recycle.

emergency shutdown a compressor's operating point approaches its stability limit quickly. Consequently, the anti-surge system requires an anti-surge valve with both a fast opening time and a large flow area. In contrast, during normal operation an anti-surge system is required to precisely control anti-surge valve position to avoid introducing oscillations into the gas flowing through the piping.

SURGE PHENOMENON

Wachter and Rohne (1984) have explained a centrifugal compressor's characteristics during surge (Figure 3.4). As the compressor approaches its stability limit, the compressor's ability to generate pressure reduces with further flow reductions. At the stability limit the flow through the compressor reverses and gas now flows from discharge to suction side. Once the flow through the compressor reverses, the flow rate is dependent on the compressor's pressure ratio as the compressor now has a characteristic that engineers usually associate with an orifice plate. The pressure ratio across the compressor can rise quickly as the flow reversal through the compressor results in the pressure downstream of the compressor falling quickly.

The pressure reduction speed depends primarily on the volume downstream of the compressor. Once the pressure reduces below a critical limit, the compressor will

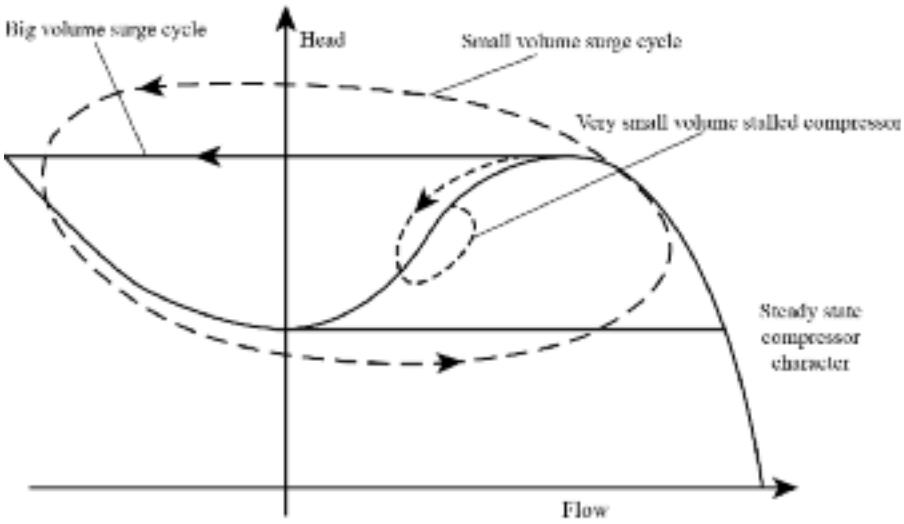

FIGURE 3.4. Simplified surge cycle (Wachter and Rohne, 1984).

recover and gas will once again flow from the suction to the discharge side. As the compressor operating point remains beyond its stability limit, the compressor will surge again. Ongoing surge can damage thrust bearings as a consequence of the thrust loads' changing magnitude and direction. Seals are also prone to damage, and if allowed to continue long enough the compressor will suffer a mechanical failure (Ribi and Gyarmathy, 1997).

MODELING THE PIPING SURGE CONTROL INTERACTION

Compression system piping and valve design, together with instrumentation selection and placement, significantly affects an anti-surge control system's performance. Control system performance is a major consideration for engineers during the design of compression systems. Changing any aspect of the recycle system piping layout or its associated instrumentation once a compression system is operational is difficult. A recycle system's generic configuration incorporates a flow-measuring element on the compressor suction side, pressure and temperature measurements at both compressor suction and discharge. Additionally, the recycle system includes an after-cooler, a discharge check valve and a recycle line with a control valve connected upstream of the discharge check valve and compressor flow-measuring device.

The discharge check valve, compressor and anti-surge valve establish boundaries for gas volume on the discharge side. The volume on the suction side is typically orders of magnitude larger than the discharge volume and, therefore, we regard it as infinite. When modeling the discharge it is therefore reasonable to assume that suction pressure remains constant. When modeling a compressor's surge control system, the worst case is an emergency shutdown for a compressor already operating close to its stability limit. As the compressor decelerates, its pressure developing capacity falls with the square of speed and consequently, the anti-surge valve must be able to relieve about half of the flow through the compressor for a one-third reduction in compressor speed.

The larger the volumes upstream and downstream of the compression system, the longer it will take for pressure across the compressor to equalize. The larger the anti-surge valve, the higher the flow rate through it when open, and consequently, the higher its potential to avoid surge. However, the larger the anti-surge valve the higher its inertia, and consequently, the slower its opening time. The faster an anti-surge valve can open, the more quickly flow can start to pass through it. Irrespective of anti-surge valve size there is a limit to the speed with which it can open.

Both the need to control the valve in intermediate positions and the physical limits on the actuator's size in practical applications affect the anti-surge valve actuation's design. A way to compensate for the effect of an anti-surge valve that cannot protect the compressor in the event of an emergency shutdown induced surge is to include a "hot gas bypass" (Figure 3.3). A hot gas bypass short-circuits the recycle loop and allows the compressor discharge to feed directly back into the compressor inlet.

Engineers can predict the pressure in the compression system piping if they calculate the downstream volume and assume that the suction side pressure will remain constant. The gas turbine and compressor decelerate together. They are linked and must reduce at the same rate. We may calculate compressor power consumption for a series of steady-state operating points. During an emergency shutdown the discharge pressure will dictate the operating points which then dictate the pressure across the compressor if we assume that the suction side pressure is to remain constant. The pressure across the compressor determines the flow through the compressor at a specific speed.

In a compression system during an emergency shutdown, it is important to maintain mass and momentum balance (Sentz, 1980; Wachter and Rohne, 1984). We may characterize the anti-surge valve flow as a function of the pressure differential across the anti-surge valve, with p_v the pressure just upstream of the valve:

$$Q_v = \sqrt{\frac{1}{K_v}(p_v - p_1)} \tag{2}$$

unless the flow across the valve is choked, thus:

$$Q_v = C\sqrt{\frac{p_v}{p_v}} \tag{3}$$

while mass and energy balance yield:

$$\frac{dp_v}{dt} = \frac{k}{V}\left[p_2 Q - p_v Q_v - \frac{k-1}{k} H_{cooler}\right] \tag{4}$$

and the momentum balance:

$$\frac{d(p_2 Q)}{dt} = \frac{p_2 - p_v}{L}\left[ART_2 - \frac{p_2 Q^2}{AP_v}\right] \tag{5}$$

where p_2 is a function of the compressor operating point, expressed by:

$$\frac{p_2}{p_1} = \left[1 + \frac{k-1}{k} \cdot \frac{h(Q,N) \cdot SG}{287 \cdot ZT_1}\right]^{k/k-1} \quad \frac{h}{N^2} = \alpha\left(\frac{Q}{N}\right)^2 + \beta\frac{Q}{N} + \gamma \tag{6}$$

We can use the above relationship for positive flow through the compressor. If flow through the compressor reverses, we cannot characterize the compressor as an orifice plate and hence:

$$Q = -\sqrt{\frac{1}{K_{v,compr}}(p_2 - p_1)} \tag{7}$$

where $K_{v,comp}$ is the compressor's flow resistance against the reverse flow. Although crude, this formulation is acceptable for the present study as it primarily focuses on establishing if a compressor will surge during an emergency shutdown. The study does not focus on accurately predicting reverse flow through the compressor during a surge. Therefore, the ability to predict post-surge reverse flow is not important, but we introduce it only to ensure that their numerical model remains stable.

When considering compressor speed during an emergency shutdown we must consider the inertia (J) of the power turbine, coupling, compressor rotating system and, when applicable, the gearbox. The rotating system has a torque (T) acting upon it that the fluid induces within the compressor. Assuming that we may neglect mechanical losses, a balance of forces gives:

$$T = -2\pi \cdot J \cdot \frac{dN}{dt} \tag{8}$$

Knowing the system's inertia and measuring the speed variation with time during rundown yields the torque and, thus, the power transferred to the gas:

$$P = T \cdot N \cdot 2\pi = -(2\pi)^2 \cdot J \cdot N \cdot \frac{dN}{dt} \tag{9}$$

Assuming an empirically derived proportionality factor (k) and accepting that power is proportional to speed cubed then:

$$\frac{dN}{dt} = \frac{k}{J}\frac{N^2}{(2\pi)^2} \rightarrow \int N^{-2} dN = \frac{k}{J(2\pi)^2}\int dt + c \rightarrow N(t) = -\frac{1}{-\frac{k}{J(2\pi)^2}t - \frac{1}{N_{t=0}}} \tag{10}$$

The proportionality factors (k) for power and speed are approximately constant irrespective of where the compressor's operating point is on its performance map when an emergency shutdown commences. Therefore, the deceleration rate is independent of the operating point and consequently, the time constant *dN/dt (t = 0)* for an emergency shutdown is proportional to *k/J*.

We may make some simplifying assumptions as a consequence of the model's intended application. Relatively short lengths of piping volumes will be smaller and consequently, the pressure at the anti-surge valve and compressor discharge will be approximately the same. Therefore, we may express the compressor discharge pressure's rate of change with time as:

$$\frac{dp_2}{dt} = \frac{k \cdot p_2}{V}[Q - Q_v] \tag{11}$$

Change in discharge pressure is therefore dependent on the capability of the anti-surge valve's ability to discharge flow at a higher rate than the compressor.

We may simplify the above-mentioned model further to assist the design engineer to determine if a combination of discharge volume and valve size can prevent the compressor from surging during an emergency shutdown. The design engineer can vary surge valve size and opening speed for a given discharge volume. Alternatively, the design engineer can limit the maximum discharge volume for a given anti-surge valve configuration. In practice, design engineers typically work within the limits of available anti-surge valves. For a given anti-surge valve it makes sense to reduce discharge volume until the anti-surge valve is able to relieve pressure quickly enough for the compressor to remain stable during an emergency shutdown.

In practical applications a design engineer can use the model to calculate the maximum discharge volume where the pressure across the compressor reduces by half in 1 second. A consequence of the assumed decay rate is that it eliminates the need to calculate instant compressor speed. The assumed pressure decay rate implies that the compression system power turbine and compressor lose approximately a quarter of their speed in the first second of deceleration. Bakken *et al*. (2002) observed that gas turbine driven compression systems lose between 20 and 25 percent of their speed in the first second after an emergency shutdown, while the electric motor driven compression systems lose approximately 30 percent of their speed in the first second. A 25 percent loss of speed reduces a compressor's pressure developing capability by 56 percent, if we assume that the fan laws apply.

The compression system's control system always initiates an emergency shutdown. There are delays that occur with the gas turbine's fuel valve closing and exhaustion of hot pressurized gas to the gas turbine's power turbine. In-service experience indicates that these delays are approximately the same as the anti-surge valve opening time, and consequently, a compressor's deceleration commences simultaneously with the anti-surge valve reaching its fully open position. We assume that the starting time (T_0) for the model is the time when the compressor's deceleration commences, at which time we also assume that the anti-surge valve is fully open.

The suction volume is typically more than three orders of magnitude larger than the discharge volume and, therefore, we assume that it remains at a constant pressure during an emergency shutdown. The model considers only the mass flow into the downstream piping volume from the compressor and the mass flow leaving this volume through the anti-surge valve. The gas mass in the piping volume determines the gas density and, therefore, the pressure. Knowing the downstream pressure, one may calculate the required pressure rise across the compressor, and if that pressure rise exceeds the maximum, the compressor is always capable of generating a greater pressure rise than is required to avoid surge.

We can conceptually simplify the model further by splitting the anti-surge valve's (c_v) flow coefficient into a part that is necessary to release the flow at the

compressor's steady-state operating point ($c_{v,ss}$) and a part that is actually available to reduce the pressure in the piping volume ($c_{v,avail}$). We associate a pressure drop coefficient with the anti-surge valve. The flow through the anti-surge valve is necessary to maintain the known steady-state operation $c_{v,ss}$. We also know the valve's c_v rating. Thus, we may determine the flow coefficient that can reduce the discharge pressure:

$$c_{v,avail} = c_v - c_{v,ss} \tag{12}$$

Engineers run the model at a constant temperature; however, the majority of compression systems include after-coolers. An after-cooler's thermal capacity and the piping are significantly larger than the thermal capacity of the gas that they contain. Consequently, gas temperature changes are negligible within the first second following an emergency shutdown.

We may calculate the standard flow, Q_{std}, through the anti-surge valve using the International Society of Automation method defined in the ANSI/ISA Standard 75.01.01 (2002). Usually we do not know the piping geometry factor, F_p; however, we may assume it to be one. We assume the pressure to be constant throughout the entire piping volume. Therefore the pressure is the same both upstream of the anti-surge valve and at the compressor's discharge.

$$Q_{std} = 1360 \cdot F_p \cdot c_v \cdot Y \cdot \left[\frac{dp}{p_2} \cdot \frac{1}{SG \cdot T_2 \cdot Z_2} \right]^{0.5} \tag{13}$$

We calculate the compressibility, Z_2, from the Redlich-Kwong equation of state, an empirical, algebraic equation that relates temperature, pressure and gas volume (Redlich and Kwong, 1949; Murdock, 1993). We may achieve an iterative solution of Equation 11 using the following method. Initially, we know the gas mass contained in the volume, V. For each time-step, we calculate the flow from the compressor and flow through the anti-surge valve, Equation 13, using the pressure p_2 in the volume calculated at the previous step. We derive the flow from the compressor from the known compressor map, with the compressor speed reducing at an assumed rate, typically 30 percent speed loss per second. We base the flow through the anti-surge valve on an assumed opening speed. Therefore, we assume the anti-surge valve's c_v value to increase from zero at the initial time-step to the fully opened value at an assumed rate.

If the system is able to reduce the compressor discharge pressure by less than 56 percent, the volume reduces by a pre-defined small increment. If the compressor discharge pressure reduction is more than 56 percent, then the volume V increases by the same pre-defined small increment until it finds a volume V, where the compressor discharge pressure reduces by 56 percent in 1 second. This calculation method enables a design engineer to compute the maximum allowable compressor discharge piping volume for a given compression system design that will not result in the compressor surging during an emergency shutdown.

VALIDATION

Figure 3.3 and Table 3.1 respectively illustrate the anti-surge system geometry and compression system parameters. Figure 3.5 provides compressor characteristics. The individual speed lines in the compressor discharge pressure-flow map are collapsed onto a single curve by dividing the flow by the compressor speed and the isentropic compressor discharge pressure by the square of the compressor speed.

In-service data were available for a compression system where the anti-surge valve failed to open during an emergency shutdown. We ran the model with data from this in-service shutdown and Figure 3.6 presents the results. The model predicts an initial deceleration that is faster than that which we observed in-service. The discrepancy between the predicted and measured deceleration rate is probably a consequence of the power turbine continuing to produce power after shutting off the gas turbine fuel supply. The deviation between predicted and measured deceleration rate is acceptable as the purpose of the model is to assist design engineers to avoid emergency shutdowns. Despite the discrepancy between the predicted and measured deceleration rate, we accurately predicted the onset of surge and also well characterized the post-surge deceleration rate.

Table 3.1. *Problem definition (full model).*

$P1$	4938 kPa
$P2$	6100 kPa
V	21 m^3
L	42 m
SG	0.59
$T1$	305 K
J	34.593 kg m^2
Anti-surge valve K_v	N/A

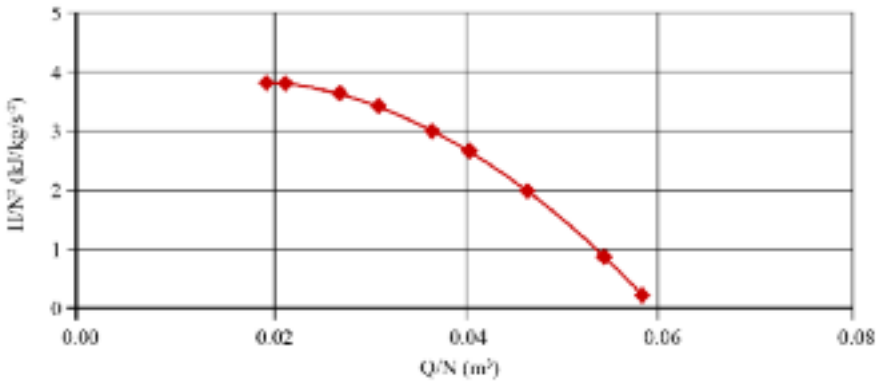

FIGURE 3.5. Compressor performance characteristics. The individual speed lines in the compressor discharge pressure-flow map are collapsed into a single curve by dividing the flow by the compressor speed and the isentropic compressor discharge pressure by the square of the compressor speed.

Both measured data and model prediction show the speed line's characteristic flattening in surge. This flattening occurs primarily as a consequence of the compressor absorbing less power when surging. We verified compressor surge through an analysis of vibration data which we recorded at the compressor bearings (Figure 3.6). To demonstrate the complete model's capability, we used it to simulate the recycle system we defined in Table 3.2. We used the same compressor as previously, with the same compressor characteristics (Figure 3.5).

The compressor only just avoids surge at 0.1 second and then goes on to decelerate with an acceptable surge margin (Figure 3.7). Besides the reduction in

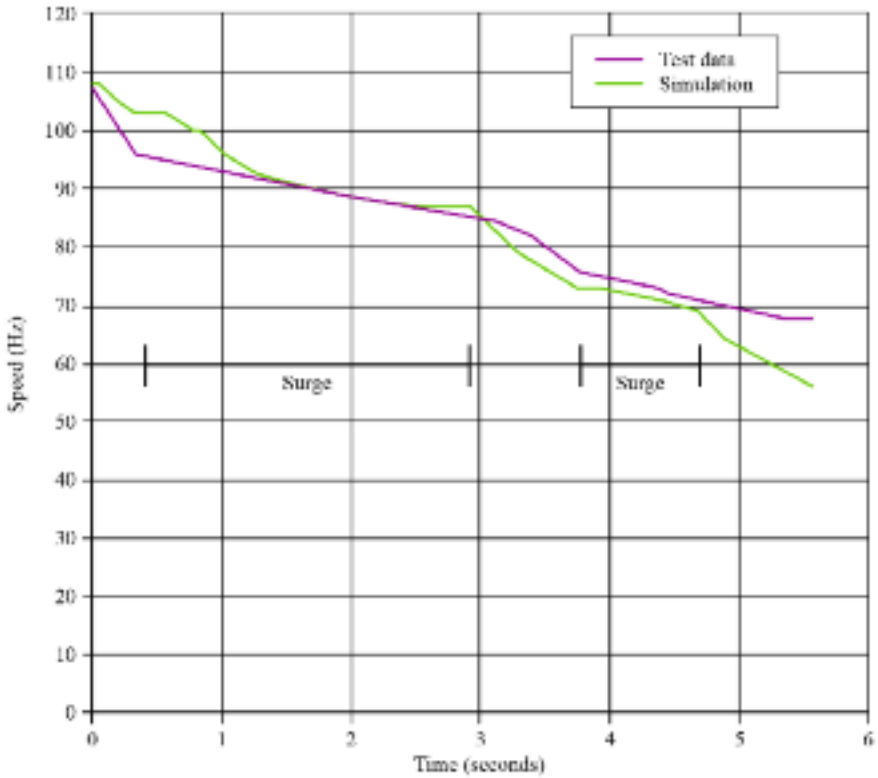

FIGURE 3.6. Emergency shutdown against closed anti-surge valve. Test data versus simulation with complete model. Time spans in surge based on vibration data from test flow and reverse flow.

Table 3.2. *Problem definition (simplified model).*

$P1$	5900 kPa
$P2$	8900 kPa
V	21 m^3
L	42 m
SG	0.59
$T1$	305 K
J	34.593 kg m^2
Anti-surge valve K_v	30,000

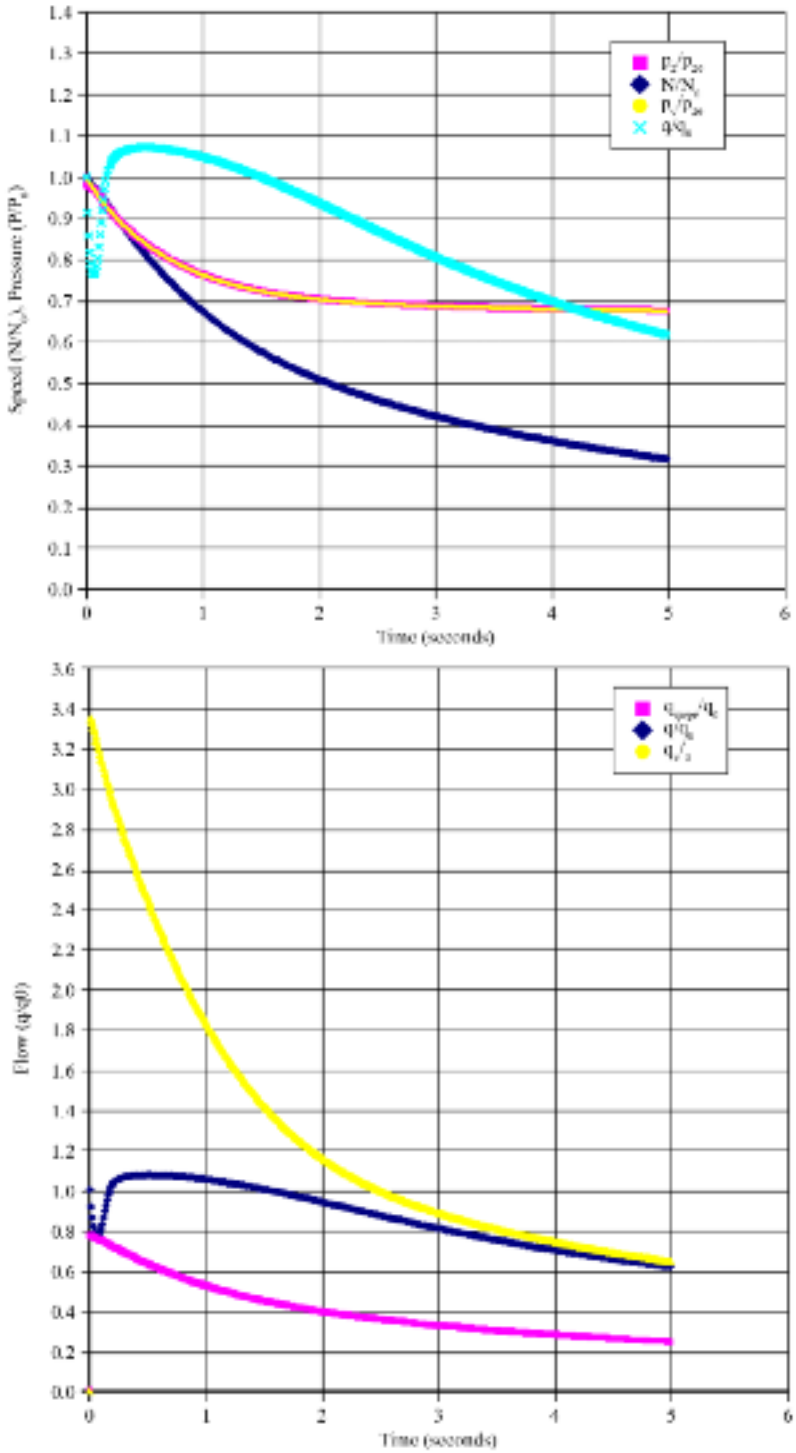

FIGURE 3.7. Emergency shutdown with anti-surge valve opening, based on calculations with the full model: (top) speed and pressures versus time, (bottom) flow versus time. All curves are normalized with the respective values at the time of initiation of the emergency shutdown.

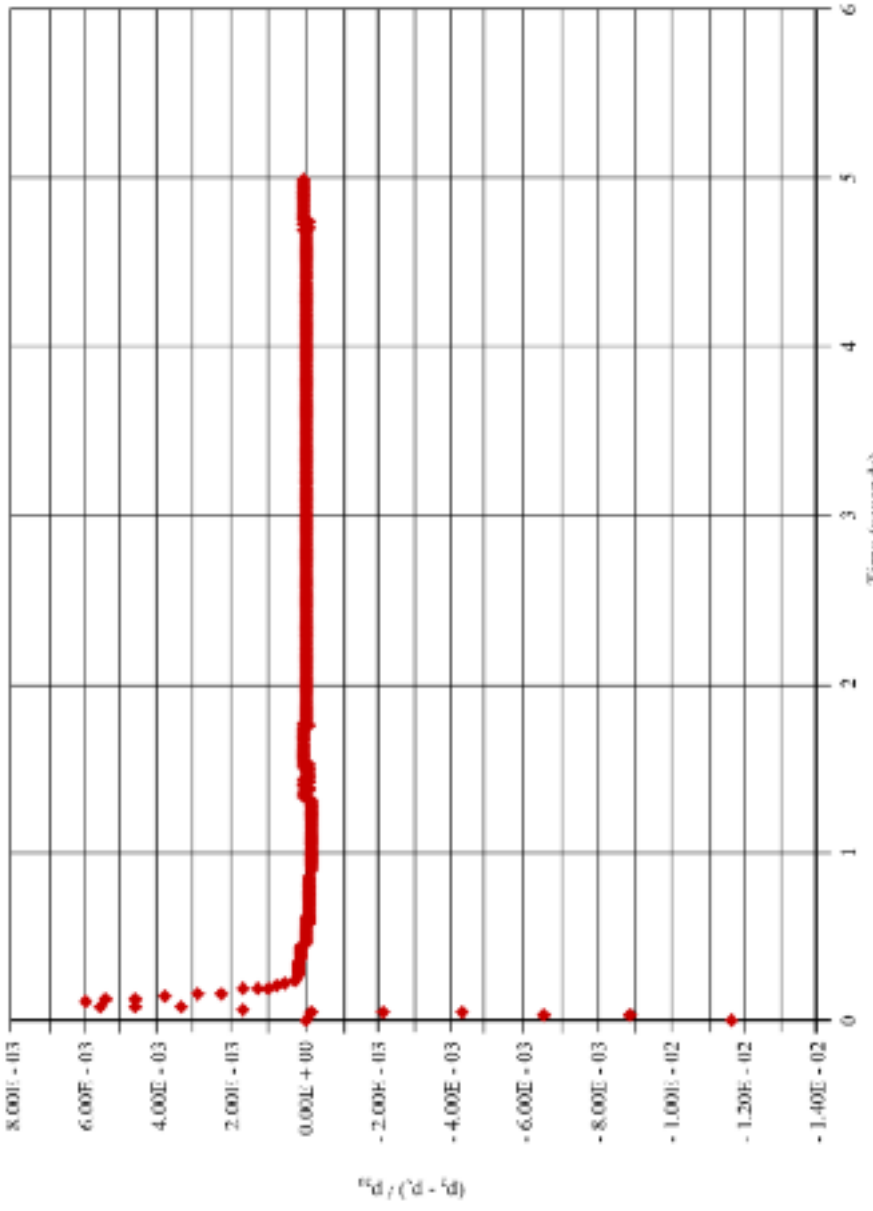

FIGURE 3.8. Relative difference between compressor discharge pressure p_2 and valve pressure p_v, based on the full model.

compressor speed of about 30 percent during the first second, the data also shows that the pressure at the compressor discharge (p_2) and the pressure upstream of the valve (p_v) are almost identical (Figure 3.8) thus confirming validity of the simplifying assumptions when we developed the models.

We may use the simplified model for the same conditions, first with a prescribed speed reduction and second, with the calculated speed reduction as in the complete model. This shows very similar results compared to the complete model (Figure 3.9). We can expand this method to situations where a relatively small suction volume leads to a fast increase in suction pressure. In the simulated system, test data did not indicate this pressure increase and therefore the assumption of a large suction volume was valid.

SUMMARY

We developed and used a model to simulate compression system emergency shutdowns to define guidelines that design engineers can use when sizing upstream and downstream compressor piping, as well as the necessary anti-surge valve. We analyzed a compression system and used in-service data to verify the model. The model predictions are in good agreement with the measured data. The model was able to predict when a surge will occur. The inaccuracies and limitations inherent in the current model are only problematic if design engineers require the entire compressor rundown characteristic. The purpose of the program was to provide design

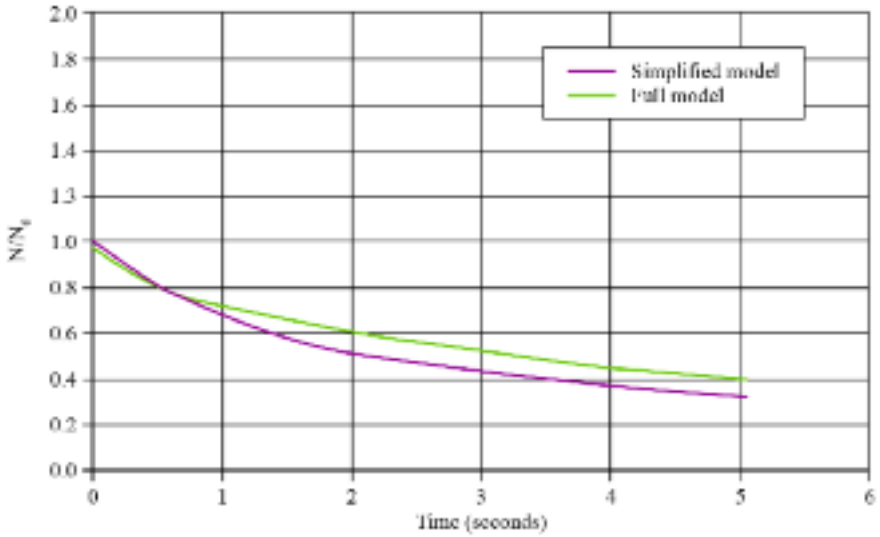

FIGURE 3.9. Comparison between full and simplified model. N_0 is the compressor speed at the initiation of an emergency shutdown.

engineers with a tool that would enable them to determine if a compression system would surge during an emergency shutdown. We showed that the simplified and the full model can predict the system's capability to avoid compressor surge during emergency shutdowns accurately. Therefore, it provides a useful tool to assist design engineers when developing a compression systems' piping design.

REFERENCES

ANSI / ISA Standard 75.01.01 (2002), "Flow Equations for Sizing Control Valves".

Arnulfi, G.L., Giannatasio, P., Micheli, D., and Pinamonti, P. (2000), "An Innovative Control of Surge in Industrial Compression Systems", *Proceedings of the 45th American Society of Mechanical Engineers Gas Turbine and Aeroengine Congress,* Munich, Germany, 8–11 May, Paper No. 2000-GT-352.

Bakken, L.E., Bjorge, T., Bradley, T.M., and Smith, N. (2002), "Validation of Compressor Transient Behavior", *Proceedings of the 47th American Society of Mechanical Engineers Gas Turbine and Aeroengine Congress,* Amsterdam, The Netherlands, 3–6 June, Paper No. 2002-GT-30279.

Blanchini, F., Giannatasio, P., Micheli, D., and Pinamonti, P. (2002), "Experimental Evaluation of a High-Gain Control for Compressor Surge Suppression", *Transactions of the ASME, Journal of Turbomachinery*, vol. 124, pp. 27–35.

Epstein, A.H., Ffowcs Williams, J.E., and Greitzer, E.M. (1994), "Active Suppression of Compressor Instabilities", AIAA Paper No. 86-1994.

McKee, R.J., and Deffenbaugh, D. (2003), "Factors that Affect Surge Precursors in Centrifugal Compressors", *Proceedings of the GMRC Gas Machinery Conference,* Salt Lake City, USA, 6–8 October.

Murdock, J.W. (1993), *Fundamental Fluid Mechanics for the Practicing Engineer,* CRC Press, New York, USA.

Redlich, O., and Kwong, J.N.S. (1949), "On the Thermodynamics of Solutions", *Chemical Review*, vol. 44, pp. 233–44.

Ribi, B., and Gyarmathy, G. (1997), "Energy Input of a Centrifugal Stage into the Attached Piping System During Mild Surge", *Proceedings of the 42nd American Society of Mechanical Engineers Gas Turbine and Aeroengine Congress*, Orlando, USA, 2–5 June, Paper No. 97-GT-84.

Sentz, R.H. (1980), "The Analysis of Surge", *Proceedings of the 9th Turbomachinery Symposium*, Houston, USA, 9–11 December, pp. 57–61.

Wachter, J., and Rohne, K.H. (1984), "Centrifugal Compressor Surge Behavior", *Proceedings of the 29th American Society of Mechanical Engineers Gas Turbine and Aeroengine Congress,* Amsterdam, The Netherlands, 3–7 June, Paper No. 84-GT-91.

Chapter 4

Compression Systems during Emergency Shutdowns

J.J. Moore, R. Kurz, A. Garcia-Hernandez and K. Brun

ABSTRACT

Compression system transient behavior, particularly under rapidly changing conditions, is of interest to both design engineers and operators. Predicting transient behavior is important if operators are to avoid damage during an emergency shutdown. A limited number of "accidental" data sets from compressor manufacturers and compression system operators are available in the public domain. Academics have developed transient compression system modeling approaches; however, the available accidental data sets are not complete. Some details of the compressor, gas turbine, valves and piping system geometry are not available in the public domain. Consequently, the data is unsuitable for validating the developed modeling approaches. Surge control system models are particularly difficult to validate, as surge is a transient phenomenon and it is difficult to obtain the transient data during a compressor surge. The primary objective of the work in this chapter is the development of a full-scale test facility that will enable one to obtain transient compressor surge data. This data facilitated the verification of transient surge models. The chapter documents the test results and model comparisons and validates the models using the test results.

This chapter is a revised and extended version of Moore, J.J., Kurz, R., Garcia-Hernandez, A., and Brun, K. (2010), "Experimental Evaluation of the Transient Behavior of a Compressor Station During Emergency Shutdowns", *Transactions of the ASME, Journal of Engineering for Gas Turbines and Power*, vol. 132, pp. 1–9.

NOMENCLATURE

C_v	valve flow coefficient ($m^3/Pa^{1/2}s$)
H	head
J	inertia (kg m^2)
N	speed (rpm)
N_{BG}	inertia number
P	power (kW)
P	pressure (kPa)
Q	flow (m^3/min)
T	compressor torque (Nm)
t	time scale (s)
V_2	discharge volume between compressor and anti-surge valve (m^3)
W	mass flow
Π	dimensionless parameter
ω	rotational speed (rad/s)
GT	gas turbine
MMSCFD	million standard cubic feet per day

Subscripts

b	discharge volume to bleed down
compr	compressor
d	compression systems rotating system deceleration
delay	surge control response
frict	friction
GT, resid	residual gas turbine
o	operating point
surge	conditions at surge
v	anti-surge valve

INTRODUCTION

The operating range of a compressor is limited by its maximum operating speed, minimum operating speed, maximum available power, choke flow and stability limit (Figure 4.1). At flows below the stability limit the compressor initially shows a reduced capability to generate pressure with reduced flow. At a critical flow the compressor experiences reverse flow, it surges, and the gas now flows from discharge to suction side. Once the compressor surges, the flow rate is a function of the compressor pressure ratio as during a surge a compressor acts like an orifice plate. The flow reversal results in the pressure downstream of the compressor reducing gradually. The pressure reduction speed depends on the volume size downstream of the compressor. Once the pressure reduces sufficiently, the compressor will recover, and gas will flow again from the suction to the discharge side. Unless the compression

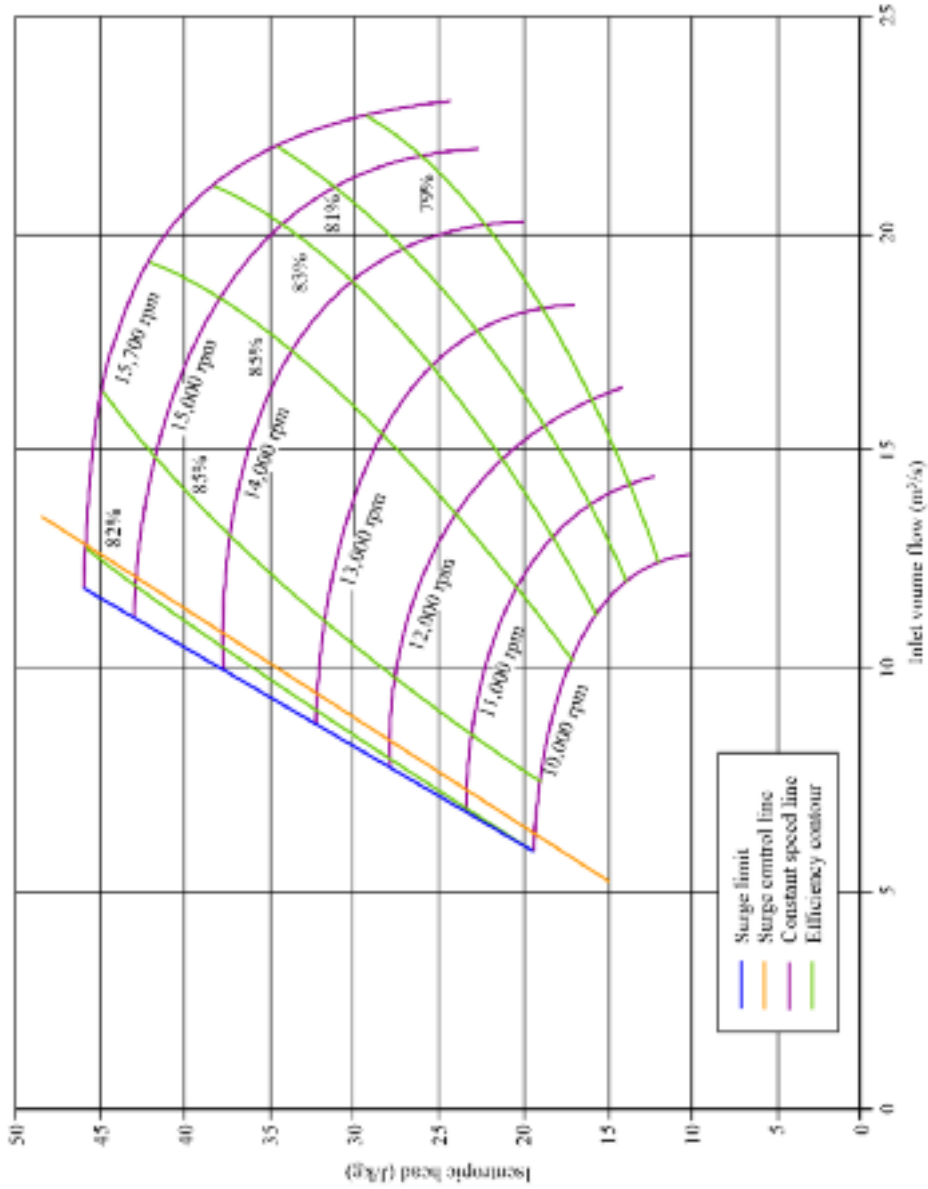

FIGURE 4.1. Typical map of a variable speed centrifugal compressor.

system operators intervene, the surge and recovery will repeat. Ribi and Gyarmathy (1997) describe the consequences of repetitive surge and recovery for a compressor. Repeated surge and recovery may damage the compressor's thrust bearing as a consequence of the thrust load's reversal during a surge event. Repetitive surge and recovery may also damage seals, and ultimately overheat the compressor.

One must avoid surge to protect the compressor. The usual method for surge avoidance consists of one or several recycle loops that fast-acting anti-surge valves can activate when the compression system control system detects that the compressor is approaching its stability limit. Typical control systems use suction and discharge pressure and temperature, together with the inlet flow into the compressor as input to calculate the present operating point's relative distance to the predicted or measured compressor stability limit (Figure 4.1). We define the surge margin (*SM*) by:

$$SM = \left. \frac{Q_o - Q_{surge}}{Q_o} \right|_{N=const} \tag{1}$$

The surge margin definition is somewhat arbitrary as it is a compression system feature, not an isolated centrifugal compressor feature. Definitions that engineers frequently use to establish compressor surge line locations when installed in a compression system include a local maximum in the compressor discharge pressure-flow characteristic, the onset of rotating stall that is classically established by monitoring and analysing compressor bearing vibration characteristics or the point where one can measure flow reversal. If the compressor operating point comes within typically 5 percent of its surge line, the control system starts to open the anti-surge valve, thereby reducing the pressure ratio across and increasing flow through the compressor.

Practitioners who have studied the role of an anti-surge control system (White and Kurz, 2006; Brun and Nored, 2007) have observed that to be effective an anti-surge control system must:

- facilitate the compression system starting and normal shutdown process;
- accommodate slow process changes to prevent process disruption; and
- accommodate fast process changes and massive system disturbances.

White and Kurz (2006) and Brun and Nored (2007) commented that the ability to accommodate slow process changes requires precision control of the anti-surge valve opening position to ensure that there are no flow oscillations through either the compressor or the wider compression system. When considering fast process changes, White and Kurz (2006) and Brun and Nored (2007) observed that during an emergency shutdown an anti-surge control system requires extremely fast-opening valves with a large flow area in order to avoid surge.

During an emergency shutdown the fuel supply to the compression system's gas turbine cuts off instantly. Some installations maintain fuel flow to the gas turbine for 1 to 2 seconds while the anti-surge valve opens; however, this practice can result in a

safety hazard and therefore, control system design engineers no longer favor it. When the compression system driver is an electric motor, tripping the motor initiates the emergency shutdown. In either case, the compression system's centrifugal compressor will decelerate rapidly under the influence of fluid forces. The magnitude of fluid forces and inertia of the compression system's rotating system govern the deceleration rate.

A compression system's rotating system comprises a centrifugal compressor impeller plus the coupling to its driver and the inertia of the driver's rotating components. Driver rotating components may comprise:

- a single-shaft gas turbine's shaft or the low-speed shaft of a two-shaft gas turbine, if the gas turbine is directly coupled to the centrifugal compressor;
- a gas turbine's power turbine, if the gas turbine has a separate power turbine; or
- an electric motor's rotor, if the centrifugal compressor's driver is an electric motor.

This set of rotating components collectively comprises a compression system's rotating system, and it is the involved inertia that is of interest to design engineers when estimating centrifugal compressor deceleration rate. In the program of work that we report in this chapter, the rotating system comprised a centrifugal compressor's impeller, coupling and gas turbine power turbine.

The compressor's pressure developing capability reduces approximately by the square of its running speed. However, the upstream and downstream piping system imposes the pressure ratio across a compressor. Therefore, the compressor will always surge during an emergency shutdown if the anti-surge valve cannot provide fast discharge pressure relief. A 30 percent loss in speed within the first second after initiating the shutdown is typical during an emergency shutdown (Kurz and White, 2004; White and Kurz, 2006) and equates to a loss in pressure developing capability of approximately 50 percent. Consequently, the anti-surge valve must reduce the pressure across the compressor by about half in the time that the compressor loses 30 percent of its speed.

The rate at which the discharge pressure can relieve itself not only depends on the anti-surge valve's reaction time, but also on the constraints which the piping system imposes. The piping system's transient behavior depends largely on the gas volume enclosed by its various components. Besides the piping itself, this may include scrubbers, knockout drums and coolers (Figure 4.2).

The larger the volumes are in the system, the longer it will take to equalize pressure. The larger the anti-surge valve, the better is its potential to avoid surge. However, the larger the anti-surge valve, the more difficult it is to control and the slower its opening time. The faster the anti-surge valve can open, the more flow can pass through it, especially in the first few critical seconds following an emergency shutdown. There are, however, limits to the anti-surge valve opening speed, dictated by practical limits on the anti-surge valve actuator's power. If the discharge volume is too large, and engineers cannot design the anti-surge valve to avoid surge, one may

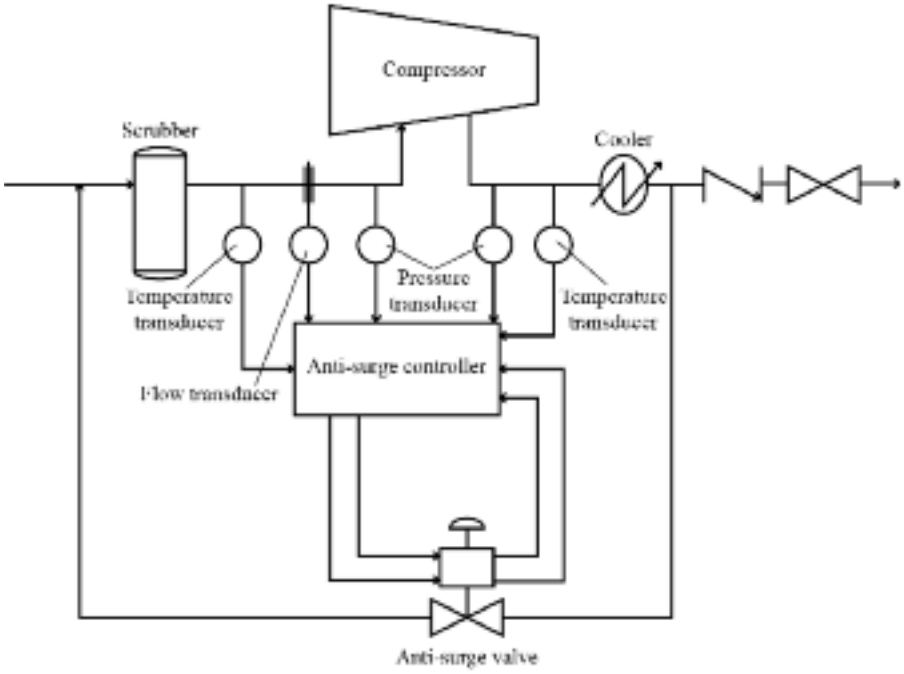

FIGURE 4.2. Surge avoidance system schematic.

consider a short recycle loop (known as a hot recycle loop). Such a loop does not include the compression system aftercooler and therefore is a last resort for design engineers as their use in-service will overheat the compressor.

Other scholars have developed transient surge models, which predict the compression system's behavior during an emergency shutdown (Morini *et al*., 2007; Botros and Ganesan, 2008). However, we can generate correlations using data from laboratory-scale compression systems. This chapter presents results from a full-scale natural gas centrifugal compressor that we designed and instrumented to reproduce compression system performance during a compressor surge. We used the acquired experimental data to validate predictions, and performed parametric studies to establish key parameter sensitivities.

MODELING THE PIPING AND SURGE CONTROL INTERACTION

Piping and valve design, together with instrument selection and placement, will significantly affect an anti-surge control system's performance. An anti-surge control system's configuration (Figure 4.2) is a major design issue because if the system fails to perform, rectifying design errors is costly once a compression system is operational. In its simplest form, an anti-surge control system includes:

- a flow-measuring element on the compressor's suction side;
- instruments to measure pressures and temperatures on both the compressor's suction and discharge side;
- an aftercooler;
- a discharge check valve; and
- a recycle line with an anti-surge valve which connects upstream of the discharge check valve and compressor flow-measuring device.

The control system calculates the compressor's location on its operating map and calculates the compressor's surge margin by comparing that position to the compressor's surge line. If necessary, an operator may open the anti-surge valve to prevent the compressor's surge margin falling below, typically, 10 percent. In the event of an emergency shutdown, where the fuel to the gas turbine or power to the electric motor shuts off, the anti-surge valve should open as the fuel valve is closing. A design engineer must consider the following system features when designing an anti-surge control system:

- the piping system's geometry, in particular the volumes of piping and vessels;
- the anti-surge valve's opening and closing characteristics;
- the compression system's rotating system inertia;
- the driver's thermal inertia;
- the compressor performance map; and
- other known factors that will introduce a delay in the anti-surge control system.

A key challenge when attempting to simulate a compression system's transient behavior is predicting its rotating system's deceleration rate. We determine the deceleration rate using the rotating system's inertia J, any residual power generated by the gas turbine ($P_{\mathrm{GT,resid}}$), the friction losses in the system and the compressor's power absorption:

$$P = P_{compr} = P_{frict} - P_{GT,resid} = T \cdot N + -J \cdot N \cdot \frac{dN}{dt} \tag{2}$$

$$\frac{dN}{dt} = \frac{P_{compr}(t) + P_{frict}(t) - P_{GT,resid}(t)}{-(2\pi)^2 \cdot J \cdot N(t)} \tag{3}$$

Assuming that all compressor operating points follow the fan laws, we may express the compressor power as:

$$P_{compr}(t) = P_o \left(\frac{N}{N_o} \right)^3 \tag{4}$$

where P_0 and N_0 are, respectively, the steady-state power and speed at the initial operating point. We may also derive compressor power from a consideration of the

compressor's instantaneous operating point. However, derivation of power from the compressor's instantaneous operating point requires a prior knowledge of the operating point locus across the compressor map during an emergency shutdown. Assuming a constant flow-to-speed ratio enables us to make a reasonable assessment of compression power. Practitioners usually assume that the compressor's steady-state flow-compressor discharge pressure-efficiency map remains accurate under transient conditions such that they may still use it to determine compressor power at any point during an emergency shutdown.

Substituting and integrating Equation 4 into Equation 3 yields the following expression for compression system speed decay:

$$N(t) = \frac{JN_o^3}{JN_o^2 + P_o t} \tag{5}$$

However, determining the compression system deceleration rate is difficult as there is residual power which the gas turbine generates after closing the fuel valve as fuel remains in the gas turbine's fuel system. Consequently, theoretically predicting the compression system deceleration rate is difficult.

TEST OBJECTIVES

This program of work in this chapter is based upon experimental data which we obtained from a full-scale centrifugal natural gas compressor that we subjected to a range of surge conditions. We studied the piping configuration's impact on compressor performance during an emergency shutdown. We selected the piping configurations and operating conditions for the surge tests as representative of actual compressor emergency shutdown events. The selected test conditions produce nondimensional volume, compressor discharge pressure and flow parameters that match actual conditions.

We selected, installed and calibrated the instrumentation to minimize test uncertainty. We studied transient events across a range of compressor operating conditions and control system settings. We selected the anti-surge control system operating points to have the compression system's rotating system inertia and gas forces typical of oil and gas applications.

The piping system's geometry, as well as the anti-surge valve and compressor behavior, are well defined. We gathered dynamic pressure, flow, temperature and speed data. The project's goal was to create an accurate data set during an emergency shutdown for a compression system with a known geometry. The intent was to use the data set to facilitate the validation of numerical simulations and provide a means of assessing the simulation accuracy.

TEST SETUP

We conducted the tests that we describe in this chapter at Southwest Research Institute's metering research facility (MRF) in San Antonio, Texas. The metering research facility comprises a gas turbine driven centrifugal compressor that we operated in a closed loop filled with natural gas (Figure 4.3). The test setup included valves on the compressor's suction (Suc *V*) and discharge (Dis *V*) sides (Figure 4.4). These valves automatically close at the initiation of a shutdown, and move from fully open to fully closed in 2 seconds.

The metering research facility compression system comprises a 1.1 MW class two-shaft gas turbine with a power turbine that drives a single-stage centrifugal compressor with a 190-mm diameter impeller. The compression system's rotating system has a maximum speed of 22,300 rpm. The metering research facility allows testing at different operating conditions in a high-pressure loop at flow rates of between 6 and 150 million standard cubic feet per day, over a pressure range of 14–73 Bar and a temperature range of 15–32°C. We initiated shutdown sequences from 13.9 Bar to 14.4 Bar compressor suction pressure.

The compressor setup included suction and discharge headers, a gas scrubber, aftercooler, isolation valves, a vibration monitoring system and an anti-surge valve. The suction header was a 300-mm diameter (schedule 80) pipe connected to an isolating suction valve and to a 790 × 2900 mm scrubber connected to the centrifugal compressor's suction side. We fitted the suction header with taps that we utilized to mount the test instrumentation. From the compressor discharge, we connected an

FIGURE 4.3. The metering research facility (MRF) at the Southwest Research Institute, San Antonio, Texas.

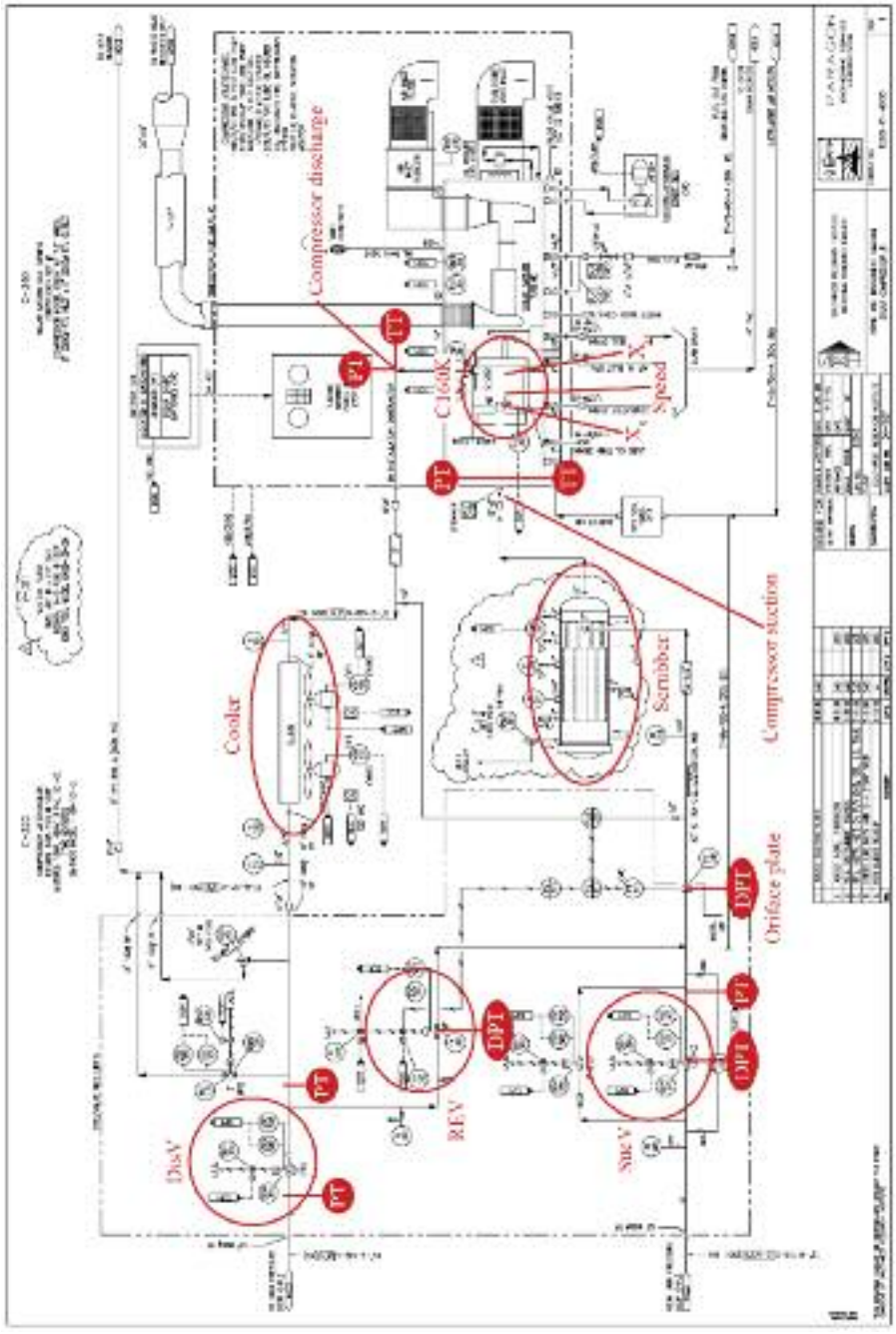
Compressor discharge
C160K
Speed
Cooler
Scrubber
Compressor station
Orifice plate
DPT
TT
PT
DisV
REV
SucV

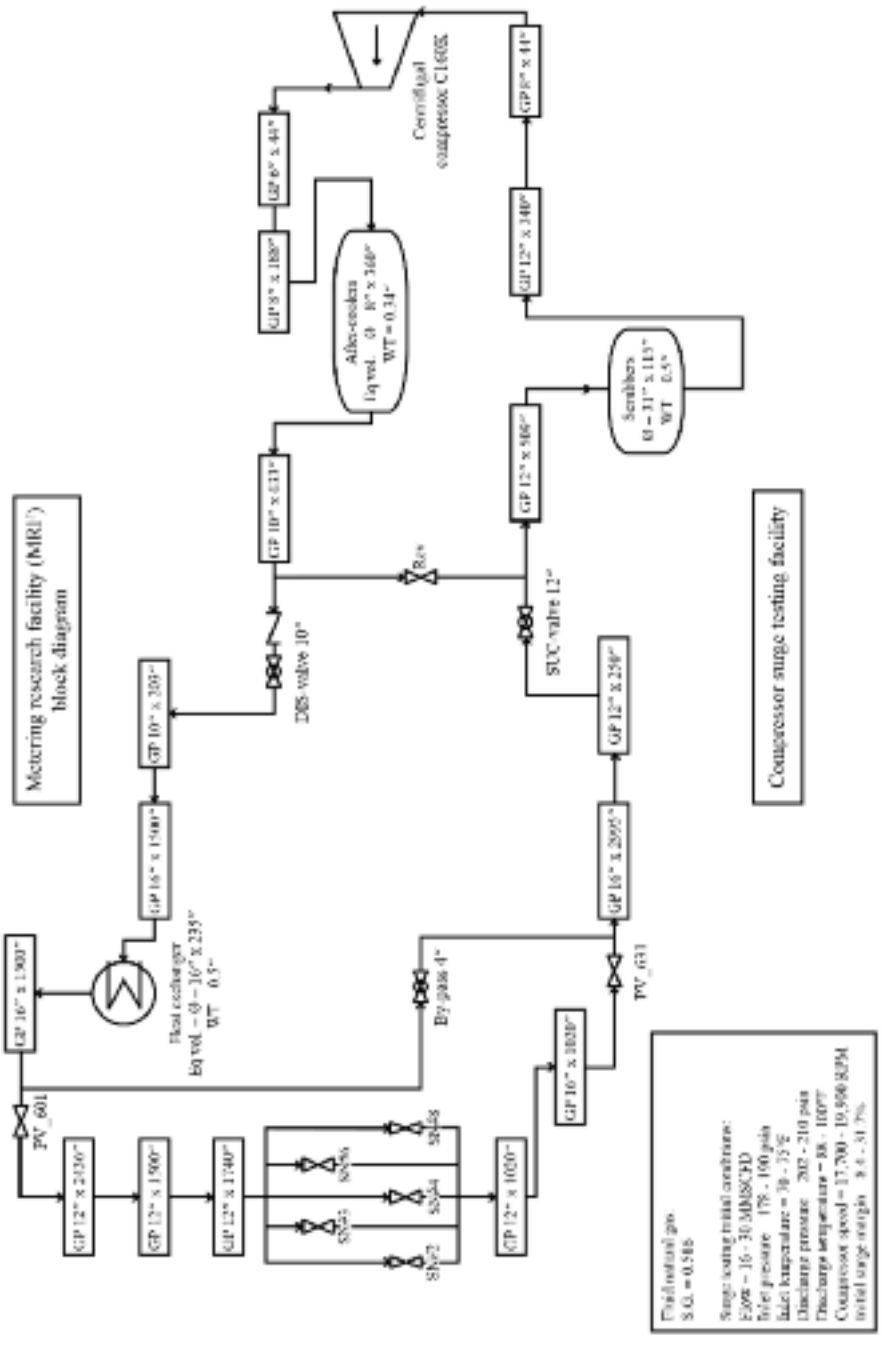

FIGURE 4.4. (Top) Piping and instrumentation diagrams for metering research facility (MRF), and (bottom) its representation in the Stoner Pipeline Simulation® (SPS) software.

8-inch diameter pipe to a fin-fan aftercooler. Downstream of this cooler was a recycle loop and a discharge isolation valve. The recycle loop was a small pipe segment that connected the compressor suction side with the compressor discharge header through an anti-surge valve. The anti-surge valve was part of the compressor's anti-surge system. The anti-surge system's control system monitored compressor suction pressure, discharge pressure and flow rate which we then used to control the anti-surge valve position. We accomplished surge control through pneumatic programmable relays. The anti-surge valve was a 6-inch diameter, equal-percentage fast-opening valve. The anti-surge valve's normal position was open.

The metering research facility setup facilitated transient testing of the compression system and enabled us to collect transient data during full-scale emergency shutdowns of a centrifugal compressor across a range of operating conditions. The transient data includes static and dynamic pressure, compressor speed, suction and discharge temperatures, plus vibration data. We mounted the absolute pressure transducers close to the piping (Figure 4.5). The transducers had a 2000 Hz bandwidth that we considered high enough to facilitate both static and dynamic pressure measurement. We acquired data using a 16-channel data acquisition system that utilized a 24 bit analog to digital converter.

We measured gas temperature using two thermocouples located at the compressor suction and discharge inside thermowells. We collected radial shaft vibration data at the compressor bearings from vibration transducers that we mounted on each bearing. With one horizontal and one vertical, we input these into an oscilloscope to enable us to study the resultant Lissajous figures in real time. We measured compressor speed using a magnetic sensor located on the gas turbine's power turbine shaft. We used a linear variable differential transducer for measuring displacement of the anti-surge valve, giving a measurement of the anti-surge valve stroke length and travel time. We calibrated all instrumentation prior to its installation in the metering research facility.

SIMILARITY CONSIDERATIONS

The metering research facility test setup simulated conditions representative of actual compression system installations. Parameters that characterise the dynamic response of the compression system's rotating system include the pipe volume, V_2, the shaft rotating system inertia, J, the rotating system speed, ω, the centrifugal compressor torque, T, at the moment that the operator initiates emergency shutdown, the rate at which the anti-surge valve opens, the pressure differential across the anti-surge valve and the anti-surge valve's flow coefficient. We may combine these parameters in four non-dimensional parameters Π_i:

FIGURE 4.5. High-frequency pressure transducer in discharge pipe.

Deceleration parameter:

$$\Pi_1 = \frac{\omega^2 J}{T} \tag{6}$$

Energy parameter:

$$\Pi_2 = \frac{\Delta p V_2}{J\omega^2} \tag{7}$$

Bleed volume parameter:

$$\Pi_3 = \frac{t_v \Delta p^{1/2} C_v}{V_2} \tag{8}$$

Time parameter (bleed time over deceleration time):

$$\Pi_4 = \frac{t_b}{t_d} = \frac{V_2 T}{\Delta p^{1/2} \omega J C_v} \tag{9}$$

These four parameters characterise the compression system's dynamic behavior. Table 4.1 compares the non-dimensional parameters Π_1–Π_4, for the metering research facility installation with non-dimensional parameters for typical in-service installations. The comparison illustrates that the metering research facility produces a representation of the in-service installation physics, both for pipeline compressors and production compressors.

Botros and Ganesan (2008) established a non-dimensional parameter, the inertia number N_{BG}, that characterized a compression system, and its propensity to surge during an emergency shutdown:

$$N_{BG} = \frac{J \cdot N^2}{W_{surge} H_{surge} t_{delay}} \tag{10}$$

By evaluating in-service compressor systems across the oil and gas industry, Botros and Ganesan (2008) found that if N_{BG} is below 30, the system will require a recycle loop to avoid surge during an emergency shutdown, while a system with N_{BG} above 100 will not surge during an emergency shutdown. If N_{BG} is between 30 and 100, Botros and Ganesan (2008) concluded that a more detailed dynamic system simulation is required to establish if surge will occur with a specific in-service compression system geometry. Table 4.2 presents the metering research facility's inertia number, N_{BG}. The metering research facility inertia number falls between 30 and 100.

Table 4.1. *Parameters Π_1–Π_4 for the metering research facility (MRF) test setup.*

Parameter	MRF value (C160K-1E)	C366	Pipeline station 1	Pipeline station 2	Production compressors
Π_1	9200–12,200	12,000–15,200	1000	1900	3200–3400
Π_2	0.28–0.33	0.23–0.54	3.8	2.3	0.50–0.80
Π_3	0.13–0.16	0.16–0.19	0.02	0.035	0.03–0.04
Π_4	1.5–2.2	0.9–1.9	18.47	7.8	2.5–2.8

Table 4.2. *Summary of the inertia number established by Botros and Ganesan (2008) for the metering research facility (MRF).*

Data point	Speed (rpm)	Inertia (kg m^2)	Mass rate at surge (kg/s)	Head at surge (J/kg)	Delay time (s)	Inertia number N_{BG}
MRF No. 1	17,800	0.19	4.49	16,487.1	0.18	50
MRF No. 2	19,800	0.19	4.78	20,532.8	0.18	47

TEST RESULTS

We gathered the first set of test data under steady-state conditions for the purpose of establishing the compressor's steady-state performance at different speeds (Figure 4.6). The results were self-consistent with the centrifugal compressor manufacturer's performance predictions.

The theoretical and measured surge lines differ significantly (Figure 4.6). The difference occurs as a consequence of the different convention that we used for setting a compressor's surge line. Each of the compressor discharge pressure-flow characteristics for the centrifugal compressor installed in the metering research facility exhibits two horizontal tangents, one at a higher flow and the other at a lower flow. The tangent at the higher flow indicates the onset of rotating stall, while the tangent at the lower flow indicates the onset of surge. The theoretical surge line is set to avoid rotating stall. The compressor manufacturer determined the theoretical surge line's location via a factory test. The measured surge line (Figure 4.6) is the stability limit for the same compressor in the metering research facility. The difference between the two constitutes the compressor manufacturer's factor of safety when predicting in-service performance from a factory test.

With the compressor's steady-state performance established in the metering research facility, we defined a matrix of tests to determine the compressor systems' transient performance (Table 4.3). We performed the tests at two different speeds, and varied the compressor's operating point when we initiated an emergency shutdown. The first series of five tests involved initiating an emergency shutdown with the centrifugal compressor running at 17,800 rpm at five different surge margins. The second series of six tests involved initiating emergency shutdowns with the compressor running at 19,800 rpm, with the compressor operating at six different surge margins.

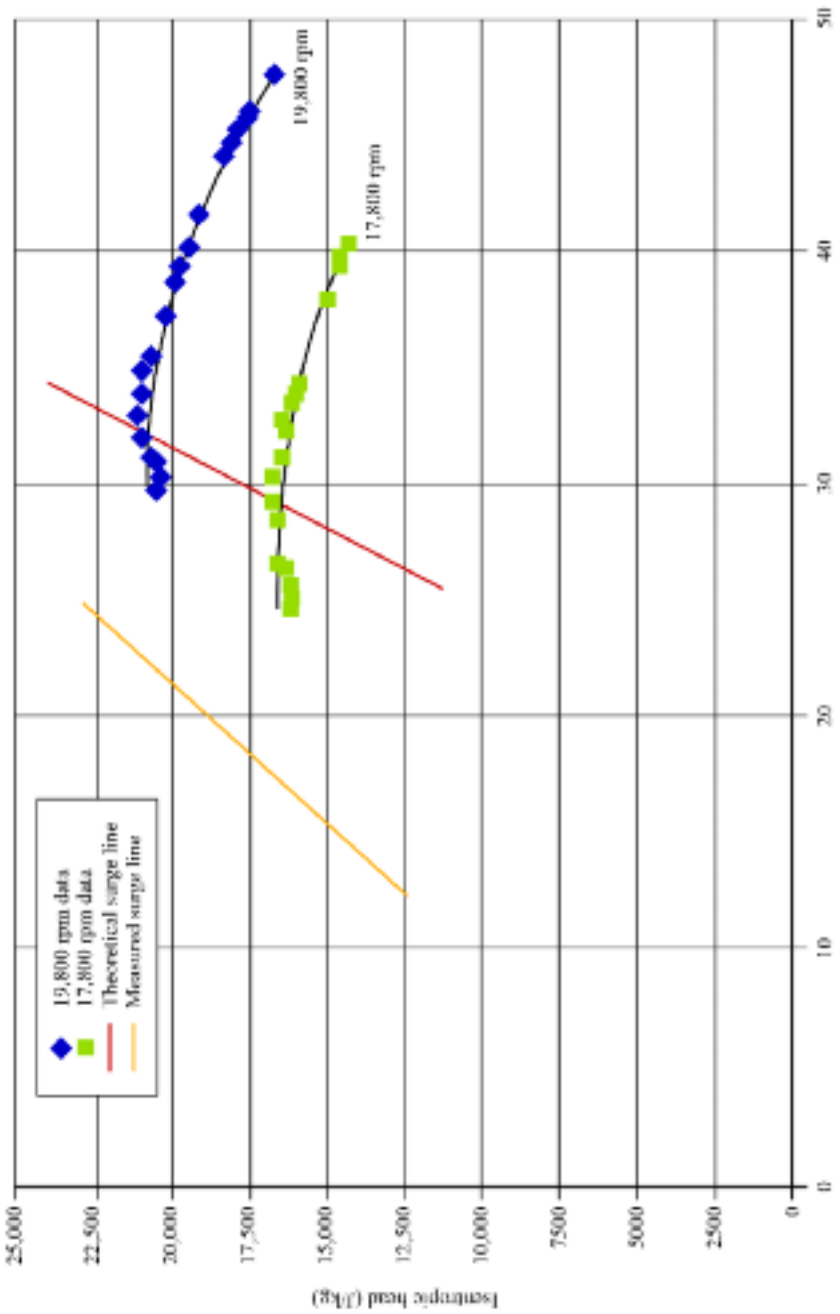

FIGURE 4.6. Steady-state compressor discharge pressure-flow map for two speeds. Solid speed lines are the compressor manufacturer's performance predictions. The theoretical surge line is also based on the manufacturer's prediction.

Table 4.3. *The metering research facility (MRF) transient performance test matrix.*

Initial point data for shutdown sequences											
Data point No.	Compressor suction (kPa)	Compressor discharge (kPa)	T_{suc} (°C)	T_{dis} (°C)	Mass flow (kg/s)	Actual flow (m^3/min)	Standard flow (MMSCFD)	Compressor speed (rpm)	P2/P1	Initial surge margin (%)	Compressor isentropic head (J/kg)
Transient No. 0	1298.3	1435.9	21.3	31.0	6.19	39.7	26.38	17,700	1.106	38.6	14,377.4
Transient No. 1	1283.6	1434.8	21.5	31.8	5.23	34.1	22.29	17,778	1.118	28.5	15,927.6
Transient No. 2	1276.1	1434.1	22.0	32.6	4.61	30.3	19.65	17,777	1.124	19.7	16,740.7
Transient No. 3	1272.4	1427.2	22.5	33.4	4.01	26.6	17.08	17,850	1.122	8.4	16,496.8
Transient No. 4	1275.9	1442.5	22.4	34.2	7.04	45.8	29.98	19,800	1.131	41.0	17,645.8
Transient No. 5	1257.6	1443.2	22.9	35.6	5.95	39.6	25.34	19,879	1.148	31.7	19,878.6
Transient No. 6	1247.6	1442.8	23.4	36.7	5.19	35.0	22.11	19,878	1.157	22.8	21,056.0
Transient No. 7	1245.0	1435.9	23.8	37.2	4.59	31.2	19.56	19,878	1.153	13.2	20,686.4
Transient No. 7.1	1248.0	1438.0	24.1	37.5	4.60	31.2	19.58	19,801	1.152	13.3	20,577.5
Transient No. 8	1245.9	1397.0	23.1	34.1	3.93	26.6	16.73	17,778	1.121	8.6	16,489.3
Transient No. 9	1223.5	1409.4	22.6	36.0	4.41	30.4	18.79	19,800	1.152	11.0	20,420.1

Data from the tests enabled us to trace the locus of the compressor's operating point across its performance map (Figures 4.7 and 4.8). A critical condition occurred when we initiated an emergency shutdown at 19,800 rpm and a low initial surge margin, transient No. 9 (Figure 4.8). The data indicates that the compressor operated past its (theoretical) surge line and reached its lowest flow when the anti-surge valve had opened 35.9 percent. As a consequence of the compression system characteristics, no flow reversal occurred. With the anti-surge valve 35.9 percent open, the discharge pressure reduction was large enough to shift the compressor operating point back across the surge line and into the stable operating region. The minimum flow of 17 cubic meters per minute was similar for each speed, but the potential for surge was greater at the higher speed.

We may clarify the sequence of events as the anti-surge valve opened by considering data that we obtained for transient No. 9 case at 19,800 rpm. When we consider the variation of measured parameters with time, it is apparent that the discharge pressure declines after we initiated the emergency shutdown (Figure 4.9) and the suction pressure starts to increase. This anti-surge valve design does not significantly impact the recycle loop's performance, as the pressure downstream of the anti-surge valve also drops. Figure 4.9 presents the data recording which commenced 8 seconds prior to initiating the emergency shutdown. The pressure that stabilises outside the now isolated recycle loop at approximately 15 seconds was approximately 0.14 Bar higher than that inside, as the pressure downstream of the anti-surge valve indicated.

After initiating an emergency shutdown, there was a rapid reduction in compressor speed and compressor discharge pressure (Figure 4.10). There was a delay of about 200 ms as a consequence of the gas turbine still producing power after shutting off the fuel. After 200 ms the gas turbine consumed the residual fuel and the compressor started to decelerate, losing approximately 15 percent of its initial speed in the first second. The minimum flow condition occurred after 1100 ms, with a corresponding anti-surge valve opening of 35.9 percent (Figure 4.10).

The differential pressure over the suction and discharge valves (Suc *V* and Dis *V* in Figure 4.4) was near zero when the valves were fully open, and it increased as they closed (Figure 4.11). The suction valve took 3 seconds to close. The discharge valve took 2 seconds to close. The differential pressure through the discharge valve became negative as a consequence of the reverse flow from the discharge volume to the suction side through the anti-surge valve. Therefore, the discharge volume flowed backward through the anti-surge valve to the suction side, from a higher to lower pressure region.

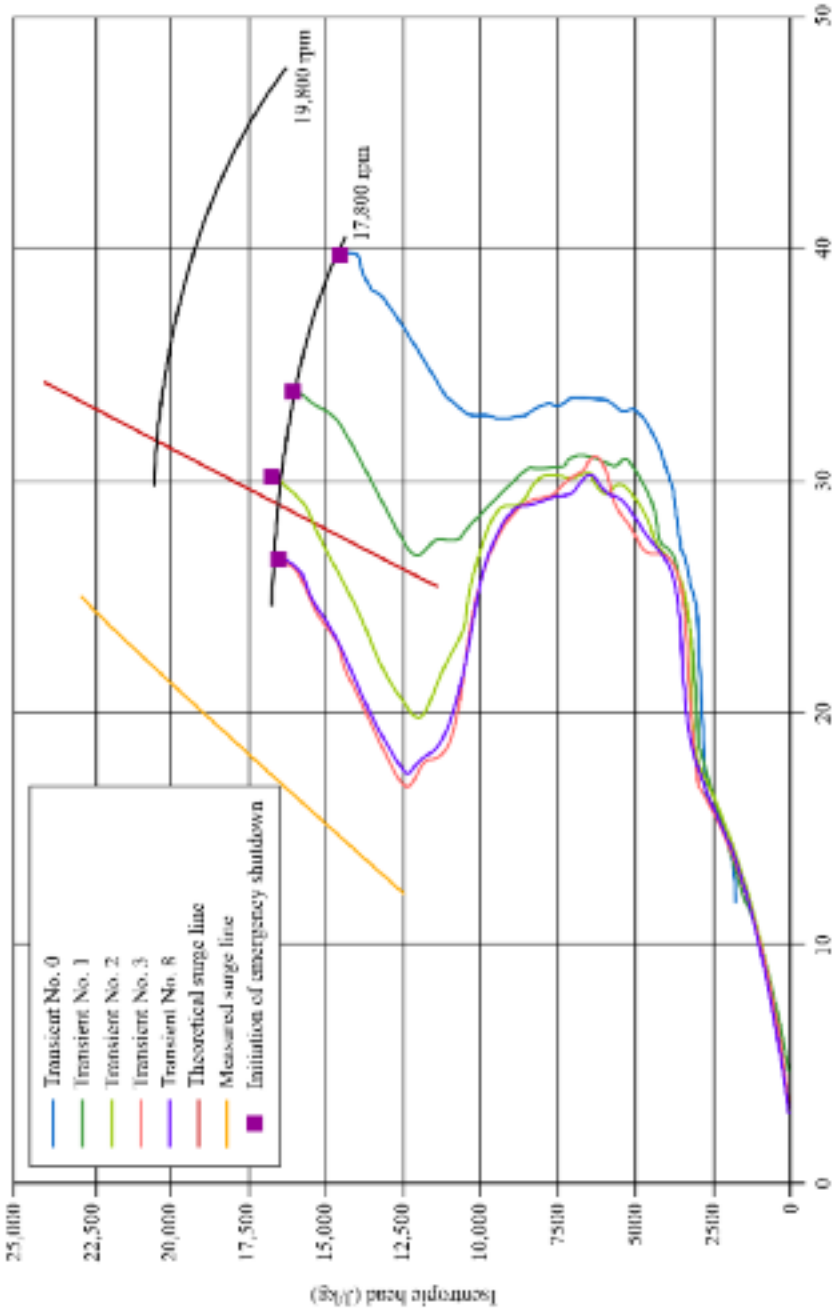

FIGURE 4.7. Transient shutdown loci measurements for 17,800 rpm.

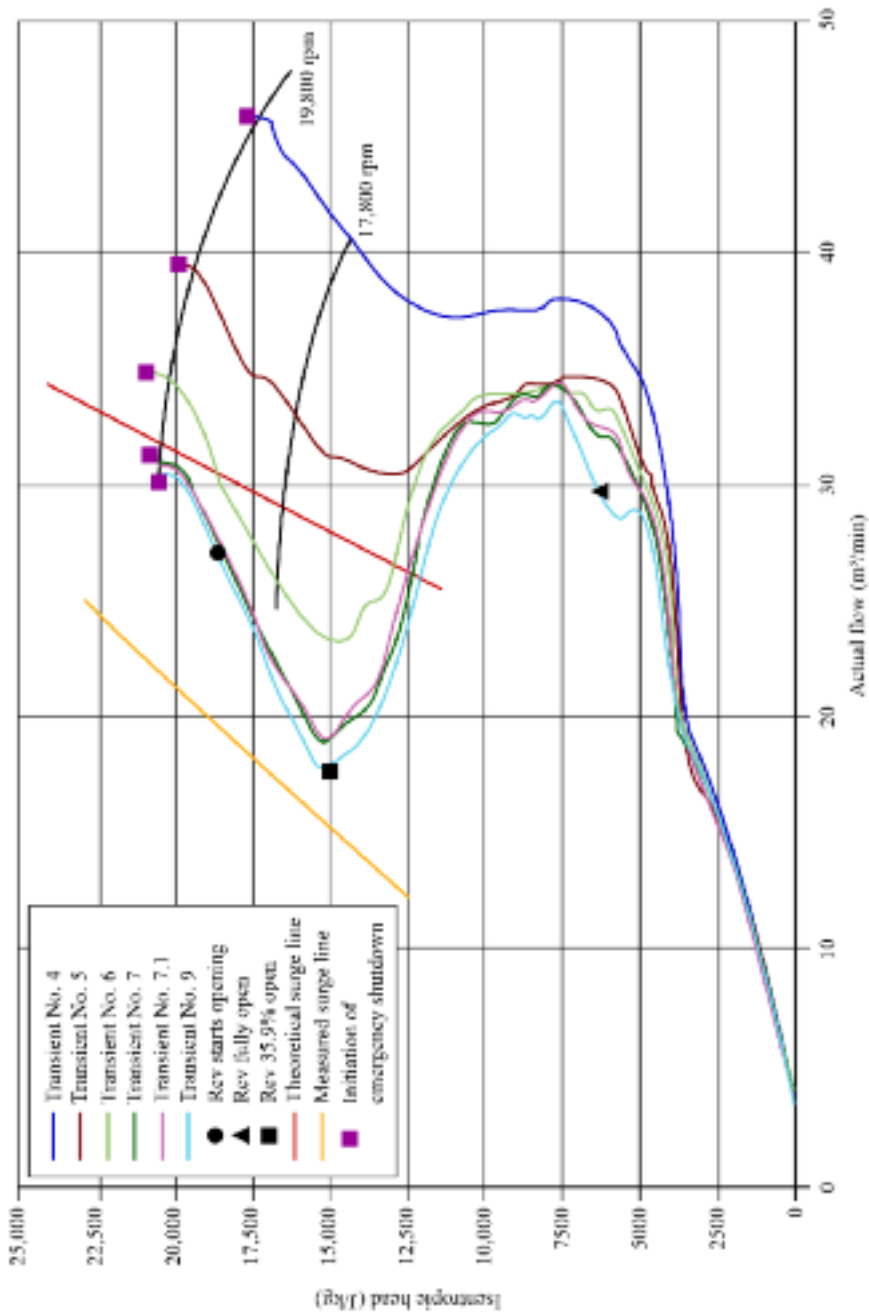

FIGURE 4.8. Transient shutdown loci measurements for 19,800 rpm.

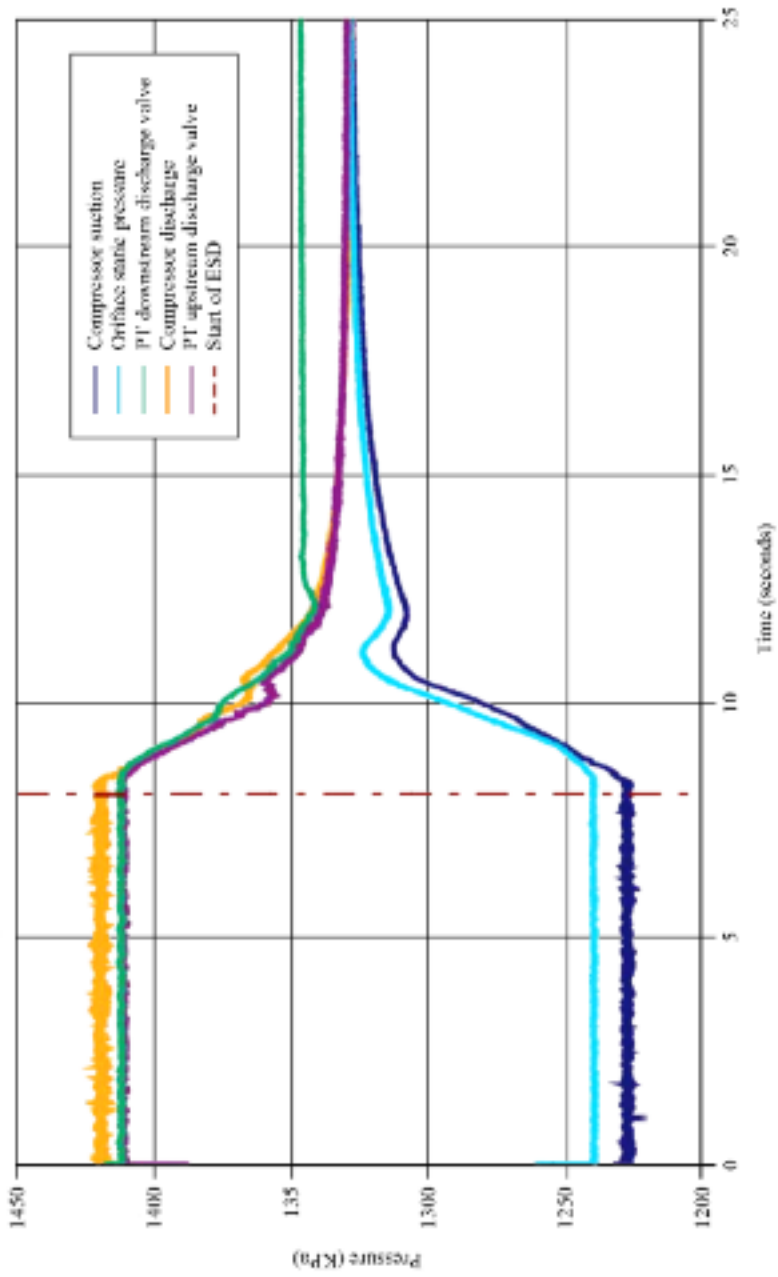

FIGURE 4.9. Pressure versus time for the transient No. 9 condition at 19,800 rpm.

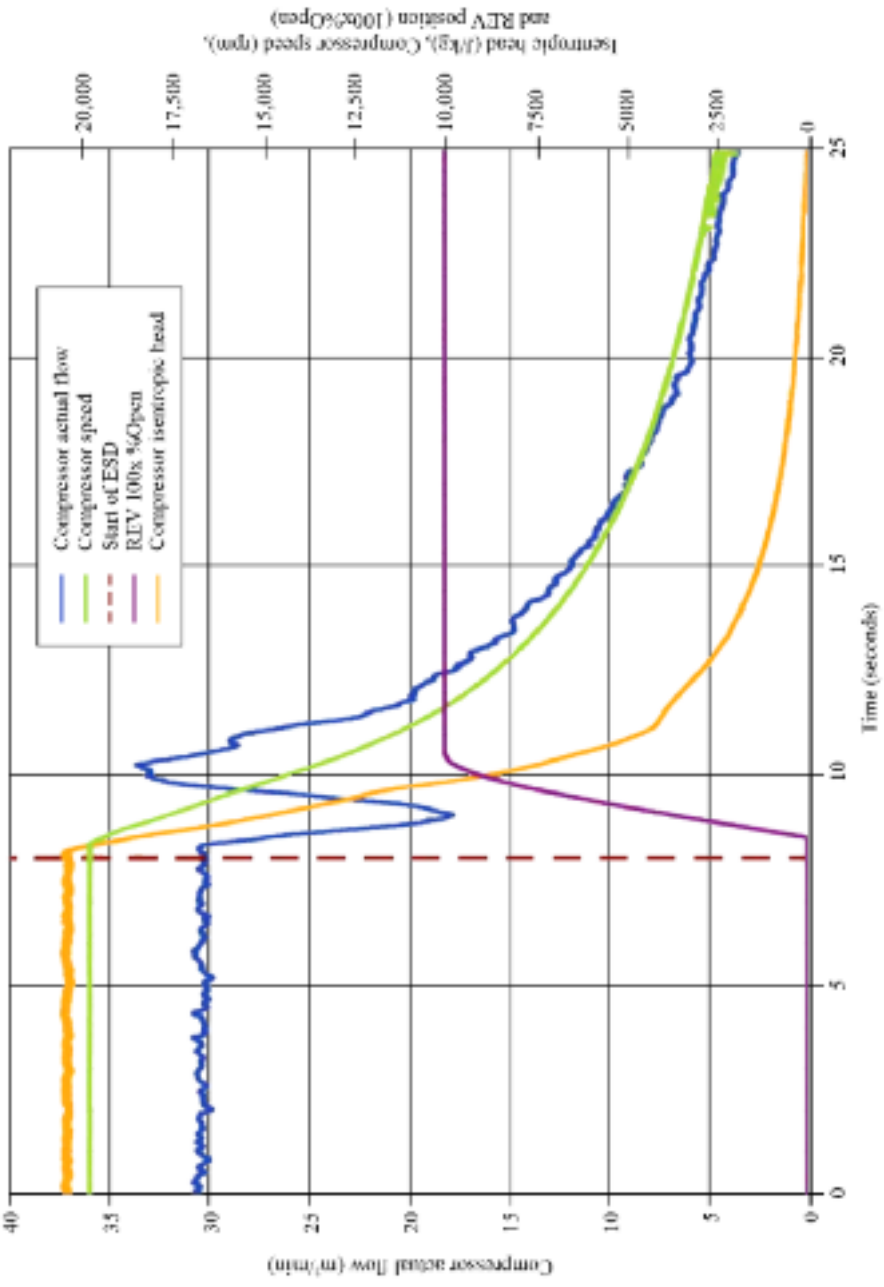

FIGURE 4.10. Compressor actual flow, compressor discharge pressure and speed, and anti-surge valve position versus time for the transient No. 9 condition at 19,800 rpm.

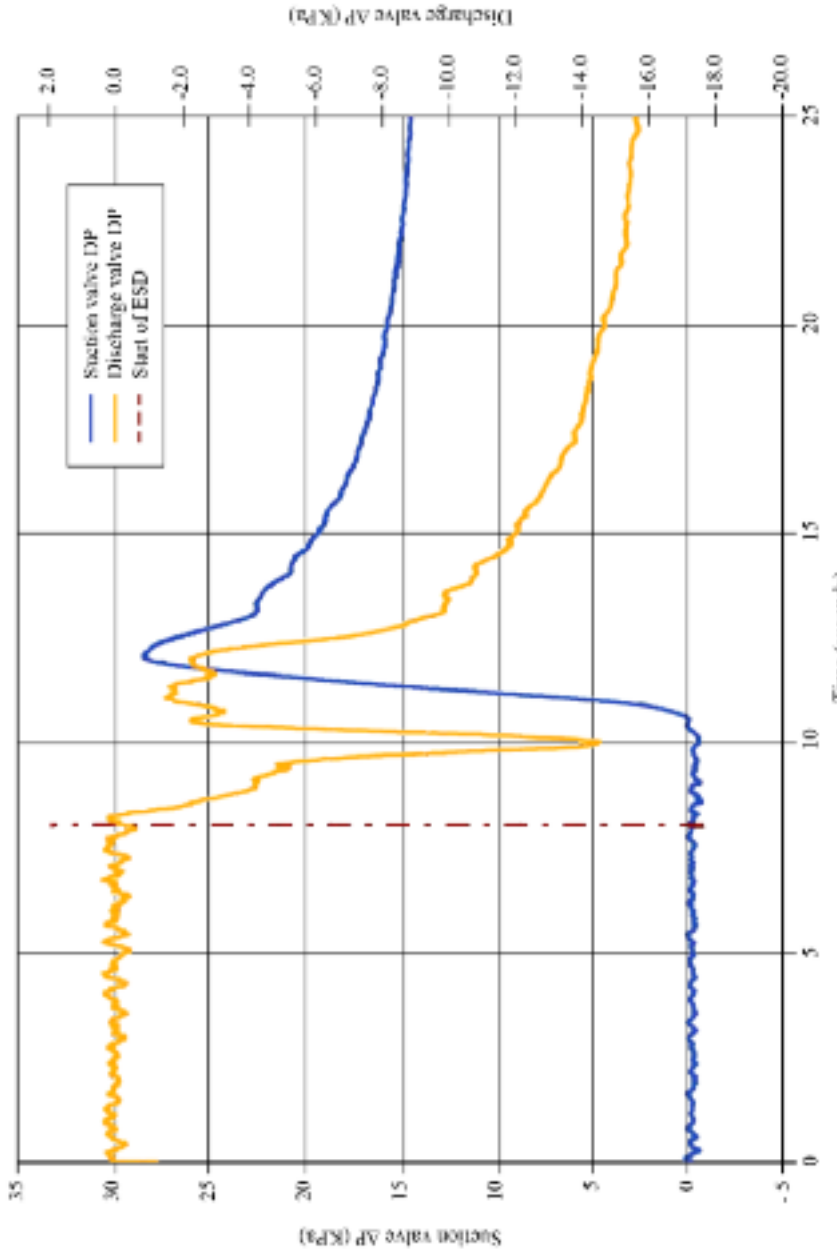

FIGURE 4.11. Differential pressure over unit valves for the transit No. 9 condition at 19,800 rpm.

Modeling

Data that we obtained from the metering research facility during the compression system's emergency shutdown comprised a complete data set which was necessary for the validation of a transient numerical simulation of compression system transient performance. We knew the compression system's geometry and its compressor characteristics. Consequently, we could use the metering research facility data to identify software-specific inaccuracies that would normally be hidden as a consequence of uncertainty associated with the input parameters. When considering how to best approach the compression system's transient numerical simulation, we can identify two stages in the modeling process:

- modeling based on known data at the beginning of a project — piping geometry, the compressors' performance maps, rotating system inertia and valve characteristics; and
- modeling based on the above and, additionally, knowledge of the compression system's rotating system deceleration rate.

We undertook a quantitative analysis of the metering research facility's compression system using the Stoner Pipeline Simulation® (SPS) software (Advantica, Inc., 2009). The Stoner Pipeline Simulation software solves non-linear systems of differential equations at each time-step. The software linearizes and discretizes the differential equations over small spatial intervals and iteratively determines a solution for the equations. The process of creating a system model commences with the creation of a functional process block diagram in the Stoner Pipeline Simulation software. One can then run a simulation using a model that the software generates from the functional process block diagram and an initial set of boundary conditions.

We created a function block diagram using the metering research facility piping and compressor geometry, plus the compressor performance map. We created a set of boundary conditions by taking valve opening and closing rates from manufacturers' datasheets and combined the actual metering research facility and compressor shutdown operating sequences into a generic emergency shutdown sequence. We ran emergency shutdown simulations from stable compressor operating points and then "tuned" the model to predict known steady-state parameters for a known operating point. We used pipe roughness, thermal and flow coefficients to adjust the model. We validated the model by comparing the simulation results to known steady-state parameters:

- compressor suction pressure;
- compressor discharge pressure;
- compressor inlet temperature;
- compressor outlet temperatures;
- compressor speed; and
- actual flow at a series of locations and operating conditions.

We both calculated and measured compressor deceleration rate, with the measured rate being slightly higher than the calculated rate (Figure 4.12). We calculated the rate using Equation 4, assuming that we could apply the incompressible fan laws to the compressor. This is probably responsible for the majority of the discrepancy between the calculated and measured compressor deceleration rate. We judged the agreement to be acceptable in those applications where it is not practical to measure the compressor deceleration rate.

A comparison between typical simulation results and measured data indicates that the prediction matched the measured data well at compressor speeds of 17,800 rpm (Figure 4.13) and 19,800 rpm (Figure 4.14). There is significant difference between the predictions when using the calculated and measured compressor deceleration rates; however, both predict well the shape of the compressor's performance characteristics during an emergency shutdown. The agreement between predicted and measured compressor performance characteristics, when based on either calculated or measured compressor deceleration rate, is good enough for either prediction to be useful in practical applications.

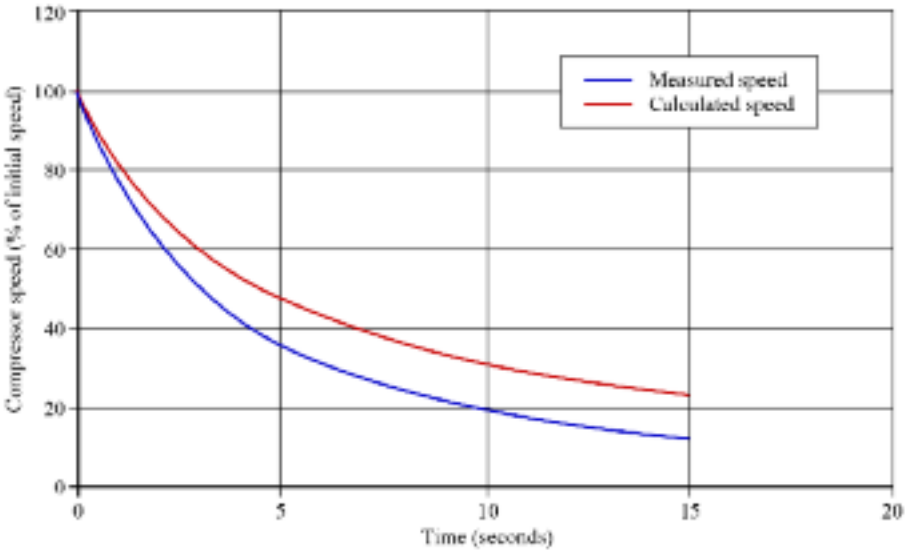

FIGURE 4.12. Measured versus calculated compressor deceleration rate.

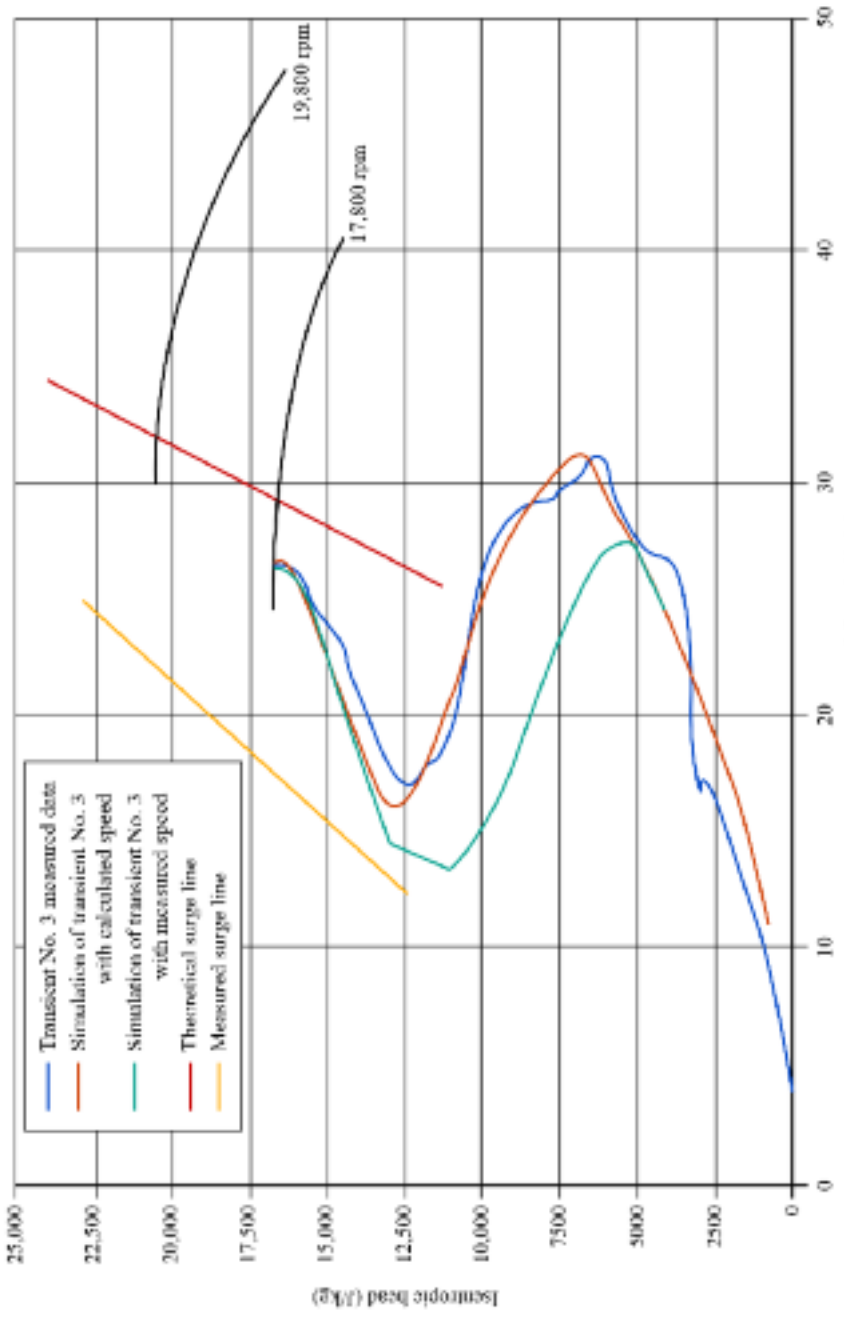

FIGURE 4.13. A comparison of measured and predicted compressor performance characteristics at 17,800 rpm. Performance is predicted using both calculated and measured compressor deceleration rates.

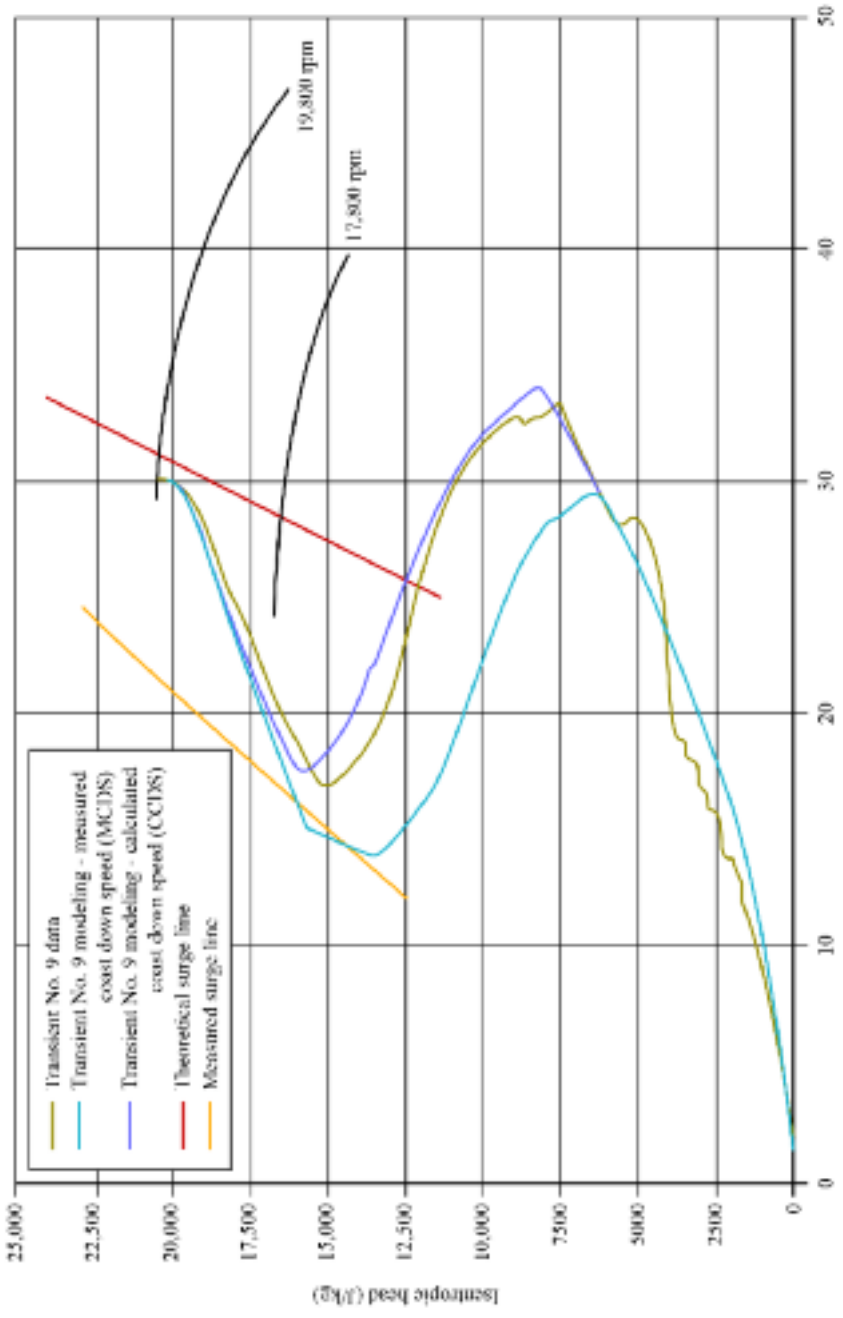

FIGURE 4.14. A comparison of measured and predicted compressor performance characteristics at 19,800 rpm. Performance is predicted using both calculated and measured compressor deceleration rates.

A comparison of measured and predicted temperature (Figure 4.15) indicates a near-constant discharge temperature during the 5 seconds following initiation of the emergency shutdown. The near-constant measured discharge temperature is primarily a consequence of the compressor's thermal mass and the thermowell's slow response time. Consequently, the measured discharge temperature does not fall with reduced compressor discharge pressure. In contrast, the measured suction temperature reacts to the hot gas inflow from the compressor discharge. A comparison between the measured and predicted pressures (Figure 4.16) indicates good agreement within the measurement's estimated 3 percent uncertainty.

MODELING SENSITIVITY ANALYSIS

We conducted a sensitivity analysis to better understand the impact of modeling errors for key parameters, comparing measured data for case No. 9 (Table 4.3) with predicted compressor performance characteristics (Figure 4.17). The installed anti-surge valve had a flow capacity, $C_{vmax} = 2.99 \times 10^{-4}$ $m^3/Pa^{½}s$, which we used in the baseline simulation. We repeated the simulation, assuming an anti-surge valve flow capacity of +50 percent, –50 percent and 200 percent of the value that we used in the base line simulation. The base line simulation showed good agreement with measured data. The –50 percent simulation resulted in a predated minimum flow just crossing the measured surge line. The +50 percent simulation resulted in a predicted minimum flow slightly further from the measured surge line than the base line simulation. The 200 percent simulation resulted in a predicted minimum flow significantly further from the measured surge line than the base line simulation. The results of the sensitivity analysis indicate that if we must estimate the anti-surge valve flow capacity, the conservative approach is to aim to underestimate, rather than overestimate, flow capacity.

SUMMARY

The purpose of this study in this chapter was to gather data during a compression system emergency shutdown. We conducted a series of emergency shutdown tests on a compression system in the Southwest Research Institute's metering research facility. We compared measured data with predicted compressor performance characteristics. We made the predictions using the Stoner Pipeline Simulation® (SPS) software. Overall, the Stoner Pipeline Simulation software predicted the compression system's transient behavior reasonably accurately without specific tuning of the model.

We used measured data to benchmark the Stoner Pipeline Simulation software prediction of transient compressor performance. The simulation underpredicts the compressor deceleration rate during an emergency shutdown. We used the Stoner Pipeline Simulation software to build a model of the metering research facility, and

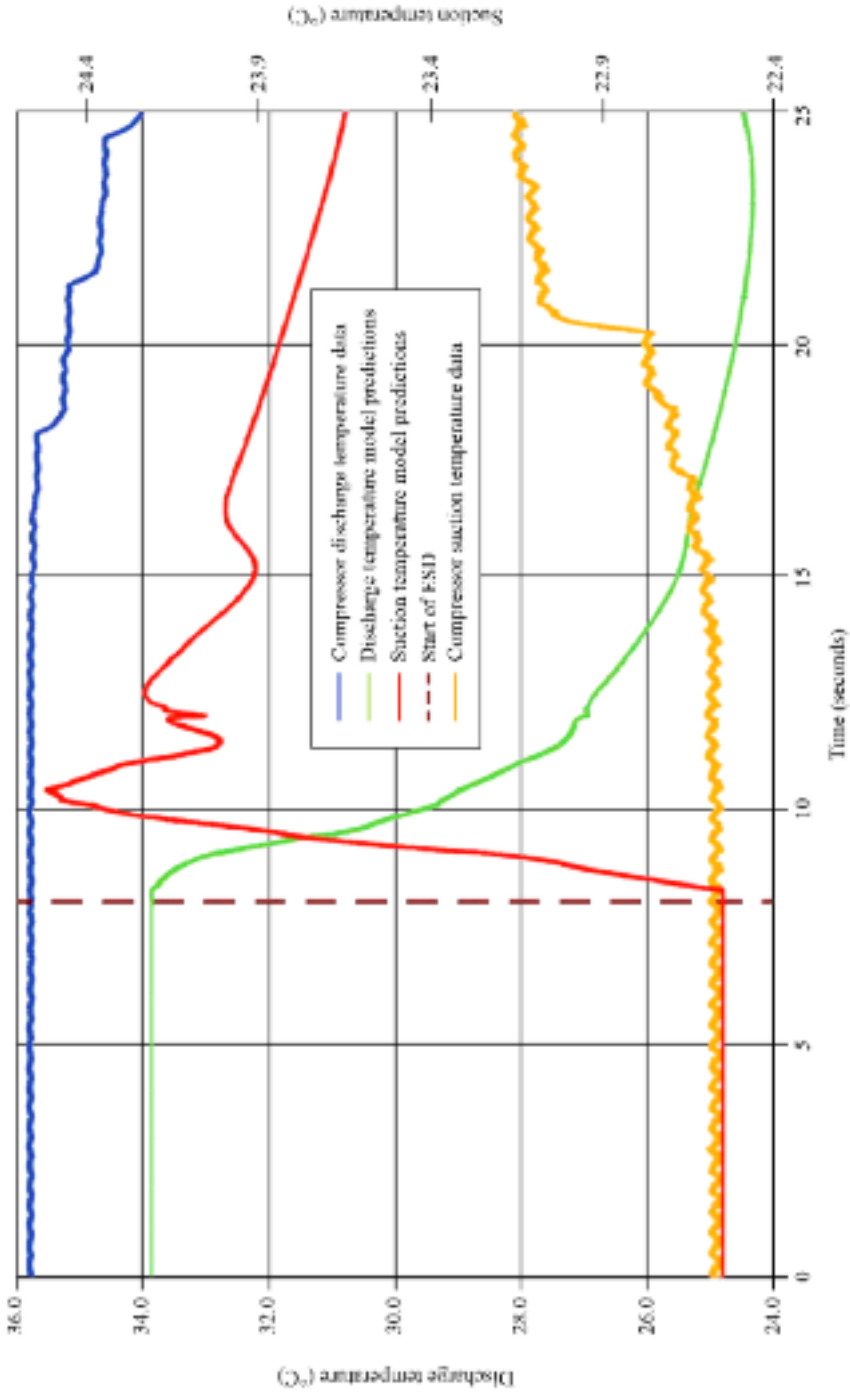

FIGURE 4.15. Temperature model predictions versus measured data for a 19,800 rpm emergency shutdown.

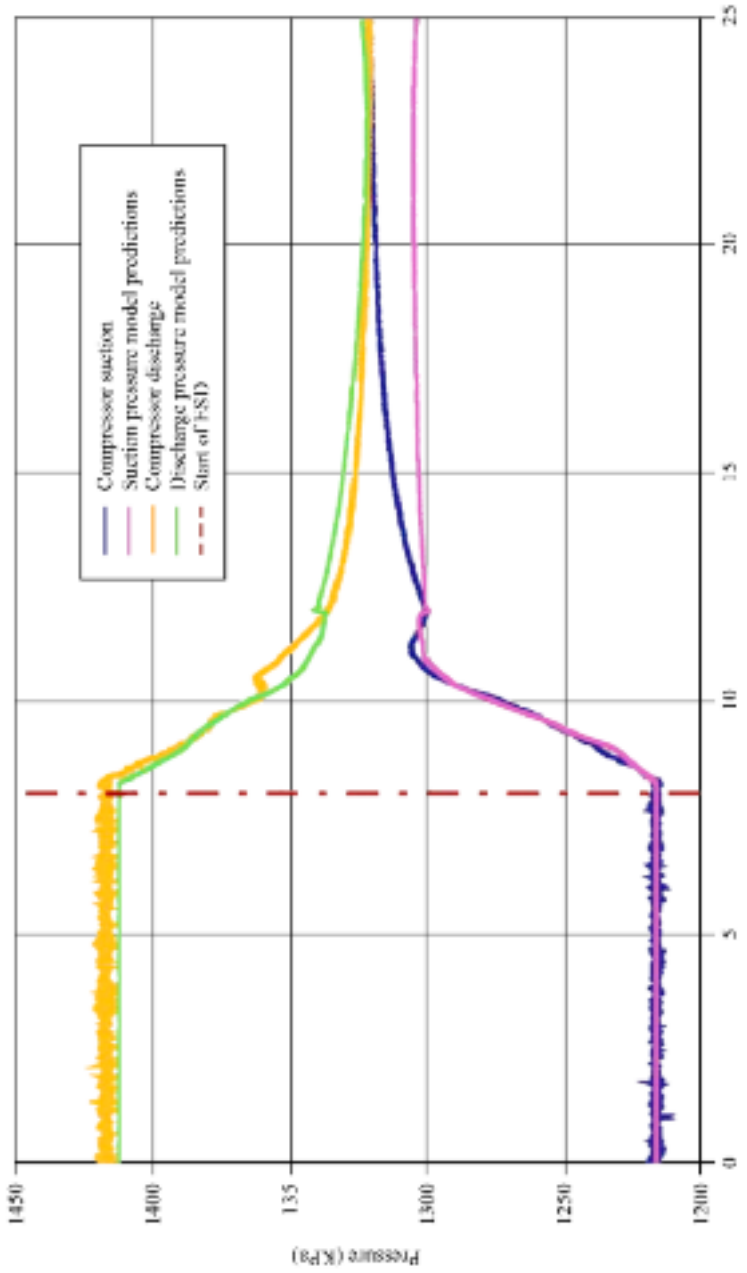

FIGURE 4.16. Pressured model predictions versus measured data for a 19,800 rpm emergency shutdown.

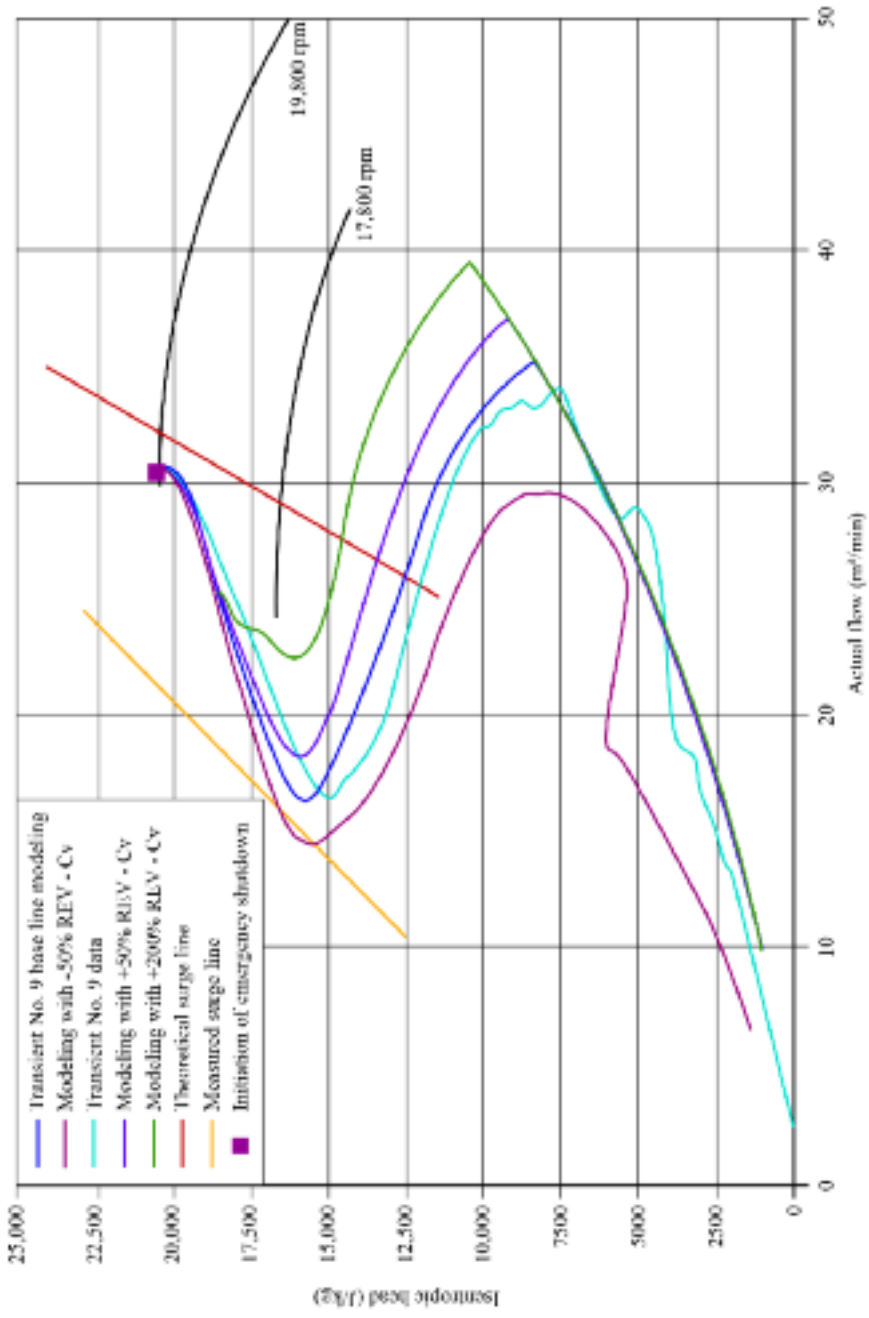

FIGURE 4.17. Anti-surge valve size sensitivity study from 19,800 rpm.

the compression system within it, that required an assumption about the compressor deceleration rate. The uncertainty in the assumed compressor deceleration rate is a source of error in the prediction, and therefore we can improve the accuracy of predictions by improving the accuracy with which we determine the compressor deceleration rate. Using measured pipe friction factors and actual valve opening times in their installed condition further refines the model.

The study in this chapter indicates that one can use the Stoner Pipeline Simulation software to predict if a compressor will surge during an emergency shutdown. When using the Stoner Pipeline Simulation software, a design engineer must remain aware that no simulation models all eventualities. Consequently, we recommend a 10 percent safety margin on flow at surge to ensure that the operator avoids surge during an in-service emergency shutdown.

REFERENCES

Advantica, Inc. (2009), "Stoner Pipeline Simulation (SPS) Reference Manual and Software".

Botros, K.K., and Ganesan, S.T. (2008), "Dynamic Instabilities in Industrial Compression Systems with Centrifugal Compressors", *Proceedings of the 37th Turbomachinery Symposium,* Houston, USA, 8–11 September, pp. 119–32.

Brun, K., and Nored, M. (2007), "Application Guideline for Centrifugal Compressor Surge Control Systems", Gas Machinery Research Council, available at: www.gmrc.org.

Kurz, R., and White, R.C. (2004), "Surge Avoidance in Gas Compression Systems", *Transactions of the ASME, Journal of Turbomachinery*, vol. 126, pp. 501–6.

Morini, M., Pinelli, M., and Venturini, M. (2007), "Application of a One-dimensional Modular Dynamic Model for Compressor Surge Avoidance", *Proceedings of the 52nd American Society of Mechanical Engineers Gas Turbine and Aeroengine Congress,* Montreal, Canada, 14–17 May, Paper No. GT2007-27041.

Ribi, B., and Gyarmathy, G. (1997), "Energy Input of a Centrifugal Stage into the Attached Piping System During Mild Surge", *Proceedings of the 42nd American Society of Mechanical Engineers Gas Turbine and Aeroengine Congress,* Orlando, USA, 2–5 June, Paper No. 97-GT-84.

White, R.C., and Kurz, R. (2006), "Surge Avoidance in Compressor Systems", *Proceedings of the 35th Turbomachinery Symposium,* Houston, USA, 25–28 September, pp. 123–34.

Chapter 5

Effects of Pulsations on the Stability of Compressors in Mixed Reciprocating and Centrifugal Compressor Stations

K. Brun and R. Kurz

ABSTRACT

Mixed operation with both centrifugal and reciprocating compressors in a compression system poses significant operational challenges. Pressure pulses and machine mismatches lead to poor centrifugal compressor performance and instability. Arrangements with reciprocating compressors placed in series with centrifugal compressors generally lead to higher suction and discharge pulsations than conventional parallel operation. By fitting pulsation attenuation devices in the interconnecting piping between compressors and matching the compressors' volumetric-flow rates, a design engineer can produce a functional compression system for even the worst case mixed centrifugal and reciprocating compressor combinations. Modeling an interconnecting piping system's transient flow characteristics during the compression system design process can assist the design engineer to avoid errors and minimize pressure losses. This chapter presents a methodology and examples of an analysis technique based on a one-dimensional transient Navier-Stokes solver. The analysis technique constitutes a tool that assists the design engineer in avoiding piping layout and compressor matching errors early in the compression station design. The chapter presents code development, discusses typical applications and provides example results for a set of mixed operational cases.

This chapter is a revised and extended version of Brun, K., and Kurz, R. (2010), "Analysis of the Effects of Pulsations on the Operational Stability of Centrifugal Compressors in Mixed Reciprocating and Centrifugal Compressor Stations", *Transactions of the ASME, Journal of Engineering for Gas Turbines and Power*, vol. 132, pp. 1–10.

NOMENCLATURE

A	pipe cross-sectional area
C	Brun-Kurz number
H	head
J	mass moment of inertia
P	pressure
Q	volume flow
V	volume
c	speed of sound
f	pipe friction
j	node number
k	pipe friction coefficient
m	Mach number
$\Delta\dot{m}$	mass flow pulsation
r	radius
t	time
u	local velocity
x, y	distance
z	piston position
γ	isentropic coefficient
λ	clearance volume
∂	viscosity
ρ	density
ϕ	crank angle
Γ	coefficient
ω	angular speed

Subscripts and superscripts

i	intersection
int	null node and intersection
j	node number
n	number of nodes in reach

INTRODUCTION

The mixed operation of centrifugal and reciprocating compressors in a single compression system has become common practice over the last 20 years. In mixed arrangement compression systems compressors are placed in parallel. Large gas turbine driven centrifugal compressors provide the base-load compression while smaller reciprocating compressors follow cyclical or peaking compression demands. In parallel operation the centrifugal compressor may experience pulsations from the reciprocating compressor on both the common suction and discharge headers. Good reciprocating compressor bottle and manifold design minimizes the impact of paral-

lel operation on centrifugal compressor operating stability, with well-designed mixed parallel compression systems having a history of good in-service reliability.

Some recent mixed compression system designs have placed reciprocating compressors in series with centrifugal compressors. Compression stations use mixed compression systems with the reciprocating compressor downstream of the centrifugal compressor in high pressure ratio applications. Reciprocating compressors are better suited to high-pressure application, and therefore placing a reciprocation compressor downstream of a centrifugal compressor can result in a more effective high pressure ratio compression system.

In gas gathering applications reciprocating compressors are placed upstream of a centrifugal compressor. Reciprocating compressors accept multiple low-pressure streams, with their collective output brought together into a single medium-pressure stream. The medium-pressure stream then forms the input to a centrifugal compressor. A system arrangement with multiple reciprocating compressors upstream of a single centrifugal compressor can lead to significantly higher pressure pulses on the centrifugal compressor inlet than those typical in parallel operation. These pressure pulses may affect the compressor's operational stability. Typically, a centrifugal compressor operating with a suction pressure of 40 Bar and discharge pressure of 70 Bar may experience upstream pulsations from a reciprocating compressor exceeding 10 Bar peak-to-peak, if one does not utilize pulsation attenuation devices such as bottles, choke tubes or orifice plates. Suction pressure variations of up to 25 percent present a challenge for any centrifugal compressor aerodynamic stability, especially if the compressor operates near its surge line.

This chapter presents a methodology and examples of an analysis technique which we derived from the chosen methodology. We modeled the pulsating pipe flow using a one-dimensional transient Navier-Stokes code. We used a reciprocating compressor model and a simple centrifugal compressor flow interface to generate the pulsating boundary conditions. We imposed the resultant impact of the combined pulsation including the effects of pipe resonant conditions on the centrifugal compressor operating map. We imposed the pulsation as either a suction or discharge pressure fluctuation to determine the effect on the compressor's operational stability. We present three case studies to illustrate the impact of pulsations on centrifugal compressor performance, surge margin and choke limit.

BACKGROUND

Classical reciprocating compressor manifold and piping design involves optimizing the selection of primary volumes, choke tubes and secondary volumes. Engineers use these elements when designing pulsation filters. The objective of a pulsation filter is to provide a settling volume for the unsteady flow entering and leaving the compressor cylinders. While providing sufficient settling volume, engineers also must design the primary volume, choke tubes and secondary volume to avoid "acoustic" resonance. Acoustic resonance is inherent in any compression system's installation piping and compressor station filter system (Smalley *et al*., 1995).

A centrifugal compressor either attenuates or amplifies pulsations at its discharge or suction side, because it reacts to any fluctuation in flow with a fluctuation in compressor discharge pressure and, thus, pressure ratio (Figure 5.1). Even well-designed pulsation dampeners for reciprocating compressors allow low-frequency pressure pulsations to enter the piping system (Kurz *et al*., 2006). When the pressure fluctuations are less than 1 Hz, the process control system may cycle the power which the gas turbine generates, and subsequently the centrifugal compressor's speed in the attempt to keep the suction or discharge pressure constant.

Sparks (1983) studied the cycling of centrifugal compressor speed and characterized the phenomenon as the interaction of a piping system with given acoustic impedance and a compressor in response to a change in flow and compressor discharge pressure. The piping impedance comprises a combination of:

- resistive impedance due to frictional losses;
- acoustic inertia due to the gas mass in the pipe; and
- stiffness due to compressibility of the gas within the pipe.

Two other published studies on the impact of flow pulsations on turbomachines complement Spark's (1983) report. Kurz *et al*. (2006) provided a literature review on the topic and Brun *et al*. (2007) presented an overview of the state-of-the-art in pulsation analysis techniques.

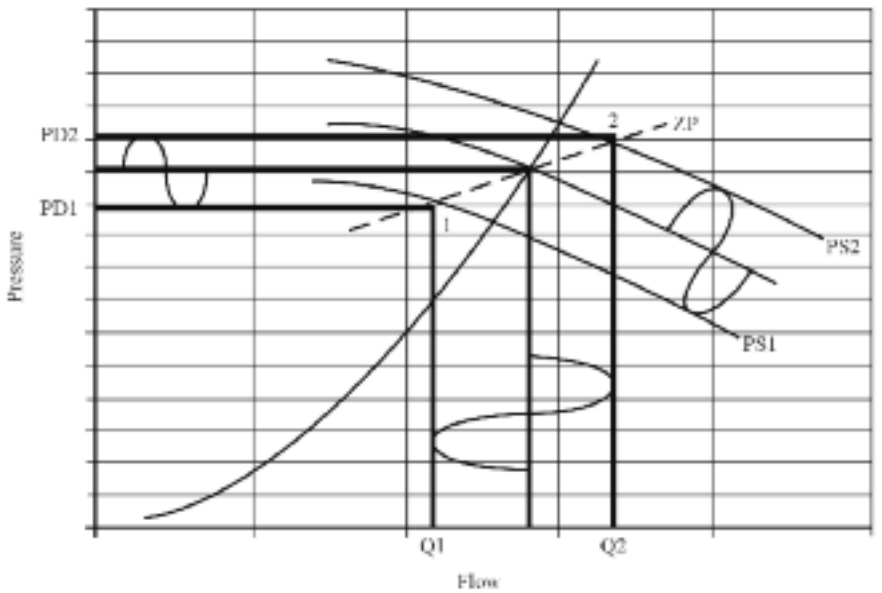

FIGURE 5.1. Pulsation transmission in centrifugal compressors (Sparks, 1983).

RATIONALE

When designing compression systems engineers have historically attempted to minimize the pressure pulsation impact by avoiding system resonant frequencies. Although pressure pulsations are undesirable and compression system performance would be enhanced if they were eliminated, simply ensuring that pressure pulse frequency does not coincide with a compression system resonant frequency is enough to avoid in-service reliability issues.

We may determine compression system resonance frequencies using transient acoustic wave equations to predict both compression system resonant frequencies and the effect of a specific compression system design on pulsation amplitudes. Resonant frequency prediction is generally good; however, predicting pulsation amplitudes is more prone to error. Predicting pulsation amplitudes is made challenging by the need for simplifying assumptions when applying the transient wave equations. The resulting equations do not fully model the compression systems and consequently, the error in predicting pulsation amplitude becomes significant.

An issue when predicting pressure pulse amplitude is that acoustic wave models focus on frequency only. They do not model the actual geometry of the interconnecting duct or take account of the pressure drops through that pipework. This inability to accurately predict pressure pulse amplitude has been tolerable when the compression system utilizes constant speed reciprocating and centrifugal compressors. However, when one or both is a variable speed device it becomes impossible to avoid compression system resonant frequencies under all operating conditions.

When we encounter compression system resonant frequencies during compression system operation, the accurate prediction of both resonant frequencies and pressure pulse amplitude becomes a critical input to the design process. First, centrifugal compressor stability is sensitive to highly pulsating flows (Kurz *et al*., 2006). Second, a failure to take into account both resonant frequency and pressure pulse amplitude during the design process has resulted in mechanical failure in-service of both the compression system piping and the piping support structure (Brun *et al*., 2007).

A one-dimensional representation of the Navier-Stokes equations can provide a physical basis for an analysis technique that can predict both compression system resonant frequencies and pressure pulse amplitude. When developing an analysis technique, one must model three transient fluid mechanisms:

1. pulsations generated by the reciprocating compressor;
2. pulsations generated by the reciprocating compressor that are amplified by an acoustic resonance within the piping system; and
3. a mismatch between the centrifugal and reciprocating compressors' operating points which causes one or both compressors to continuously "hunt" for a stable operating point.

Each of these mechanisms can drive the centrifugal compressor operating point into a surge condition, and so all are important to the design engineer. We may

analyze mechanisms 1 and 2 using the transient wave equations. However, the third mechanism requires a transient flow analysis as a consequence of the unbalance between the compressors. There is an operational unbalance because at a given running speed a reciprocating compressor is effectively a constant volume-flow machine. In contrast, centrifugal compressors have a fixed compressor discharge pressure-flow relationship. Any mismatch in volume flow between the compressors will create a pressure imbalance that moves the operating point of both centrifugal and reciprocating compressors. In most cases, this results in continuous low-frequency pressure fluctuations that are not necessarily periodic. This fluctuation is a function of the operating condition, compressor designs and the interconnecting piping geometry. The centrifugal compressor's control system often further complicates the analysis, which is designed to vary the compressor's speed to maintain either a constant discharge or suction pressure. The centrifugal compressor speed's continuous non-periodic cycling is often the result.

The challenges posed by an analysis technique that can model the three mechanisms associated with pulsating flow in a compression system are significant. Simplifying assumptions may still enable resonant frequency prediction with reasonable accuracy; however, it will inevitably compromise the accuracy of pressure pulse amplitude predictions. Consequently, an analysis technique based on a full solution of the Navier-Stokes equation, coupled with physical compressor models, is the most appropriate approach. Such an analysis technique has the potential to model the transient fluid flow through the compression system pipework and the interaction of interconnected reciprocating and centrifugal compressors.

ANALYSIS MODEL

The authors developed a full one-dimensional time-domain flow solver applicable to an interconnected manifold and piping system to determine the transient fluid pulsations in mixed reciprocating and centrifugal compression systems. This transient flow solver included all terms of the Navier-Stokes equations. We also derived physical models for both centrifugal and reciprocating compressors and implemented them into the analysis technique.

Compressor models

Two factors determine the state of the gas in any compressor manifold and attached piping system:

1. the compressor drive's kinematics, which provide a forcing inlet boundary condition to the piping system; and
2. the piping system's outlet boundary conditions.

A reciprocating compressor's piston position, z (ϕ), determines the cylinder boundary condition by:

$$z\varphi = \frac{V_x}{A_p} + r \times (1 - \cos\varphi) + \frac{r}{\lambda} \times \left(1 - \sqrt{1 - \lambda^2 \sin^2 \varphi}\right) \tag{1}$$

and the cylinder valve position, which is a function of the cylinder internal pressure. For a centrifugal compressor, we may derive boundary conditions directly from a specific compressor performance map (Figure 5.2). One must obtain this map from the centrifugal compressor manufacturer or from test data. For the sake of simplicity, we may further simplify the map by non-dimensionalizing the flow and compressor discharge pressure into characteristic psi-phi (Shapiro, 1996) curves. However, given the very short time constant of flow transients (in the order of 0.5 to 100 Hz) and the significant rotational inertia of a gas turbine driven centrifugal compressor, it is acceptable that the centrifugal compressor may be modeled as a constant speed machine. We can validate the assumption that the compressor is a constant speed machine for a given application by calculating a non-dimensional parameter that ratios pulsating aerodynamic torque on the impeller with the rotor's total angular inertia. We have derived and have successfully utilized the following non-dimensional (Brun–Kurz) number, C, for this analysis:

$$C = \frac{\omega w r^2 \Delta\dot{m}}{(2\pi) J f^2} \tag{2}$$

where $\Delta\dot{m}$ is the inlet mass flow pulsation peak-to-peak magnitude, ω is the angular speed of the centrifugal compressor, r is the tip radius of the centrifugal compressor impeller, J is the rotor's inertia and f is the pulsation frequency. For small values of the Brun–Kurz number the inertial forces dominate the pulsating aerodynamically induced torque, and one can assume that the impeller speed remains constant and unaffected by pulsations. This simplifies the centrifugal compressor boundary condition to a second order polynomial:

$$H = \Gamma_1 + \Gamma_2 Q + \Gamma_3 Q^2 \tag{3}$$

where we may determine the coefficients from the compressor map. We used a parabola here, but for some applications higher order polynomials can provide a better representation of the compressor map. The limits of this polynomial are surge on the low-flow side and choke on the high-flow side. Thus, for a given compressor speed, we utilize Equation 3 and the fan laws to obtain flow for a given pressure suction and discharge condition.

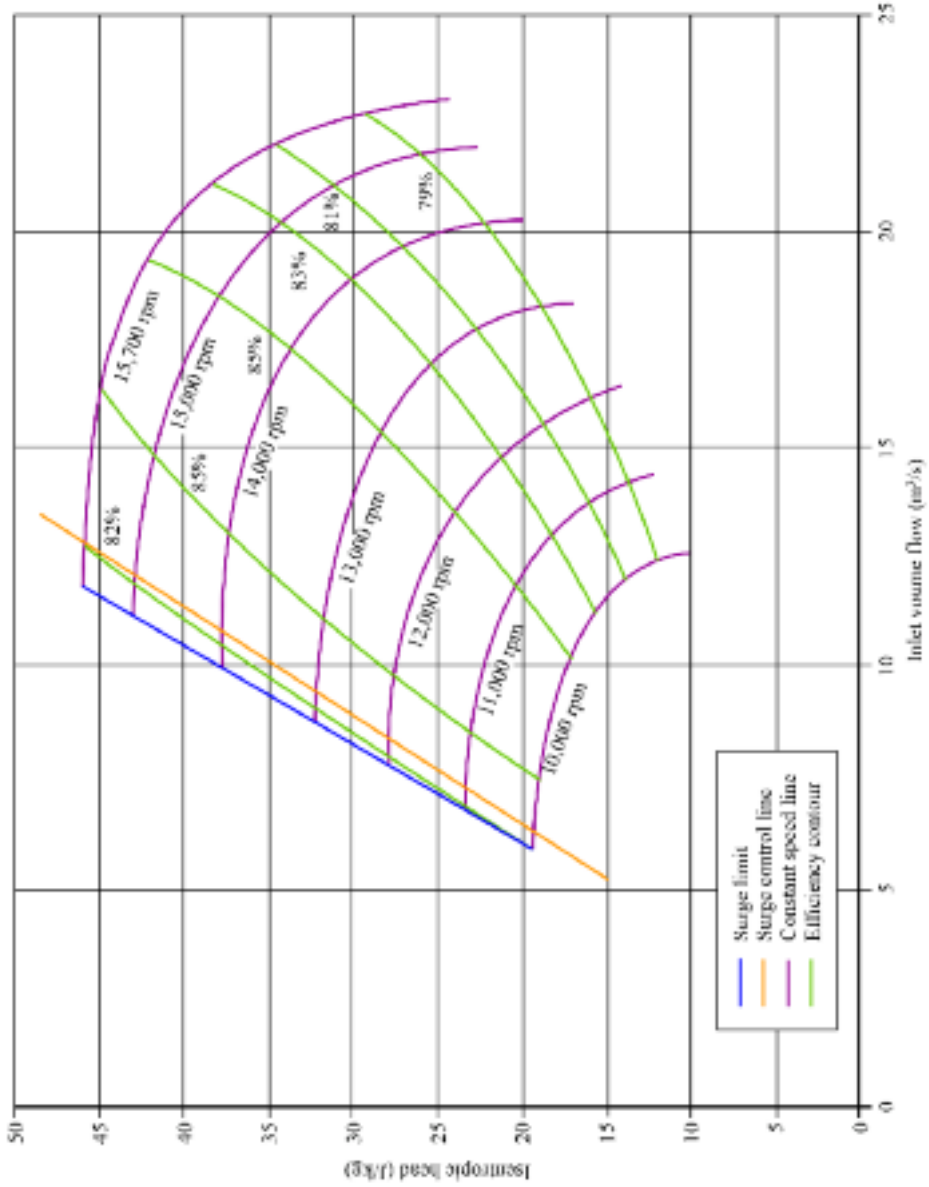

FIGURE 5.2. Typical compressor map for boundary condition.

Governing equations

Morini *et al*. (2006) provide a description of the governing equations of one-dimensional transient flow and, thus, we only briefly review the derivation. The Navier-Stokes continuity, momentum and energy equations govern compressible fluid flow in a compressor manifold system. In order to solve the Navier-Stokes equations for pressure and velocity in one dimension, we may use the momentum and continuity equations in combination with an equation-of-state. We express the transient one-dimensional momentum equation as:

$$\frac{\partial(\rho u)}{\partial t} + u\frac{\partial(\rho u)}{\partial x} + \frac{\partial P}{\partial x} = \mu\left(\frac{\partial^2 u}{\partial x^2} + \frac{\partial^2 u}{\partial y^2}\right) \tag{4}$$

The continuity equation is:

$$\frac{\partial \rho}{\partial t} + \frac{\partial(\rho u)}{\partial x} = 0 \tag{5}$$

In the above momentum equation, the viscosity, ∂, in the streamwise (x) direction is the combined viscosity and turbulent eddy viscosity, where we usually determine the turbulent eddy viscosity using a second order Reynolds number-based turbulence model. We can treat the second viscous loss term as a pipe friction loss, f:

$$f = \mu\left(\frac{\partial^2 u}{\partial y^2}\right) = \frac{1}{2}\rho u^2 k \tag{6}$$

We obtain the friction factor k from empirical models, in this case a Moody diagram. Note that the energy equation is not included here as one can solve it as a simple algebraic pressure loss equation.

A second order Reynolds number turbulence model determines and explicitly handles the turbulence eddy viscosity. In pipe flow, there are two terms in the momentum equation that include viscosity: (a) the second partial derivative in the streamwise direction, and (b) the second partial derivative in the stream-normal direction. We can treat the (b) term implicitly using a basic pipe friction loss coefficient which does not require viscosity directly. The (a) term does require viscosity and turbulence eddy viscosity and therefore requires explicit handling. To properly capture this term's non-linearity, small time-steps and fine grid spacing are necessary. Thus, the transient inviscid momentum equation is:

$$\rho\frac{\partial u}{\partial t} + \rho u\frac{\partial u}{\partial x} + \frac{\partial P}{\partial x} = 0 \tag{7}$$

Note that we eliminated the viscosity term in the above equation and so these equations are effectively Euler equations. However, we do not neglect the viscosity and pressure loss terms, but rather explicitly treat them at every time-step and use them to correct pressures and velocities at all nodes.

In order to account for changes in area in the system, we must include area in the continuity equation. We may regard area as constant with respect to time and space, and as such, we may bring it inside the derivative:

$$\frac{\partial(\rho A)}{\partial t} + \frac{\partial(A\rho u)}{\partial x} = 0 \tag{8}$$

We can rewrite the momentum equation as:

$$\frac{\partial}{\partial t}(\rho u) + \frac{\partial}{\partial x}(\rho u^2 + P) = 0 \tag{9}$$

For acoustic applications, we substitute the speed of sound, c, for density as we can determine directly the speed of sound from the equation of state:

$$c^2 = \left(\frac{\partial P}{\partial \rho}\right) \tag{10}$$

which we can also write as:

$$c = \sqrt{\frac{\gamma p}{\rho}} \tag{11}$$

for a real gas. Thus, we can write the final equations as:

$$\frac{\partial}{\partial t}\left(\frac{PA\gamma}{c^2}\right) + \frac{\partial}{\partial x}\left[\frac{PA\gamma u}{c^2}\right] = 0 \tag{12}$$

$$\frac{\partial}{\partial t}\left[\frac{P\gamma u}{c^2}\right] + \frac{\partial}{\partial x}[P\gamma m^2 + P] = 0 \tag{13}$$

Numerical method

We selected the Lax-Wendroff method for speed and stability as the most appropriate numerical approach to solve the above equations. Fletcher (1991) describes

the method, hence we will only briefly summarize it. The Lax-Wendroff method uses a basic forward time and centered space numerical approximation as a first step, but requires finding an intermediate time solution at $t = *$ and an intermediate space solution at $x = j + 1/2$. One applies a centered space and forward time scheme at the intermediate time step in the second step equation to derive the final spatial and time derivatives.

We can express the momentum and continuity equations above in the following form for the numerical approximation scheme:

$$\frac{\partial \overline{q}}{\partial t} + \frac{\partial \overline{F}}{\partial x} = 0 \tag{14}$$

where q and F are vectors:

$$q = \begin{bmatrix} \dfrac{PA\gamma}{c^2} \\ \dfrac{P\gamma u}{c^2} \end{bmatrix} F = \begin{bmatrix} \dfrac{PA\gamma u}{c^2} \\ P(1 + m^2\gamma) \end{bmatrix} \tag{15}$$

As we previously noted, the energy equation and viscosity are decoupled and treated explicitly in between time-steps to enhance computational efficiency. This results in a two-equation model with the requirement for relatively small time-steps, but a time-space step dependency. We can divide the viscous energy loss terms into pipe friction loss and through-flow viscous energy dissipation. We calculate both terms separately and apply them at all nodes. One should note that the viscous through-flow energy dissipation represents the velocity gradient losses in the pipe flow direction, which is usually very small for steady flow, but can be significant for pulsating flows. One must also include the conventional pipe friction loss, as it accounts for the normal flow gradient viscous losses, which are primarily steady-state effects.

Within the research that we report in this chapter, we also developed a three-equation model with the energy equation coupled and compared it to the two-equation model. As differences were negligible, we chose to develop the two-equation model. Note that the system's energy losses are effectively pressure drops which we can obtain from empirical pipe friction formulations. In contrast, the viscosity term results in an enthalpy reduction that one must convert to a pressure drop if we are to take it into account in the above model.

Unless one utilizes a cooler, measurements at many compression stations have shown that gas temperature drops between compressor discharge and station exit are less than 0.5ºC because of the dominant convection heat transfer from the process gas. Even at very low ambient conditions, the gas temperatures throughout compressor systems are usually constant and, thus, we can neglect the influence of heat transfer on the pulsation. Nonetheless, the model does allow for gas temperature changes,

but they are included in the model in the form of gas property changes from the particular gas mixture's real equation-of-state rather than heat transfer in the energy equation.

Equation discretization

We solved the spatial derivative at every half-step using the following equation to yield an intermediate transient derivative at time = *:

$$\left[\frac{\partial q}{\partial t}\right]^{*}_{j+1/2} = -\left[\frac{\partial F}{\partial x}\right]^{n}_{j+1/2} \tag{16}$$

In discretized form, using a forward time and centered space method, the above derivatives become:

$$\frac{q^{*}_{j+1/2} - q^{n}_{j+1/2}}{0.5\Delta t} = -\left[\frac{F^{n}_{j+1} - F^{n}_{j}}{\Delta x}\right] \tag{17}$$

We solved the time derivative for the intermediate time-step. We assumed that a linear relationship exists, q_j and q_{j+1}, and we used a weighted value based on the physical length of ∂x_{j-1} and ∂x_j to estimate q at $j + 1/2$ for $t = n$:

$$q^{n}_{j+1/2} = q^{n}_{j} + (q^{n}_{j+1} - q^{n}_{j})W_i \tag{18}$$

where:

$$W_i = \text{weighting factor} = \frac{\Delta x_{j-1}}{(\Delta x_{j-1} + \Delta x_j)} \tag{19}$$

The resultant equation for the first time-step was:

$$q^{*}_{j+1/2} = -\frac{0.5\Delta t \cdot (F^{n}_{j+1} - F^{n}_{j})}{\Delta x} + 0.5 \cdot (q^{n}_{j+1} + q^{n}_{j})_i \tag{20}$$

For the second time-step, we applied the governing equation to provide the final q values at $x = j$ and $t = n + 1$, namely:

$$\left[\frac{\partial q}{\partial t}\right]^{n+1}_{j} = -\left[\frac{\partial F}{\partial x}\right]^{*}_{j} \tag{21}$$

The discretized version of the second time-step equation, using a forward time and centered space scheme, resulted as follows:

$$q_j^{n+1} = q_j^n - \frac{\Delta f}{(0.5\Delta x_{j-1} + 0.5\Delta x_j)} \cdot [F^*_{j+1/2} - F^*_{j-1/2}] = q_j^n - \frac{2\Delta t}{(\Delta x_{j-1} + \Delta x_j)} \cdot [F^*_{j+1/2} - F^*_{j-1/2}] \tag{22}$$

Figure 5.3 graphically represents this discretization formulation. Fletcher (1991) describes the advantages and limitations of the above described method, so we do not discuss them further here.

In a complex piping system, one must solve the above set of equations individually for all pipe segments with the appropriate inlet and outlet conditions updated at each time-step. Within each pipe segment, we utilized the simple central difference discretization and time-space forward marching solution. We determined pressure losses inside the pipe and at the interfaces from basic pipe friction loss models and viscosity losses which we directly calculated from the momentum equation's discretized viscosity term. We applied these two terms at every time-step at every applicable node. Thus, we did not treat the viscous terms simply as a pipe friction loss, but also included a discretization of the x viscous term in the flow direction. We calculated the x discretized term and the pipe friction viscous term for each node after

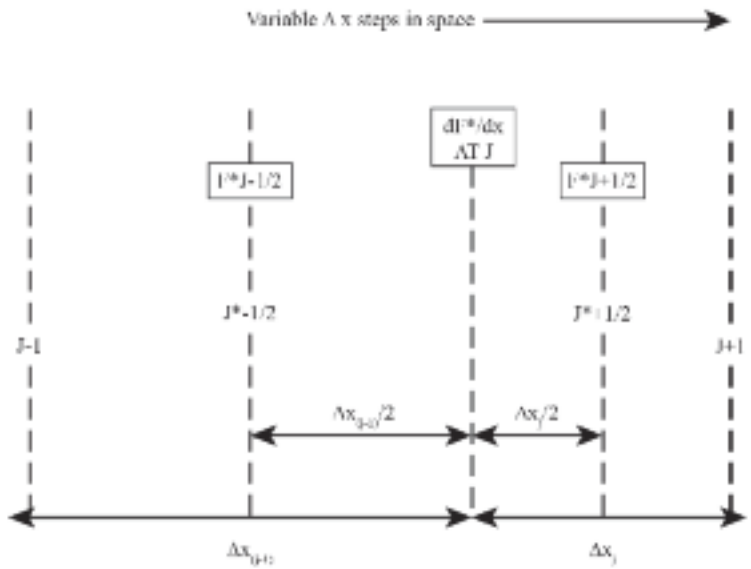

FIGURE 5.3. Lax-Wendroff discretization.

determining the half-step ($j + 1/2$) and then included them to determine the full-step ($j + 1$). This allows for coupling the viscous terms with the momentum equations' inertial and pressure terms.

Pipe inlet and outlet boundary conditions were enforced at every time-step. These boundary conditions were either forced, re-active or passive functions. For example, a simple sine wave or square wave pipe inlet or outlet boundary condition is a forced boundary condition. In contrast to pipes, reciprocating and centrifugal compressors required reactive boundary conditions as their responses are functions of the pressures and velocities at the pipe inlet or outlet from the previous time-step. For the same reason boundary conditions for pipe intersections were also re-active, as they depend on the surrounding nodes' previous time-step flow conditions. Finally, closed ends, wide-open ends and infinite pipes required passive boundary conditions as they simply enforce fixed or floating pressure and velocity values at every time-step.

Pipe interfaces

Formulations are necessary to determine boundary conditions at multiple pipe interfaces, such as pipe tees or joints. One may apply the continuity equation to determine the resulting velocity in each pipe inlet and outlet. Figures 5.4 and 5.5 show examples for two case studies.

If two inlet flows (Reach 0 and 1) combine to provide a final output flow (Reach 2) as in Figure 5.4, then we can derive the equations for the velocity at the intersection point based on the velocities in each reach as follows:

$$u_{\text{int}}^{0} = \frac{u_{j-1}^{0} \cdot A_{j-1}^{0}}{A_{\text{int}}} \tag{23}$$

$$u_{\text{int}}^{1} = \frac{u_{j-1}^{1} \cdot A_{j-1}^{1}}{A_{\text{int}}} \tag{24}$$

where:

$$A_{\text{int}} = \frac{(A_{j}^{0} + A_{j}^{1} + A_{j}^{2})}{3} \tag{25}$$

$$u_{\text{int}}^{2} = \frac{u_{\text{int}}^{0} \cdot A_{j}^{0} + u_{\text{int}}^{1} \cdot A_{j}^{1}}{A_{j}^{2}} \tag{26}$$

We used the intersection point's average area to solve for the inlet velocity in each reach. We assumed that pressure was equal at the intersection point at each time-step. We used the pressure in each reach at the node previous to the reach ($j - 1$)

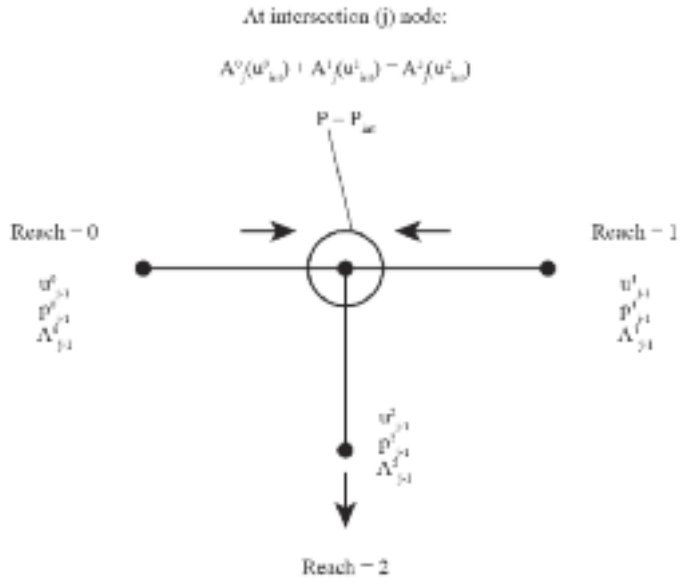

FIGURE 5.4. Branching node intersection (two inlets/one outlet).

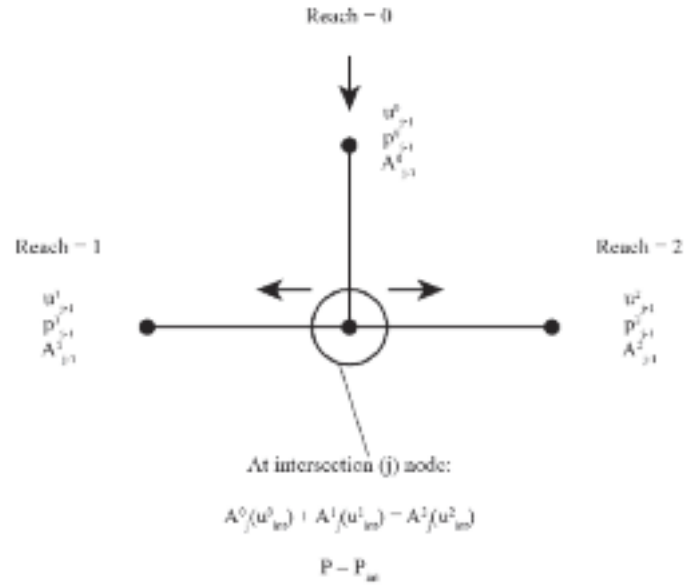

FIGURE 5.5. Branching node intersection (one inlet/outlet).

to determine the weighted contribution towards the pressure at the intersection point. The pressure is weighted by multiplying by the area of the reach and its corresponding delta *x* length. We used the following equation to determine pressure at the intersection point:

$$P_{\text{int}} = \frac{\sum_{n-1}^{3} (P_{j-1}^{i} \cdot A_{j-1}^{i})}{\sum_{n-1}^{3} (A_{j-1}^{i})} \tag{27}$$

Using these equations, we based the velocity at the intersection point in each reach on continuity, and based the pressure at the intersection point on the pressures' weighted average in each reach. The interface nodes are actually zero-volume nodes and, thus, although we used integral expressions, there is no difference between this approach and any differential interface implementation. As we determined the interface pressures and mass flows from a balance of the surrounding nodes, we implicitly included the governing equations' transient terms.

End conditions

We also must define boundary end conditions, such as open-ended pipe, closed pipe or infinite pipe, which we relatively straightforwardly determine from basic physics. At an open-ended pipe, we set the interface node pressure to ambient while conserving velocity. Similarly, at a pipe closed-end, we set the velocity to zero to maintain pressure. As compressor cylinders are varying-volume machines, we found that boundary conditions based on velocity rather than pressure were more practical to implement. Table 5.1 presents applicable boundary and interface conditions.

Code implementation

We coded the unsteady one-dimensional Navier-Stokes equations for a system of pipes with multiple interfaces and standard boundary conditions. Interfaces between pipe segments can be one-on-one, two-on-one, one-on-two, one-on-three or three-on-one and include discrete pressure drops at the segment interfaces. Other boundary conditions are either passive (closed wall, open wall, infinite pipe) or active (compressor, sine wave, square wave). The pipe areas can change either gradually (transition piece) or abruptly (open-end or bottles) within the pipes or at the pipe segment interfaces. We successfully tested models with up to 60 interconnected pipe segments. We also implemented a Windows file pre-processor, graphical user interface and graphical post-processor for frequency and time domain data. Figure 5.6 presents the user interface for a typical compression station model. Brun *et al.* (2007) present a detailed validation of the code.

Table 5.1. *Pipe interface and end conditions.*

Active	Passive	Pipe interfaces	In-pipe
Compressor cylinder	Infinite end	1-1 pipes	Orifice plate
Centrifugal compressor	Open end	2-1 pipes	Discrete pressure drops
Sine wave	Closed end	3-1 pipes	
Square wave	Transitions		

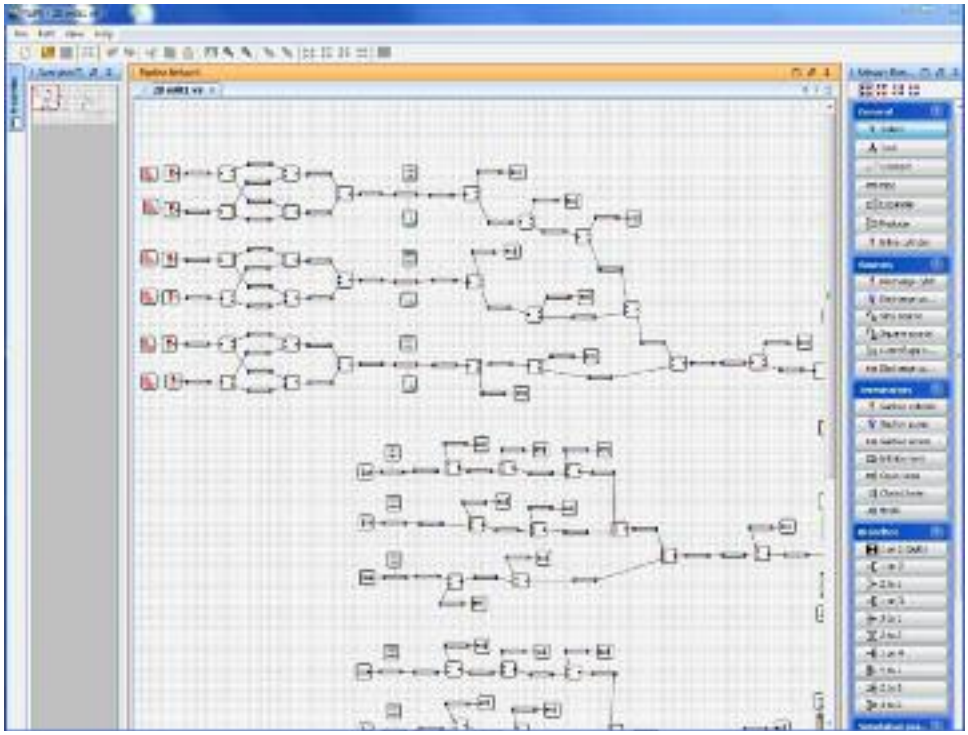

FIGURE 5.6. Graphical user interface for the solver.

CASE STUDIES

We utilized the above-described code to determine the transient flow and operation of a set of simple compression systems (Figures 5.7, 5.8 and 5.9). We chose these idealized cases to illustrate the methodology. In these cases, we mounted a double-acting reciprocating compressor comprising two single-ended cylinders at 180 degrees out of phase 30 meters upstream from a centrifugal compressor. Case 1 is straight pipe, while Cases 2 and 3 include pulsation attenuation devices in the pipe system. Case 2 incorporates an orifice with an area ratio 1:5, while Case 3 has a

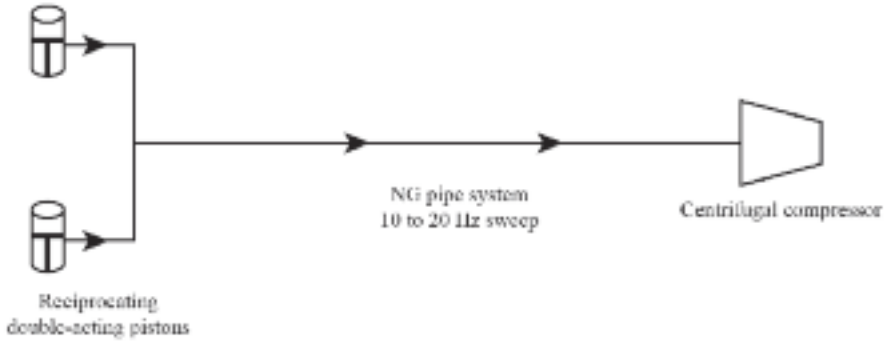

FIGURE 5.7. Case 1 — reciprocating compressor upstream of centrifugal compressor.

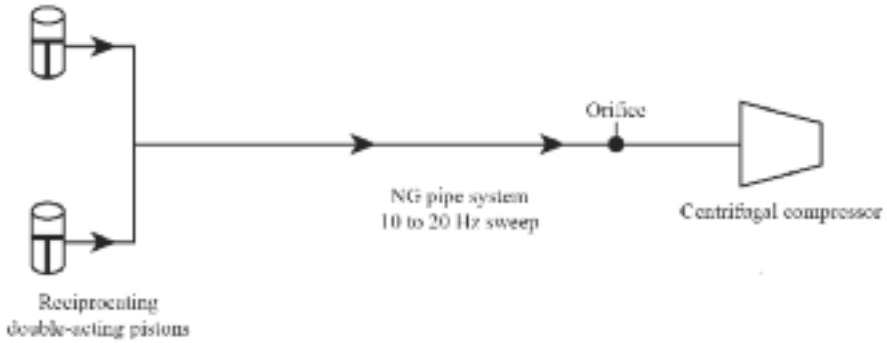

FIGURE 5.8. Case 2 — reciprocating compressor upstream of centrifugal compressor with orifice plate.

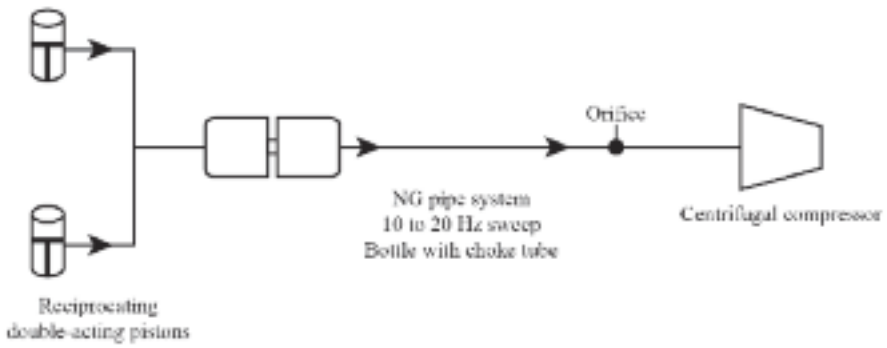

FIGURE 5.9. Case 3 — reciprocating compressor upstream of centrifugal compressor with bottle, choke tube and orifice plate.

bottle with internal choke tube (bottle area ratio 6:1, choke tube area ratio 1:4) and also an orifice plate (area ratio 1:5). The fluid in the system is methane at an absolute pressure of 2089 kPa at the reciprocating compressor discharge, a speed of sound of 444 meters per second and an isentropic coefficient of 1.35. The reciprocating compressor has the following design data:

Stroke: 0.2 m
Bore area: 0.05 m^2
Rod length: 0.5 m
Speed: 10–20 Hz
Pressure ratio: 2.0
Clearance volume: 5 percent (0.0005 m^2)

The resulting flow ranged between 1.6 and 3.3 kilograms per second and the power ranged between 160 and 340 kW depending on compressor speed. Figure 5.10 shows the power required and flow produced by the reciprocating compressor over a speed sweep from 10 to 20 Hz. For this example, the centrifugal compressor modeled as operating at the lower end of its compressor discharge pressure-flow map at a constant speed of 8000 rpm. The non-dimensional Brun–Kurz number that relates rotor inertia to aerodynamic pulsation torque ranges between 0.001 and 0.002, which indicates that the centrifugal compressor's angular speed will not fluctuate due to the inlet pulsations. To simplify the example, we assumed that the compressor operates on constant speed control. Thus, as the reciprocating compressor speed and flow increases, the downstream centrifugal compressor will simply follow its speed line and decrease compressor discharge pressure until it reaches choke. The surge limit at 8000 rpm is at a minimum flow of 1.7 kilograms per second and choke is at a minimum pressure ratio of 1.1.

Compressor inlet pulsations

Figure 5.11 presents the transient flow field at the compressor inlet. We can observe high-velocity fluctuations, with the compressor inlet flow velocity fluctuations largest at about 7 seconds into the speed sweep. Inlet flow velocity pulsations continuously reach negative values between 6 and 10 seconds of the sweep. In this case, we performed a 10 to 20 Hz frequency sweep over a 10 second interval, and deduced that the compressor would experience inlet flow reversal and therefore surge at any reciprocating compressor operating speed above 16 Hz. Thus, it was apparent that the compression system would not operate as designed over the full speed range.

To perform a more rigorous analysis, it is convenient to plot pressure versus frequency to determine not just pulsations, but also any low-frequency total pressure trends. Figures 5.12, 5.13 and 5.14 present the compressor inlet pressure as a frequency function for Cases 1, 2 and 3, respectively. Both Cases 2 and 3 utilize pulsation attenuation devices and thus, have significantly lower pulsations than Case 1. We see peak amplitudes at compressor speeds of 18, 17 and 19 Hz for Cases 1, 2 and 3, respectively.

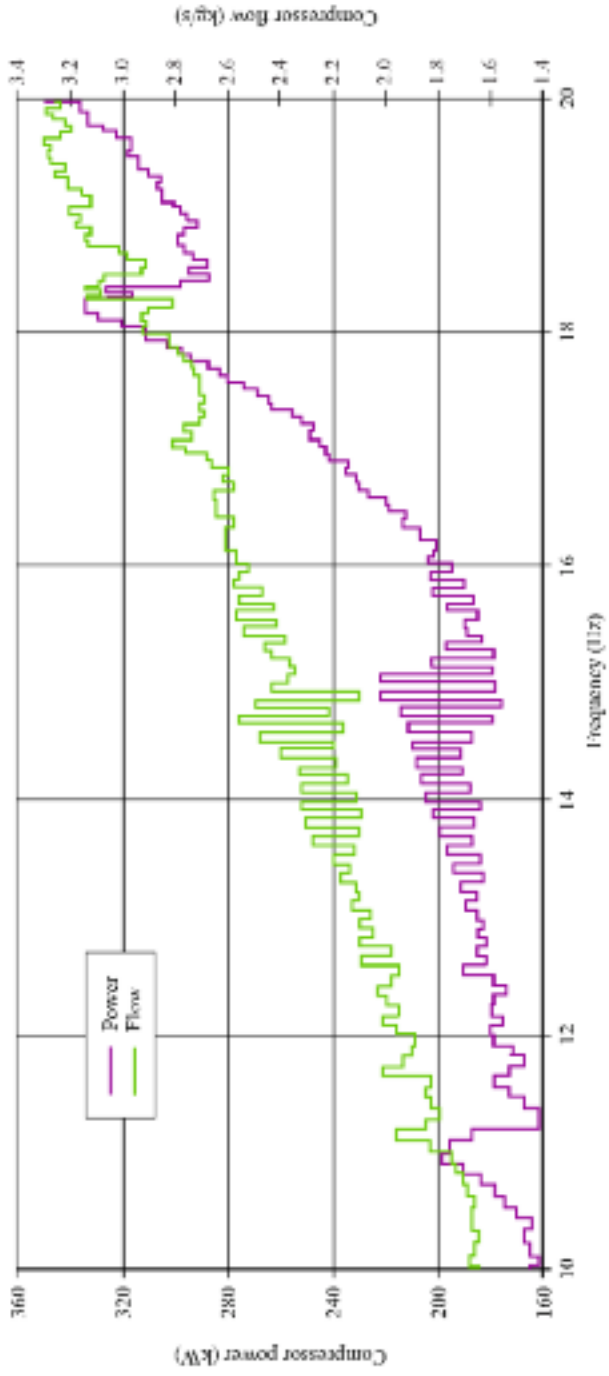

FIGURE 5.10. Reciprocating compressor power required.

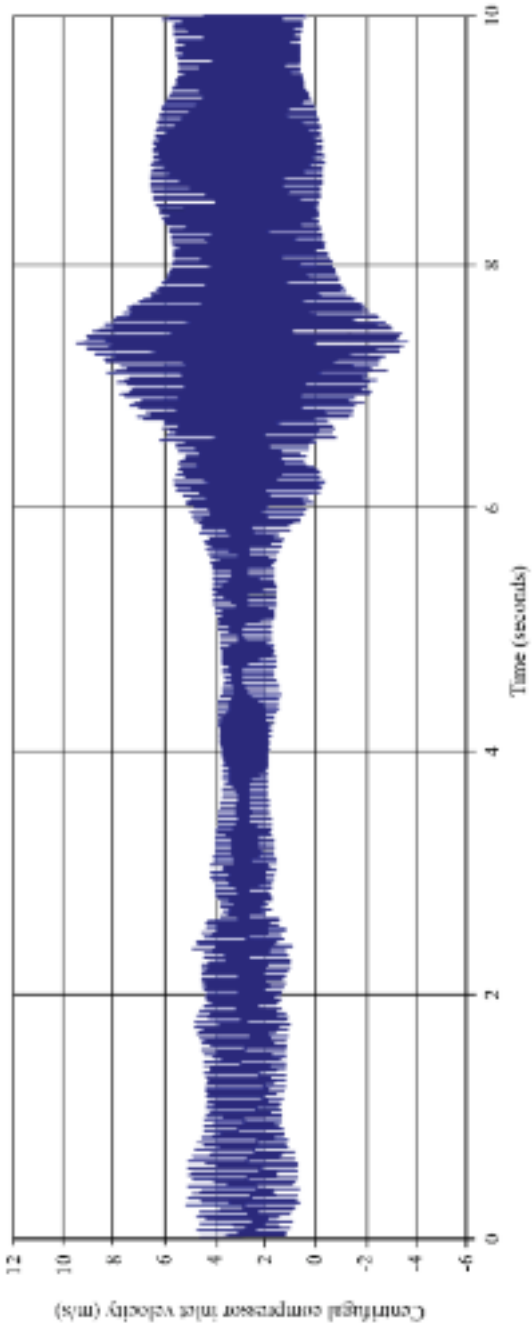

FIGURE 5.11. Case 2 — centrifugal compressor inlet velocity versus time.

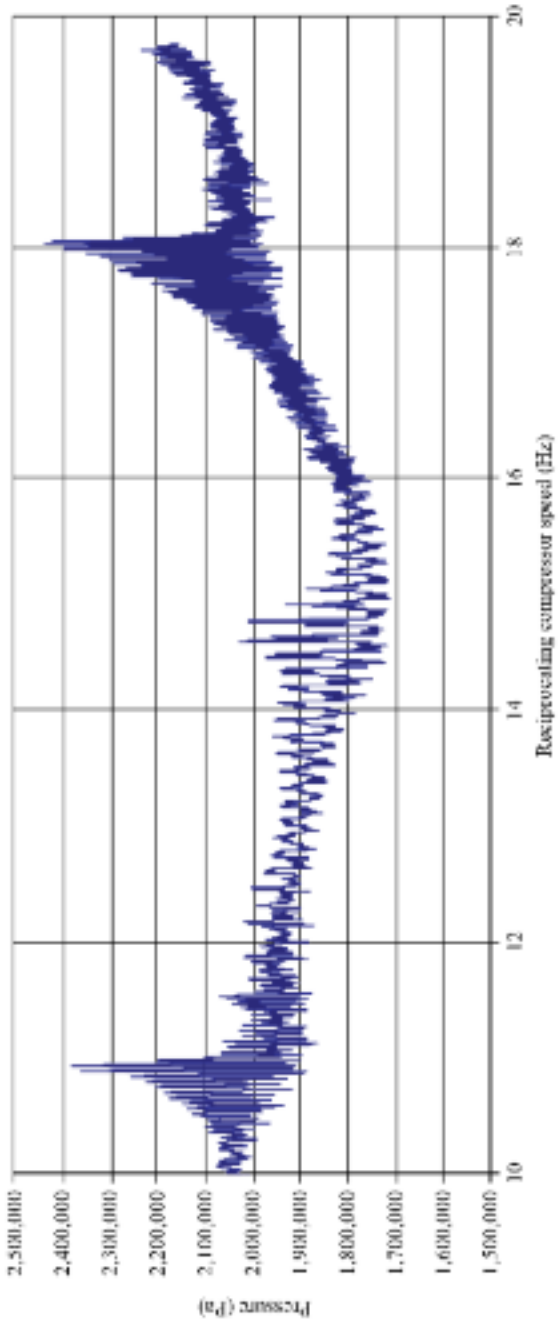

FIGURE 5.12. Case 1 — centrifugal compressor inlet pressure fluctuation versus frequency.

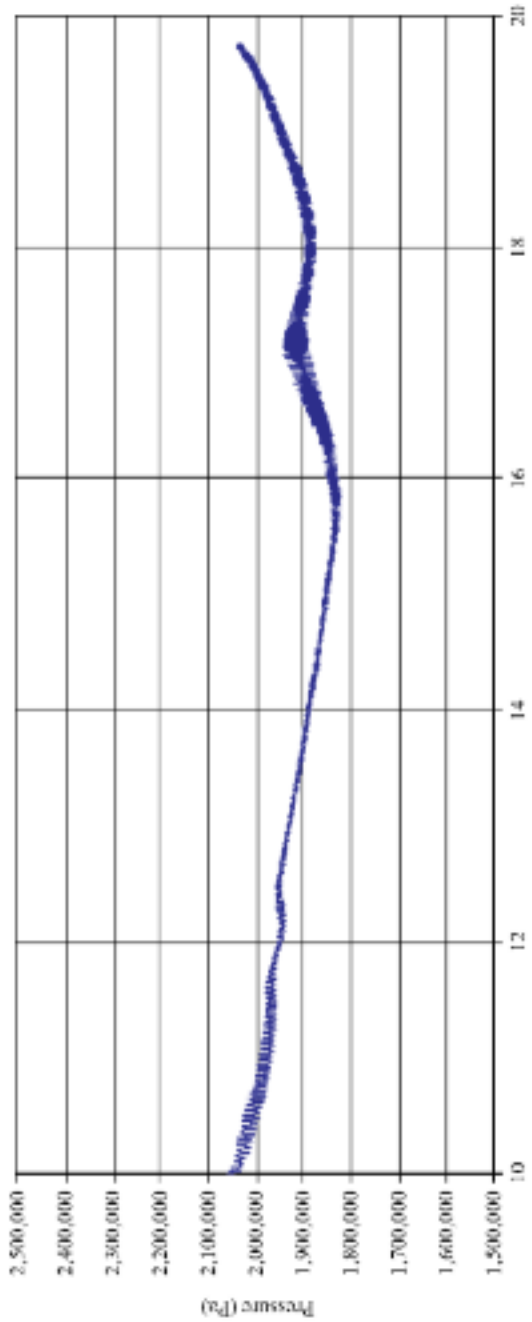

FIGURE 5.13. Case 2 — centrifugal compressor inlet pressure fluctuation versus frequency.

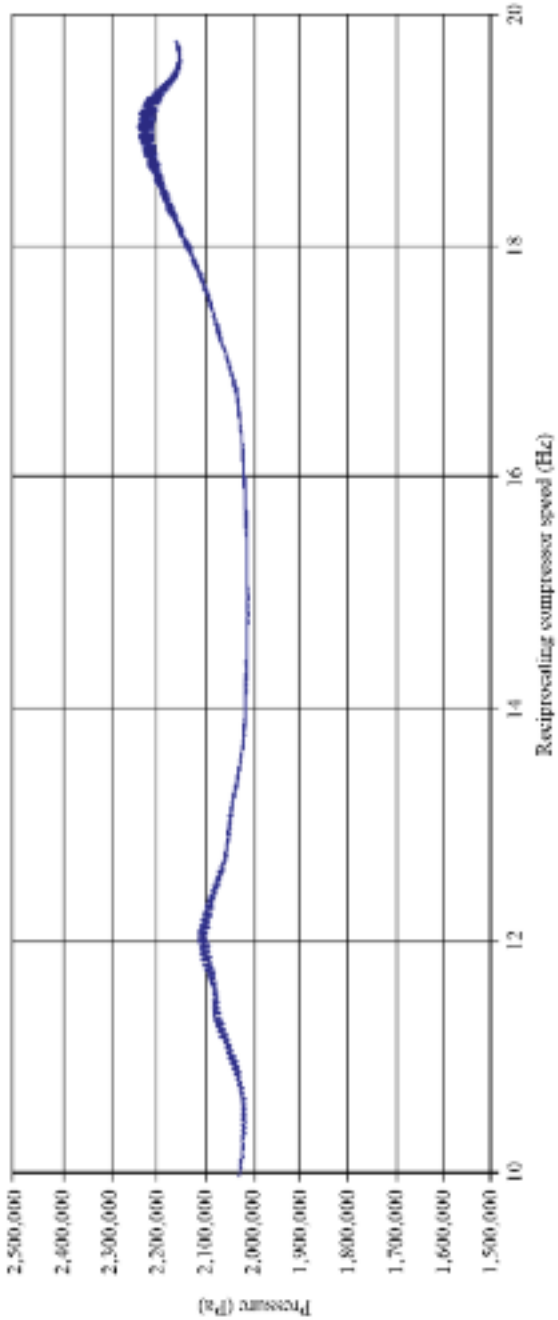

FIGURE 5.14. Case 3 — centrifugal compressor inlet pressure fluctuation versus frequency.

Although Case 3 utilizes a bottle, choke tube and an orifice, the pulsation amplitude reduction when compared to Case 2 which only uses an orifice is not significant. Furthermore, low-frequency flow transients are more pronounced for Case 3 than for Case 2. This indicates that the pulsation attenuation for Case 3 is not well designed and that the compressors are not matched. When comparing Cases 1, 2 and 3, one should also note that the attenuation devices not only affect the pulsation magnitudes, but also result in a pronounced resonance frequency shift.

Figure 5.15 presents the inlet pressure pulsations when converted to the frequency domain using a fast Fourier transform. The plot compares the peak-hold pressures in the frequency domain to determine all critical system resonance frequencies excited by the reciprocating compressor over its design operating range. The frequency domain results show that, except for Case 1 where high first-order pulsations are in the 10 to 20 Hz range, the majority of peak-to-peak pulsations for Cases 2 and 3 are second-order synchronous. This type of system response is relatively common for double-acting reciprocating piston cylinders on a common and well-balanced header. Case 1 shows a strong first-order resonance at 11 Hz and then equally strong second- and third-order resonances at 22 and 33 Hz. For Case 2, the orifice filtered the first-order response, but weak second- and third-order responses are still evident. As we previously noted, the addition of a bottle and choke tube for Case 3 did not provide significant additional pulsation damping, but shifted resonance frequencies to above 26 Hz (second order) and 39 Hz (third order). Shifting resonance frequencies away from a desired operating speed is a useful feature of bottle–choke–tube combinations and is commonly used in piping pulsation design.

Piping system compressor discharge pressure losses

When designing a compression station piping system, minimizing the total pressure drop across the piping system is a critical design objective, once flow stability is assured. A well-designed interconnect piping should have minimum pressure losses while providing adequate pulsation damping to avoid damaging the machinery and piping. Acoustic attenuation devices, such as orifice plates, bottles and choke tubes, have inherently high pressure losses. Table 5.2 presents the pressure drop across the piping systems for the above Cases 1, 2 and 3. Table 5.2 also illustrates the reciprocating compressor's total power that is lost due to these pressure drops.

Table 5.2. *Interconnect pipe pressure losses.*

Case	Pressure loss (Pa)	Power loss
1 (Straight pipe)	200	0.0%
2 (Pipe, orifice)	26,000	2.5%
3 (Pipe, bottle, choke tube, orifice)	32,000	3.1%

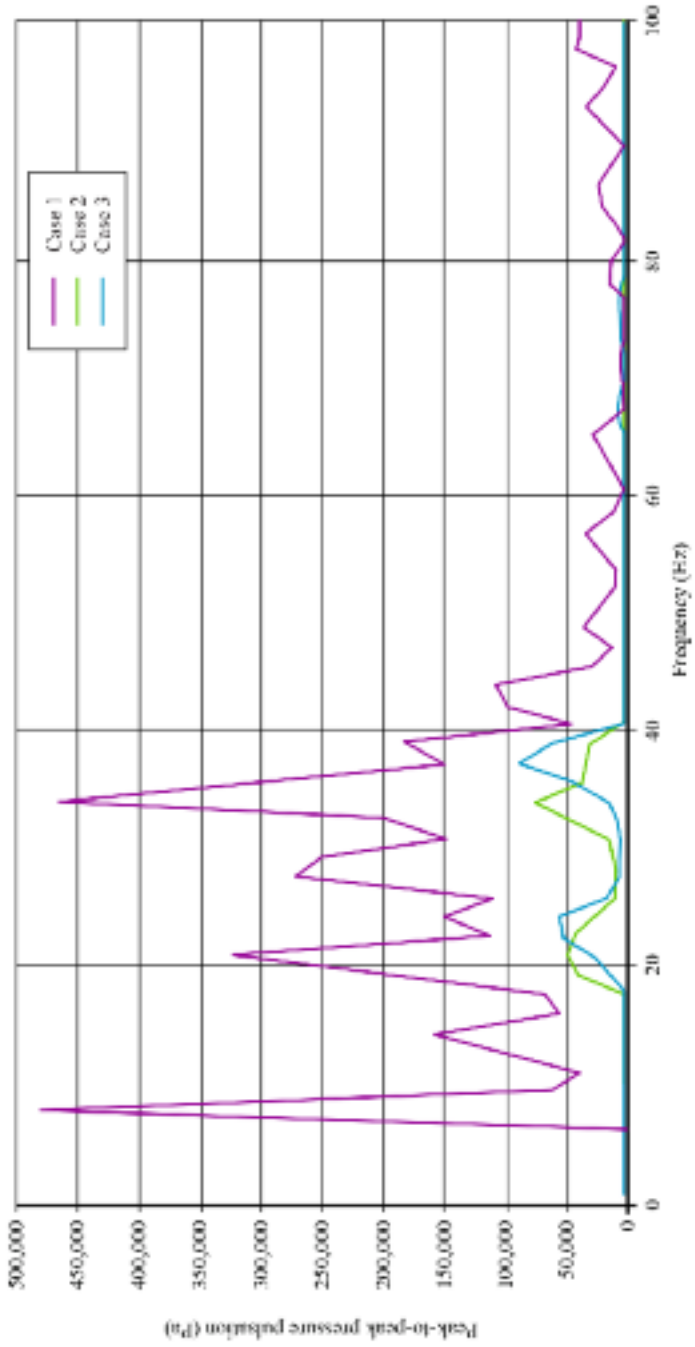

FIGURE 5.15. Cases 1, 2 and 3 pulsation spectrum.

The attenuation devices in Cases 2 and 3 result in significant pressure loss and therefore total system efficiency. For Case 3, approximately 3.0 percent of the power required to compress the gas is lost through pulsation attenuation devices in the downstream piping.

Impact on centrifugal compressor

As we previously noted, when developing a model it is acceptable to assume that the relatively fast flow transients experienced by the centrifugal compressor do not affect the compressor's operating speed. The centrifugal compressor continues to operate at a constant speed as the compressor's rotational inertia and power turbine will torsionally dampen any unsteady flow. Thus, the compressor will operate on a fixed compressor discharge pressure-flow speed line, which is limited by surge on the low-flow–high-pressure side and choke on the high-flow–low-pressure side.

Although one should avoid choke, as it is an inefficient operating regime, it is not necessarily damaging to the compressor. In contrast, it is critical to avoid surge, as surge can cause bearing or seal damage, blade rubbing or even catastrophic compressor failures. A flow limit usually defines the compressor's surge limit at a given speed, whereas a minimum compressor discharge pressure defines choke. Strong pulsations in pressure and flow have the capability to move a centrifugal compressor into surge or choke. For example, Figure 5.11 (Case 2) illustrates that the centrifugal compressor would experience very low and even negative inlet flows for short periodic time intervals when the upstream reciprocating compressor runs at any speed above 16 Hz (960 rpm). In this case, a strong pulsation second order harmonic at 33 Hz is evident in Figure 5.15. Thus, the time intervals of significant negative flows at the centrifugal compressor inlet are approximately 0.029 seconds. During these short periods, the centrifugal compressor would likely surge periodically. However, if the reciprocating compressor speed is limited to 15 Hz, the centrifugal compressor would remain stable.

For Case 3, the stable centrifugal compressor operating range shifts to slightly above 18 Hz, as Figure 5.14 illustrates. Here, minimum inlet flow velocities stay above the 1.7 kilograms per second surge limit on the 8000 rpm speed line, as long as the reciprocating compressor operates below 18 Hz. We can plot the periodic cycling of the centrifugal compressor's operating point on its compressor discharge pressure-flow curve to visualize the impact of inlet pulsations on its performance and stability. For example, Figure 5.16 shows the centrifugal compressor operating point variations due to inlet flow pulsations when the reciprocating compressor is operating at 17 Hz. Although the centrifugal compressor's operating point fluctuates significantly on the constant speed line the compressor will not cross the surge line at this operating condition.

The wide operating point fluctuations associated with Case 3 are not desirable as: (1) the compressor operates a significant percentage of time away from its best efficiency point, and (2) any small operating change could move the compressor

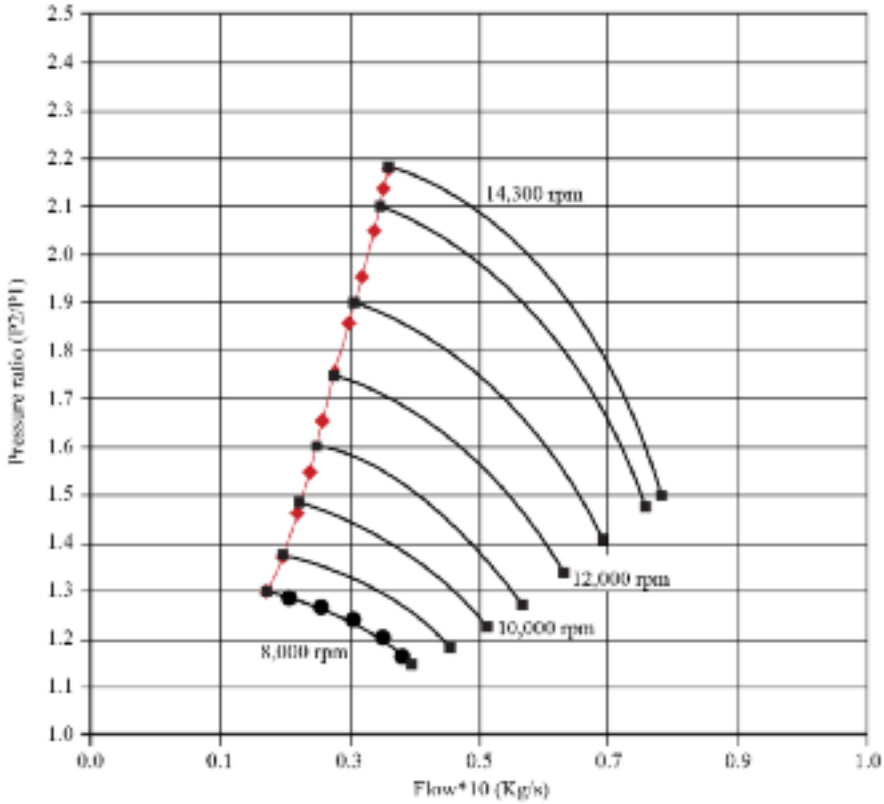

FIGURE 5.16. Operating range of centrifugal compressor due to inlet pulsations.

across the surge line. A reduction of less than 15 percent in flow, or increase of 10 percent in system suction pressure, would lead to compressor surge, which indicates a severely restricted system operating range. Also, centrifugal compressor's isentropic efficiencies vary widely between 72 percent and 56 percent, with a time-averaged mean value of only 61 percent. Although we achieved a functional compression system solution, we concluded that a further piping pulsation and machine design optimization was desirable for this case.

SUMMARY

The three cases demonstrate that by analyzing and designing the interconnecting piping between the compressors, utilizing pulsation attenuation devices and matching the compressor's mass-flow rates, one can achieve a functional compression system design for even the worst cases of mixed centrifugal and reciprocating compressor operation. Nonetheless, the cases also make apparent that even small

analysis errors, design deviations or machine mismatches can lead to an operationally restricted compression system. Also, pulsation attenuation designs result in significant piping pressure losses. Utilizing analysis tools in the design process can enable the design engineer to model the piping system's transient fluid dynamics, the pulsation attenuation devices and the compressor behavior. This analysis is critical to minimize piping pressure losses and to avoid pulsation induced pipe or compressor failures.

Traditionally, design engineers utilize acoustic analysis software to solve the linearized transient wave equations for the piping resonance analysis of reciprocating compression systems. However, these solvers were inadequate for the analysis of the pulsating flows in mixed centrifugal and reciprocating compression systems, as they do not account for non-linear fluid effects. Also, as these solvers do not model physical flow, just perturbations from mean flow, they cannot predict real compressor performance and system pressure losses. Where the reciprocating and centrifugal compressor mass flows and performances are mismatched, the resultant compression system can continuously "hunt" for a stable operating point, resulting in low-frequency non-periodic pressure transients in the piping system.

We developed a fully transient one-dimensional Navier-Stokes equation solver for systems of interconnected pipes which enabled us to predict flows, pulsation amplitudes and frequencies in mixed compression systems. This solver serves as a tool that design engineers may use to avoid piping design and compressor matching errors early in the compression system design process.

REFERENCES

Brun, K., Deffenbaugh, D.M., and Bowles, E.B., Jr. (2007), "Development of a Transient Fluid Dynamics Solver for Compression System Pulsation Analysis", *Proceedings of the Gas Machinery Conference,* Dallas, USA, 1–3 October.

Fletcher, C.A.J. (1991), *Computational Techniques for Fluid Dynamics, Volume I*, Springer-Verlag, Berlin, Germany.

Kurz, R., McKee, R., and Brun, K. (2006), "Pulsations in Centrifugal Compressor Installations", *Proceedings of the 51st American Society of Mechanical Engineers Gas Turbine and Aeroengine Congress*, Barcelona, Spain, 8–11 May, Paper No. GT2006-90700.

Morini, M., Pinelli, M., and Venturini, M. (2006), "Development of a One-Dimensional Modular Dynamic Model for the Simulation of Surge in Compression Systems", *Transactions of the ASME, Journal of Turbomachinery*, vol. 129, pp. 437–47.

Shapiro, L. (1996), *Performance Formulas for Centrifugal Compressors*, Solar Turbines Publication, San Diego, USA.

Smalley, A.J., Jungbauer, D.E., and Harris, R.E. (1995), "Reciprocating Compressor Reliability Issues", *Proceedings of the Gulf Publishing Company and Hydrocarbon Processing 4th Process Plant Reliability Conference*, Houston, USA, 14–17 November.

Sparks, C.R. (1983), "On the Transient Interaction of Centrifugal Compressors and Their Piping Systems", *Proceedings of the 28th American Society of Mechanical Engineers Gas Turbine and Aeroengine Congress,* Phoenix, USA, 27–31 March, Paper No. 83-GT-236.

Chapter 6

Aerodynamic Instability and Life Limiting Effects of Inlet and Inter-stage Water Injection into Gas Turbines

K. Brun, R. Kurz and H.R. Simmons

ABSTRACT

End-users are employing gas turbine power enhancement technologies such as inlet fogging, inter-stage water injection, saturation cooling, inlet chillers and combustor injection, and do not evaluate the potentially negative effects that these devices may have on the gas turbine's operational integrity. Engineers often overlook the effect of these add-on devices on off-design operating conditions and specifically, the effect of non-standard fuels, compressor degradation and fouling on the gas turbine's compressor surge margin and aerodynamic stability. Nonetheless, we can directly link the compressor aerodynamic instabilities which these factors cause to blade high-cycle fatigue and subsequent catastrophic gas turbine failure. An analysis should always precede applying power enhancement devices, especially if one operates the gas turbine at full power, uses older internal parts that are degraded and weakened or uses non-standard fuels.

This chapter discusses a simplified method to evaluate the principal factors that affect a single-shaft gas turbine compressor's aerodynamic stability. We applied the method to a frame-type gas turbine and present the results. These results show that inlet cooling alone will not cause gas turbine aerodynamic instabilities, but that it can be a contributing factor if the machine's surge margin is already slim for other reasons. An operator can employ this approach to identify high-risk applications and bound the gas turbine operating regions. Bounding the operating regions limits the risk of compressor aerodynamic instability and the associated unsteady blade aerodynamic forces. It is important to avoid elevated unsteady aerodynamic forces as they induce elevated unsteady blade stress which then reduces blade life and consequently, increases the probability of a catastrophic compressor blade failure.

This chapter is a revised and extended version of Brun, K., Kurz, R., and Simmons, H.R. (2005), "Aerodynamic Instability and Life Limiting Effects of Inlet and Inter-stage Water Injection into Gas Turbines", *Proceedings of the 50th American Society of Mechanical Engineers Gas Turbine and Aeroengine Congress*, Reno, 6–9 June, Paper No. GT2005-68007. This paper won the International Gas Turbine Institute Oil & Gas Application Committee 2005 best paper award.

NOMENCLATURE

c_1, c_2	local velocities
c_p	specific heat
dm/dt	mass flow
h	enthalpy
k	specific heat ratio
P	pressure
Q	volumetric flow
r	radius
SM	surge margin
T	temperature
V	velocity
W	power
ω	angular speed
α	flow incidence angles
η	stage efficiency
τ	torque
θ	tangential direction

Subscripts

d	discharge
i	inlet
s	suction
1, 2	inter-stage

INTRODUCTION

As the widespread introduction of inlet cooling and water injection technologies for gas turbines is a relatively recent development, only limited historical field operating data and information on the effect on parts life is available. Nonetheless, because of the strong commercial advantage that these technologies may bring to the operator, manufacturers have installed a large number of the devices over the past 5 years. Since the introduction of inlet cooling and water injection technologies for ground-based gas turbines, manufacturers have built or retrofitted over 800 gas turbine installations worldwide with these technologies. However, inlet air-cooling, in combination with off-design operating conditions, non-standard fuels, combustion dilution and compressor blade degradation, can lead to compressor aerodynamic instabilities and subsequent gas turbine high-cycle fatigue induced blade failures.

A number of different gas turbine power augmentation technologies are currently available. We can generally classify them into two categories:

1. evaporative cooling: these include wetted media, fogging, wet compression, overspray and inter-stage injection;
2. chillers: mechanical and absorption chillers with or without thermal energy storage.

In general, chillers only affect the gas turbine by reducing the inlet air temperature. This increases the gas turbine's output power, but has otherwise minimal effects on its internal aerodynamics. In effect, the gas turbine behaves as if it is running on a cold day. Other than some cases where ice formation on the gas turbine inlet has caused problems with casing distortion, rubbing and foreign object damage, researchers have linked few gas turbine failures directly to inlet chilling. However, inlet chillers are generally large, expensive to operate and rarely offer more than marginal economic benefits. Thus, the industry does not widely employ them.

In contrast, evaporative inlet cooling relies on injecting water droplets or vapor into the gas turbine's compressor. Within the context of this chapter, we will treat fogging and conventional evaporative cooling as having the same thermodynamic effect on the gas turbine. However, we employ two different principles: evaporative coolers utilise a wetted media that is exposed to the inlet air flow, while inlet fogging sprays water mist into the gas turbine inlet system. Engineers normally design either system to avoid liquid water carry-over into the gas turbine inlet, but fogging systems can sometimes "overspray". This results in a significant amount of water that does not evaporate before entering the gas turbine inlet. Overspraying has a similar effect to inter-stage water injection because water droplets will be present inside the compressor's first stages.

Evaporative cooling provides between 5 and 10 percent power augmentation on hot, dry days and is thus commercially attractive. The principal difference between the various commercially available evaporative cooling technologies is the percentage air saturation, the water droplet size and the location of the water injection ports into the gas turbine. However, the basic principle of all inlet water augmentation technologies is that they effectively reduce the gas turbine's inlet air temperature from the air's dry bulb temperature to the ambient air's wet bulb temperature. This temperature difference depends on the ambient air's relative humidity and temperature, as well as the evaporative cooler's efficiency. We typically measure the efficiency of evaporative devices as the percentage difference between the achieved dry and wet bulb temperatures. Researchers have reported efficiencies of 80 to 95 percent.

When discussing gas turbine compressor aerodynamic instability, one must also address the issues of combustor diluent injection and low heating value fuels. Although these technologies are primarily concerned with NO_x reduction and fuel flexibility, gas turbine power output increases which can affect the gas turbine's aerodynamic stability. Most combustor diluent injection applications employ steam or water, but some process power plants have successfully utilised CO_2 or nitrogen

for NO_x reduction. Similarly, the use of low heating value fuels in a gas turbine produces the same net aerodynamic effect as combustor diluent injection. Thus, this chapter also briefly discusses the influence of diluent injection and low heating value fuel combustion on gas turbine operational stability.

Previous work on evaporative cooling and wet compression

Because of the recent popularity of water inlet injection, a number of researchers have studied the effects of the various technologies that are available on the market. For example, Horlock (2001), Bhargava and Meher-Homji (2002), Chaker *et al.* (2002a, 2002b), Zheng *et al.* (2002), Bhargava *et al.* (2003a, 2003b), Hartel and Pfeiffer (2003) and White and Meacock (2003) all studied various aspects of wet compression in gas turbines. Most of this analysis focused on thermodynamic effects and did not evaluate the long-term effects on gas turbine operation and life, or the effects of water injection in combination with other non-standard gas turbine conditions.

The study of wet compression technology in gas turbines dates back to the 1940s, as is evident from Kleinschmidt's (1947) and Wilcox and Trout's (1951) work on jet engine water injection. However, detailed thermodynamic analysis of wet compression in ground-based gas turbines is more recent. For example, Utamura *et al.* (1999) studied the impact of droplet size in an industrial gas turbine. Later, Zheng *et al.* (2002) and Hartel and Pfeiffer (2003) performed an analysis of the thermodynamic effects of wet compression inside a gas turbine. Also, Ingistov (2001) discussed inter-stage water injection methods for gas turbine compressors.

Operational effects of evaporative cooling

In natural gas power generation applications, operators have reported few operational problems that they could directly attribute to inlet evaporative cooling. Ingistov (2002) even commented that water injection has reduced compressor fouling and improved maintenance intervals. However, in a number of cases where researchers combined excessive inlet water injection with other factors such as low heating value fuels, combustor steam injection, highly degraded blades and off-design operating conditions, they have anecdotally reported performance issues and failures. Thus, prior to installing an evaporative cooling system on an existing gas turbine plant or determining the feasibility of water augmentation for a green-field plant, one should undertake a design review to identify any damaging operating regions.

The two most critical effects of gas turbine inlet evaporative cooling are the influence on the aerodynamic stability of the gas turbine's compressor and the air–water vapour-fuel mixture's increased heat transfer on the gas turbine's high-pressure turbine vanes and blades. We separately treat these two effects for single-shaft gas turbines and provide analysis and discussion on:

1. The onset of aerodynamic compressor instabilities such as rotating stall and surge that can result from using evaporative cooling power augmentation technologies in gas turbines. We discuss a method to determine the compressors' operational safety margin. One can employ this method as a design tool for new installations or as a safety check on existing facilities.
2. The increased heat transfer due to the exhaust's higher water vapor content. We present a life fraction curve to assist design engineers in estimating the gas turbine's high-pressure turbine life reduction which aids the operator in evaluating the increase in operating costs and maintenance intervals of gas turbines fitted with water inlet injection.

COMPRESSOR AERODYNAMIC INSTABILITY

A typical performance map for a compressor shows pressure ratio as a function of inlet volumetric flow for a range of compressor speeds. This compressor map indicates that there are limits on the compressor's operating range (Figure 6.1). Surge sets the limit for low-flow operation. The exact location on the compressor map at which surge occurs can range widely depending on operating condition and, as a result, one usually establishes a surge line with a 10 percent margin above the flow at which we expect surge to occur. While centrifugal compressors can actively avoid surge using a recycle loop and anti-surge valve, most compressors in a gas turbine have no active surge control system other than start-up compressor discharge bleed and inlet guide vane modulation.

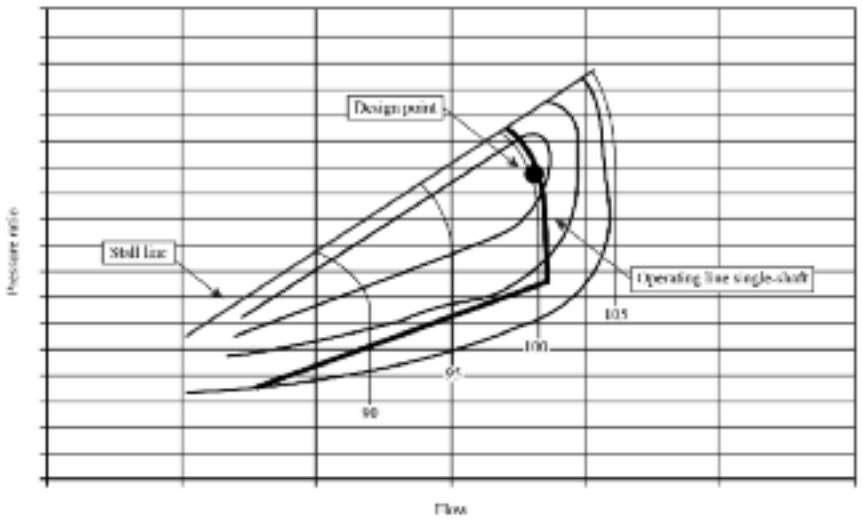

FIGURE 6.1. Axial compressor performance map.

Compressors will surge when they can no longer maintain forward flow through the compressor. Once surge occurs, the flow reversal reduces the discharge pressure or increases the suction pressure, thus allowing forward flow to resume until the pressure rise again reaches the surge point. This surge cycle continues at a low frequency until some change takes place.

Thus, surge is instability in a compressor's flow that results in a complete breakdown and flow reversal through the compressor. Surge occurs just below the minimum flow that the compressor can sustain against the existing suction to discharge pressure rise. When surge occurs, both flow rate and compressor discharge pressure decrease rapidly and air flows backward through the compressor. Prior to reaching a surge event, a number of other aerodynamic flow instabilities are likely to occur within a compressor. These phenomena include rotating stall and blade flutter. Rotating stall is a localized flow reversal cell that rotates at about 30 to 70 percent rotor speed in the direction of the compressor blades. As the compressor's operating condition moves close to the surge line, rotating stall typically initiates in the stator first and then, once it fully develops, enters the blades.

Compressor rotating stall is a well-studied phenomenon in compressor aerodynamics. Rotating stall occurs when the blade exceeds aerodynamic stability margins and results in periodic blade loading. Emmons *et al.* (1955) describe rotating stall as a momentary aerodynamic overloading of an already highly loaded blade, which causes this particular blade to exhibit separation and blockage. This blockage restricts the flow through a blade passage, and consequently diverts the incoming flow, causing an increase in incidence on one side of the blade passage, and a reduction on the other. The increased incidence on the adjacent blade row will cause separation and blockage there, and therefore a stall cell will propagate from blade to blade at a speed different from the compressor running speed.

As a compressor operating point passes its surge line, multiple rotating stall cells from both the compressor's rotors and stators combine to generate a surge with fully reversed flow through the entire compressor. We must distinguish rotating stall from surge. Rotating stall occurs when flow through the compressor separates on both vane leading and trailing edges. We associate flow separation with vortex shedding. If the vortex shedding frequency coincides with any blade natural frequency, the blade will "flutter". Flutter results in significant aerodynamic forces on the blades that can have a detrimental effect on the blade's life. For example, Figure 6.2 illustrates a gas turbine compressor blade that failed due to flutter-induced high-cycle fatigue. Compressor blades typically experience both rotating stall and flutter when the compressor's surge margin falls to less than 5 percent (Boyce, 2011). Gas turbine instrumentation has not historically been able to identify that either of these precursors surge, although recently Sheard *et al.* (2010, 2011) demonstrated an acoustic stall warning system that can identify stall precursors.

Analysis method

To investigate whether a compressor is operating in a region where rotating stall or flutter may occur, we performed aerodynamic surge analysis of the compressor. A

FIGURE 6.2. Compressor blade failed due to flutter-induced high-cycle fatigue.

compressor surge analysis consists of a one-dimensional thermodynamic and two-dimensional mean streamline flow analysis for each stage of a multi-stage compressor. The two-dimensional mean streamline analysis yields the power that each stage absorbs, total compressor power and blade-to-blade flow angles. Using the results from the two-dimensional analysis, we mapped the one-dimensional analysis results for each stage's operating point on the stage's characteristic performance curve to determine the local surge margin. We may define surge margin (*SM*) for compressors as:

$$SM = \frac{Q_{design} - Q_{surge}}{Q_{design}} \tag{1}$$

where Q is the volumetric flow rate.

For evaporative cooling, the model assumes that all water instantly vaporizes unless the flow is already saturated, in which case the model assumes that the flow carries the water through the compressor until the flow can absorb higher moisture content. Evaporative cooling primarily affects the gas turbine's inlet air temperature. Water injection also affects flow density and the specific heat of air, but the dominant effect is cooling. Nonetheless, although changes in these physical properties have a minimal impact on the gas turbine's overall performance, they do affect the compressor's

aerodynamic stability. Moving the compressor's operating point closer to the surge line affects the aerodynamic stability (Figure 6.3), and we therefore included them in the surge analysis. Thus, the model locally recalculates the mixture's physical properties based on the moisture content in the air.

Characteristic compressor stage performance curves are typically not available from the gas turbine manufacturer, so operators must adopt generic single-stage compressor curves for the application by matching performance parameters with compressor geometry. Using the general equation for stage efficiency:

$$\eta_s \approx \frac{T_d - T_i}{T_i\left(\left(\frac{P_d}{P_i}\right)^{\frac{k}{k-1}} - 1\right)} \tag{2}$$

we can determine the compressor's stage power requirements from:

$$W = \Delta h \cdot \frac{dm}{dt} = \frac{dm}{dt} \cdot c_p \cdot (T_d - T_i) \tag{3}$$

and

$$W = \Delta\tau \cdot \omega = \omega \cdot \frac{dm}{dt} r(V_d^\theta - V_i^\theta) \tag{4}$$

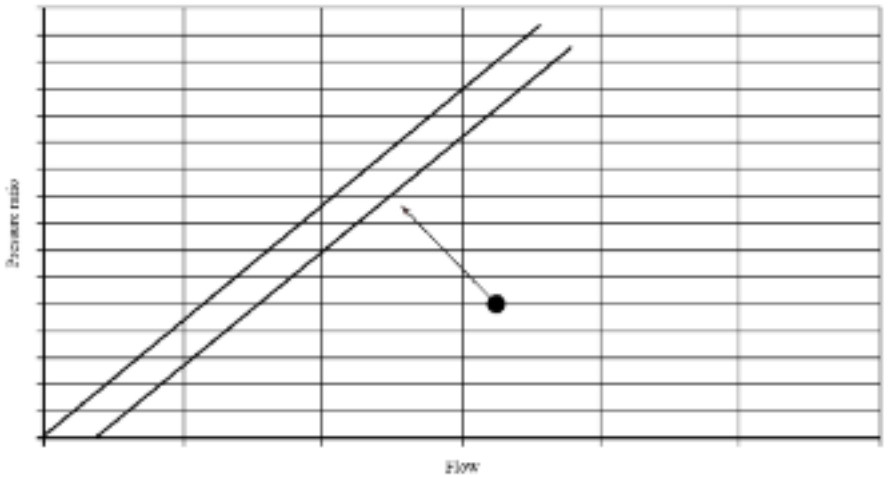

FIGURE 6.3. Operating point moving toward surge line.

Unless specific information on the compressor stages is available, a 15 percent original design surge margin is a reasonable and conservative assumption for all stages. Also, we can estimate individual stage compressor blade design angles using Euler's equation:

$$\frac{P_d}{P_s} = \left(1 + \frac{\eta r \omega}{c_p T_s} (c_s \sin \alpha_2 - c_1 \sin \alpha_1) \frac{k}{k-1} \right) \tag{5}$$

We can subsequently use the same equation to determine actual blade incidence angles in the surge-flutter analysis. As the aim of the method is to determine changes in surge margin, rather than the total surge margin for a given operating condition, small errors in the characteristic compressor stage maps do not significantly affect the individual decreases in surge margin calculation.

Aerodynamic stability criteria

The results from the characteristic stage curve operating point mapping should ensure that the stage surge margin of any stage is always above 5 percent to avoid operating the compressor in a region of local surge. In addition, the two-dimensional analysis identifies the highest local stator and rotor blade incidence angles. These should not exceed 8 degrees and 12 degrees, respectively, as high incidence angles indicate rotating stall.

To avoid stall, most gas turbines employ variable pitch inlet and stator guide vanes. One may use variable pitch inlet and stator guide vanes to reduce the gas turbine's airflow at low load and during both start-up and shut-down (Figure 6.1). At low load and during start-up and shut-down the gas turbine's compressor's surge margin decreases due to high incidence angles. The design engineer must therefore ensure that he or she maintains the gas turbine's stall margin not only at design point, but also off design.

Factors that can have a significant effect on surge margin in a gas turbine and that the design engineer should evaluate as part of an analysis of surge margin are:

- inlet water injection (evaporative cooling);
- inter-stage compressor water injection;
- combustor diluent (steam, water or nitrogen) injection;
- compressor blade degradation and fouling; and
- low or medium equivalent heating value fuels.

As each of these factors can individually affect a gas turbine compressor's surge margin, we must determine their total impact for a given gas turbine operating condition. One should note that this analysis treats effects on surge margin as net additive. If, for example, 5 percent of surge margin is lost due to degradation and 6 percent of surge margin is lost due to fogging, the total surge margin decreases by 11 percent. Namely:

$$\Delta SM = \sum_{i=1}^{n} \frac{\partial SM}{\partial \Phi_i} \cdot \Delta \Phi_i \tag{6}$$

where Φ is the individually assessed factor influencing the stage surge margin. By parametrically mapping the individual factors' effects on surge margin, we can establish a global operation limit.

INSTABILITY FACTOR INFLUENCE ANALYSIS

Although we based our surge analysis on the sequential application of one-dimensional thermodynamic and two-dimensional mean streamline equations that are readily available in the public domain (see Zheng *et al.* (2002) for a comprehensive review), few operators perform this safety check prior to installing water inlet and stage injection on their gas turbine. This has led to some gas turbine operational problems, including in-service blade failures. Thus, we provide a parametric study of the relative influence of each factor on compressor surge margin for a typical large gas turbine. Although the analysis results that we present here are based on single-shaft gas turbines, one can develop a similar methodology and apply it to two-shaft gas turbines.

Evaporative cooling

Inlet air evaporative cooling into a gas turbine has become a popular method to increase a gas turbine's power. Researchers originally developed this technology to provide a power boost during peak demand times, but some plants now use evaporative cooling for base load power generation. Evaporative cooling's short-term effect is to reduce the inlet air's temperature from its dry to its wet bulb temperature. Researchers do not understand fully evaporative cooling's long-term impact on the gas turbine. Typically, a gas turbine can achieve a power increase between 5 percent and 10 percent on hot, dry days using evaporative cooling.

To demonstrate surge margin reduction due to evaporative cooling, we include example results of a surge analysis for a 100 MW industrial frame type gas turbine. Evaporative cooling moves the compressor operating point closer to the surge line (Figure 6.4). With 100 percent saturation of the inlet air, we can decrease the surge margin by approximately 4 percent, if the ambient relative humidity is between 20 and 30 percent. Although a 4 percent reduction in surge margin is significant, it is not enough for evaporative cooling to decrease the surge margin sufficiently to result in compressor surge. However, evaporative cooling can be a contributing factor if for other reasons the gas turbine's surge margin is already low.

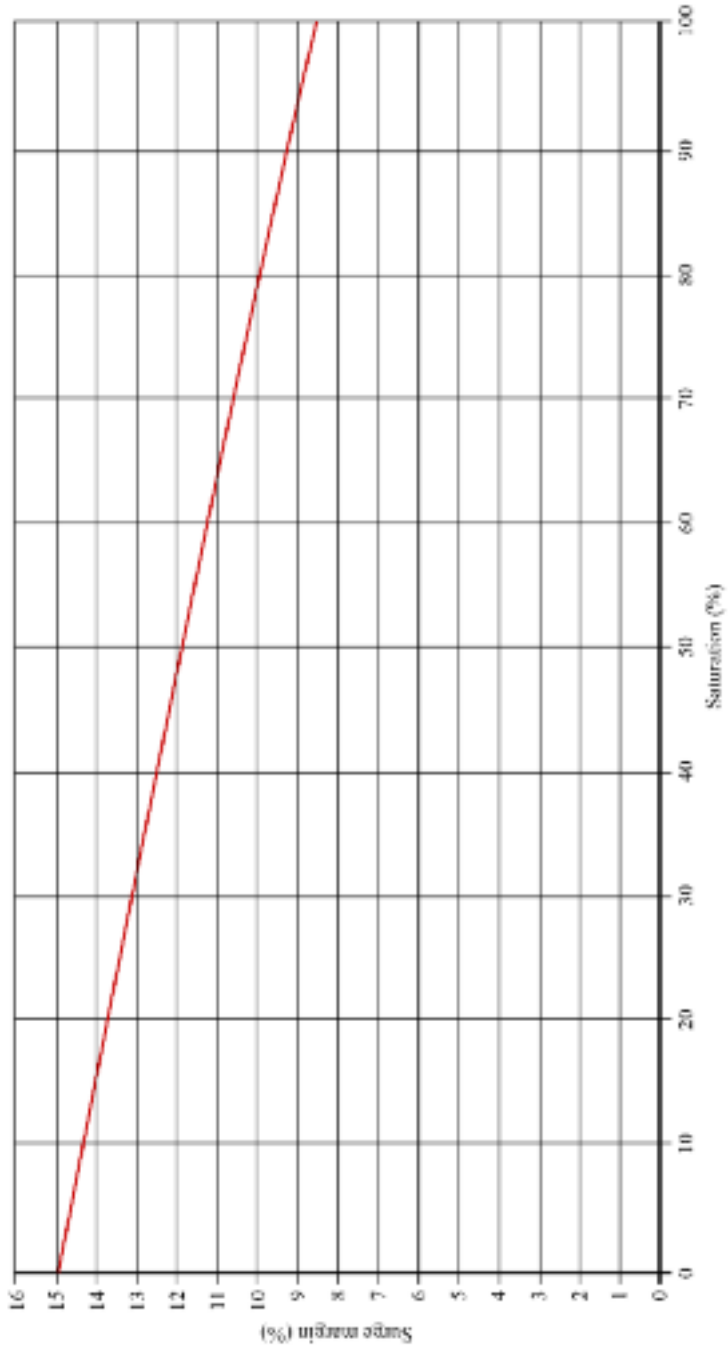

FIGURE 6.4. Surge margin versus percent air saturation.

Inter-stage water injection

Some operators inject water directly into the compressor through ports in the first stages of the gas turbine's compressor. Injecting water downstream from the gas turbine's inlet has a similar effect as over-spraying, as the water droplets travel beyond the compressor's first stage. Inter-stage water injection locally reduces the temperature to the wet bulb temperature. This increases the gas turbine's output power, but also decreases the compressor's surge margin. Parametric study results to evaluate the effect of water injection (Figure 6.5) evaluate the impact of:

- compressor stage 1 water injection (spray);
- compressor stage 2 water injection (spray); and
- both stage 1 and 2 water injection (spray).

Compressor inter-stage water injection has a significant impact on a compressor's surge margin. Study results showed that the further downstream in the compressor that one injects water, the larger the loss of surge margin. This is primarily because a temperature reduction from dry bulb to wet bulb temperature in a downstream stage has a more significant effect on the blade flow incidence angles than in an upstream stage.

We conservatively assume that the net effect on a compressor's surge margin of evaporative cooling and inter-stage water injection is additive. When we combine evaporative cooling with inter-stage water injection, the effect on surge margin (Figure 6.6) is large enough to eliminate surge margin and therefore results in a compressor surge. Again, the further downstream the water injection occurs, the more detrimental the effect on surge margin.

Equivalent lower heating value

Operating a gas turbine with a fuel that has a heating value lower than that of its design fuel can affect compressor surge margin. Most gas turbine fuel systems are designed for natural gas, which has a heating value of approximately 5×10^7 J/kg, and can tolerate a Wobbe Index variation of ±10 percent. Steam or water injection into the combustor to reduce NO_x emissions has a similar effect as using lower heating value fuels, since it decreases the fuel mixture's equivalent heating value in the combustor. If the fuel mixture's heating value is significantly lower than the design fuel, the operator must inject more fuel into the combustor to achieve the required equivalent gas turbine heat input. However, the increased volumetric input into the combustor also increases the compressor backpressure and decreases the compressor's surge margin.

We conducted a parametric study on the effect of fuel equivalent lower heating value on surge margin (Figure 6.7). We define equivalent heating value as the resulting net heating value of a fuel/steam/water mixture in the combustor. The study indicates that we can reduce the compressor's surge margin by about half when burning

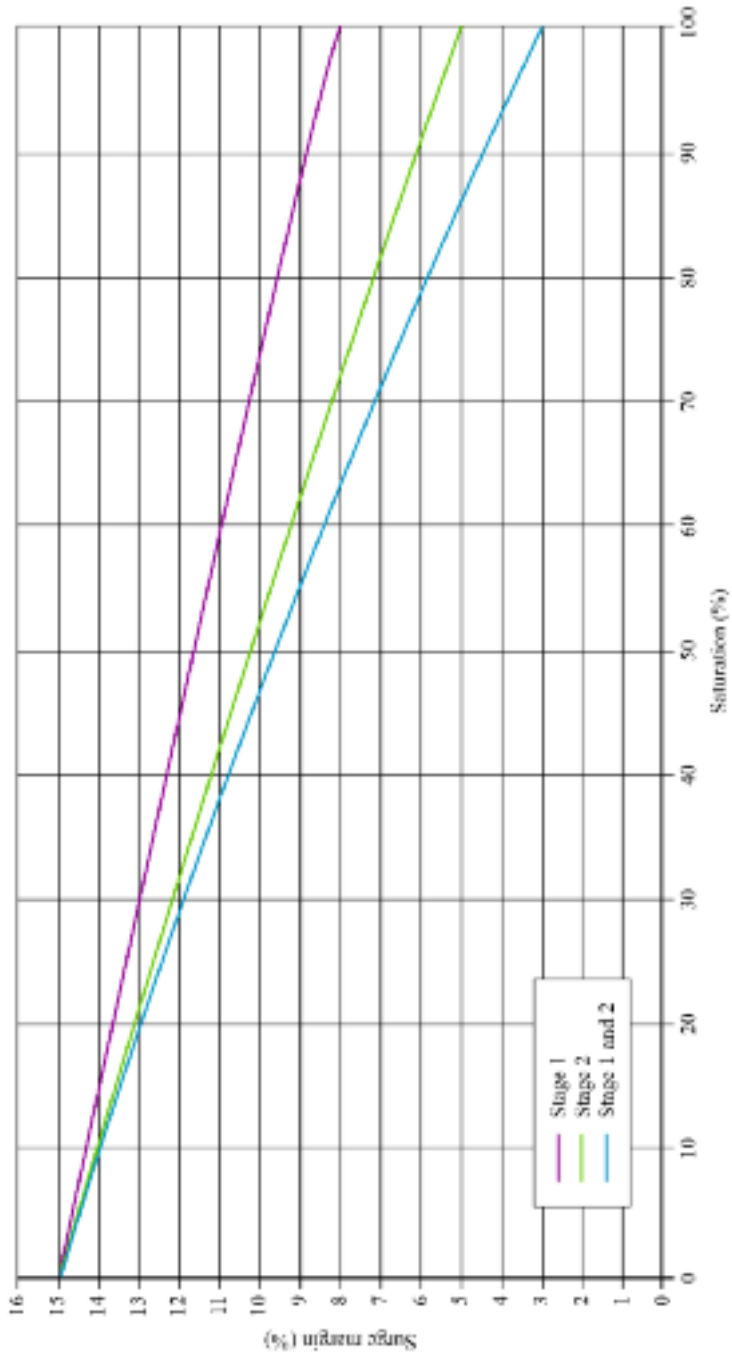

FIGURE 6.5. Surge margin versus inter-stage injection.

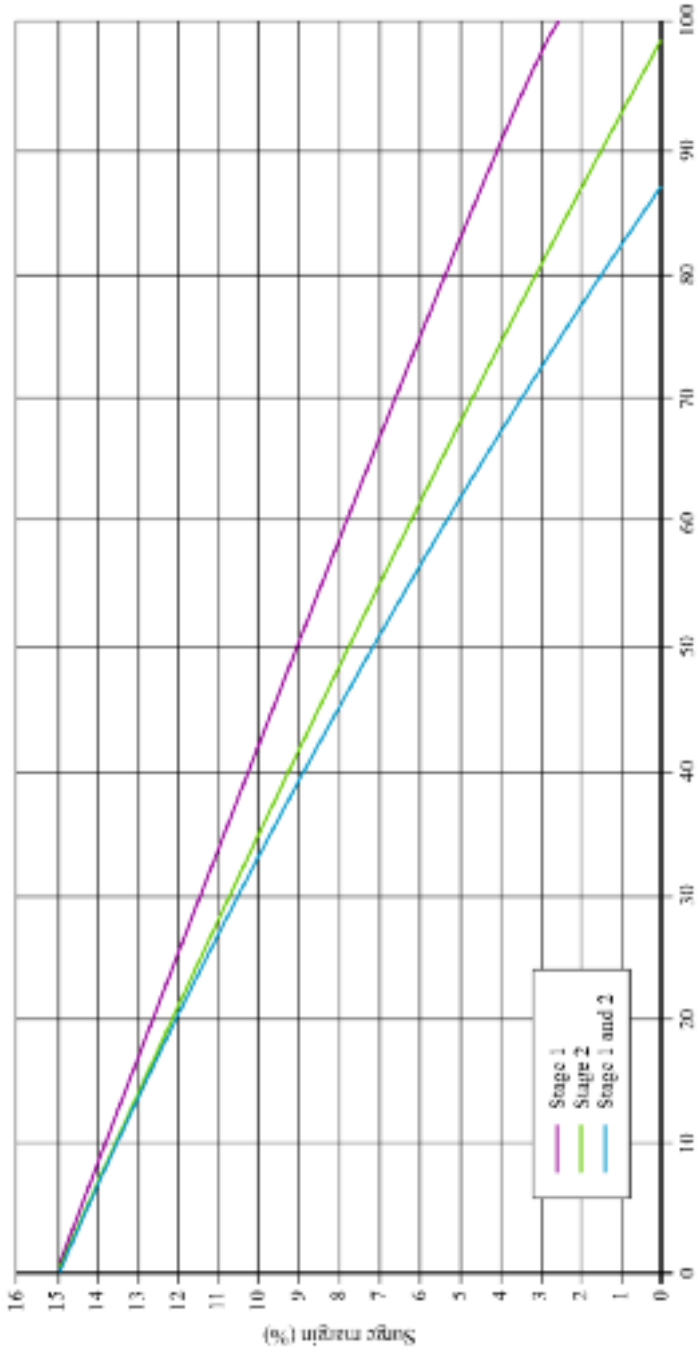

FIGURE 6.6. Surge margin versus inlet evaporative cooling and inter-stage injection.

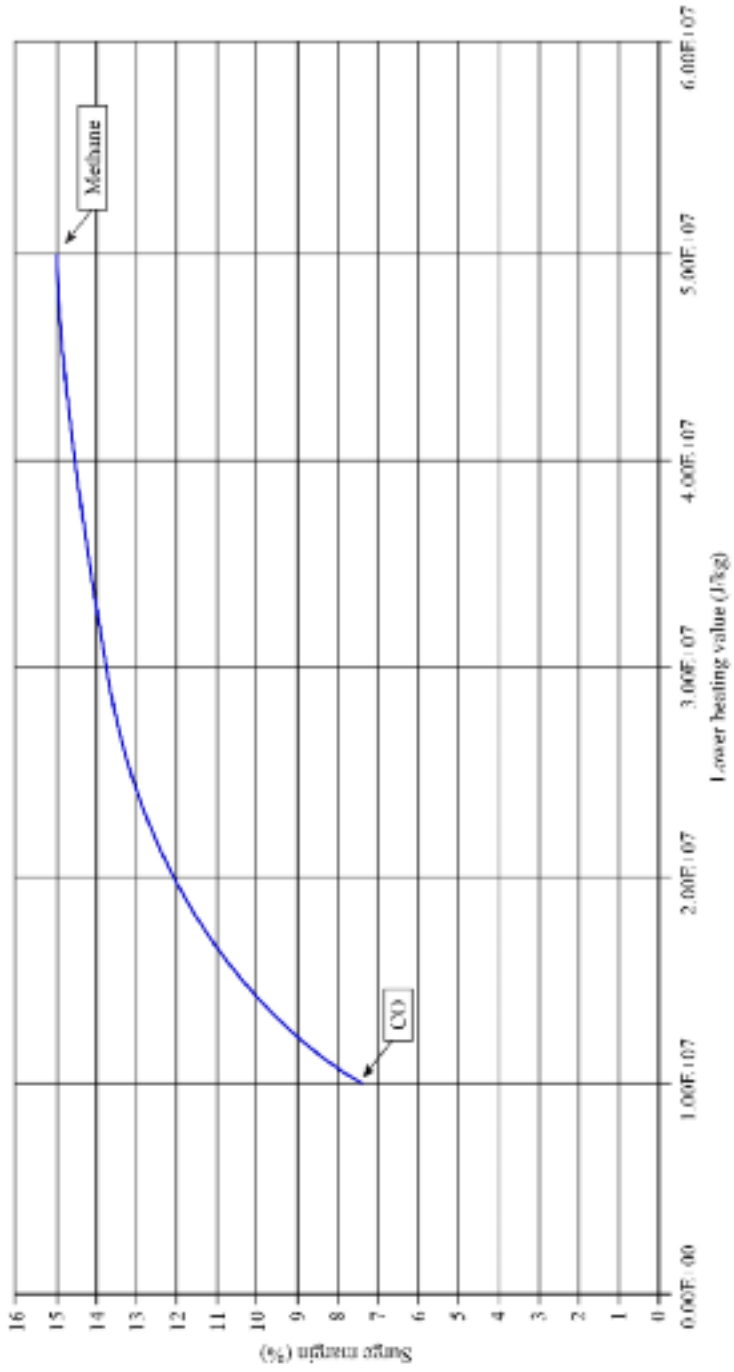

FIGURE 6.7. Surge margin versus equivalent lower heating value of the gas turbine's fuel.

extremely low heating value fuels. In most applications, it is unlikely that an operator will use fuel with more than a 10 percent deviation in heating value than that of natural gas. A 10 percent deviation translates into a surge margin reduction of about 1 percent. Thus, the effect of burning lower heating value fuel on the compressor surge margin is probably negligible for the majority of gas turbine applications.

Compressor blade degradation

While the effects that we discussed above cause a compressor's operating point to move closer to its surge line, compressor blade degradation as a consequence of a loss of material on the blades' leading and trailing edges because of erosion and corrosion, plus a build-up of material on the blade as a result of fouling, move the surge line towards the operating point (Figure 6.8). Nonetheless, the net effect is the same in that the compressor surge margin is reduced. Particle fusing and pitting do not affect a compressor's performance. These effects are more generally related to crack formation on compressor blades. Degradation affects compressor performance as shortening blade chord, change in blade profile or increasing surface roughness may result in flow slip or separation (Kurz and Brun, 2001; Corsini *et al.*, 2012). Slip is an indicator of how effectively a blade imparts kinetic energy into the flow and is, thus, a direct function of blade degradation.

We conducted a parametric analysis of the effect of compressor blade degradation on surge margin (Figure 6.9). We present degradation as an equivalent chord loss parameter, which we define as the equivalent chord loss divided by the total chord length. Design engineers employ the equivalent chord loss parameter to account for all types of degradation in one parameter. The equivalent chord loss parameter assumes that we can equate aerodynamic degradation due to fouling to the blade chord's equivalent decrease.

Typical values for the equivalent chord loss parameter range from 0 to 0.3 percent in frame type gas turbines, and 0 to 1 percent in aero-derivative gas turbines. The parametric analysis indicates that even significant compressor blade degradation results in a relatively small reduction in surge margin, when compared to the evaporative cooling or inter-stage water injection. However, if we install evaporative cooling on a gas turbine with a severely degraded compressor, the combined effect could be significant enough to result in compressor surge.

HOT-SECTION EFFECTS

The heat transfer coefficient between hot combustion products and the high-pressure turbine vanes and blades is a direct function of the combustion product's composition. For a given mixture temperature, the higher the water vapor content, the higher the energy content and, therefore, the more heat will transfer to the turbine vanes and blades. Since evaporative cooling and water injection increase the airflow's water vapor content, the heat transferred to the high-pressure turbine vanes and blades must increase and, therefore, so must their temperature.

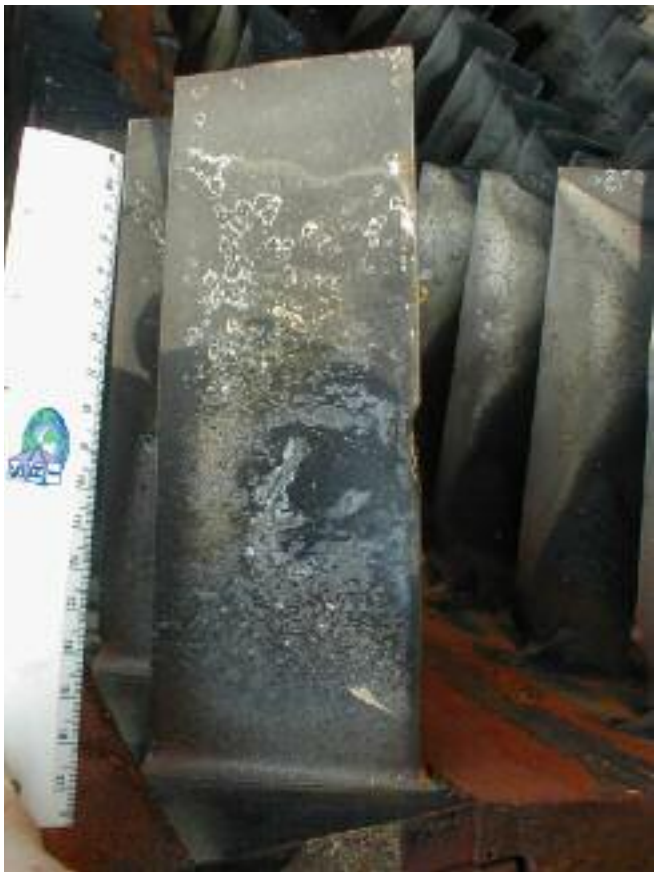

FIGURE 6.8. Degraded compressor blade.

Design engineers optimize high-pressure turbine vanes and blades for operation at a specific design point that occurs with a specific temperature. The margin on material properties is minimal, and even small increases in average temperature lead to rapid vane and blade oxidation. The added heat that transfers to the vanes and blades because of evaporative cooling or water injection is most problematic in older gas turbine designs that operate without vane or blade cooling.

More recent gas turbine designs are less susceptible to the increase in high-pressure turbine vane and blade temperature as compressor delivery air cool both vanes and blades. As this also contains additional water vapor, it cools the vanes and blades more effectively. Nonetheless, an analysis indicates that improved cooling effectiveness does not fully compensate for increased heat transfer to vanes and blades. An analysis of the effect of inlet evaporative cooling on a 100 MW industrial gas turbine illustrates that the life of high-pressure turbine vanes and blades reduces with increasing water content (Figure 6.10). This reduced life will translate into a significant increase in the gas turbine's maintenance costs and a corresponding reduced availability.

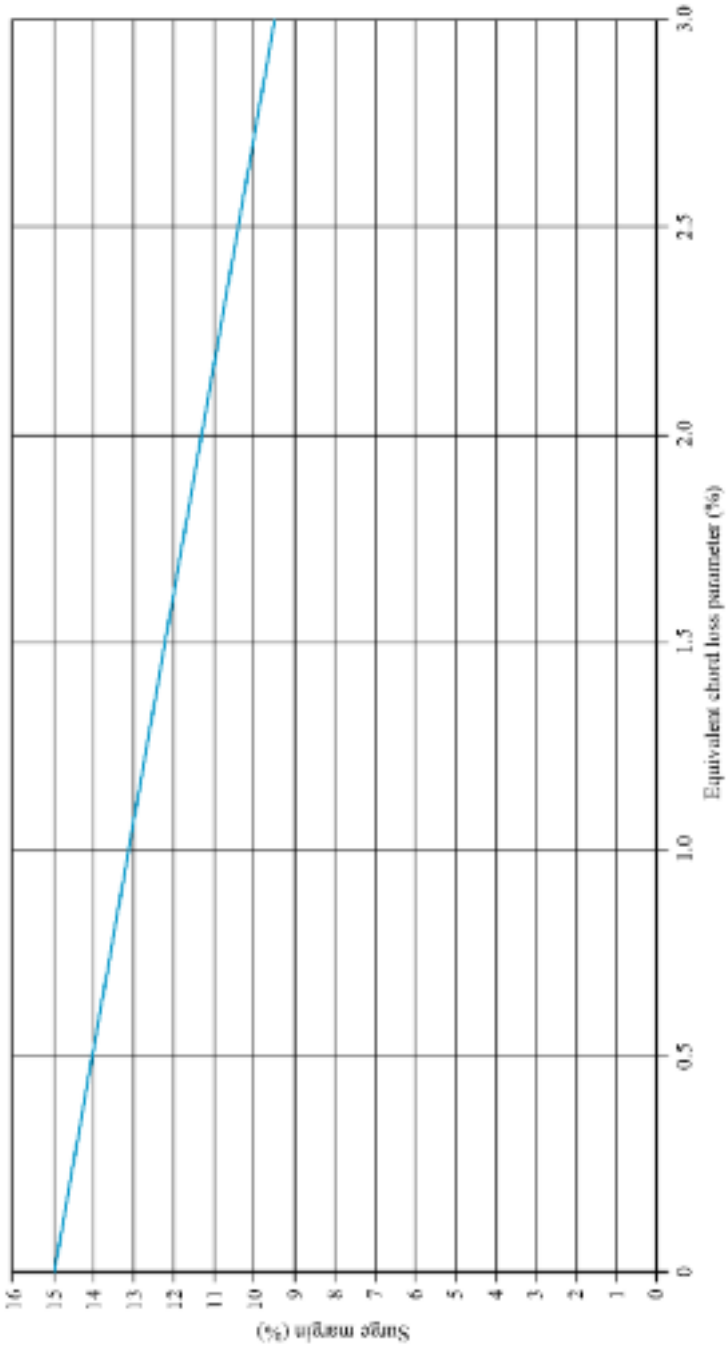

FIGURE 6.9. Surge margin versus blade degradation.

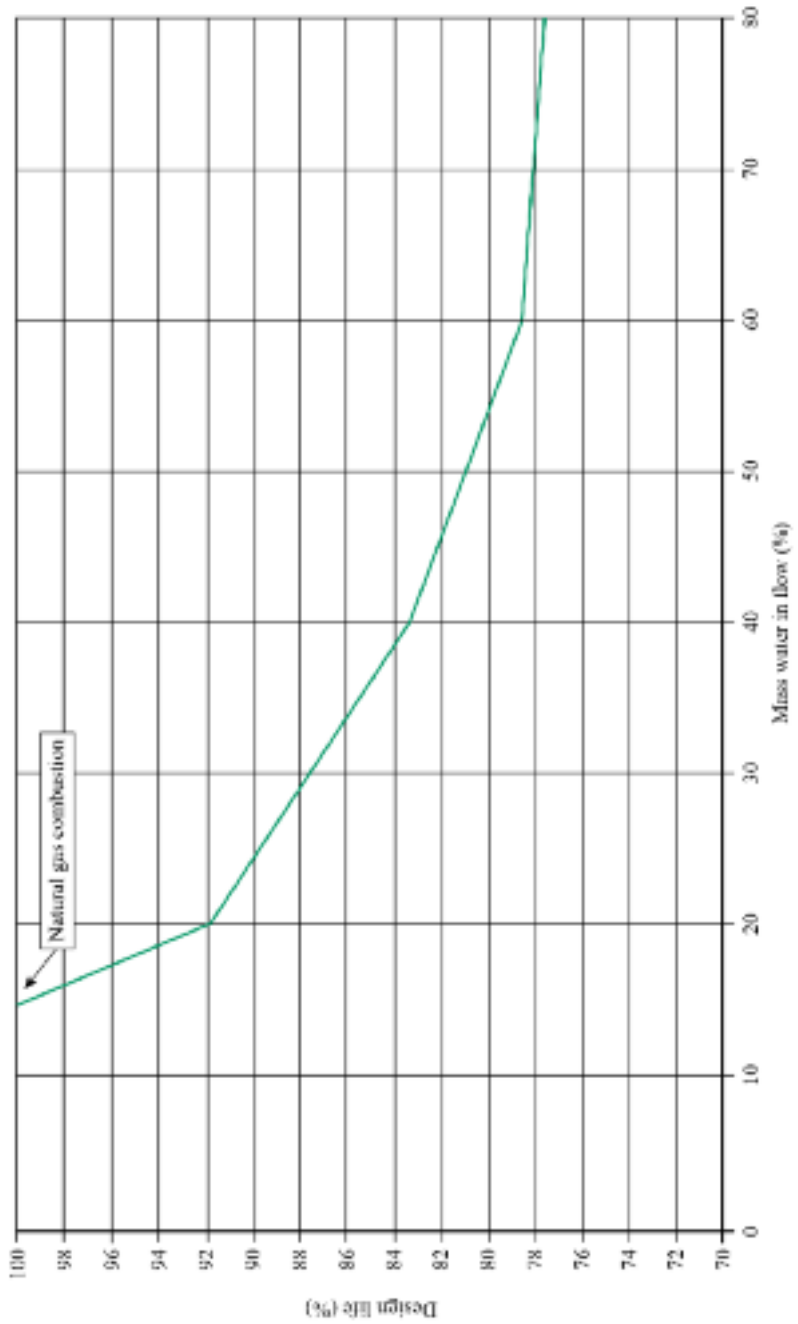

FIGURE 6.10. Hot-section parts life fraction.

SUMMARY

Only limited historical operating data on the long-term effect of gas turbine inlet evaporative cooling and water injection is available. However, over the past 15 years, manufacturers have built or retrofitted more than 800 gas turbine installations worldwide with these technologies. The basic functional principle of all evaporative cooling technologies is that they reduce the gas turbine's inlet air temperature from the air's dry bulb to wet bulb temperature. Prior to utilizing evaporative cooling systems, a design engineer should undertake a stability review of the compressor in order to establish the reduction in compressor surge margin.

This chapter presented a method to evaluate the principal factors that affect a single-shaft gas turbine's compressor surge margin. We applied the method to a frame type gas turbine, and presented the results. The findings showed that when one combines inlet evaporative cooling and inter-stage water injection with other factors, the compressor aerodynamic surge margin can reduce to the point where the compressor will surge. We can directly link compressor aerodynamic instability to blade high-cycle fatigue and possible catastrophic gas turbine failure. Furthermore, any water injection into a gas turbine will reduce the high-pressure turbine vane and blade life. Operators can employ the method which this chapter describes to identify high-risk applications, and bound the gas turbine operating range to limit the potential risk of compressor surge.

REFERENCES

Bhargava, R., and Meher-Homji, C.B. (2002), "Parametric Analysis of Existing Gas Turbines with Inlet Evaporative and Overspray Fogging", *Proceedings of the 47th American Society of Mechanical Engineers Gas Turbine and Aeroengine Congress*, Amsterdam, Netherlands, 3–6 June, Paper No. GT-2002-30560.

Bhargava, R., Bianchi, M., Melino, F., Peretto, A., Meher-Homji, C.B., and Chaker, M.A. (2003a), "Inlet Fogging for Gas Turbine Power Augmentation — A State-of-the-Art Review", *Proceedings of the International Conference on Power Engineering-03* (ICOPE-03), Kobe, Japan, 9–13 November, pp. 129–35.

Bhargava, R., Bianchi, M., Melino, F., and Peretto, A. (2003b), "Parametric Analysis of Combined Cycles Equipped with Inlet Fogging", *Proceedings of the 48th American Society of Mechanical Engineers Gas Turbine and Aeroengine Congress*, Atlanta, USA, 16–19 June, Paper No. GT-2003-38187.

Boyce, M.P. (2011), *Gas Turbine Engineering Handbook*, 4th edn, Butterworth-Heinemann, Oxford, UK.

Chaker, M., Meher-Homji, C.B., and Mee III, T.R. (2002a), "Inlet Fogging of Gas Turbine Engines," Part A: Fog Droplet Thermodynamics, Heat Transfer and Practical Considerations", *Proceedings of the 47th American Society of Mechanical Engineers Gas Turbine and Aeroengine Congress*, Amsterdam, Netherlands, 3–6 June, Paper No. GT-2002-30562.

Chaker, M., Meher-Homji, C.B., and Mee III, T.R. (2002b), "Inlet Fogging of Gas Turbine Engines, Part B: Fog Droplet Sizing Analysis, Nozzle Type, Measurement and Testing",

Proceedings of the 47th American Society of Mechanical Engineers Gas Turbine and Aeroengine Congress, Amsterdam, Netherlands, 3–6 June, Paper No. GT-2002-30563.

Corsini, A., Marchegiani, A., Rispoli, F., Sheard, A.G., and Venturini, P. (2012), "Predicting Blade Leading Edge Erosion in an Axial Induced Draft Fan", *Transactions of the ASME, Journal of Engineering for Gas Turbines and Power*, vol. 134, pp. 1–9.

Emmons, H.W., Pearson, C.F., and Grant, H.P. (1955), "Compressor Surge and Stall Propagation", *Transactions of the ASME*, vol. 77, pp. 455–69.

Hartel, C., and Pfeiffer, P. (2003), "Model Analysis of High-Fogging Effects on the Work of Compression", *Proceedings of the 48th American Society of Mechanical Engineers Gas Turbine and Aeroengine Congress*, Atlanta, USA, 16–19 June, Paper No. GT-2003-38117.

Horlock, J.H., (2001), "Compressor Performance with Water Injection", *Proceedings of the 46th American Society of Mechanical Engineers Gas Turbine and Aeroengine Congress,* New Orleans, USA, 4–7 June, Paper No. 2001-GT-0343.

Ingistov, S. (2001), "Interstage Injection System for Heavy Duty Industrial Gas Turbine Model 7EA", *Proceedings of the 46th American Society of Mechanical Engineers Gas Turbine and Aeroengine Congress*, New Orleans, USA, 4–7 June, Paper No. 2001-GT-407

Ingistov, S. (2002), "Interstage Injection into Axial Compressor, Gas Turbine Model 7EA", *Proceedings of the 47th American Society of Mechanical Engineers Gas Turbine and Aeroengine Congress,* Amsterdam, Netherlands, 3–6 June, Paper No. GT-2002-30656.

Kleinschmidt, R.V. (1947), "Value of Wet Compression in Gas-Turbine Cycles", *Mechanical Engineering*, vol. 69, pp. 115–16.

Kurz, R., and Brun, K. (2001), "Degradation in Gas Turbine Systems", *Transactions of the ASME, Journal of Engineering for Gas Turbines and Power*, vol. 123, pp. 70–77.

Sheard, A.G., Corsini, A., and Bianchi, S. (2010), "A Method of Detecting Stall in an Axial Fan", Patent No. GB 2 468 571 B.

Sheard, A.G., Corsini, A., and Bianchi, S. (2011), "Stall Warning in a Low-Speed Axial Fan by Visualisation of Sound Signals", *Transactions of the ASME, Journal of Engineering for Gas Turbines and Power*, vol. 133, Paper No. 041601, pp. 1–10.

Utamura, M., Kuwahara, T., Murata, H., and Horii, N. (1999), "Effects of Intensive Evaporative Cooling on Performance Characteristics of Land-Based Gas Turbine", *Proceedings of the 1999 International Joint Power Generation Conference and Exhibition, Sponsored by the Fuels and Combustion Division of ASME*, Burlingame, USA, 25–28 July, pp. 321–8.

White, A.J., and Meacock, A.J. (2003), "An Evaluation of the Effects of Water Injection on Compressor Performance", *Proceedings of the 48th American Society of Mechanical Engineers Gas Turbine and Aeroengine Congress*, Atlanta, USA, 16–19 June, Paper No. GT-2003-38237.

Wilcox, E.C., and Trout, A.M. (1951), "Analysis of Thrust Augmentation of Turbojet Engines by Water Injection at Compressor Inlet including Charts for Calculating Compression Process with Water Injection", NACA Report No. 1006.

Zheng, Q., Sun, Y., Li, S., and Wang, Y. (2002), "Thermodynamic Analysis of Wet Compression Process in the Compressor of Gas Turbine", *Proceedings of the 47th American Society of Mechanical Engineers Gas Turbine and Aeroengine Congress*, Amsterdam, Netherlands, 3–6 June, Paper No. GT-2002-30590.

Chapter 7

Transient Pressure Loss in Compressor Station Piping Systems

K. Brun, M. Nored, D. Tweten and R. Kurz

ABSTRACT

Engineers use the term "dynamic pressure loss" to describe the added loss that occurs with time-varying components of an unsteady flow through a piping system in centrifugal and reciprocating compression systems. Conventionally, one determines dynamic pressure losses by assuming a periodically pulsating one-dimensional flow profile and calculating the transient pipe friction losses by multiplying a friction factor by the average flow dynamic pressure component. In reality, the dynamic pressure loss is more complex, comprising different physical effects which include the piping arrangement, structural supports, piping diameter and the level of unsteadiness in the flow effect. The pressure losses due to fluid–structure interactions represent one of these physical loss mechanisms and are presently the most misrepresented loss term. Researchers have not previously quantified the dynamic pressure losses, dominated at times by fluid–structure interactions for transient flows in compressor piping systems. This chapter presents experimental results from an instrumented piping system fitted in a closed loop compressor facility that we used to determine the dynamic pressure loss component. Comparisons between predictions from a numerical model and experiments revealed that pressure losses that occur with the piping fluid–structure interactions can be significant, but conventional three-dimensional fluid models may not account for them.

This chapter is a revised and extended version of Brun, K., Nored, M., Tweten, D., and Kurz, R. (2010), "Transient Pressure Loss in Compressor Station Piping Systems", *Proceedings of the 55th American Society of Mechanical Engineers Gas Turbine and Aeroengine Congress*, Glasgow, Scotland, 14–18 June, Paper No. GT2010-22017. This paper won the International Gas Turbine Institute Oil & Gas Application Committee 2010 best paper award.

NOMENCLATURE

F_S	force matrix
P	pressure
K	structural stiffness matrix
S	displacement vector
T	temperature
V	velocity vector
c	specific heat
t	time
u	Cartesian x-direction velocity
x, y, z	Cartesian direction normal vectors
δ	finite displacement
∂_T	turbulent fluid and eddy viscosity
ρ	density
Φ	viscous dissipation function

INTRODUCTION

The fluid flow in compression station piping is typically highly transient as a consequence of pipe length acoustic resonances coupled with flow excitation. We may divide pipe flow pressure losses into steady-state pipe friction and time-transient losses. The centrifugal and reciprocating compression industry uses the term "dynamic pressure loss" to describe the sum of the time-transient pressure losses. For this chapter, dynamic pressure losses include periodic flow fluctuations, process system transients and random flow unsteadiness. These losses in centrifugal and reciprocating compression systems comprise an energy loss that one associates with the flow's unsteady component through the compression system's piping.

Flow through a compression system's piping may become unsteady as a consequence of vortex shedding from control valves or sensors and other protrusions into the piping. These unsteady flows are periodic in nature, typically pulsating at discrete frequencies which correspond to the vortex shedding frequency and the vortex shedding frequency's multiple harmonics. The compression system piping's design can result in a vortex shedding frequency, or one of its harmonics, coinciding with a piping acoustic resonance length which results in the unsteady flow component's amplification.

Furthermore, if a pipe vortex shedding frequency or harmonic aligns with a piping structural resonance, the compressor, piping or support structure may vibrate. Structure resonance in any rotating equipment will reduce the equipment's service life. These resonances also constitute a direct transfer of energy from the gas within the pipeline to the structure. This constitutes a transient pressure loss. Brun *et al*. (2007) observed that the peak-to-peak pulsation amplitude that occurs with a compression system's piping when in resonance may be in excess of 10 percent of the mean flow pressure. A 10 percent variation in the piping system pressure level results in a signifi-

cant compression system pressure loss. To avoid these pressure losses, engineers must design compression system piping to avoid acoustic and structural resonances.

Reciprocating compression systems are prone to piping resonance that result from the magnitude of flow pulsations emanating from the compressor. Typical reciprocating compressor outlet pressure varies between 1 and 5 percent of the mean value. This variation in outlet pressure is typically from 10 Hz for low-speed reciprocating compressors and up to 300 Hz for high-speed reciprocating compressors.

Broerman and Gatewood (2009) studied the magnitude of structural vibration and pressure pulsation levels and presented data from an in-service compression system (Figures 7.1 and 7.2). Broerman and Gatewood (2009) observed vortex shedding from the compression system anti-surge valve at 49 Hz. This corresponded to both an acoustic and structural resonance in the compression system. As the anti-surge valve induced the vibration, the anti-surge valve's position had a significant impact on the magnitude of both structural vibration and pressure pulsation level. A weakness of Broerman and Gatewood's (2009) research was their inability to record unsteady pressure data. Therefore, it was not possible to correlate the observed system resonance at different anti-surge valve positions with dynamic pressure loss.

Engineers conventionally calculate the dynamic pressure loss in a compression system by assuming a periodically pulsating one-dimensional flow profile. They then obtain the piping friction factor from a Moody diagram. A Moody diagram is a graph in non-dimensional form that relates the friction factor, Reynolds number and relative roughness for fully developed flow in a circular pipe. They then multiply the friction factor by the dynamic pressure for each time-step through a single time-discretized pulsation period.

LITERATURE REVIEW

Researchers have studied extensively loss mechanisms within turbomachinery (Denton, 1993). The academic community has paid less attention to loss mechanisms within compression system piping and the effects of pulsating flow in that piping. Despite the lack of attention, unsteady losses within a compression system's piping can affect compressor performance and in extreme cases result in compressor surge. As such, we need to understand and be able to model loss mechanisms within compression system piping if we are to provide design engineers with a tool to help them design the piping for a new compression system.

An origin of pulsating flow in a compression system's piping is the compressor's blade-passing frequency. Pulsating flow can also originate from valves in the piping, either upstream or downstream from the compressor. When flow passes a side branch in the piping, or there is a reciprocating compressor included in the compression system, flow pulsations can also occur. When the pulsating flow's frequency coincides with a system resonance, it creates additional energy loss through the fluid–structure interaction. If the resonance is poorly damped it may result in visible vibrations through the piping structure. The piping structure's vibration results in a net loss of energy from the system that translates into pressure loss in the piping.

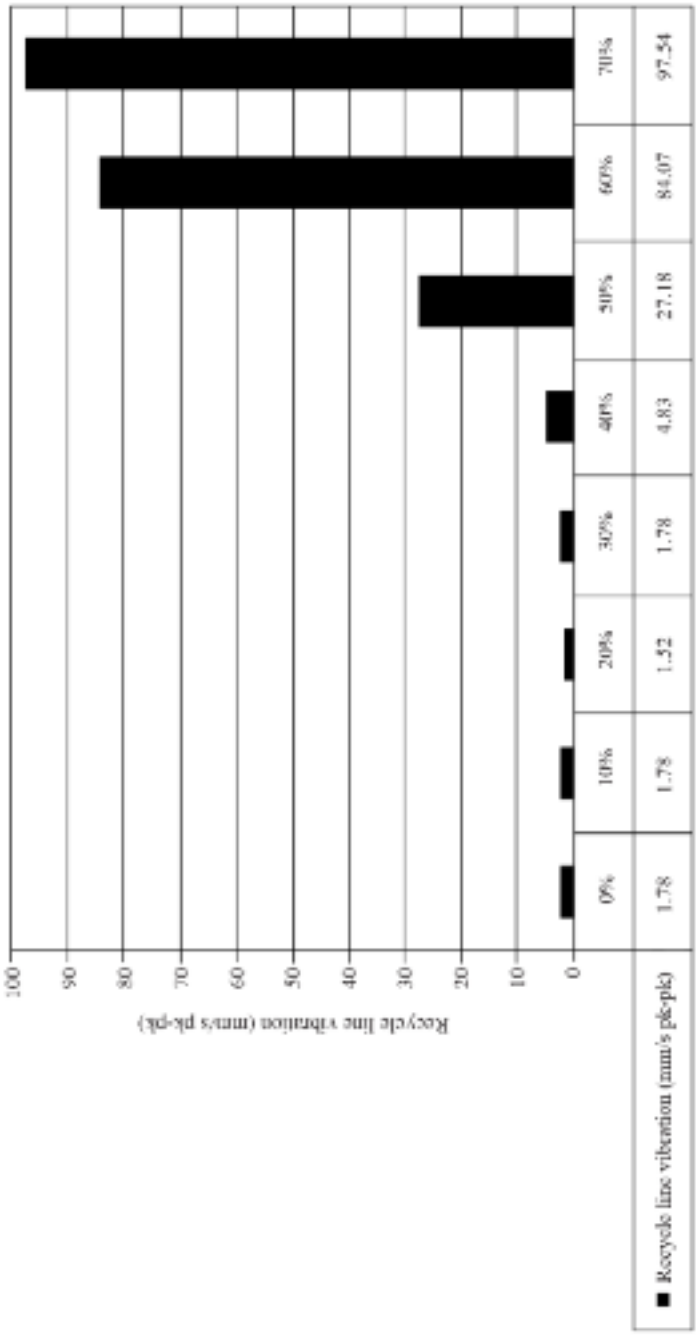

FIGURE 7.1. Measured vibration levels near a compression system recycle line anti-surge valve, from Broerman and Gatewood (2009).

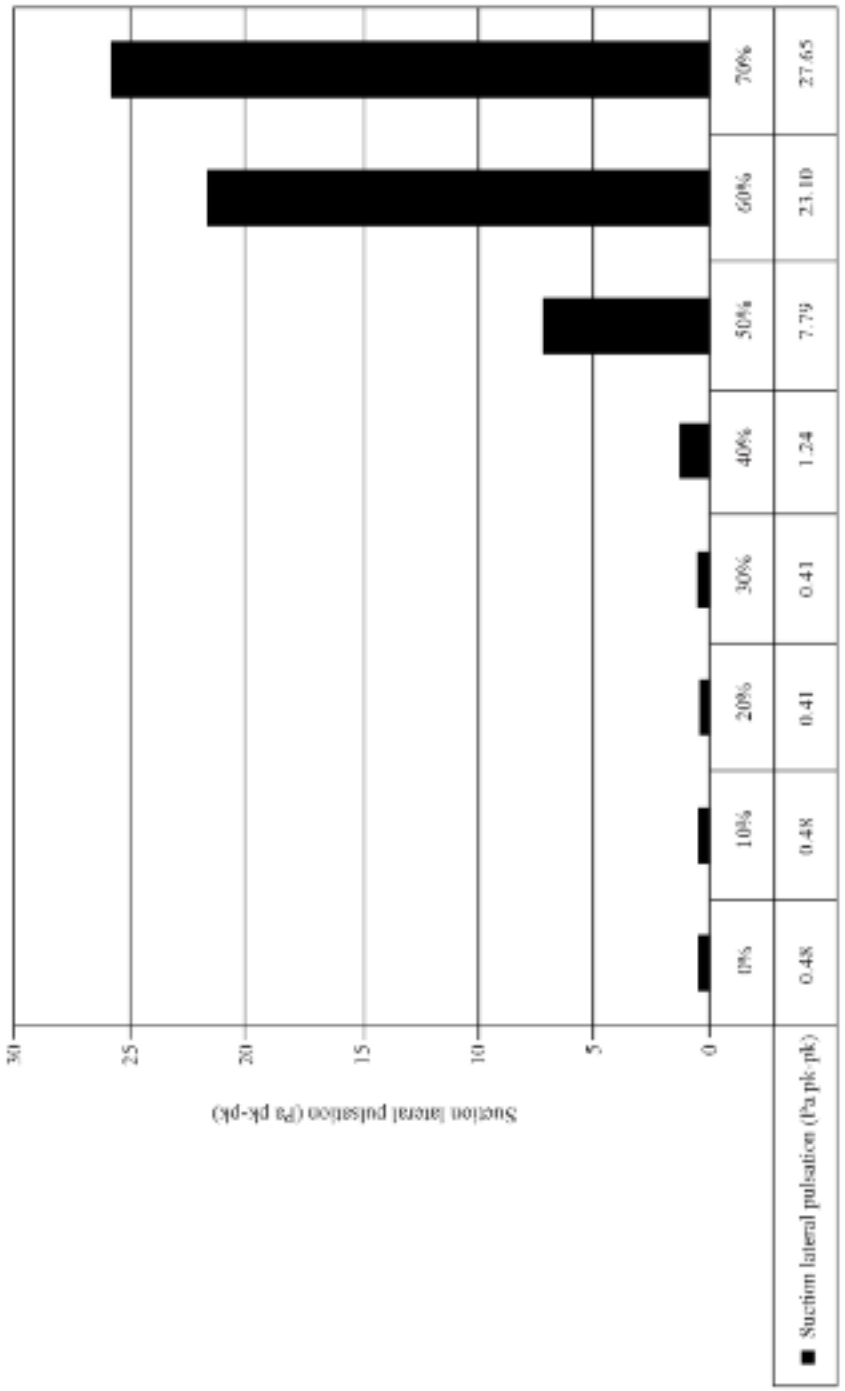

FIGURE 7.2. Measured pressure pulsation near a compression system recycle line piping tee, from Broerman and Gatewood (2009).

Researchers have studied compression system piping's influence on centrifugal compressor transient performance from:

- a fluid–structure interaction perspective;
- a compressor flow stability and surge perspective; and
- an active and passive control perspective.

Sparks' (1983) landmark piping system interaction research identified that a centrifugal compressor may amplify or attenuate pulsations and can induce surge. Sparks highlighted the importance of system design to avoid resonance, concluding that a centrifugal compressor feeding into a pipe or vessel's center is less prone to resonance than the same compressor feeding into a capped pipe end. As piping systems are composed of varying lengths, diameters and end designs, there are numerous reflection points in the piping that can result in almost any pulsating flow resonating. Sparks' field data indicated that low-frequency pulsations may be present regardless of the pulsating flow's magnitude or frequency within the piping. In effect, the compression system piping becomes a complex acoustic system that will always resonate.

Van Helvoirt and de Jager (2007) extended Sparks' (1983) work, focusing on the acoustic modes that occurred within a gas compression system. Their research concluded with an observation that one must utilize a non-linear model to predict piping acoustics and their effect on centrifugal compressor surge. Specifically, Van Helvoirt and de Jager (2007) concluded that the addition of acoustic damping terms to a lumped parameter surge model did not result in a model accurate enough to predict experimental results.

Jungowski *et al*. (1996) studied the effect of a pressure pulsation and its reflection points in a piping system and conducted a series of laboratory experiments on piping systems. They found that they could relate the surge condition's severity to the position of a 2-inch globe valve in the system piping for a 10-horsepower centrifugal compressor. When the globe valve was located near the compressor suction or discharge flange, the system flow impedance lowered and thus reduced the compressor's tendency to surge. Jungowski *et al*. (1996) also studied active control technologies using a throttled, controllable sleeve valve and a side-branch oscillator. The surge margin extended 30 percent by actively controlling the compression system's piping acoustic resonance characteristics and effectively eliminating the potential for surge-acoustic resonance coupling.

When studying the performance of a surge control system, Kurz and White (2004) commented on the actions required to avoid compressor surge. Specifically, they required a start-up and shut-down procedure that avoided destabilizing transient flow through the compressor. Tweten *et al*. (2008) studied the physics of pulsating flow in pipelines. They focused primarily on the behavior of pressure pulses across a matrix of configurations covering typical reciprocating compressor installations. Tweten *et al*. (2008) considered the influence of friction, orifice plate restrictions, branch lines and choke-volume systems, highlighting the improvements in pulsation analysis methods realized by a new Navier-Stokes equation formulation. This new

formulation included terms which acoustic wave equation based methods did not consider, therefore offering the potential of more accurate unsteady pressure loss predictions.

Researchers have studied fluid–structure interaction extensively in liquid flow systems. Recently, Wiggert and Tijsseling (2001) presented a one-dimensional model that linked a pipe's axial, lateral and torsional motion to one of four fluid loadings. These fluid loadings are:

1. T-section loading due to transmission and reflection of pressure and stress waves at a T-shaped piping branch;
2. closed end forces because of doubling of pressure waves due to unmovable closed end reflection;
3. moveable bends which couple the fluid and structure when the in-plane vibration occurs around an elbow; and
4. column separations which occur in liquid systems when the liquid pressure falls far enough for it to vaporize.

The researchers applied finite element modeling combined with fluid loading to predict the resulting fluid–structure interaction loads and resultant stresses. Wiggert and Tijsseling (2001) concluded that fluid–structural interaction is a complex phenomenon that is dependent on a piping layout and piping supports.

The majority of previous unsteady loss numerical modeling and experimental investigation has focused on incompressible flows. NASA also studied "sloshing" effects caused by fluid dynamic loads within the context of spacecraft design between the early 1960s through to 1980. Researchers found that "fluid slosh" in liquid propellant tanks influenced the astronaut's ability to control the spacecraft if not restrained (Abramson, 1966). Control and stabilization of the fluid and structure systems governed the resulting propellant tank design. Kana (1966) further extended Abramson's work (1966) by analyzing compressible fluids with inertial forces. Kana (1966) discusses the wave equation's solution with boundary conditions for the unsteady fluid pressure at the cylinder wall in a tank.

Moody (1990, 2007) undertook similar research to Kana (1966). He related gas effects to acoustic amplifications in liquids. In Kana's previous work (1966), the use of the acoustic wave equation was relevant as fluid flow in a tank was negligible. Both Moody and Kana were able to utilize the governing equations' linearized acoustic form since higher order pressure terms in the momentum equation were much smaller than the pressure forces. This is no longer the case in gas flows with high-pressure pulsations.

Diwakar and Lin (2007) utilized a combination of computational fluid dynamics and finite element analysis to predict vibration frequency and amplitude in compressor discharge piping. The computational fluid dynamics code simulated the unsteady flow rate from two compressors which researchers use as input to a finite element analysis code to predict vibration in a 12-inch diameter header connected by 10-inch diameter lateral pipes. Diwakar and Lin's research (2007) was helpful in that it established the possibility of developing a fluid–structural interaction model

based on a combined use of computational fluid dynamics and finite element analysis. Unfortunately, Diwakar and Lin (2007) had no experimental data to verify their predictions.

Researchers have studied dynamic pressure loss related to acoustic modes within the context of gas turbine combustor instabilities. Although the present work does not include combustion, one may apply some of the principles when attempting to elucidate loss mechanisms. Eckstein *et al*.'s experimental study (2006) showed that a normalized pressure loss produced by oscillations in the combustor chamber governed the combustor instability limit. Although entropy waves caused by local hot spots or temperature non-uniformities were measurable contributions to the oscillations, Eckstein *et al*. (2006) linked the dominant thermo-acoustic mode to the instability to which they referred to as combustor "rumble".

When considering the sources of loss in turbomachines, Denton (1993) highlights the influence of unsteady flow. Denton (1993) considers a loss as any flow feature that reduces the turbomachine's efficiency. Unsteady flow without regard to a fluid–structure interaction mechanism will create a velocity difference between the mainstream flow and the "center of the unsteadiness". Denton (1993) concluded that unsteady flows can result in a vortex stretching and compressing longitudinally. This reduces the stream tube diameter and increases the streamwise vorticity. This in turn results in higher viscous dissipation due to the unsteady streamwise velocity. Although Denton's (1993) work focuses on specific loss mechanisms within the turbomachine, it is possible to view the turbomachine and its piping system as a system whereby we can characterize and identify entropy losses to improve efficiency.

GOVERNING EQUATIONS

This conventional approach to the calculation of dynamic pressure loss does not include all the physical mechanisms that contribute to the actual dynamic pressure loss. The dynamic pressure loss is not a single pressure loss, but the sum of four different and discrete physical mechanisms. In order to better understand dynamic pressure loss, we must understand each mechanism and quantify its relative contribution to the overall pressure loss.

Transient flow

We can identify the origin of three of these mechanisms in the Navier-Stokes equations. The Navier-Stokes equations consist of: (1) conservation of mass, (2) conservation of momentum and (3) conservation of energy equations:

Conservation of mass:

$$\frac{\partial \rho}{\partial t} + \frac{\partial (\rho u)}{\partial x} = 0 \tag{1}$$

Conservation of momentum:

$$\rho \frac{\partial u}{\partial t} + \rho u \frac{\partial u}{\partial x} + \frac{\partial p}{\partial x} = \mu \nabla^2 u \tag{2}$$

Conservation of energy:

$$\rho c_v \frac{\partial T}{\partial t} + \rho c_v u \frac{\partial T}{\partial x} = \mu \nabla^2 T + \Phi \tag{3}$$

where temperature is related to pressure and density through an equation of state and Φ is the viscous dissipation function. Brun *et al*. (2007) have previously described the individual terms of these equations and their physical meaning in transient pipe flow and thus, we do not further discuss them here.

The aforementioned four dynamic pressure loss mechanisms are mathematically coupled by the Navier-Stokes equations and are functions of the equations' dependent variables and the fluid's physical properties. However, the dynamic loss mechanisms are only weakly physically inter-related and one can individually assess them to determine an additive combined pressure drop of unsteady and periodically pulsating flow in centrifugal and reciprocating compressor piping networks. These four dynamic pressure loss components are:

1. transient boundary layer viscous losses;
2. non-uniform flow internal profile shear stresses, secondary flows and turbulence;
3. inertial momentum change losses; and
4. fluid to piping driven dynamic structural losses.

We derive the first mechanism from the streamwise normal and bi-normal viscous terms of the momentum equation:

$$\mu_T \nabla^2 u = \mu_T \left(\frac{\partial^2 u}{\partial x^2} + \frac{\partial^2 u}{\partial y^2} + \frac{\partial^2 u}{\partial z^2} \right) = \mu_T \frac{\partial^2 u}{\partial x^2} + \frac{1}{2} \rho V^2 \frac{1}{d} c_f \tag{4}$$

where ∂_T is the combined viscosity and turbulent eddy viscosity, V is the streamwise bulk-flow velocity and c_f is a viscous loss coefficient for pipe flow. As described above, we determine this from pipe friction loss coefficients using Moody diagrams or other empirical tabulations. The dynamic pressure loss is:

$$\Delta P = \iint \mu_T(x,t) \nabla^2 u(x,t) \cdot dx dt \tag{5}$$

When calculating the dynamic pressure loss, it is important to consider the effects of the local Reynolds number. For high flow velocities, it is also important to

consider the effect of the profile-averaged pipe flow's Mach number on the empirical loss coefficient, c_f.

The second dynamic loss mechanism comprises non-uniform flow profile shear stresses, secondary flows and turbulence losses. This second dynamic loss mechanism usually represents a small proportion of the overall dynamic pressure loss in pipe flow and does not contribute significantly to the associated dynamic pressure drop. However, this dynamic loss mechanism can be a primary generator of acoustic emission in pipe flow, especially for highly turbulent or three-dimensional flow profiles. To calculate the dynamic pressure loss attributable to this second dynamic loss mechanism, one must integrate the viscous loss terms from the three-dimensional form of the energy equation:

$$\Delta P = \iint \Phi(x,t) \cdot dxdt = \iint \mu \left(2 \cdot \left(\frac{\partial u}{\partial x} \right)^2 + \left(\frac{\partial u}{\partial y} \right)^2 + \left(\frac{\partial u}{\partial z} \right)^2 \right) \cdot dxdt \tag{6}$$

The energy equation's three-dimensional form captures boundary layer losses if the integration continues into the flow's boundary layer region. However, continuing the integration into the flow's boundary layer region is mathematically inconvenient. Since for most piping transient flow analysis one assumes that the flow is one-dimensional, it is often difficult to perform this three-dimensional calculation. Sometimes one can estimate the secondary flow losses' relative contribution to the overall pressure drop from empirical correlations, but for three-dimensional piping configurations, these approximations are usually poor.

The third dynamic loss mechanism is the fluid's inertial momentum change. The fluid molecules' continuous acceleration and deceleration in unsteady pipe flow drives this dynamic loss mechanism. We can determine the energy which this momentum change expends from an integration of the momentum equation:

$$\Delta P = \iint \rho(x,t) \left(\frac{\partial u}{\partial t} + u \frac{\partial u}{\partial x} \right) dxdt \tag{7}$$

Researchers often overlook this third dynamic loss mechanism which can significantly contribute to the dynamic pressure loss in highly pulsating flows. However, if one utilizes a transient flow solver and computes the momentum equation's discretized inertial terms, the pressure loss that occurs with this third dynamic loss mechanism becomes implicit in the solution. It is therefore not necessary to separately calculate it.

The fourth dynamic loss mechanism that contributes to dynamic pressure losses in pipe flow is the fluid to piping driven dynamic structural losses. This fourth dynamic loss mechanism requires a physical understanding of the piping system as it originates from a fluid–structural interaction. This fourth dynamic loss mechanism is the only mechanism that we cannot characterize using the governing fluid flow equa-

tions. The governing fluid flow equations do not account for the fluid's interaction with externally applied body forces. These external body forces become significant when pressure pulsations from the unsteady pipe flow become excessive. Excessively large pressure pulsations result in structural pipe vibrations. These structural vibrations require energy to overcome the piping's damping. To generate piping vibrations, the flow must transfer some energy to the pipe structure which manifests itself as a pressure loss.

Researchers have historically neglected this fourth dynamic loss mechanism as it requires a dynamic model of the energy transfer from wall pressure fluctuations onto the piping structure. This dynamic modeling is challenging, and therefore design engineers usually overlook pressure losses that occur with this fourth dynamic loss mechanism. Overlooking the pressure loss is potentially problematic, as these losses can comprise a significant proportion of the overall dynamic pressure loss.

This chapter presents the experiments that we performed in a transient reciprocating compressor closed loop facility to determine the magnitude of the pressure loss associated with each of the dynamic loss mechanisms using dynamic pressure and vibration measurements. We repeated the experiments for different structural constraint conditions on the same reciprocating compressor discharge piping system. In the first test, we added structural constraints to the piping to eliminate horizontal and vertical motion. We repeated the tests with the pipe constraints removed, allowing free structural motion in the horizontal and vertical directions. We performed the first and second tests over a speed range of 400 to 900 rpm. The speed range included flow rates where the fluid flow excited the piping structure. This chapter presents experimental results and quantitatively assesses and compares them to computational predictions in an effort to establish the relative contribution of the four dynamic loss mechanisms to the overall dynamic pressure loss.

Fluid–structure interaction

We may present the fluid–structural interaction equations in terms of energy conservation, where the system's overall energy is conserved. Shaaban's (1979) formulation provides one of the expressions of the energy conservation approach. The structural force equation includes a coupling matrix multiplied by the incident pressure:

$$\{F_x\} = [K]\{\delta_U\} + [C]\{\dot{\delta}_U\} + [M + ADM]\{\ddot{\delta}_U\} + [S]^T\{\delta_{Pi}\} \tag{8}$$

We define the added mass matrix [*ADM*] as the product of the transposed coupling matrix, a stiffness matrix and the coupling matrix itself:

$$[ADM] = [S]^{\mathrm{T}}[K_{UU}]^{-1}[S] \tag{9}$$

The *ADM* term represents the inertial fluid mass responsible for the force exerted on the structure. The pressure in the system (*Pu*) is represented by:

$$\{\delta_{Pu}\} = \{\delta_{Pr}\} + \{\delta_{Pi}\} \tag{10}$$

The fluid–structural interaction equations define a relationship between stiffness, affected by clamping the pipe in place, movement of the pipe wall and the incident pressure force exerted on the structure by the fluid as a consequence of a coupling coefficient.

We have simplified the fluid–structural interaction equations to avoid the complexity that occurs with calculating terms likely to be second or third order. Despite the formula simplification, we were able identify that the pipe's higher order acceleration term at resonance dominates the system's behavior. At resonance the higher order acceleration term drives the coupling between the fluid system and the damping term in the structural equation. It is the structural equation's damping term that defines the rate at which energy transfers from the fluid system to the piping system.

In our formulation of the fluid–structural equations we chose to use the acceleration term for coupling in contrast to other researchers who had chosen to use the velocity term (Shaaban, 1997; Diwakar and Lin, 2007). Fluid–structural interaction only becomes significant if the piping is able to move under load. If the piping is rigid, displacement, velocity and acceleration terms within the fluid–structural equations will be negligible. If the piping is rigid the total system energy remains within the fluid itself, and no energy is lost through damping in structure. Assuming that there is some flexibility in the piping to allow energy to transfer from the fluid to the structure, the coupling term becomes significant at resonance. It is at resonance that a significant energy transfer from the fluid to structure occurs. During a non-resonant condition, the coupling term effect is small and does not contribute significantly to the compression system's dynamic pressure loss. The net effect of fluid–structural interaction is that structural vibrations dissipate energy from the fluid. This results in an energy loss from the fluid which can comprise a significant proportion of the overall compression system's dynamic pressure loss.

The present research focuses on compression systems with large pressure pulses relative to the mean fluid pressure in compression system piping flows during a resonant condition. In this context we define a large pressure pulse as a pressure pulse of at least 5 percent of the mean fluid pressure, and more typically 10 percent. Reciprocating compressor-generated pressure pulses classically result in a strongly coupled piping structure to the fluid force at a single resonant frequency.

Despite strong coupling at the reciprocating compressor operating frequency, the resulting pressure pulses are also reflected from piping bends, joints and splits. Consequently, the fluid–structural interaction equations become progressively less accurate as the pipework becomes progressively more complex. We observe that we could extend usefully the research that we report in this chapter to further study the mechanisms by which piping fluid and the piping structure couple at resonant conditions in complex piping geometries. Such research has the potential to improve the accuracy with which computational models predict the dynamic pressure loss in compression systems.

Because of the pressure pulse behavior's complexity, the piping system response and the fluid–structure coupling, the classic fluid–structural interaction equations may not directly apply in all instances. Furthermore, the present findings suggest that further study of the coupling between fluid and structure at resonance is warranted in order to predict the dynamic pressure loss accurately.

EXPERIMENTAL SETUP

We constructed an experimental facility using a Southwest Research Institute (SwRI) reciprocating air compressor laboratory. This experimental facility had the instrumentation to provide dynamic pressure data during pressure pulsations to compare with predictions from a computational fluid dynamics model. We configured the experimental facility such that we could operate it both in resonant and non-resonant conditions. The goal was to accurately determine the flow pulsations' dynamic pressure losses and pipe displacement and acceleration in three directions, in a normal operating mode without an acoustic resonance and in a resonant condition when the half-mode wavelength frequency coincided with the compressor excitation frequency.

We extended compressor discharge piping with an 18-foot straight length of 4-inch diameter pipe, linking the compressor discharge valve to the first volume bottle's entrance (Figures 7.3 and 7.4). We instrumented the discharge piping with

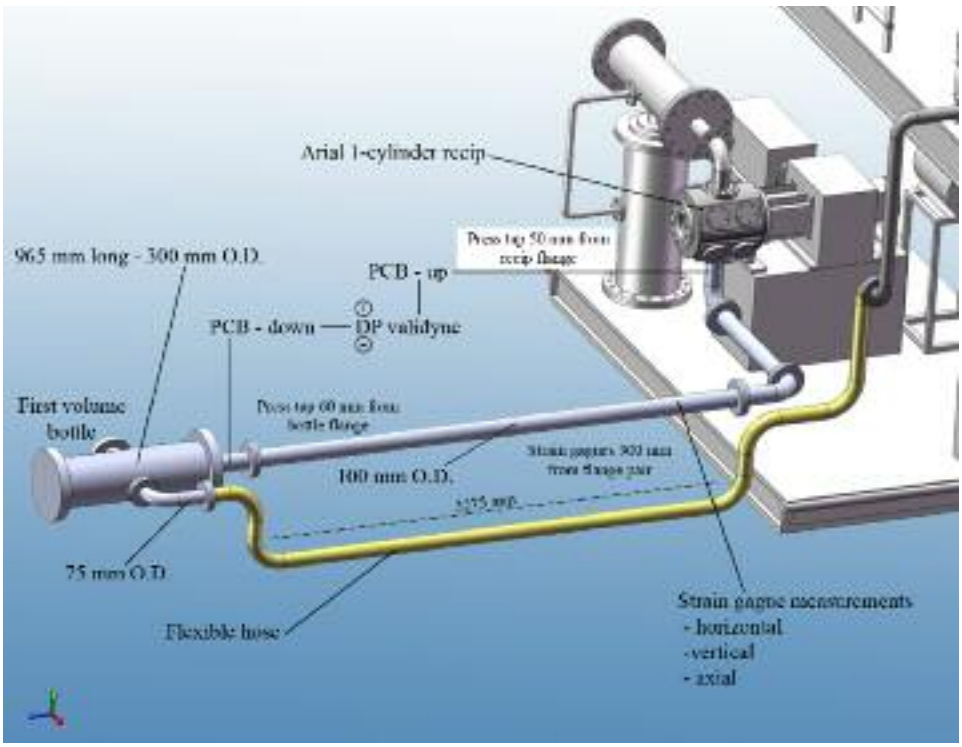

FIGURE 7.3. Schematic of experimental test setup and measurement points.

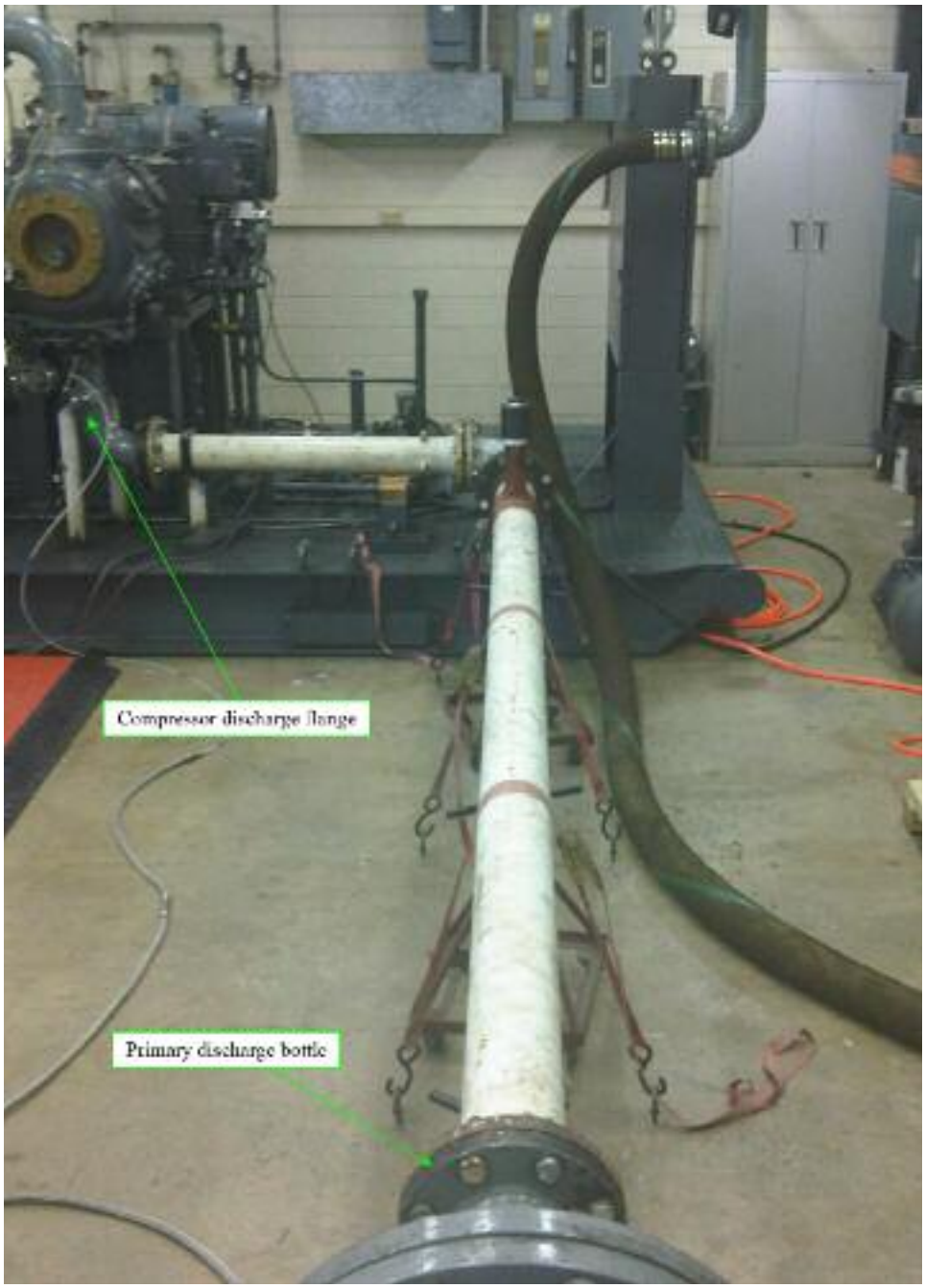

FIGURE 7.4. Southwest Research Institute air compressor discharge piping.

fast response dynamic pressure transducers as well as strain gages that were oriented in the horizontal, vertical and axial directions on the primary discharge pipe. The test setup facilitated pressure pulsation measurements in the reciprocating compressor discharge flow at the compressor nozzle, immediately downstream of the discharge valve and at the inlet to the first volume bottle. We also measured differential pressure drop between these two test points with a fast response dynamic pressure transducer.

We tuned the experimental facility piping resonant length's half-wave mode to 14.5 Hz as a system comprising the primary 4-inch compressor discharge piping and the loop piping back to the volume control bottles (Figure 7.3). We purposefully tuned the facility piping resonant length's half-wave mode to coincide with the reciprocating compressor's 435 rpm second order harmonic (Figure 7.5).

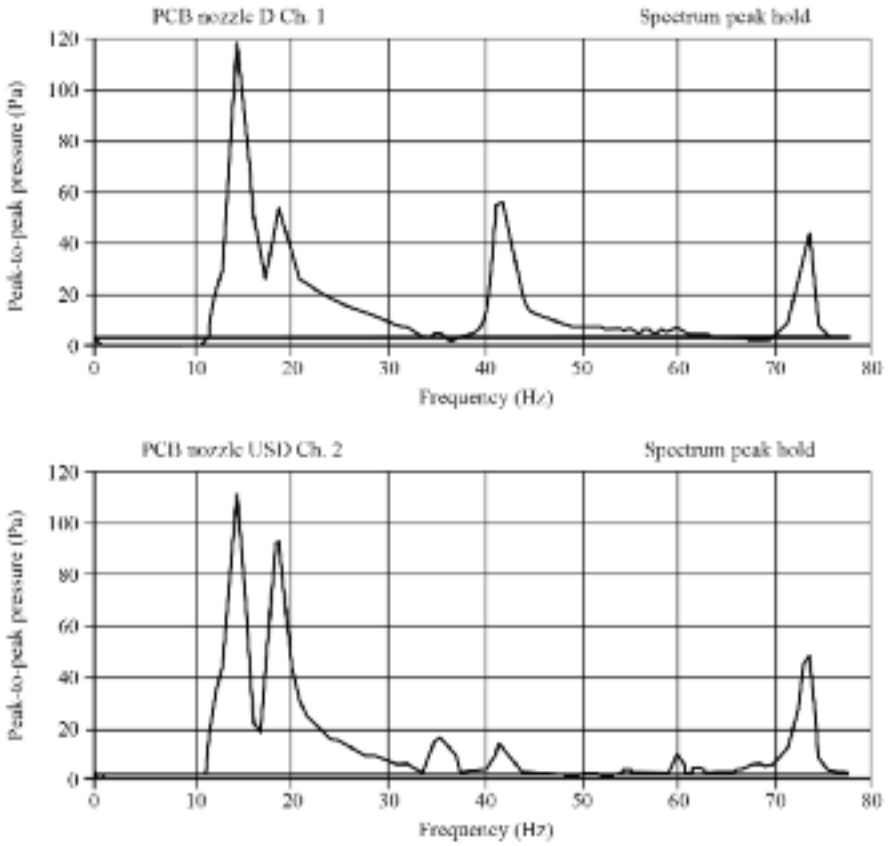

FIGURE 7.5. Speed sweep data to determine system resonance at 435 rpm for 2 × order (both dynamic pressure transducers on upstream and downstream end of the pipe are shown).

We used a calibrated Validyne dynamic differential pressure transducer to measure dynamic pressure loss across the discharge pipe. We used the experimental facility data acquisition system to average dynamic pressure for each 2-minute "steady state" test. We used the three-directional strain gages to record pipework vibration from which we could subsequently derive total pipe movement.

We operated the experimental facility's reciprocating compressor at a pressure ratio of 2.5 with a fixed suction pressure of 172 kPa over its speed range of 300 to 1000 rpm. We defined a test matrix at 300, 435, 600, 870 and 1000 rpm. At each speed we measured the fluid pressure pulse and structural vibrations with the experimental facility both in and out of resonance. We then repeated the test matrix with the piping constrained using two clamps prior to the elbow and two downstream prior to the bottle inlet. The clamps effectively reduced all pipe structural motion in the vertical and horizontal directions, but not the axial direction.

We calculated measurement uncertainty using Brun and Kurz's (2001) method for each sensor and its associated signal conditioning and data acquisition system. Brun and Kurz (2001) base individual uncertainties on total bounds for individual instruments and statistical bounds for data acquisition and analysis methods. Using the uncertainty analysis, we estimated the total dynamic pressure uncertainty that we associated with the experimental facility at ±0.7 kPa peak-to-peak.

TEST RESULTS

At non-resonant speeds of 20, 28 and 34 Hz, the dynamic pressure loss is less than 0.7 kPa for both the unconstrained and constrained conditions (Figure 7.6). The measured unconstrained and constrained pipe pressure losses were the same within

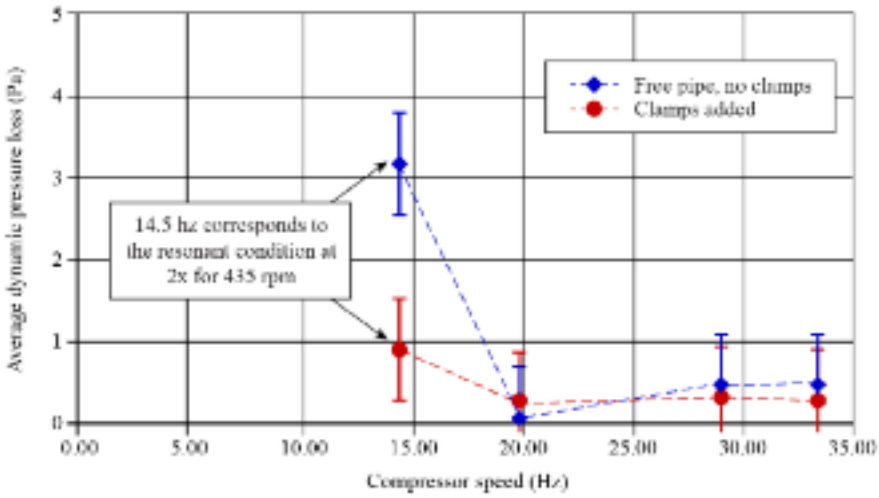

FIGURE 7.6. Experimental dynamic pressure losses for free (unrestrained) and constrained pipe.

the uncertainty of the measurement. However, at the resonant condition of 14.5 Hz, the free pipe dynamic pressure loss was 0.35 kPa, significantly greater than the 1.0 kPa that we measured with the constrained pipe.

The increase in dynamic pressure loss at 14.4 Hz illustrates the difference in dynamic pressure loss at resonance and non-resonant conditions. The reduced dynamic pressure loss that occurs with the constrained pipe illustrates the benefit of restraining pipe movement. We illustrate the importance of structural movement as a loss mechanism in fluid flow through piping for the resonant condition. If we had considered only flow-induced pressure pulses at the resonant condition, we would have underestimated substantially the dynamic pressure loss for an unrestrained pipe.

FLUID DYNAMIC MODELS

We created models of the compression system piping geometry and operating conditions using the commercially available CFDesign V.10 computation fluid dynamics software package. The CFDesign software package discretizes the governing equations using a finite element method derived from Galerkin's weighted residual method (Zienkiewicz, 1977). The CFDesign software package uses a two-equation k-epsilon turbulence model to determine the turbulent flow eddy viscosity and enforces the "Law of the Wall" to obtain turbulent boundary layer profiles. The package treats the non-linear advection terms using Rice and Schnipke's (1985) monotone streamline upwind method. One can solve the discretized equations using a segregated approach based on Patankar's (1980) SIMPLER method. Because of the non-linear and close-coupling of the governing equations, the package solver uses a Picard iterative process. We considered a solution converged when the governing equation's residuals were less than 10^{-4}.

We created two models of the compression system piping geometry and operating conditions: a steady-state flow model and a transient flow model. The transient flow model better represented the actual reciprocating compressor discharge flow. The two models modeled the compression system from the reciprocating compressor discharge to the first volume bottle (Figure 7.7). For both models, we used an unstructured mesh with 1,450,421 elements and 427,072 nodes configured as uniform tetrahedral elements. The models usually converged within 500 iterations when using a k-epsilon turbulence model.

The models predicted the pressure loss in the discharge pipe due solely to fluid effects. We then predicted energy dissipation to the structure by subtracting the computational prediction of the dynamic pressure loss due to fluid effects from the experimentally measured total dynamic pressure loss. We did not extend the computational modeling to include a finite element model of the pipework.

The computational model predicted a harmonic flow at the reciprocating compressor discharge nozzle. We modeled the peak flow and frequency at the discharge nozzle using experimental measurement. The applied harmonic flow had a magnitude of 3.95 meters per second and a frequency of 14.5 Hz. The pressure at the outlet was 632 kPa. The model began with initial conditions of no velocity and a

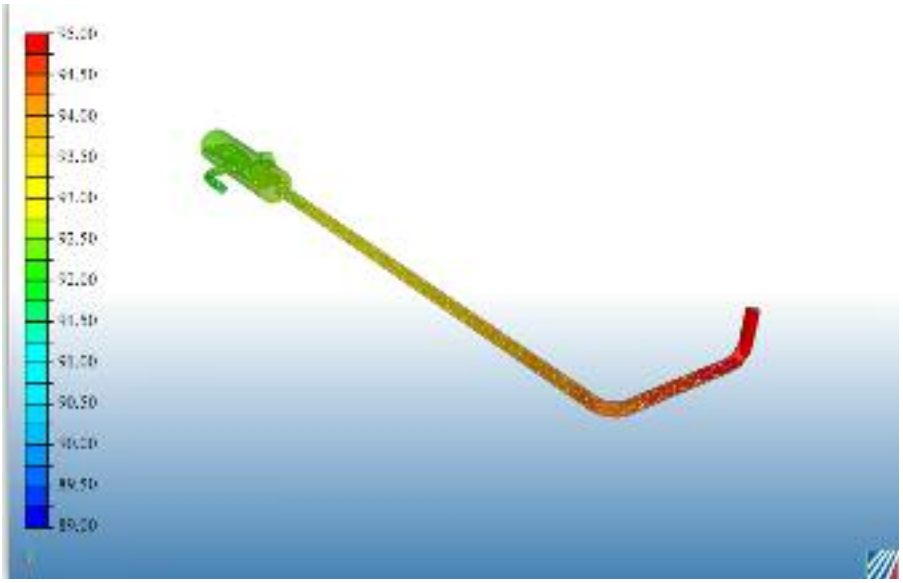

FIGURE 7.7. Computational fluid dynamic model of the experimental system (variation in color is a measure of the pressure intensity).

pressure of 632 kPa. The transient model had a time-step size of 0.0003 seconds, with the software saving results every 0.007 seconds for a sample rate of 143 Hz. We discarded the first two full cycles and retained results for the third cycle. The transient model's output included velocity and static pressure at each time-step. The software saved the velocity and static pressure's cross-sectional average at the discharge nozzle and bottle inlet for each time-step. We then calculated dynamic pressure at both locations from velocity and then added the calculated dynamic pressure to static pressure to give total pressure. We averaged total pressures over each cycle at each location and we defined the difference between the nozzle average and the bottle inlet average as the piping total pressure drop.

The second computational fluid dynamic model was a steady-state model. We applied a single constant flow to this steady-state model at the reciprocating compressor discharge nozzle which was equivalent to the average flow through the experimental facility. The steady-state model only included losses that occurred with steady flow.

In addition to the two computational fluid dynamic models, we also calculated the experimental facility dynamic pressure loss using a one-dimensional Navier-Stokes time domain solver. Brun *et al*. (2007) describe in detail the one-dimensional solver. The solver models a pulsating fluid system. However, since the model is one-dimensional it does not account for piping geometry and therefore is not as accurate as a computational fluid dynamic model. We created two one-dimensional models to match the dynamic and steady computational fluid dynamic models. The one-dimensional models include the cylinder gas passages, discharge pipe, bottle, flexible hose and a second bottle at the end of the hose.

COMPARISON AND RESULTS

The experimental results constituted the actual pressure loss due to both steady and unsteady effects. A comparison between the constrained and unconstrained measured data provided an assessment of the dynamic loss for the freely vibrating pipe. The four dynamic pressure loss components were:

1. transient boundary layer viscous losses;
2. non-uniform flow internal profile shear stresses, secondary flows and turbulence;
3. inertial momentum change losses; and
4. fluid to piping driven dynamic structural losses.

We found it helpful to first compare steady and dynamic computational predictions with experimental results (Figure 7.8). All predictions assume the same geometry, pipe length, friction factor and gas conditions. We compared four fluid models with experimental results:

1. a steady flow one-dimensional calculated loss solely based on the viscous loss coefficient and the steady flow term (steady one-dimensional);
2. a three-dimensional computational fluid dynamic model with calculated loss based on steady flow predictions including the effect of shear layer and viscous (steady enhanced three-dimensional);
3. a full Navier-Stokes implementation in one-dimension (dynamic one-dimensional); and
4, a full Navier-Stokes implementation in three-dimensions (dynamic three-dimensional).

When considering the data in Figure 7.8, the reader should bear in mind that of the computational predictions of dynamic pressure loss, none of the computational methods model the fourth dynamic pressure loss mechanism: fluid to piping driven dynamic structural losses.

The comparison of measured and calculated pressure losses in the discharge pipe (Figure 7.8) provides insight into the relative importance of the four dynamic pressure loss mechanisms. Comparison of the predicted one-dimensional steady flow loss to the predicted one-dimensional dynamic flow (dynamic one-dimensional) loss highlights that the unsteady flow loss is ten times that of the steady flow loss. The most likely reason the unsteady loss is an order of magnitude greater than the steady flow loss is a consequence of the dynamic flow and the model differences in accounting for the fluid's inertial momentum change. The dynamic steady flow loss prediction therefore models the fluid flow physics more accurately than the one-dimensional steady flow prediction.

The one-dimensional steady flow calculation uses both the average velocity and the associated "average" Reynolds number based on the average velocity. Calculating the pressure drop using the steady flow as representative of the true pulsating

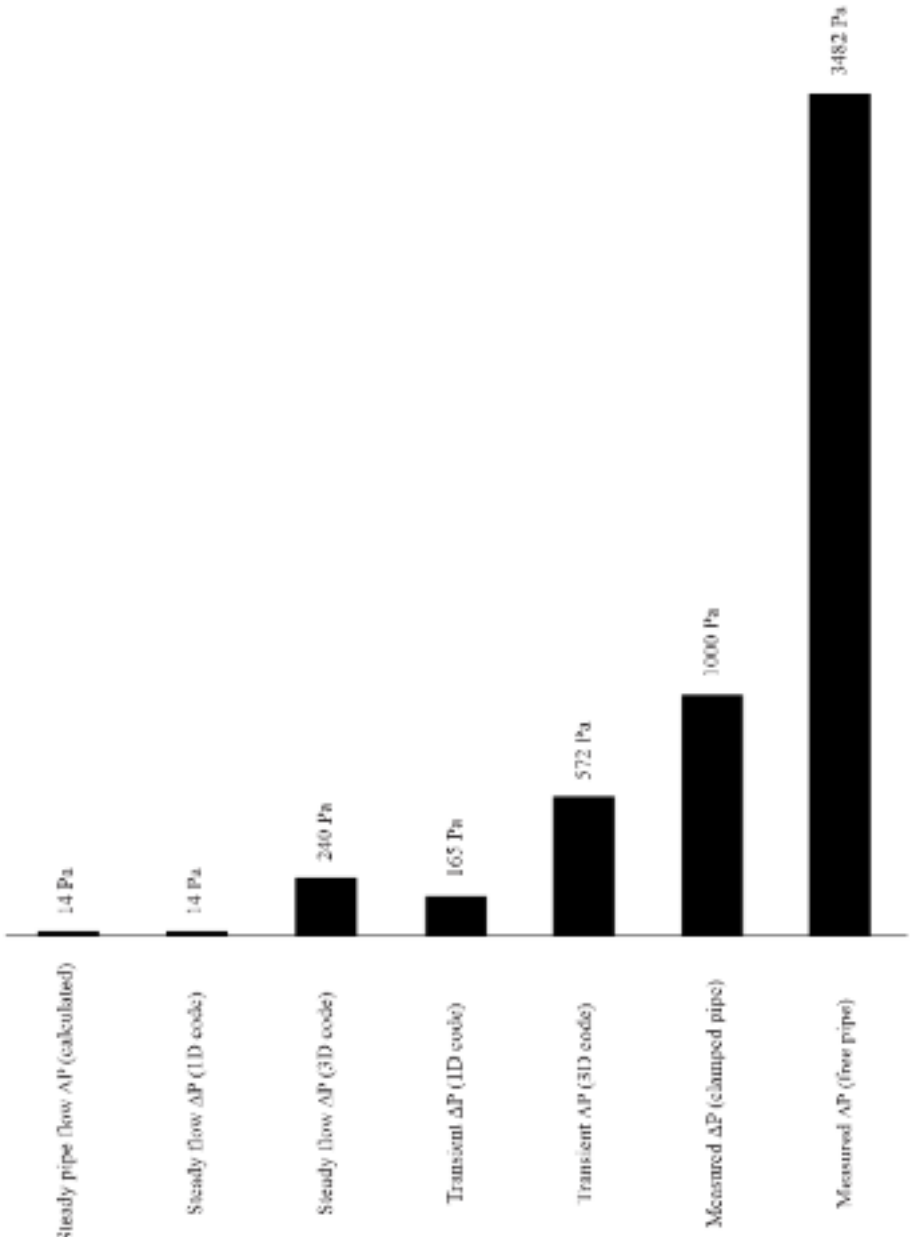

FIGURE 7.8. Comparison of measured and calculated pressure losses in the discharge pipe.

flow will always result in underestimating the total pressure drop in the piping because the pressure drop is proportional to the instantaneous velocity squared.

Both one-dimensional models underpredict the actual dynamic pressure loss. The three-dimensional steady flow models account for the effect of three-dimensional geometry on steady flow loss. The additional losses that occur with three-dimensional flow originate from boundary layer turbulence and shear layer losses. These boundary layer turbulence and shear layer losses vary with piping geometry. Compression system piping invariably includes application-specific discharge piping expansions, contractions and bends. The cumulative effect of the piping geometry on the boundary layer turbulence and shear layer losses resulted in the three-dimensional steady flow loss increasing. The steady one-dimensional model predicted a pressure loss of 14 Pa. The predicted one-dimensional dynamic flow loss from the dynamic one-dimensional model was 150 Pa greater than the steady one-dimensional model, predicting a total pressure drop of 165 Pa. The loss predicted by the steady enhanced three-dimensional model was 240 Pa, which was 228 Pa greater than the steady flow model.

In combination, the deltas from the base one-dimensional steady model using the one-dimensional dynamic flow model and the three-dimensional steady flow model (228 Pa and 150 Pa, respectively) identify the additional losses over and above the inertial momentum losses and the steady flow three-dimensional boundary layer losses. Neither model accounts for both of these terms but both of these loss terms are of the same order of magnitude. One should include both loss terms in any assessment of actual pressure loss in combination with the simplified one-dimensional steady flow loss prediction of 0.002 psi. Since the models depict different loss terms, one can estimate the total pressure drop at 392 Pa (14 + 228 + 150 Pa), accounting for all three terms. However, this estimate still does not account for all sources of pressure loss and therefore, one must consider the dynamic three-dimensional model.

The three-dimensional dynamic prediction of 572 Pa comes closer to the measured dynamic pressure loss of the constrained pipe of 1000 Pa (Figure 7.8). The three-dimensional dynamic model combines all fluid-based losses with the exception of losses that occur with fluid–structural interaction effects. Although the experimental facility piping was constrained during the "constrained" test, it is likely that the piping clamps did not fully constrain the pipe and consequently, some energy transferred to the structure and dissipated. This dissipated energy is probably responsible for the difference in the measured dynamic pressure loss and the three-dimensional dynamic code prediction (approximately 428 Pa (1000 – 572 Pa)), and we can attribute it to the fluid–structural losses for which we did not account in the solely fluid-based model.

The results from the three-dimensional dynamic prediction suggest that it is possible to use a three-dimensional computational fluid dynamic model to estimate the dynamic pressure loss if the fluid structural losses are not significant. Note that we assumed incompressible flow in the three-dimensional dynamic model to increase the speed of the calculations. It is possible that if the three-dimensional dynamic model were enhanced to include compressibility effects, the predicted

dynamic pressure loss would be closer to the constrained pipe's 1000 Pa measured dynamic pressure loss.

The measured unconstrained pipe pressure loss was 3482 Pa compared to 165 Pa using the dynamic one-dimensional model indicating that the true pressure loss was 21 times greater than we predicted using the dynamic one-dimensional model (Figure 7.8). Using the enhanced three-dimensional model, the predicted pressure loss was 240 Pa. This indicated that the true pressure loss was 14 times greater than we predicted using the enhanced three-dimensional model. Using the three-dimensional dynamic model, the predicted loss was 572 Pa. This indicated that the true pressure loss was six times greater than we predicted using the three-dimensional dynamic model. Without integrating the piping structure's finite element analysis into the prediction of dynamic pressure loss, the three-dimensional model will not predict the dynamic pressure loss that occurs with fluid–structural interaction effects when the piping is in resonance. When in a resonant condition, dynamic pressure losses that occur with fluid–structural interaction dominate the other three dynamic pressure loss mechanisms.

SUMMARY

In many compression system piping arrangements, acoustic and mechanical resonance do occur. The research in this chapter provides insight into the distribution of steady and unsteady losses, one-dimensional and three-dimensional driven piping loss mechanisms.

We have also clarified the magnitude of the additional dynamic pressure loss that occurs with fluid–structural interaction when in resonance. The experimental results illustrate that structural motion which unsteady fluid flow drives can significantly increase the dynamic pressure loss through compression system piping. The increase in dynamic pressure loss between constrained and unconstrained pipes occurs as a consequence of fluid forces coupling with the piping structure. This results in the pipe vibrating.

When a compression system's piping is not in resonance, a three-dimensional dynamic model has the potential to produce a reasonably accurate prediction of dynamic pressure loss. When a compression system's piping is resonating, fluid pulsations couple with the piping structure and both one- and three-dimensional dynamic predictions underpredict dynamic pressure loss. The three-dimensional dynamic prediction does not model fluid–structural interaction. It produced results that were the same order of magnitude as the constrained pipe experimental data. The agreement between the three-dimensional dynamic prediction and the constrained pipe experimental data illustrates the importance of structural movement as a loss mechanism at resonance. A large and unpredicted pressure loss will manifest itself in an inadequately constrained compression system piping.

The experimental results indicate that as the structure becomes more compliant, the pressure loss at resonance conditions increased by up to 21 times the value predicted using the dynamic one-dimensional model and up to six times the value pre-

dicted by the most advanced dynamic three-dimensional model. Using a dynamic three-dimensional model and applying structural constraints to the piping system illustrated that a reasonably accurate dynamic pressure loss is possible. Design engineers may use a three-dimensional dynamic model to estimate the effects of dynamic pressure losses on compressor performance, surge stability and different piping arrangements. However, the design engineer's primary objective must be to configure the compression system piping to avoid fluid–structural induced resonance. Neither the one- or three-dimensional dynamic models accounted for losses that occur with fluid–structural induced resonance.

When we consider differences between predicted and measured dynamic pressure losses, we can draw the following conclusions regarding the relative importance of the four dynamic pressure loss mechanisms:

1. Transient boundary layer viscous losses: when calculating the dynamic pressure loss, the local Reynolds number effects will be significant for pulsating flows. The local Reynolds number variation modeling is the reason why the dynamic one-dimensional model was closer to the measured pressure loss than the steady one-dimensional model.
2. Non-uniform flow internal profile shear stresses, secondary flows and turbulence: the "second term" dynamic loss mechanism can be a primary generator of acoustic emission in pipe flow, especially for highly turbulent or three-dimensional flow profiles. The three-dimensional steady flow models account for the effect of three-dimensional geometry on steady flow loss. Some of these second term additional losses associated with three-dimensional flow originate from boundary layer turbulence and shear layer losses. The calculated pressure loss from the dynamic one-dimensional model is 21 times lower than the measured pressure drop, compared to the steady enhanced three-dimensional model, which was 14 times lower than the measured value. We can expect this difference since one-dimensional models are less accurate than computational fluid dynamic models when calculating pressure drop even if one accurately predicts the pulsation levels because the three-dimensional models account for the "second term" influences.
3. Inertial momentum change losses: the fluid molecules' continuous acceleration and deceleration in an unsteady pipe flow drive this dynamic loss mechanism. At resonance, the fluid acceleration and deceleration amplitudes amplify and a steady flow model underestimates the dynamic flow's inertial momentum changes. In addition, we should include compressibility to accurately model inertial momentum variations. The dynamic pressure loss in the three-dimensional fluid model was within 43 percent of the pressure loss which we measured off-resonance. The incompressible assumption likely lowered the velocity peaks in the fluid model. This reduced the overall pressure drop in the model.
4. Fluid to piping driven dynamic structural losses: typically, engineers do not consider fluid–structure interactions in fluid models of centrifugal and reciprocating compressor systems and these structural energy dissipations will

increase the pressure drop at resonance. Based on the data in this chapter, the structural energy dissipation at resonance is two to six times. This depends on constrained or unconstrained pipes and the predicted dynamic pressure loss due to fluid effects alone.

An accurate prediction of dynamic pressure loss must consider the fluid–structural induced loss mechanism, as well as the three loss mechanisms that we associate with fluid forces. Currently, there is no commercially available simulation package that combines an analysis of pulsating fluid flow with a structural vibration analysis. Although it may be possible to combine and couple a fluid-based model and its resulting forces with a finite element analysis model, the prediction of the fluid-driven structural energy losses and the coupling between the fluid and the structure is complex. At present, this type of coupled analysis is not something that the design engineer can realistically undertake during compression system piping design. The experimental results in the chapter illustrate the importance of avoiding resonance. The design engineer should therefore focus piping design efforts around the avoidance of both acoustic and fluid–structural induced resonance.

REFERENCES

Abramson, H.N. (1966), *The Dynamic Behavior of Liquids in Moving Containers*, NASA SP-106, Washington, D.C., USA.

Broerman, E., and Gatewood, J. (2009), Personal communications.

Brun, K., and Kurz, R. (2001), "Measurement Uncertainties Encountered During Gas Turbine Driven Compressor Field Testing", *Transactions of the ASME, Journal of Engineering for Gas Turbines and Power*, vol. 123, pp. 62–9.

Brun, K., Deffenbaugh, D.M., and Bowles, E.B., Jr. (2007), "Development of a Transient Fluid Dynamics Solver for Compression System Pulsation Analysis", *Proceedings of the Gas Machinery Conference*, Dallas, USA, 1–3 October.

Denton, J.D. (1993), "The 1993 IGTI Scholar Lecture: Loss Mechanisms in Turbomachines", *Transactions of the ASME, Journal of Turbomachinery*, vol. 115, pp. 621–56.

Diwakar, P., and Lin, L. (2007), "Study of Dynamic Stress in Piping Networks and Pressure Vessels using Fluid-Solid Interaction Models", *Proceedings of the ASME Pressure Vessel and Piping Division Conference*, San Antonio, 22–26 July, Paper No. PVP 2007-26009.

Eckstein, J., Freitag, E., Hirsch, C., and Sattelmayer, T. (2006), "Experimental Study on the Role of Entropy Waves in Low Frequency Oscillations in a RQL Combustor", *Transactions of the ASME, Journal of Engineering for Gas Turbines and Power*, vol. 128, pp. 264–70.

Jungowksi, W.M., Weiss, M.H., and Price, G.R. (1996), "Pressure Oscillations Occurring in a Centrifugal Compressor System With and Without Passive and Active Surge Control", *Transaction of the ASME, Journal of Turbomachinery*, vol. 118, pp. 29–40.

Kana, D.D., Lindholm, U.S., and Abramson, H.N. (1966), "An Experimental Study of Liquid Instability in a Vibrating Elastic Tank", *Journal of Spacecraft and Rockets,* vol. 3, pp. 1183–8.

Kurz, R., and White, R.C. (2004), "Surge Avoidance in Gas Compression Systems", *Transactions of the ASME, Journal of Turbomachinery*, vol. 126, pp. 501–6.

Moody, F.J. (1990), *Unsteady Fluid Mechanics Examples from Reactor and Containment*, American Society of Mechanical Engineers, New York, USA.

Moody, F.J. (2007), "Acoustic Amplification of a Vertical Liquid Column Bouncing on a Gas Volume", *Proceedings of the ASME Pressure Vessel and Piping Division Conference,* San Antonio, USA, 22–26 July, Paper No. PVP 2007-26031.

Patankar, S.V. (1980), *Numerical Heat Transfer and Fluid Flow,* Hemisphere Publishing, New York, USA.

Rice, J.G., and Schnipke, R.J. (1985), "A Monotone Streamline Upwind Finite Element Method for Convection Dominated Flows", *Computational Methods in Applied Mechanics and Engineering*, vol. 48, pp. 313–27.

Shaaban, S.H. (1979), "Implicit Three-Dimensional Finite Element Solution to Fluid-Structure Interaction Induced by Hydrodynamic Accidents", *Proceedings of the 3rd National Congress on Pressure Vessel and Piping: Dynamics of Fluid–Structure Systems in the Energy Industry,* San Francisco, USA, 25–29 June, pp. 67–75.

Sparks, C.R. (1983), "On the Transient Interaction of Centrifugal Compressors and Their Piping Systems", *Transactions of the ASME, Journal of Engineering for Power*, vol. 105, pp. 891–901.

Tweten, D., Nored, M., and Brun, K. (2008), "The Physics of Pulsations", *Proceedings of the Gas Machinery Conference,* Albuquerque, USA, 6–8 October.

Van Helvoirt, J., and de Jager, B. (2007), "Dynamic Model Including Piping Acoustics of a Centrifugal Compression System", *Journal of Sound and Vibration*, vol. 302, pp. 361–78.

Wiggert, D.C., and Tijsseling, A.S. (2001), "Fluid Transients and Fluid Structure Interaction in Flexible Liquid Filled Piping", *Applied Mechanical Review*, vol. 54, pp. 455–81.

Zienkiewicz, O.C. (1977), *The Finite Element Method*, McGraw Hill, New York, USA.

Chapter 8

Degradation in Gas Turbine Compression Systems

R. Kurz and K. Brun

ABSTRACT

Any prime mover exhibits the effects of wear and tear over time. The problem of predicting the effects of wear and tear on a gas turbine's performance is still a matter of discussion. Because a gas turbine's function is the result of the fine-tuned cooperation of many different components, the emphasis of this chapter is on the gas turbine and its driven equipment (compressor or pump) as a system, rather than on isolated components.

We will discuss the degradation effects on the package as part of a complex system such as a pipeline or reinjection station. Treating the gas turbine package as a system facilitates insight into degradation effects on the match of components, as well as the match with driven equipment. The chapter discusses degradation effects based on studies of the mechanisms that cause gas turbine degradation, primarily changes in blade surfaces due to erosion or fouling and the effect on the blade aerodynamics; changes in seal geometries and clearances, and the effects on parasitic flows; and changes in the combustion system.

The chapter goes on to present a methodology that simulates gas turbine and driven equipment degradation. With a relatively simple set of equations that describe the gas turbine behavior, and a set of linear deviation factors which we can derive from gas turbine performance maps or test data, we studied the equipment behavior for various degrees of degradation. We then used a stage-by-stage model for the gas turbine compressor to characterise compressor deterioration. We have avoided presenting figures focused on degradation rate as it is subject to operational and design factors that one typically cannot fully control.

This chapter is a revised and extended version of Kurz, R., and Brun, K. (2001), "Degradation in Gas Turbine Systems", *Transactions of the American Society of Mechanical Engineers, Journal of Engineering for Gas Turbines and Power*, vol. 123, pp. 70–77. This paper won the International Gas Turbine Institute Oil & Gas Application Committee 2000 best paper award.

NOMENCLATURE

H	head
N	speed
P	power
p	pressure
Q	volumetric flow
R_a	roughness
s	chord length
T	temperature
u	tip speed
W	mass flow
η	isentropic efficiency
$\psi = H / (u^2/2)$	non-dimensional compressor discharge pressure
$\phi = Q / (u/A)$	non-dimensional flow
ρ	density

Subscripts

a	air
c	compressor
corr	corrected
f	fuel
g	exhaust gas
gp	gas turbine
gpt	gas turbine's turbine
m	mechanical
opt	optimum
PT	power turbine
1	inlet plane
2	compressor diffuser exit plane
3	gas turbine inlet plane
5	power turbine inlet plane
7	turbine diffuser exit plane

INTRODUCTION

The performance of a gas turbine and the compression system into which it is packaged is the result of the fine-tuned cooperation of many different components (Figure 8.1). Any of these parts can exhibit wear and tear over the compression system's lifetime, and thus can adversely affect the system's operation. In particular the gas turbine compressor, turbine and driven compressor have to operate in an environment that will invariably degrade their performance. Understanding the mechanisms that cause degradation, as well as individual components' degradation effects for the overall system, are a matter of interest.

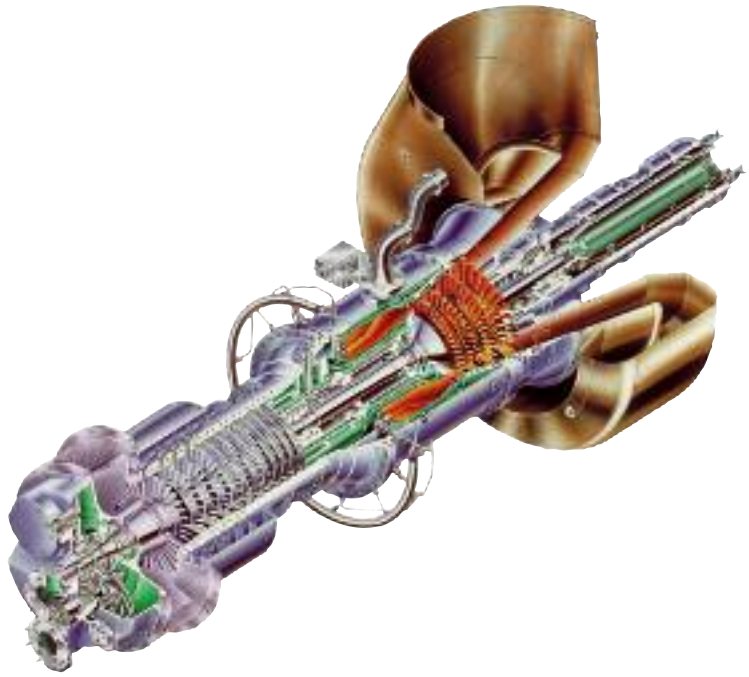

FIGURE 8.1. Gas turbine cross section.

DEGRADATION MECHANISM

Six separate and identifiable mechanisms cause gas turbine degradation. First, particle adherence to aerofoils and annulus surfaces causes fouling. Oil or water mists increase the chance that particles adhere to these surfaces. The result is a build-up of material that causes increased surface roughness and, to some degree, changes the aerofoil's shape if the material build-up forms thicker deposit layers. Many of the contaminants are smaller than 2 μm. Cleaning normally eliminates fouling.

Next is hot corrosion, the loss of material from flow path components which chemical reactions between the component and certain contaminants, such as salts, mineral acids or reactive gases, cause. The products of these chemical reactions may adhere to the aero components as scale.

Corrosion, in contrast to hot corrosion, is the chemical reaction between the components' metal atoms and oxygen from the surrounding hot gaseous environment. Any mechanical damage, such as cracking or spalling during thermal cycles, will in turn reduce the protection from an oxide scale.

Erosion is the abrasive removal of material from the flow path by hard particles impinging on flow surfaces. These particles typically have to be larger than 20 mm in diameter to cause erosion by impact. Erosion is probably more a problem for flight gas turbine applications, because state-of-the-art filtration systems for industrial ap-

plications will typically eliminate the bulk of the larger particles. Erosion can also become a problem for driven compressors or pumps where the process gas or fluid carries solid materials.

Abrasion occurs when a rotating surface rubs on a stationary surface. Many engines use abradable surfaces, where a certain amount of rubbing is permissible during the gas turbine's run-in, in order to establish proper clearances. The material removal will typically increase seal or tip gaps. While we can reverse some of these effects by cleaning or washing the gas turbine, others require the adjustment, repair or component replacement (Diakunchak, 1991).

Foreign objects striking the flow path components cause damage. These objects may enter the gas turbine with the inlet air, or the gas compressor with the gas stream, or are the result of pieces breaking off the gas turbine itself. Pieces of ice breaking off the inlet, or carbon build-up breaking off from fuel nozzles, can also cause damage.

Note that the determination of performance degradation in the field is difficult. Test uncertainties are typically significant, especially if one uses instrumentation intended for use with a control system as opposed to a calibrated test facility (Brun and Kurz, 1998). Even trending involves significant uncertainties, because in all cases one must correct the gas turbine performance from actual to a reference condition (Bakken and Skorping, 1996).

DEGRADATION OF COMPONENTS

Aerofoils

In order to judge the degradation of aerodynamic components, we will first evaluate the effects of fouling, erosion, corrosion and other damage on the individual aerofoil. Fouling, and to some extent erosion, generate a blade surface with increased roughness. Any increased roughness can increase the friction losses. It may also cause early transition from laminar to turbulent boundary layers, which increases loss production. Erosion, deposits or aerofoil damage changes its shape. For a well-designed aerofoil, optimized for the application, this will always reduce its performance.

Bammert and Sonnenschein (1967) reported early investigations on turbine blade performance change due to changes in blade geometry caused by erosion, corrosion and fouling, which they modeled after inspecting gas turbine blades that had operated in-service (Bammert and Fiedler, 1965). Changes in exit angles and increased losses were found to accompany turbine blade deterioration. Bammert and Fiedler (1965) report profile loss increases of 100 percent for 1 percent added or reduced thickness on well-designed subsonic turbine blades. More recently, Kind *et al.* (1996) reviewed the same topic, with emphasis on the increased surface roughness associated with degradation. It became clear that the primary influence of degradation appears around the optimum incidence angles, while there was little influence on off-design performance. It also became clear that added roughness on the blades' pressure side has a small effect compared to added roughness on the suction side.

In contrast to Kind *et al.*'s conclusions (1996), Boelcs and Sari (1988), who tested transonic turbine blades with and without deposits on the pressure side, conclude that in general, "a carefully designed blade will not significantly change its flow properties in a soiled condition". Kurz (1995) found a 100 percent increase in profile losses on a transonic annular turbine cascade with blades with scratches on the suction side. Note that on transonic turbine cascades the shock position often determines transition to turbulent flow, and is thus less dependent on the boundary layer condition. Losses will increase because the shock position on the suction side will move upstream, typically causing an earlier boundary layer transition from laminar to turbulent flow (Boelcs and Sari, 1988; Kurz, 1991).

If the blade operates at or near transonic velocities, increased roughness will also reduce the possible flow through the blade row due to thicker boundary layers. Thicker boundary layers on the blades and sidewalls reduce the flow capacity, especially near choking conditions. However, if the trailing edge erodes, the blade's throat width increases, thus allowing more flow. Schmidt (1992) describes the effect of a deliberate chord length reduction in a power turbine nozzle that significantly reduced the work output of the said turbine. Milsch (1971) reports increases in profile losses from 2 percent at $k_s/s = 0.3 \times 10^{-3}$ to 10 percent at $k_s/s = 5 \times 10^{-3}$ for NACA65-(12)06 compressor cascades, as well as significantly reduced turning. Significantly increased boundary layer growth, premature transition to turbulent flow and premature flow separation cause this reduction in performance. In general, all the above influences will create higher losses and less turning. The result is that the following row of aerofoils will see different incidence angles, higher temperatures, lower (for compressors) or higher (for turbines) pressures and densities.

Erosion typically has the most significant effects on the blade leading edges. This can affect the location of transition from a laminar to turbulent boundary layer, and turbulent boundary layer thickness (Pinson and Wang, 1994). The boundary layer's heat transfer characteristics are a function of its thickness and state. Consequentially leading edge erosion can result in an increase in the blade's average temperature.

Clearances

Clearances between stationary blades and the rotating hub or between rotating blades and the stationary casing have a tendency to increase in size as the equipment ages. This results in higher and unwanted leakage flows. These leakage flows reduce the possible compressor discharge pressure capability and the components' efficiency (Frith, 1992; Shabbir *et al*., 1997; Khalid *et al*., 1998). In compressors, a rotor tip clearance increase from 1 percent of blade chord to 3.5 percent of blade chord reduces the stage's pressure ratio by up to 15 percent (Sheard, 2012).

The loss production occurs as a consequence of leakage flow mixing with the main flow, producing losses and reducing the effective flow area. Singh *et al*.'s (1996) simulation on a set of compressor stages suggests that tip clearance effects and added roughness after sand ingestion lead to a similar magnitude of performance deterioration. However, the degradation mechanism by sand ingestion is more rele-

vant for aero applications than for industrial applications as industrial gas turbines can be fitted with inlet filtrations systems.

When considering driven equipment, such as compressors and pumps, increased clearances in inter-stage labyrinth seals, balance piston seals or shroud seals increase the absorbed power. For high pressure ratio machines with low flow, increased balance piston recirculation due to worn balance piston seals can cause a significant increase in absorbed power.

Compressor

Three major effects determine the compressor's performance deterioration: increased tip clearances (Khalid *et al*., 1998), changes in aerofoil geometry (Singh *et al*., 1996) and changes in aerofoil surface quality (Elrod *et al*., 1990). While the first two effects typically lead to non-recoverable degradation, washing the compressor can, at least partially, reverse the latter effect (Stalder, 1998). We can describe the overall degradation effect on a gas turbine compressor through added losses and a lowered capability to generate compressor discharge pressure. Typically, a degraded compressor will also have a reduced surge or stall margin (Spakovszky *et al*., 1999). This will not have a significant effect on the steady-state operation.

For a given speed of a degraded compressor, each subsequent stage will see lower Mach numbers (because of the higher temperature) and an increased axial velocity component (because $p = p/\mathrm{RT}$, where p is reduced, T is increased, thus the density reduces). The net effect will be that while in a new gas turbine all compressor stages are working at their optimum efficiency point and design surge margins, the degradation will force all stages after the first to work at off-optimum surge margins and lower than design efficiency. This will not only lower the overall compressor efficiency and pressure ratio that the gas turbine can achieve, but also the operating range. Readjusting variable geometry, where available, can counteract some of the degradation effects.

Singh *et al*. (1996) presented a model for estimating the deterioration of three different single-stage compressors. While the model includes the effects of increased roughness and tip clearance due to erosion, it omits the effects of blunting the blade leading edges and shortening the chord. We typically do not see the latter effects on industrial gas turbine compressors due to more effective inlet air filtration. Singh *et al*.'s results (1996) show that while the shape of the stage's ϕ-ψ-η characteristics are only marginally affected, the achievable pressure ratio and efficiency for the stage reduce. Blade roughness effects and tip clearance contribute equally to the deterioration. Aerodynamic performance loss was higher for the higher loaded test case. Also, further increased roughness from initially $R_a = 4.0$ µm to $R_a = 6.0$ µm for the stator and 8.0 µm for the rotor created only a small increase in deterioration. In addition to a reduced efficiency, added clearances will also increase the axial flow blockage, and thus will result in reduced flow through the compressor.

Given the above, we were able to design a computational model that could simulate single component degradation effects on the compressor's performance. We made the following assumptions:

1. At the design point, all compressor stages operate at the same optimum non-dimensional flow, ϕ_{opt}. In practice this is accomplished by profiling the compressor's meridional plane. In the model, we sized flow areas so that we achieved the same non-dimensional flow for all stages.
2. We implemented Mach number dependency by linear variations of ψ. We justified this because the changes in the model's operating points will be relatively small.
3. We calculated inlet conditions for the next compressor stage using updated pressure, temperature and volume.
4. We modeled compressor stage characteristics (ϕ-ψ and ϕ-η) as third-order polynomials with explicit limits for surge and choke. The stage characteristics for each stage are identical.
5. We simulated fouling by multiplying the compressor discharge pressure and efficiency of the affected stage by two constant "fouling factors" (one each for compressor discharge pressure and efficiency).
6. We modeled the effects of increasing gaps by reducing the effective blade diameters, thus modeling the increasing blockage.

Applying the above model to a typical compressor reveals that the combined effects of aerofoil fouling and increased clearances (Figures 8.2 and 8.3) lead to the loss of pressure ratio and efficiency and the increased clearances cause choke at lower flow. The model thus reproduces the effects described by Spakovszky *et al*. (1999), Shabbir *et al*. (1997) and Singh *et al*. (1996).

Turbine

Thicker boundary layers on the blades and sidewalls may reduce the turbine flow capacity, especially near choking conditions. We might assume that the lower Mach numbers counteract this effect. However, we do not normally see lower Mach numbers at the gas high-pressure turbine's nozzle, because turbine inlet temperature determines the temperature there. We don't see lower Mach numbers at the first power turbine stage nozzle either, because the compressor power requirement dictates the necessary work, and thus the temperature drop across the power turbine.

Boyle (1994) found a turbine efficiency loss of 2.5 percent for a 10.2 μm surface roughness when compared to smooth blades. He also found that the most pronounced differences appear at the optimum operating point at the turbine. When operating off-design, turbine efficiency was almost the same for rough and smooth blades. In all cases losses associated with clearances were the same order of magnitude as profile losses. Clearance losses are approximately linear with the clearance (Traupel, 1988):

$$\Delta\eta = k_1 \cdot (\delta + k_2) \tag{1}$$

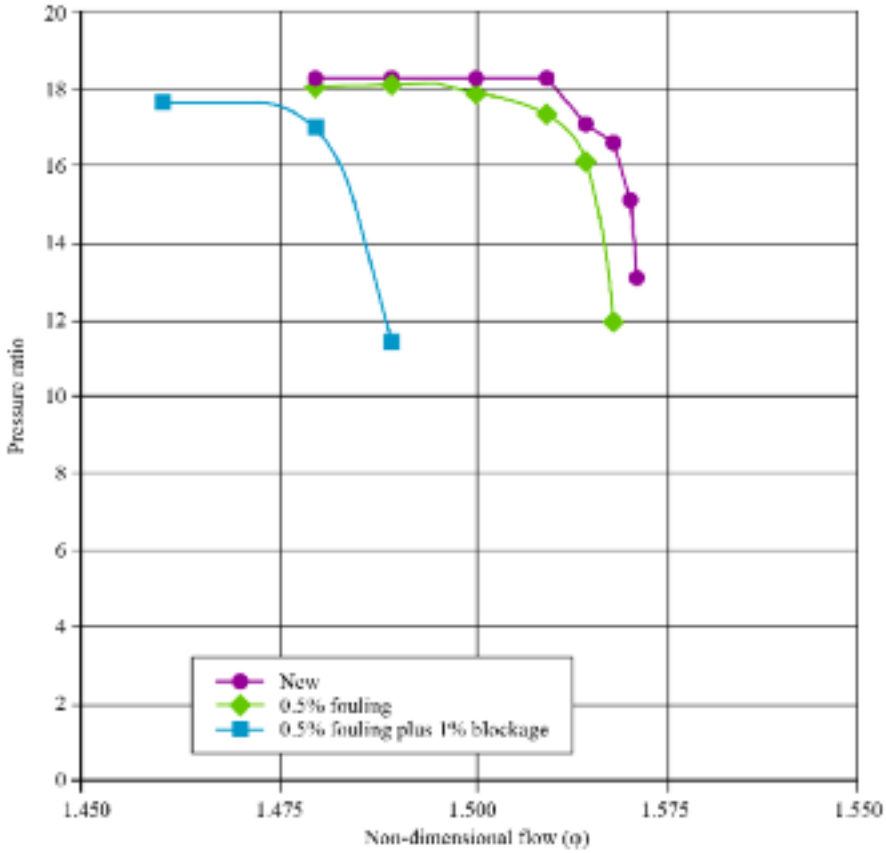

FIGURE 8.2. Effect of fouling on an axial compressor pressure ratio, comparing a new compressor, a compressor with 0.5 percent fouling and a compressor with 0.5 percent fouling and an additional 1 percent blockage.

Traupel (1988) also indicates that clearance losses increase with increasing flow rate. In addition to a reduced efficiency, increased clearances will also increase the axial flow blockage, and thus will reduce flow and increased velocities. Radtke and Dibelius (1980) report a reduction in multi-stage turbine efficiency by 0.6 percent when they increased the radial clearances from 0.5 percent of the blade height at the rotors and 0.4 percent of the blade height at the stators to 0.8 percent of the blade height at rotors and stators. If the turbine degradation leads to material removal, especially in the nozzle area, we will see the opposite effect: the flow capacity increases for a given pressure ratio. The effective throat area limits any nozzle's flow capacity. If the trailing edge erodes, the throat area increases. At the same time, the exit flow angle becomes more axial. Trailing edge erosion in the power turbine causes a shift in the pressure ratio distribution $(p_3/p_5)/(p_5/p_7)$, resulting in a gas turbine consuming a larger portion of the overall pressure ratio p_3/p_7.

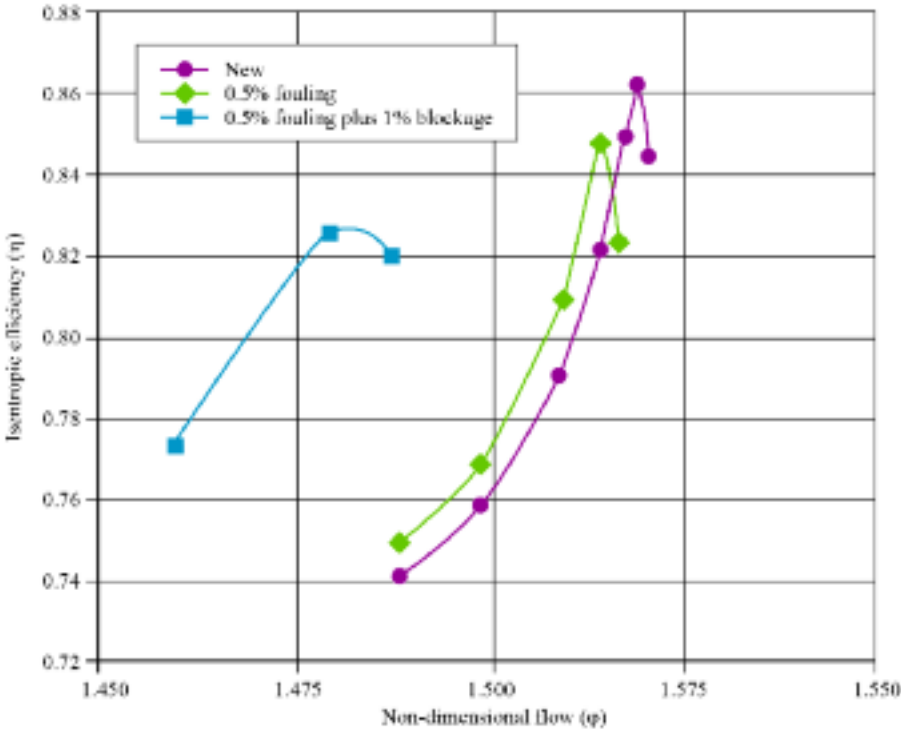

FIGURE 8.3. Effect of fouling on an axial compressor comparing a new compressor, a compressor with 0.5 percent fouling on compressor discharge pressure and efficiency, and a compressor with additionally 1 percent blockage: efficiency.

Combustor

The combustion system degradation is not likely to result in gas turbine performance degradation. The combustion efficiency will usually not decrease. However, deterioration may lead to a variation in the combustor exit temperature profile. The problems with distorted exit temperature distributions are threefold:

1. local temperature peaks can damage turbine blades and vanes;
2. the altered temperature profile will increase secondary flow activity, thus reducing turbine efficiency; and
3. because we measure the control temperature at discrete circumferential points, the average measured temperature is not the same as the true thermodynamic average temperature. Therefore, a factory test is needed to establish a correlation between the measured average and the true thermodynamic average temperature.

If the temperature profile alters due to 1 or 2, the correlation 3 is no longer valid. Figure 8.4 shows two temperature profiles in the T_5 measuring plane with

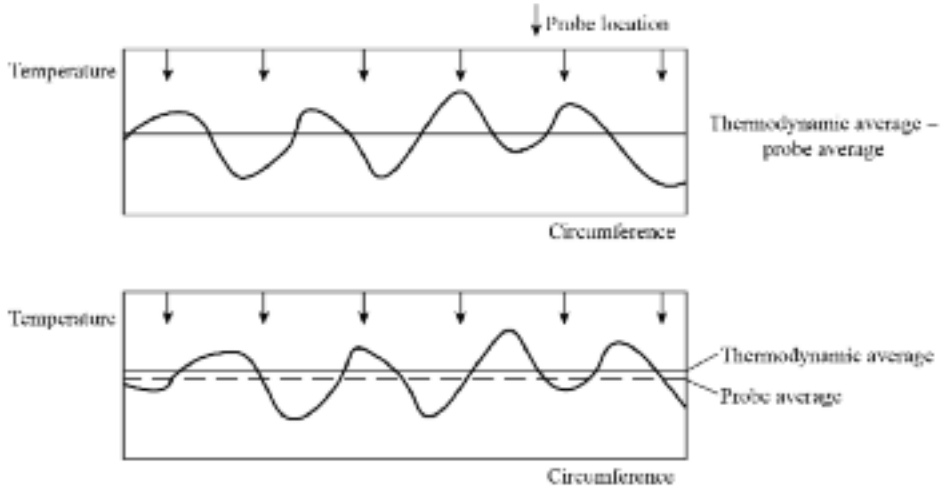

FIGURE 8.4. Effect of probe location on the measured average temperature.

probe locations. Both temperature profiles have the same thermodynamic average temperature, but different probe averages. The gas turbine could therefore be over-fired, thus producing more power but shortening its life, or under-fired, thus losing power.

Driven equipment

Not only will the driver show performance degradation over time, but also the driven equipment. Solid and liquid contaminants in the process gas can damage impellers, or can form a dirt layer on the aerodynamic surfaces which can increase friction losses. There are documented cases where pipeline compressors lost 5 percent efficiency due to oily dust layers on the impeller and diffuser surfaces. One of the known contaminant sources is reciprocating compressors. Reciprocating compressors release significant quantities of lubrication oil into the process piping that then contaminate downstream driven equipment. Heavier hydrocarbons tend to form polymers at elevated temperatures, which can also cause fouling (Haq *et al*., 1998).

GAS TURBINE MODEL

We modeled the gas turbine's overall behavior using the governing equations (Cohen *et al.*, 1996; Tarabrin *et al*., 1998) for:

Flow compatibility:

$$\frac{W\sqrt{T_3}}{p_3} = \frac{W\sqrt{T_1}}{p_1}\,\frac{p_1}{p_2}\,\frac{p_2}{p_3}\sqrt{\frac{T_3}{T_1}} \tag{2}$$

Work compatibility:

$$\frac{\Delta T_{34}}{T_3} = \frac{\Delta T_{12}}{T_1}\frac{T_1}{T_3}\frac{c_{pa}}{c_{pg}\eta_m} \tag{3}$$

$$\eta_m c_{pg}\Delta T_{34} = c_{pa}\Delta T_{12} \tag{4}$$

Flow compatibility for the gas turbine's power turbine:

$$\frac{W\sqrt{T_5}}{p_5} = \frac{W\sqrt{T_3}}{p_3}\frac{p_3}{p_5}\sqrt{\frac{T_5}{T_3}} \tag{5}$$

The gas turbine and power turbine's flow capacity impose another condition. From a pressure balance, we get the identity:

$$\frac{p_3}{p_5} = \frac{p_3}{p_2}\frac{p_2}{p_1}\frac{p_1}{p_5} \tag{6}$$

where the pressure drop in the combustor determines p_3/p_2. Consequently, for any compressor pressure ratio, the power turbine pressure ratio fixes the gas turbine pressure ratio. Specifically, if the power turbine is choked, then the gas turbine pressure ratio is a unique fixed value.

Furthermore, we determine the fuel flow from:

$$W_f = \frac{c_{pg}(T_3 - T_2)W_1}{LHV} \tag{7}$$

A performance map can represent any gas turbine component. To allow for small deviations from the design point, we can linearize the dependency of operating parameters as we do not necessarily need to model each component's entire performance map (Table 8.1). Despite the limitations of the above approach, we can simulate the behavior of a two-shaft gas turbine.

Table 8.1. *Linearized operating parameters.*

Linearized parameter	Depending on	Equation
Compressor pressure ratio	Corrected gas turbine speed	$k_{prc} = \Delta TT_c/\Delta N_{gpcorr}$
Compressor flow function	Corrected gas turbine speed	$K_{Wc} = \Delta W_c/\Delta N_{gpcorr}$
Compressor efficiency	Corrected gas turbine speed	$k_{\eta rc} = \Delta\eta c/\Delta N_{gpcorr}$
Gas turbine pressure ratio	Compressor pressure ratio	$k_{gpt} = \Delta TT_{gpt}/\Delta TT_c$
Gas turbine efficiency	Gas turbine speed	$k_{\eta gpt} = \Delta\eta_{gpt}/\Delta(\lvert Q_3/N_{gp}\rvert)$

The power turbine's optimum speed will depend on the gas turbine operating point. With:

$$\left(\frac{u}{c_{ax}}\right)_{opt} \alpha \left(\frac{N_{pt}}{Q_5}\right)_{opt} \tag{8}$$

we derive the optimum power turbine speed from:

$$N_{PT,opt} = \left(\frac{N_{pt}}{Q_5}\right)_{opt} Q_5 = \left(\frac{N_{Pt}}{Q_5}\right)_{opt} W \frac{RT_5}{p_5} \tag{9}$$

We can approximate the reduction in power turbine efficiency at off-optimum speeds by:

$$P = P_{opt}\left[2.0\frac{N_{PT}}{N_{PT,opt}} - \left(\frac{N_{PT}}{N_{PT,opt}}\right)^2\right] \tag{10}$$

These conditions are sufficient to explain the gas turbine behavior at off-design conditions, for example, at ambient temperatures different from the original design point temperature. At higher ambient temperatures, the pressure ratio p_2/p_1 reduces because the same compressor discharge pressure produces less pressure ratio, and the mass flow reduces because the choked power turbine nozzle limits the flow (temperature topping). At lower ambient temperatures, gas turbine speed limits override a limit in firing temperatures (speed topping).

Increasing the power turbine nozzle area reduces the power turbine resistance and consequently increases flow capacity, allowing a higher portion of the overall pressure ratio across the gas turbine. This reduces the turbine inlet temperature required for the gas turbine to drive its compressor. When one operates a gas turbine matched to a fixed turbine inlet temperature at fixed gas turbine speed, the turbine inlet temperature is reached before one can reach the gas turbine speed. To increase the gas turbine speed, one would have to increase the power turbine area.

EFFECT OF DEGRADATION ON THE GAS TURBINE

We used the following relationships in the model above to describe the effect of degradation: the loss of compressor efficiency $\Delta\eta_c$, compressor pressure ratio Δp_c, compressor flow ΔW_c, gas turbine efficiency $\Delta\eta_{GPT}$ and power turbine efficiency $\Delta\eta_{PT.}$

For two-shaft gas turbines, the degradation effects also depend on the gas turbines' control mode. If the gas turbine is operating at ambient temperatures below its design temperature, it will be in speed topping mode and the maximum allowable

gas turbine speed limits the gas turbine output. If the gas turbine is operating at ambient temperatures above the design temperature, it will be in turbine inlet temperature topping mode and the firing temperature limits the gas turbine output. This is similar to the conclusion reached by Tarabrin *et al*. (1998) when comparing the effect of degradation on single- and two-shaft gas turbines.

A single-shaft gas turbine must run at a fixed speed. A two-shaft gas turbine at speed topping will run at maximum speed during full load operation. Thus, degradation effects are less severe than for a gas turbine at temperature topping, which the model confirms. Figures 8.5 and 8.6 show the gas turbine's full load output and efficiency. They are at varying ambient temperatures and degradation levels. The different degradation levels include case 1/0, where compressor flow, pressure ratio and efficiency reduce by 1 percent. Case 1/1 is similar to the previous case, except that additionally, the gas turbine's turbine and power turbine efficiencies reduce by 1 percent. Case 2/2 has all values of case 1/1 reduced by 2 percent. While the case for as new performance (0/0) shows the correct design temperature of 288 K recognizable by the change in slope for the power and efficiency line, all other cases exhibit a match point at lower temperatures. Therefore, the impact of degradation at temperatures below 288 K somewhat reduces.

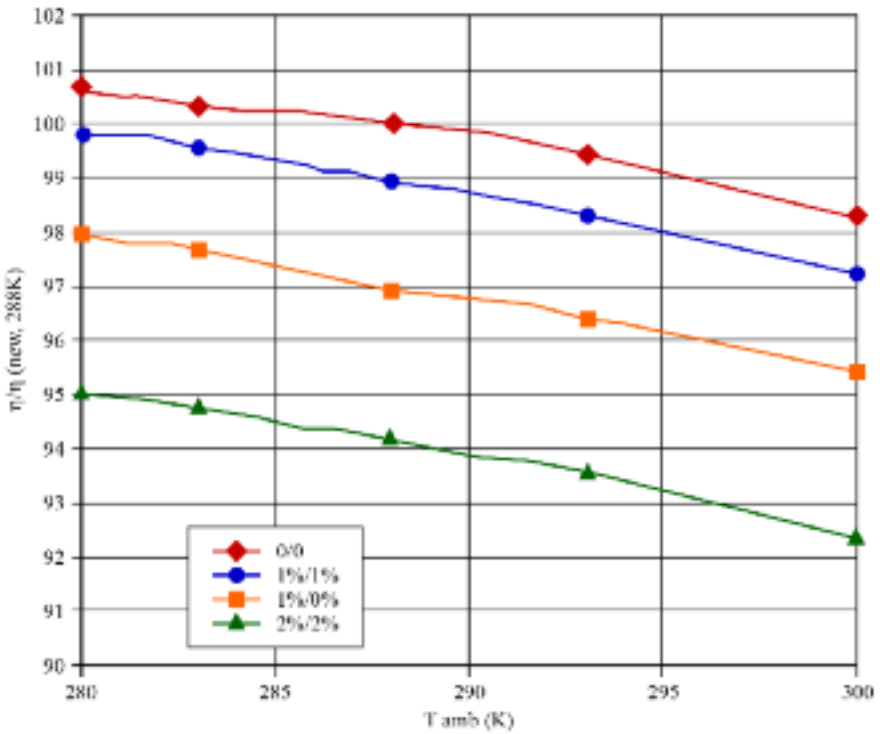

FIGURE 8.5. Degradation of engine efficiency at full load.

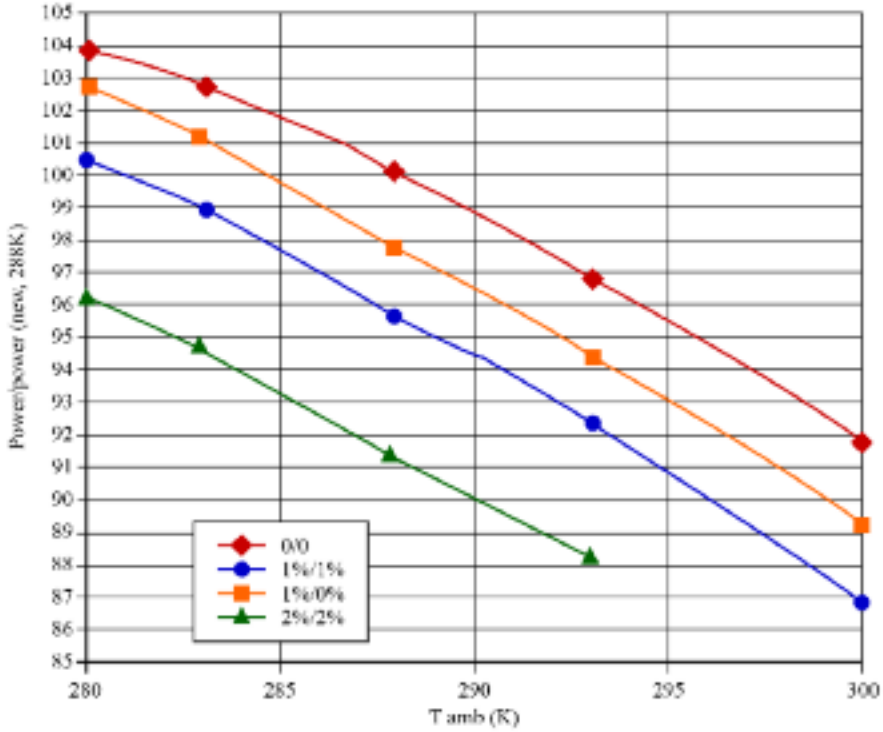

FIGURE 8.6. Degradation of engine power output.

Figure 8.7 shows the gas turbine efficiency at a given load for various ambient temperatures assuming different degradation levels. The degradation levels for "all components" are such that 1 percent would correspond to case 1/1 in the previous example, while 1 percent degradation severity for "compressor only" corresponds to case 1/0. It shows that the decline in efficiency slows down at higher levels of degradation, both for the cases where degradation affects all components, as well as cases where it affects only the compressor. This is because the operating point in the example was at 95 percent load for the new gas turbine, while for the respective curve end points, the gas turbine is operating again at design firing temperature, thus at full load.

An operating point may still be maintained at part load, a load below maximum firing temperature and below maximum gas turbine speed with a degraded gas turbine, albeit at a higher firing temperature and a higher gas turbine speed than for the new condition. The relative loss in efficiency is significantly lower than for a gas turbine at full load for the same amount of degradation.

Compressor deterioration by itself will usually result in higher efficiency losses than losses in heat rate, because a higher compressor exit temperature due to lower efficiency at a fixed firing temperature will reduce the achievable fuel flow. Tarabrin *et al*. (1998) point out that the degradation effect is typically more severe for two-shaft gas turbines than for single-shaft gas turbines. However, this is only true if

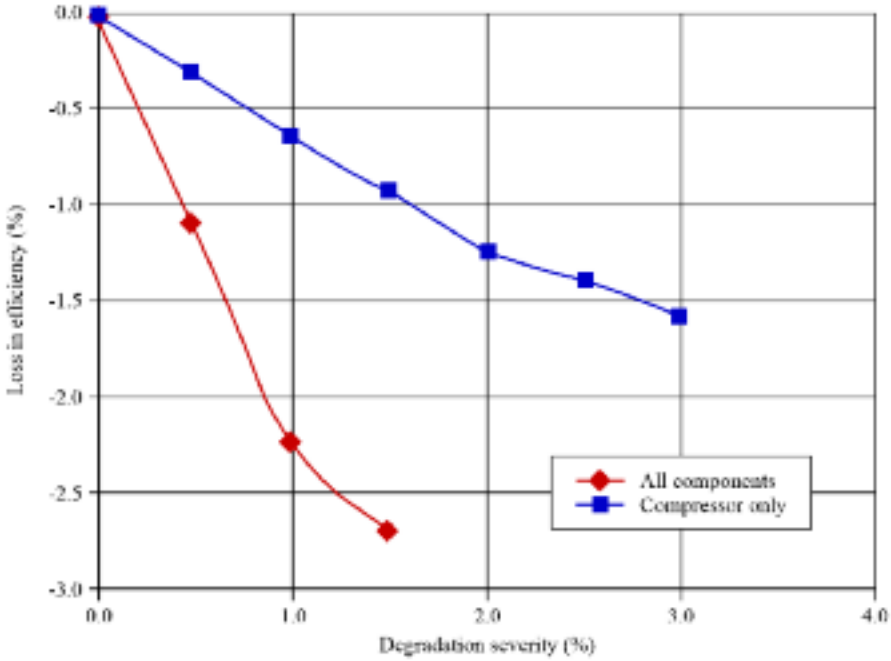

FIGURE 8.7. Degradation of engine efficiency at constant load.

compressor degradation on the two-shaft gas turbine leads to a drop in gas turbine speed. If variable geometry is available (in Tarabrin *et al.*'s (1998) example, adjustable power turbine nozzles; in our example, adjustable compressor inlet guide vanes and stators), one can avoid this drop in speed and compressor degradation effects are roughly the same for single- and two-shaft gas turbines.

Another form of turbine nozzle degradation occurs when erosion or corrosion removes material. In this case, both the pressure ratio over the turbine and its efficiency will drop. This leads to a reduction in gas turbine speed, and again a shift in the match point to a lower temperature. The effect on the overall gas turbine performance depends on the compressor's speed characteristic, but if we assume that the compressor efficiency does not change with speed, then we see a significant reduction in gas turbine output and efficiency. For some compressor designs, the design operating point is at slightly higher speeds than the compressor's optimum efficiency point. In this case, the increase in compressor efficiency at reduced speeds can partially counteract gas turbine efficiency loss.

Not directly measuring the turbine inlet temperature introduces another effect. It is more usual to measure the power turbine inlet temperature and the exhaust gas temperature, from which one can calculate the turbine inlet temperature. The measured exhaust gas temperature is not the thermodynamic average temperature, but the arithmetic average of several point measurements. Gas turbine degradation can lead to a shift in the ratio between turbine inlet temperature and exhaust gas temperature, thus causing the gas turbine to over- or under-fire.

Degradation also affects optimum power turbine speed. If a lower gas turbine compressor ratio or deterioration of the turbine itself leads to a lower gas turbine pressure ratio, then the flow through the power turbine will increase slightly, thus increasing the optimum speed. However, the effect on the gas turbine output at fixed power turbine speed is less than 0.1 percent for modern power turbines with relatively wide operating ranges.

For comparison purposes, we developed a second method to study gas turbine degradation using a non-ideal gas turbine cycle analysis concept. Hence, we developed a non-ideal Brayton cycle analysis program using compressor, combustor and turbine operating maps for a typical midsize two-shaft gas turbine. For this method, we assumed that we could model the gas turbine degradation using a non-ideal Brayton cycle analysis if the individual component operating maps accurately reflected each component's performance when the gas turbine operates off-design. While the previous method linearized the pressure ratio flow and efficiency relationships for each component, this method employs the actual non-linear operating maps for each component. It is thus more accurate at higher degradation levels or when operating the gas turbine further off-design. The following examples will demonstrate that the linearization is accurate as long as the degradation level remains small.

GAS TURBINE DATA

MacLeod *et al*. (1991), who investigated the effect of component deterioration on overall gas turbine performance on a single-shaft turboprop gas turbine, found that an increase in high-pressure turbine nozzle through flow area of 6 percent due to erosion, cracking, bowing and corrosion caused an increase in heat rate of 3.55 percent, but virtually no loss in power. Our model for a two-shaft gas turbine shows under the same conditions a significant reduction in gas turbine speed, with 7 percent loss in power and 3 percent loss in efficiency.

Frith (1992) tested a helicopter gas turbine with compressor blades cropped to simulate increased clearances. A 3 percent crop of the compressor blades reduced flow by 4.6 percent and pressure ratio by 3 percent. The compressor discharge temperature remained unchanged, which indicates a reduction in compressor efficiency of about 2.5 percent. Since the gas turbine was essentially the same as that tested by Schmidt (1992), the compressor, gas turbine's high-pressure turbine and power turbine characteristics were available. The model predicts a loss in power of 7.8 percent and a loss in efficiency of 2.7 percent, which matches the gas turbine test data (loss in power 8 percent and loss in efficiency 3.4 percent) closely.

Figure 8.8 shows the result of a set of actions to reverse the effect of degradation. In the example, the operator returned the gas turbine to the factory after approximately 5000 hours' in-service operation. The initial gas turbine run, without any adjustments and at the inlet guide vane and compressor delivery topping temperature from the original factory test, showed that the turbine inlet temperature was 22°C below design T_3 and the gas turbine speed was 3 percent below design speed.

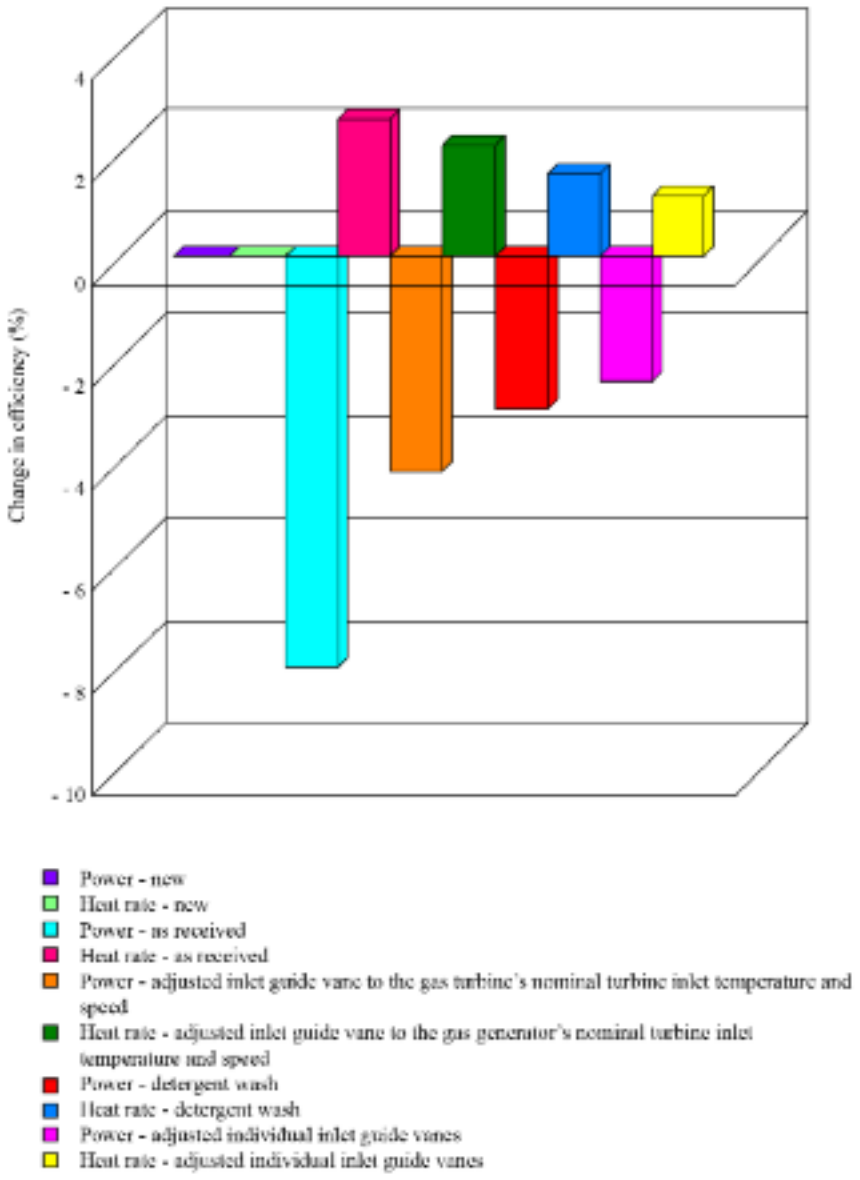

FIGURE 8.8. Performance recovery.

After adjusting the compressor inlet guide vanes to return the gas turbine to the desired design T_3 and speed, the gas turbine showed improved power and reduced heat rate. We washed the gas turbine with detergent. This resulted in a further improvement in performance. Next, we adjusted the compressor stage's variable guide vanes to the factory settings which resulted in a further improvement in power. After the adjustments, the gas turbine, compared to the original as-new factory test, had lost 2.5 percent in power and 1.2 percent in heat rate. These results illustrate that washing and adjustments can reverse a significant proportion of apparent degradation.

We operated a second gas turbine for approximately 3500 hours without a detergent wash. The environment was laden with gas turbine exhaust fumes and salt air. Borescope inspections enabled us to identify deposits on both the compressor and turbine. We recommended a detergent wash. Figure 8.9 presents control system data at full load before and after detergent washing. We took the data with the ambient temperature below the design point temperature.

The improvements in compressor pressure ratio, efficiency, power and heat rate are as expected because the washing detergent was dirty. This indicated a high degree of fouling. The gas turbine was also under-fired because one of the effects of degradation is a reduction in the T_3/T_5 ratio. The improvements explain the 9.7 percent increase in output power. After washing, and given the test uncertainties, this gas turbine appears to be performing essentially as it did when new. The model predicts this behavior: if we use a 2.1 percent loss in compressor efficiency, a 5 percent reduction in airflow and pressure ratio and a 0.5 percent reduction in gas turbine efficiency, we see a reduction in power of 8.6 percent, the efficiency drops by 3.5 percent, while gas turbine speed stays almost constant, and T_3 drops due to a reduction in T_3/T_5 ratio (Figure 8.10). Interestingly, while Tarabrin *et al*. (1998) indicate that smaller gas turbines may be more susceptible to degradation, Aker and Saravanamuttoo's study (1988) reaches the opposite conclusion.

DEGRADATION EFFECTS ON THE OVERALL SYSTEM

The net effect of gas turbine degradation is a reduction of available power and an increase in heat rate, while the driven equipment will require more power for a given operating point. Consequently, degradation of a gas turbine and its driven equipment will reduce that system's ability to achieve its design duty point. The significance of degradation effects can be clarified through a consideration of four scenarios.

Compression where compressor discharge pressure requirements depend on the flow

A typical example is a gas turbine driven centrifugal compressor operating in a pipeline. The pressure losses in the pipeline increase approximately with the square of flow velocity. Because the compressor must overcome these losses, the relationship between compressor discharge pressure and flow is also roughly quadratic (Figure 8.11). The consequence of degradation will therefore be less flow. Since

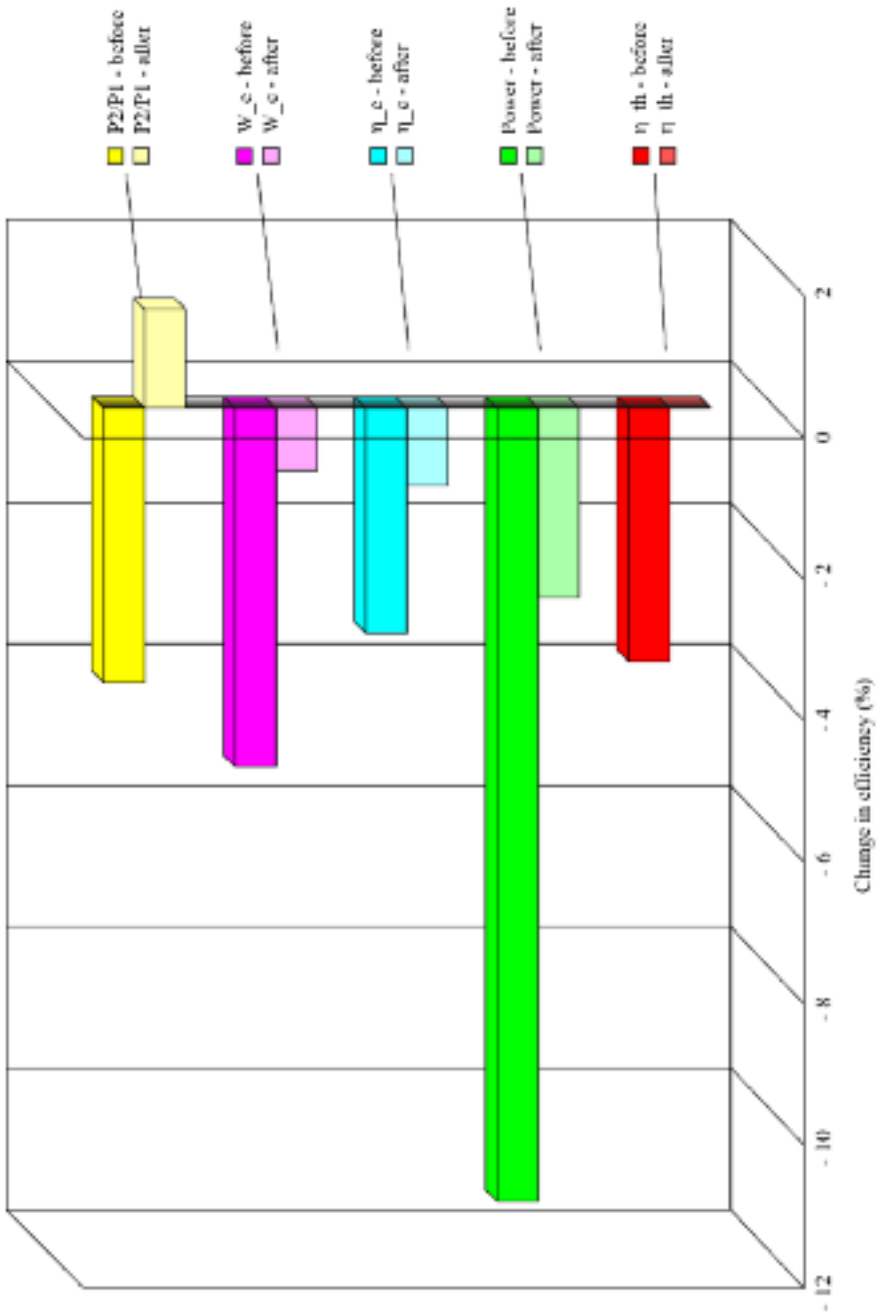

FIGURE 8.9. Effects of detergent washing.

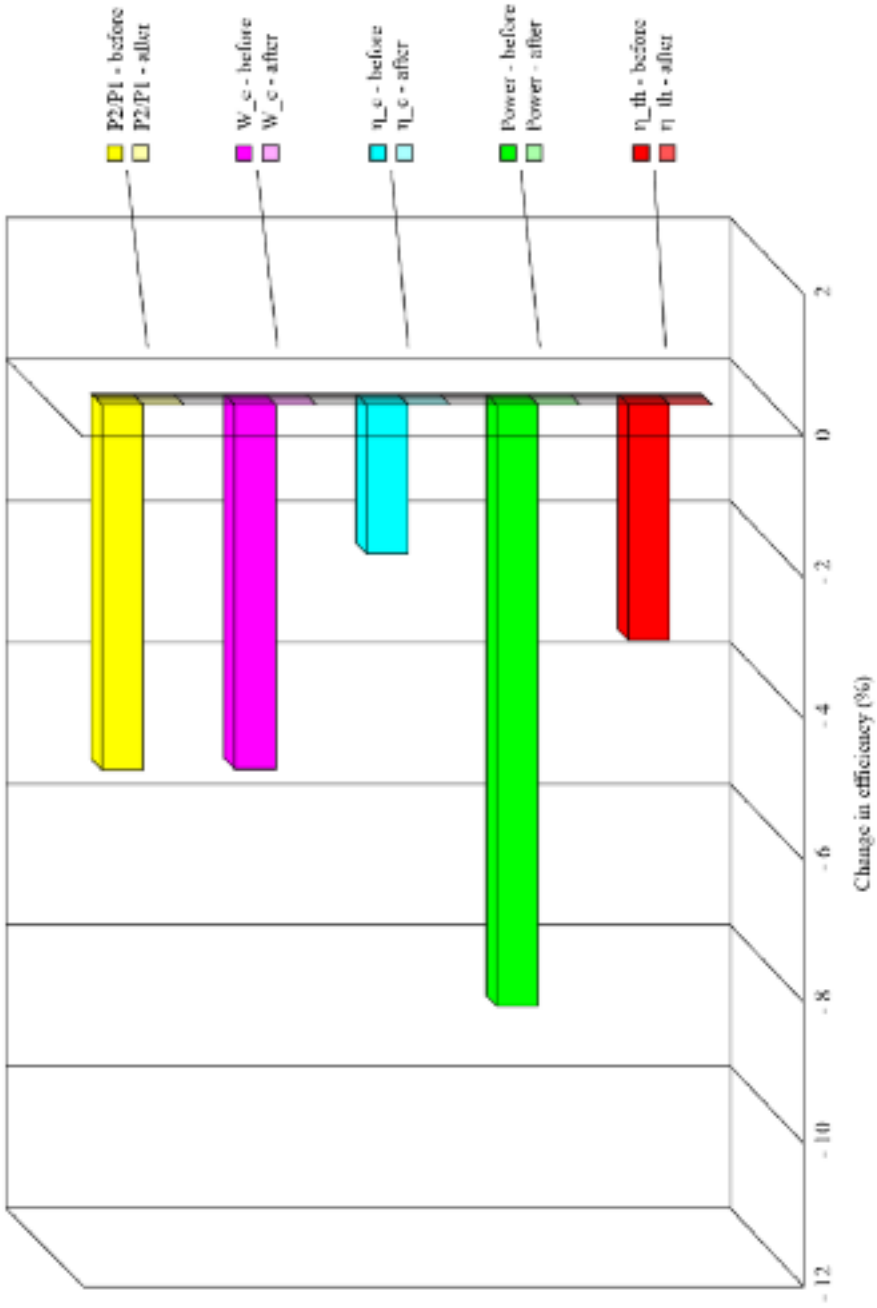

FIGURE 8.10. Simulation of effects of detergent washing.

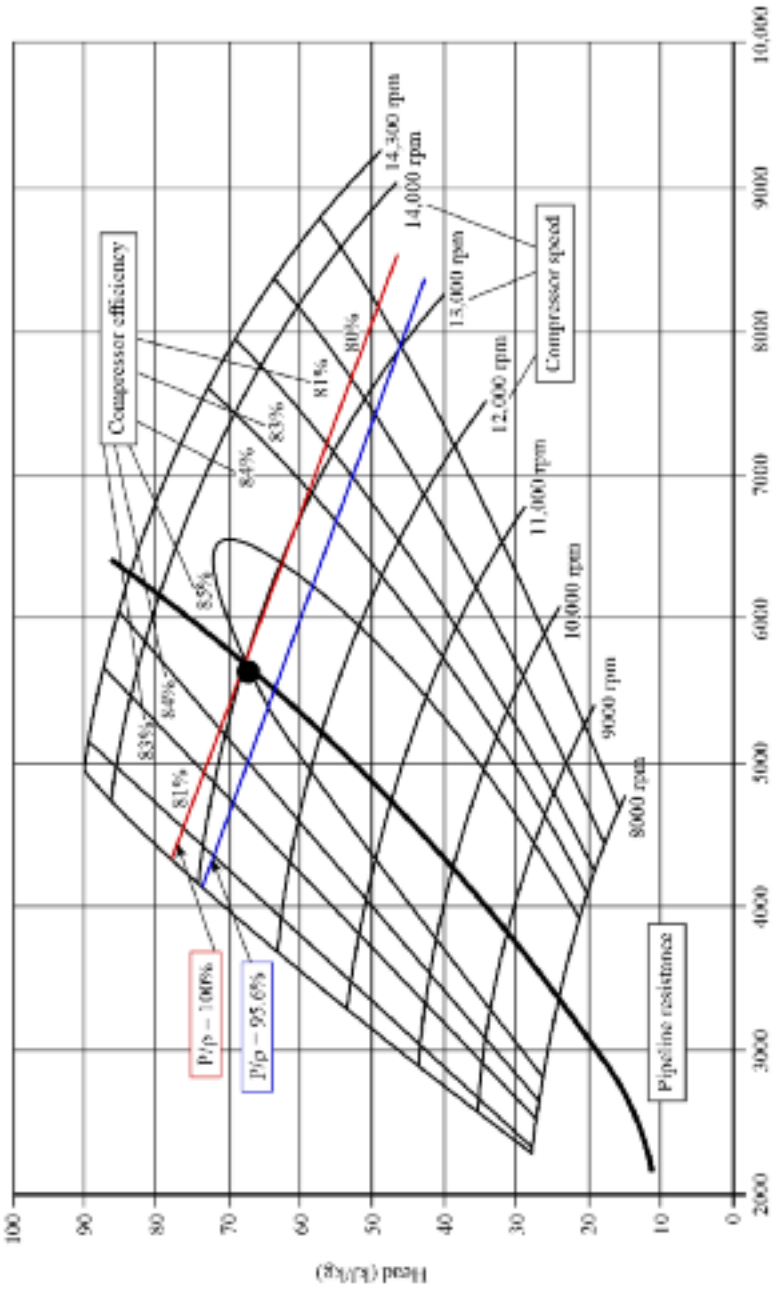

FIGURE 8.11. Effects of system degradation on a gas turbine driven pipeline compressor.

most compression system designs have gas turbines sized for the highest ambient temperatures, line packing will allow one to maintain the compression system performance, albeit with a higher fuel consumption. As we discussed earlier, the loss in power will be more significant than the loss in efficiency.

Compression where the compressor discharge pressure requirements are constant

In applications where the suction and discharge pressures are fixed, such as the cases where a compression system feeds into a pipeline that operates at a constant pressure or in processing applications, the compressor has to produce a fixed compressor discharge pressure to generate any flow. If we reduce the available power, the flow reduces. This will move the compressor's operating point closer to the surge line. At a critical flow, the available power will no longer be sufficient to generate the flow required for the compressor to operate. In process applications degradation may result in a process shutdown during the hotter parts of a day. Depending on criticality, it may be prudent to oversize the compression system's gas turbine.

Power generation

For power generation applications, gas turbine degradation will lead to higher fuel consumption, less power generation, but also more exhaust heat. In some cogeneration applications the increase in exhaust heat may be beneficial.

Pipeline application

The degradation levels from case 1/1 result in a centrifugal compressor's operating point moving on its performance map (Figure 8.11). In this example, a map represents the compressor characteristics, showing isentropic compressor discharge pressure versus flow for different operating speeds. It also shows lines of constant efficiency and shaft power that are derived from:

$$\frac{P}{\rho} = \frac{QH}{\eta} \tag{11}$$

Because the resistance of any pipeline is approximately proportional to the square of the flow velocity, the compressor's operating points will fall on a single "system" curve. The compressor's duty point will therefore be at the intersection of flow and system curve that corresponds to the available compressor power. Available compressor power is also a function of the speed (Equation 10) and therefore flow reduces with increasing levels of gas turbine degradation. However, as Table 8.2

Table 8.2. *Effect of various cases of degradation on power reduction and flow reduction.*

Case	Reduction in power (%)	Reduction in flow (%)
0/0	0	0
1/0	3.4	2.5
1/1	4.4	3.3
2/2	8.6	6.5

indicates, the loss in flow capability is smaller than the actual loss in power, because any reduction in flow also leads to a reduction in compressor discharge pressure.

RECOVERABLE AND NON-RECOVERABLE DEGRADATION

The distinction between recoverable and non-recoverable degradation is somewhat misleading. The majority of degradation is recoverable; however, the effort required to do so is different depending on the degradation type. The recovery effort may be minimal, associated with online washing or on-crank washing. We usually refer to the degradation recovery by any form of washing as recoverable degradation. However, we can recover a significant amount of degradation by adjusting a gas turbine's variable geometry. Additionally, component replacement during an overhaul can bring gas turbine or centrifugal compressor performance back to as-new conditions.

PROTECTION AGAINST DEGRADATION

While we cannot entirely avoid gas turbine degradation, there are precautions that we can take that slow its effects. These include the appropriate selection and maintenance of the air filtration equipment, and the treatment of fuel, steam or water that one injects into the combustion process. It also includes following manufacturers' recommendations regarding shut-down and restarting procedures. For the driven equipment, surge avoidance, process gas free of solids and liquids and operation within the compressor design limits are mandatory. With regards to steam injection, the requirements for contaminant limits for a gas turbine are more stringent than those typically associated with steam turbines. This is due to the higher temperatures associated with gas turbine combustion and therefore utilizing boiler feed water for steam injection will result in a gas turbine degrading.

Site location and environmental conditions are also significant when selecting an inlet air filtration system. Site location and environmental consideration dictate the presence of airborne contaminants, their size, concentration and composition. Humidity, precipitation, mist, fog, smog, dust, oil fumes and industrial exhausts will primarily affect the gas turbine compressor. Fuel quality will impact the gas turbine's

turbine. The cleanliness of the process gas, entrained particles or liquids will affect the driven equipment performance. Given these variables, it is challenging to predict the degradation rate.

While frequent online washing slows the deterioration rate, on-crank washing can yield a more significant recovery. However, if one uses the wrong detergents, some of the solvent may stick to the blades, or the washing process simply transports contaminants from the compressor's front stages to the rear stages. No matter how effective the washing, online washing will not fully clean the compressor's rear stages. If one can access the compressor blades, for example when the compressor casing is horizontally split, hand cleaning blades can be effective.

SUMMARY

The study presents a methodology to simulate the effect of gas turbine and driven equipment degradation. With a relatively simple set of equations that describe the gas turbine behavior, and a number of linear deviation factors which one can obtain from gas turbine performance maps or test data, one can study the equipment behavior for various degrees of degradation. We have avoided presenting degradation rates for specific applications because degradation rate is subject to operational and design factors that a compression system design engineer typically cannot control.

REFERENCES

Aker, G.F., and Saravanamuttoo, H.I.H. (1988), "Predicting the Gas Turbine Performance Degradation due to Compressor Fouling Using Computer Simulation Techniques", *Proceedings of the 33rd American Society of Mechanical Engineers Gas Turbine and Aeroengine Congress*, Amsterdam, Netherlands, 6–9 June, Paper No. 88-GT-206.

Bakken, L.E., and Skorping, R. (1996), "Optimum Operation and Maintenance of Gas Turbines Offshore", *Proceedings of the 41st American Society of Mechanical Engineers Gas Turbine and Aeroengine Congress*, Birmingham, England, 10–13 June, Paper No. 96-GT-273.

Bammert, K., and Sonnenschein, H. (1967), "Der Einfluss verdickter und verduennter Turbinenschaufeln auf die Gittereigenschaften", *Archiv fur das Eisenhuettenwesen*, vol. 38, heft 4, pp. 287–99.

Bammert, K., and Fiedler, K. (1965), "Ueber Korrosion, Erosion and Verschmutzung bei Gichtgasturbinen", VIK Bericht No. 164, Essen, Germany.

Boelcs, A., and Sari, O. (1988), "Influence of Deposit on the Flow in a Turbine Cascade", *Transactions of the ASME, Journal of Turbomachinery*, vol. 110, pp. 512–19.

Boyle, R.J. (1994), "Prediction of Surface Roughness and Incidence Effects on Turbine Performance", *Transactions of the ASME, Journal of Turbomachinery*, vol. 116, pp. 745–51.

Brun, K., and Kurz, R. (1998), "Measurement Uncertainties Encountered During Gas Turbine Driven Compressor Field Testing", *Proceedings of the 44th American Society of Mechanical Engineers Gas Turbine and Aeroengine Congress*, Stockholm, Sweden, 1–4 June, Paper No. 98- GT-1.

Cohen, H., Rogers, G.F.C., and Saravanamuttoo, H.I.H. (1996), *Gas Turbine Theory*, 4th edn, Longman, Harlow, UK.

Diakunchak, I.S. (1991), "Performance Degradation in Industrial Gas Turbines", *Proceedings of the 36th American Society of Mechanical Engineers Gas Turbine and Aeroengine Congress*, Orlando, USA, 3–6 June, Paper No. 91-GT-228.

Elrod, W.C., King, P.I., and Poniatowsky, E.M. (1990), "Effects of Roughness, Freestream Turbulence, and Incidence Angle on the Performance of a 2-D Compressor Cascade", *Proceedings of the 35th American Society of Mechanical Engineers Gas Turbine and Aeroengine Congress*, Brussels, Belgium, 11–14 June, Paper No. 90-GT-208.

Frith, P.C. (1992), "The Effect of Compressor Rotor Tip Crops on Turbo-shaft Engine Performance", *Proceedings of the 37th American Society of Mechanical Engineers Gas Turbine and Aeroengine Congress*, Cologne, Germany, 1–4 June, Paper No. 92-GT-83.

Haq, I.U., Bu-Hazza, A.L., and Al-Baz, K. (1998), "Multistage Centrifugal Compressor Fouling Evaluation at High Power Settings", *Proceedings of the 43rd American Society of Mechanical Engineers Gas Turbine and Aeroengine Congress*, Stockholm, Sweden, 1–4 June, Paper No. 98-GT-53.

Khalid, S.A., Khalsa, A.S., Waitz, I.A., Tan, S.C., Greitzer, E.M., Cumpsty, N.A., Adamczyk, J.J., and Marble, F.E. (1998), "End-wall Blockage in Axial Compressors", *Proceedings of the 43rd American Society of Mechanical Engineers Gas Turbine and Aeroengine Congress*, Stockholm, Sweden, 1–4 June, Paper No. 98-GT-188.

Kind, R.J., Serjak, P.J., and Abbott, M.W.P. (1996), "Measurements and Predictions of the Effects of Surface Roughness on Profile Losses and Deviation in a Turbine Cascade", *Proceedings of the 41st American Society of Mechanical Engineers Gas Turbine and Aeroengine Congress,* Birmingham, England, 10–13 June, Paper No. 96-GT-203.

Kurz, R. (1991), "Transonic Flow Through Turbine Cascades With 3 Different Pitch-to-Chord Ratios", *Proceedings of the International Society for Air Breathing Engines (ISABE) 10th International Symposium on Air Breathing Engines*, Nottingham, England, 1–6 September, pp. 659–68.

Kurz, R. (1995), "Effects of Non-uniform Blade Pitch on the Flow through an Annular Turbine Nozzle", *International Rotating Machinery*, vol. 2, no. 1, pp. 59–65.

MacLeod, J.D., Taylor, V., and Laflamme, J.C.G. (1991), "Implanted Component Faults and Their Effects on Gas Turbine Engine Performance", *Proceedings of the 36th American Society of Mechanical Engineers Gas Turbine and Aeroengine Congress*, Orlando, USA, 3–6 June, Paper No. 91-GT-41.

Milsch, R. (1971), "Systematische Untersuchung ueber den Einfluss der Rauhigkeit von Verdichterschaufeln auf den Gitterwirkungsgrad", Ph.D. Thesis, University of Hannover, Germany.

Pinson, M., and Wang, T. (1994), "Effects of Leading-Edge Roughness on Fluid Flow and Heat Transfer in the Transitional Boundary Layer of a Flat Plate", *Proceedings of the 39th American Society of Mechanical Engineers Gas Turbine and Aeroengine Congress*, The Hague, Netherlands, 13–16 June, Paper No. 94-GT-326.

Radtke, F., and Dibelius, G. (1980), "Reynoldszahleinfluss bei hochbelasteten axialen Turbinenbeschaufelungen", VDI-Berichte No. 361, Duesseldorf, Germany.

Schmidt, K.J. (1992), "Experimentelle und theoretische Untersuchungen zum instattionaeren Betriebsverhalten von Gasturbinentriebwerken", VDI, Duesseldorf, Germany.

Shabbir, A., Celestina, M.L., Adamczyk, J.J., and Strazisar, A.J. (1997), "The Effect of Hub Leakage on Two High Speed Axial Flow Compressor Rotors", *Proceedings of the 42nd*

American Society of Mechanical Engineers Gas Turbine and Aeroengine Congress, Orlando, USA, 2–5 June, Paper No. 97-GT-346.

Sheard, A.G. (2012), *Tip Clearance Measurement in Aero and Industrial Turbomachinery*, Sigel Press, Cambridge, England.

Singh, D., Hamed, A., and Tabakoff, W. (1996), "Simulation of Performance Deterioration in Eroded Compressors", *Proceedings of the 41st American Society of Mechanical Engineers Gas Turbine and Aeroengine Congress*, Birmingham, England, 10–13 June, Paper No. 96-GT-422.

Spakovszky, Z.S., Gertz, J.B., Sharma, O.P., Paduano, J.D., Epstein, A.H., and Greitzer, E.M. (1999), "Influence of Compressor Deterioration on Engine Dynamic Behavior and Transient Stall Margin", *Proceedings of the 44th American Society of Mechanical Engineers Gas Turbine and Aeroengine Congress*, Indianapolis, USA, 7–10 June, Paper No. 99-GT-439.

Stalder, J.P. (1998), "Gas Turbine Compressor Washing State of the Art Field Experiences", *Proceedings of the 43rd American Society of Mechanical Engineers Gas Turbine and Aeroengine Congress,* Stockholm, Sweden, 1–4 June, Paper No. 98-GT-420.

Tarabrin, A.P., Schurovsky, V.A., Bodrov, A.I., and Stalder, J.P., (1998), "Influence of Axial Compressor Fouling on Gas Turbine Unit Performance Based on Different Schemes and With Different Initial Parameters", *Proceedings of the 43rd American Society of Mechanical Engineers Gas Turbine and Aeroengine Congress*, Stockholm, Sweden, 1–4 June, Paper No. 98-GT-416.

Traupel, W. (1988), *Thermische Turbomaschinen*, Springer, Berlin, Germany.

Chapter 9

Fouling Mechanisms in Axial Compressors

R. Kurz and K. Brun

ABSTRACT

Compressor blade fouling is a mechanism that over time leads to performance deterioration in gas turbines. Particle adherence to airfoil and annulus surfaces causes fouling. Particles responsible for fouling typically have a diameter of 2 μm or less. Smoke, oil mists, carbon and sea salts are common sources of fouling particles. Appropriate air filtration systems can minimize fouling, and detergent-washing components can reverse fouling to some extent. The adherence of particles is impacted by oil or water mists. The result of particle adherence is a build-up of material that results in increased surface roughness. Additionally, a build-up can change an airfoil's shape if it forms a thick layer. Changes in surface roughness or the blade shape will degrade gas turbine performance. This chapter evaluates fouling mechanisms based on observed data, presents a discussion on fouling susceptibility and considers the factors which design engineers must take into account when defining air filtration system specifications.

This chapter is a revised and extended version of Kurz, R., and Brun, K. (2012), "Fouling Mechanisms in Axial Compressors", *Transactions of the ASME, Journal of Engineering for Gas Turbines and Power*, vol. 134, pp. 1–9.

NOMENCLATURE

c	cord
c_p	heat capacity
d	diameter
D	diffusion coefficient
E	capture rate
I	particle flux
k	roughness
L	length
N	number
P	power
r	radius
Re	Reynolds number
St	Stokes number
T	temperature
U	velocity
W	work
β	direction of relative flow
ρ	density
∂	viscosity
ν	viscosity
η	efficiency

Subscripts

c	compressor
f	fluid
l	laminar
out	output
p	particle
t	turbine
0	initial

INTRODUCTION

Compressor blade fouling is a mechanism that results in gas turbine performance deterioration over time. Compressor fouling occurs as a consequence of the size, quantity and chemical composition of an aerosol of particles in the gas turbine inlet flow. This aerosol comprises dust, insects, organic matter such as seeds from trees, rust or scale from the inlet ductwork, carryover from a media type evaporative cooler, deposits from dissolved solids in a water spray inlet cooling system, oil from leaky compressor bearing seals, or ingestion of power plant stack gas or plumes from nearby cooling towers. Adherence of particles smaller than 10 μm to airfoils typically causes fouling.

We must distinguish fouling from erosion, the abrasive removal of material from the flow path by hard particles impinging on flow surfaces. These particles typically have to be larger than 10 μm in diameter to cause erosion by impact. Erosion is more a problem for aero gas turbine applications because state-of-the-art filtration systems for industrial applications will typically eliminate the bulk of larger particles. However, erosion can become a problem for gas turbines that use water droplets for inlet cooling or water washing.

This chapter aims to determine which mechanisms play a role in airfoil fouling. One might argue that the mechanisms are well known and that numerous papers have described them. However, there has not been a systematic effort to correlate the location and severity of observed deposits on compressor blades with the aerodynamic features of the particle laden flow around airfoils. This study brings a deeper insight into the relative importance of different particle sizes and the gas turbine compressor blades' capture efficiency, in particular transonic front stages. The chapter thus comprises two parts: an assessment of the aerodynamic mechanisms that occur with fouling, and a review of actual, contaminated blades.

Researchers understand, at least theoretically, the mechanisms that lead to particle entrainment. However, they less clearly understand conditions under which particles on impact actually stick to a blade's surface. When one disassembles a gas turbine that has been in service for some time and studies the fouled blades, it is apparent that small particles sticking to airfoils cause performance deterioration. The deterioration in this case is usually reversible, as water-washing can remove the particles (Kurz and Brun, 2009). This distinction is important, because recoverable and non-recoverable degradation have different economic impacts.

Offline water-washing can remove fouling and online water-washing can slow it down. Theoretically, one can keep a gas turbine at a small degradation level if one frequently washes online, and if one carries the cost of lost production that occurs with shutting down the gas turbine for offline washing. The decision to shut down a gas turbine for offline washing is a balance between loss of production that occurs with the gas turbine's degraded performance due to fouled blades and loss of production that occurs with shutting down the gas turbine for typically half a day to conduct the offline water-wash.

The reversal of non-recoverable degradation requires one to disassemble and overhaul a gas turbine. Although theoretical considerations (Tarabrin *et al*., 1998) indicate that smaller gas turbines show more fouling than larger ones, there is no anecdotal evidence that this is true. If there is an impact of gas turbine size, it is probably obscured by the fact that smaller gas turbines usually have fewer compressor stages, and the variability in fouling rates occurring with site-by-site variations in dust load and air filtration system specification.

INLET FILTRATION SYSTEMS

Design engineers fit industrial gas turbines with effective inlet filtration systems. Modern filtration systems virtually eliminate particles bigger than 10 μm that

cause erosion in gas turbine compressors (Figure 9.1). When considering filtration system specification, there is a tradeoff between system size, weight and cost versus filtration efficiency and pressure loss (Wilcox *et al*., 2010).

Schroth *et al*. (2007) compared the power loss for two different air filtration systems when fitted to a 165 MW gas turbine. The filtration systems that they compared were a two-stage and a three-stage system. The three-stage system causes a significant reduction in finer particles entering the gas turbine. The power loss after 3000 hours of operation was 4 percent with the two-stage system and 2 percent with the three-stage system. If a gas turbine ingests 100 kilograms per year of contaminants without a filtration system in a typical offshore application, an F5 filter designed in accordance with the requirements of EN 779 would reduce the ingestion rate to approximately 21 kilograms per year, an F6 filter to approximately

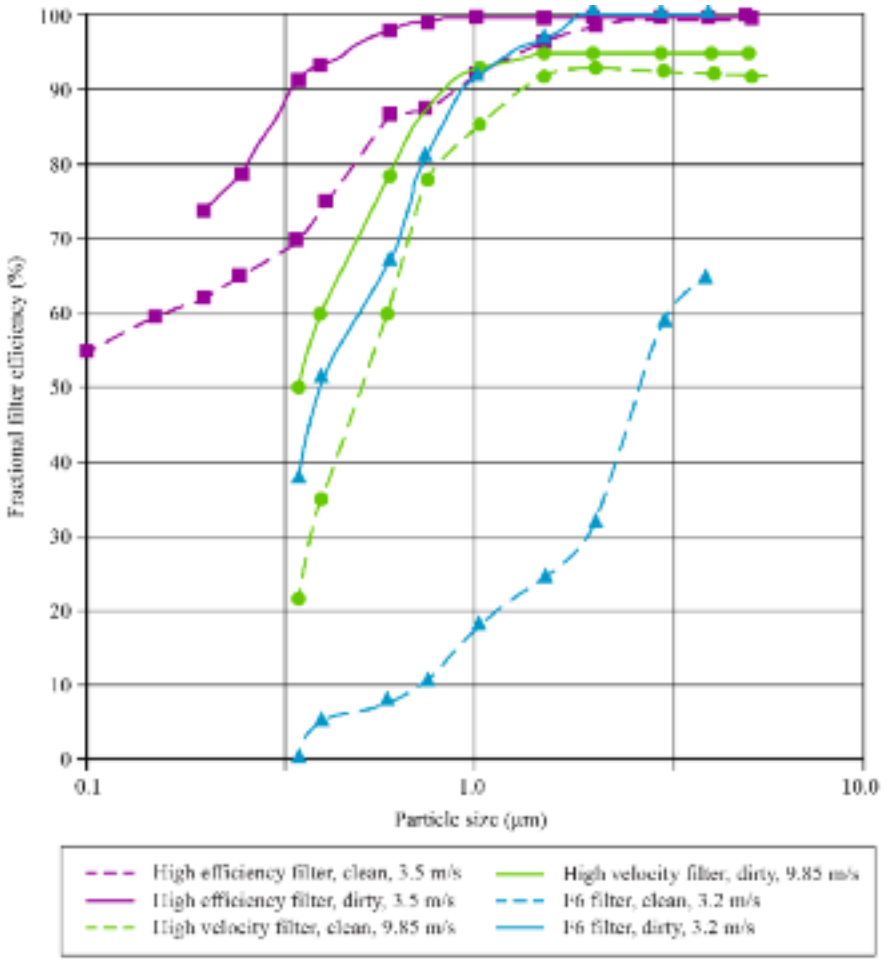

FIGURE 9.1. Comparison of fractional efficiency for filter elements from different suppliers and different face velocities in new and dirty conditions, from Brekke and Bakken (2010).

6 kilograms per year, a two-stage filtration system with F7/H10 filters to approximately 0.2 kilograms per year and a three-stage filtration system with F7/F9/H10 filters to as little as 0.05 kilograms per year. The filter designations (F5, F6, F7, F9, H10) refer to EN 779. A Class H filter has superior filtration efficiency for small particles over an F Class filter.

The different gas turbine particle ingestion rates, when fitted with different inlet filter standards, highlights the impact of air filtration quality on the performance deterioration due to fouling. One may reduce overall contaminant ingestion to 0.01 percent of the unfiltered value by using an appropriate air filtration system. With any of these multi-stage filter systems, there are virtually no particles larger than a few microns entering the gas turbine. The observed fouling therefore depends on mechanisms that bring the very small particles that do pass through the inlet filter to the compressor airfoils' surfaces.

OBSERVED DATA

To assess the fouling mechanisms that occur with a gas turbine compressor, one can analyze fouling patterns on compressor airfoils. Vigueras Zuniga (2007) reports deposits on the gas turbine compressor rotor and vanes, with deposits both on suction and pressure surface. There is evidence of increased deposits in the rotor blade suction side's leading edge region. Figure 9.2 shows a typical salt deposit on the gas turbine's compressor in offshore service. The deposits exist on both the rotor blades'

FIGURE 9.2. Salt deposits on compressor blades after 18,000 hours of operation. This is the view on the suction side. There are fewer deposits near the leading edge and in the hub region.

suction and pressure sides, with fewer deposits near the leading edge and in the hub region. Figure 9.3 shows another example of a gas turbine compressor rotor from an onshore application. The deposits indicate the location of boundary layer transition.

Parker and Lee (1972) studied fouling patterns on rotating blades for very fine (0.13 to 0.19 μm) particles and found high deposition rates at the blade leading edge, relatively low deposition on the pressure side and a higher deposition rate on the suction side toward the trailing edge (Figure 9.4). The deposition rates on the suction surface near the trailing edge are where the boundary layer is thick and turbulent. The particle distribution deposition rates are strikingly similar to the heat transfer rates around a turbine blade according to Lefebvre and Arts' study (1997) (Figure 9.5). In both cases the turbulent boundary layer drives the deposition mechanism, leading to both a higher heat transfer rate and diffusion. A comparison with the heat transfer mechanism applies to particles less than 1 μm in diameter that, as a consequence of their small size, diffuse to the surface in proportion to their original concentration via Brownian motion.

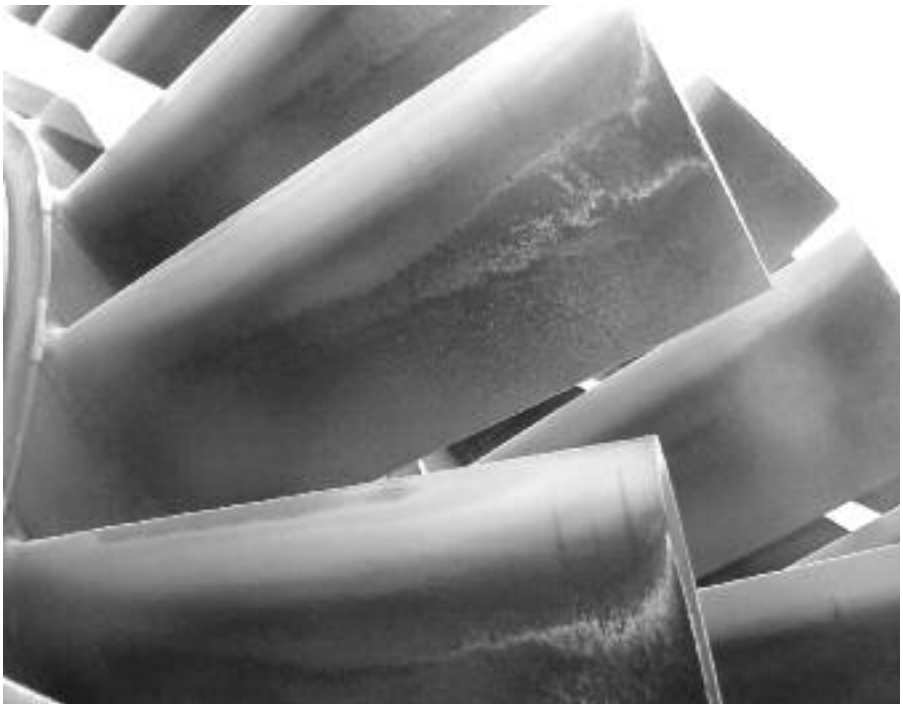

FIGURE 9.3. Deposits on the suction side of a compressor rotor. Deposits are visible in an area (halfway between leading and trailing edges) where the flow across the blade's suction side probably transitions from laminar to turbulent flow.

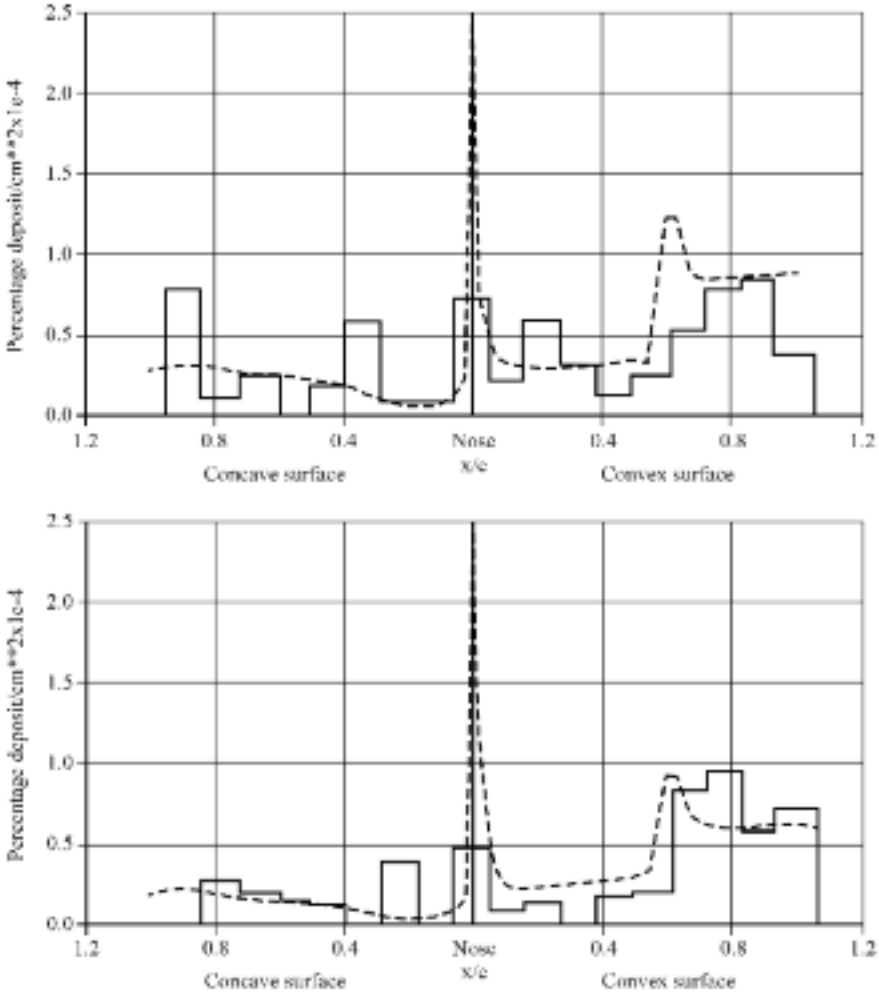

FIGURE 9.4. Fouling deposition rates on an axial compressor airfoil. The solid lines represent experimental data and the dotted lines are predicted deposition rates. Particle mass median diameter is (top) 0.13 μm and (bottom) 0.19 μm. This figure is reproduced from Parker and Lee (1972).

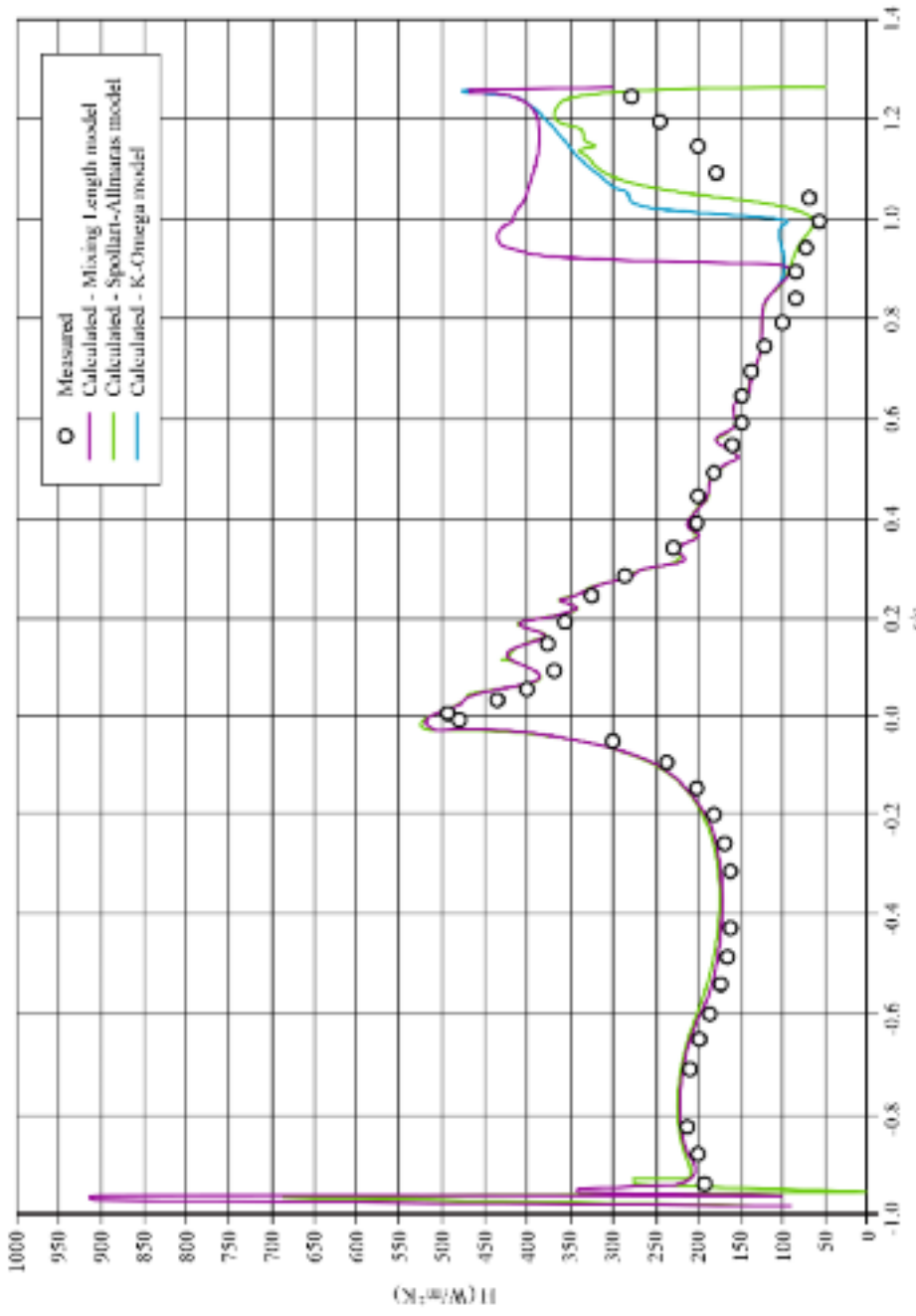

FIGURE 9.5. Blade heat transfer h on a turbine blade. s/c is a coordinate along the blade surface, starting at the stagnation point (s/c = 0) with positive s/c along the suction side and negative s/c along the pressure side, from Lefebvre and Arts (1997).

In contrast with Parker and Lee's findings (1972), Syverud *et al*. (2007) identified deposits primarily on the blade pressure side and leading edge that resulted in a significant increase in surface roughness. They also identified that the majority of the deposits occurred with the compressor's early stages. Syverud *et al*. (2007) utilized a salt water spray that formed droplets of approximately 23 μm median diameter. Therefore, their data are only of limited value for studying fouling patterns in industrial gas turbines since typical particles in industrial gas turbines' air filters will be much smaller. Adiabatic compression through the compressor stages results in the relative humidity dropping in the latter compressor stages due to the temperature increase, which reduces the droplet size for the rear stages. This is probably one reason why Syverud *et al.* (2007) found very few deposits on the rear stages of their compressor.

As a result of the inlet air's acceleration as it enters the compressor through a bell mouth and inlet guide vanes, the air's temperature will drop and therefore its relative humidity will increase. A drop in temperature can lead to saturation, and therefore condensation as the flow enters the compressor's inlet guide vanes, even if the air's relative humidity is as low as 80 percent. The droplets that can form due to this temperature drop may scrub entrained solids, such as salts or gases. Because the droplets form downstream of the filter, their size can be larger than the particle sizes that normally cannot pass through the air filter. These larger droplets may be acidic as a consequence of the presence of CO_2 or SO_x, which react with the water within the compressor. Acidic droplets cause corrosion pitting of the blades which can be prevented by utilizing compressor blade coatings.

Fouling also affects the compressor casing. Elrod and Bettner (1983) compared the performance of a gas turbine's compressor with different levels of casing roughness. Comparing the results for design roughness (1.8 μm) with a rough (13 μm) casing, the compressor lost approximately 1 percent flow capacity and 1 percent peak efficiency. The degradation in performance occurs as a consequence of the added wall roughness increasing the casing boundary layer displacement thickness.

The types of particles responsible for compressor fouling vary from site to site. Oil and grease particles are common in industrial locations as a result of emissions from refineries, petrochemical plants and internal oil leaks within the gas turbine itself (Meher-Homji *et al*., 2009). Oil and grease deposits act as an adhesive, entrapping other material that enters the compressor. Centrifugal force spreads oil ingested into the flow path, generating a film on the blades that enables larger particles to stick to the surface (Figure 9.6). Coastal locations usually result in the ingestion of sea salt. We associate desert regions with dry sand and dust particles. In agricultural regions compressors ingest dust and fertilizer chemicals. Sand, dust and other solid particles stick to blade surfaces in the presence of oil or water, and therefore result in fouling.

FIGURE 9.6. Oily deposits on axial compressor blades from bearing oil leakage on a large heavy duty gas turbine (Meher-Homji *et al*., 2009). Oil streaks originate at the hub region and are distributed over the airfoil by centrifugal forces and blade boundary layer shear stresses.

MECHANISMS

A discussion on fouling mechanisms should address three fundamental issues (Table 9.1):

1. Entrainment mechanisms: how do particles of various sizes reach blade and wall surfaces?
2. Sticking mechanisms: when do particles that reach the surface actually stick to it?
3. Performance deterioration mechanisms: what is the impact of particles on the blade surface or the walls on compressor performance?

The compressor's susceptibility to fouling affects each of the above fouling mechanisms. Meher-Homji *et al*. (2009) introduced the concept of a distinction between susceptibility and sensitivity to fouling. Susceptibility is the amount of fouling a compressor incurs under a specified contaminant load, while sensitivity describes the effect on compressor efficiency. Individual gas turbine compressors will have both a different susceptibility and sensitivity to fouling. However, the mechanisms that underpin the fouling process are generic, and apply to all gas turbine compressors.

Table 9.1. *Fouling mechanisms that bring particles into contact with blade surfaces.*

Parameter	Possible deposition mechanism for particle size (μm)	Reachable surface	Generate surface roughness	Chance to stick
Impact (Tarabrin *et al*., 1998)	> 5	Leading edge and pressure side	X	—
Diffusion (Fuchs, 1964)	< 0.1	All	—	X
Turbulent diffusion (Fuchs, 1964)	< 0.5	All	(X)	X
Bouncing particles (Beacher *et al*., 1982)	> 5	Leading edge, pressured side, (suction side near leading edge)	X	—

Entrainment mechanisms

How do the contaminants find their way to the compressor surfaces? Particles can reach surfaces in one of five ways (Fuchs, 1964):

- settling;
- inertial impaction;
- interception;
- diffusion; and
- electrostatic forces.

The above mechanisms have been the subject of study within the context of inlet air filtration system performance (Poon *et al*., 2010; Wilcox *et al*., 2010). When analyzing particle sizes responsible for fouling, it is important to consider the effect of impaction, interception and diffusion (Figure 9.7). Settling only applies to large particles in slow-moving flows. Inertial impact and interception are important mechanisms for larger particles in fast-moving flows. Inertial impaction describes the behavior of large particles in fast-moving flows around obstacles, where the particles' inertia does not allow them to follow the streamlines. Interception describes an effect where particles, while following the streamlines, are large enough to penetrate the boundary layer and come into contact with the surface. Diffusion mechanisms are particularly important for sub-micron particles. Electrostatic forces, while a significant consideration in the design of inlet air filtration systems, play no role in compressor fouling.

Tarabrin *et al*. (1998) presented a correlation to describe a compressor's susceptibility to fouling. Song *et al*. (2003, 2004) expanded Tarabrin *et al.*'s (1998) correlation. Tarabrin *et al.* (1998) and Song *et al*. (2003, 2004) use an inertial impaction

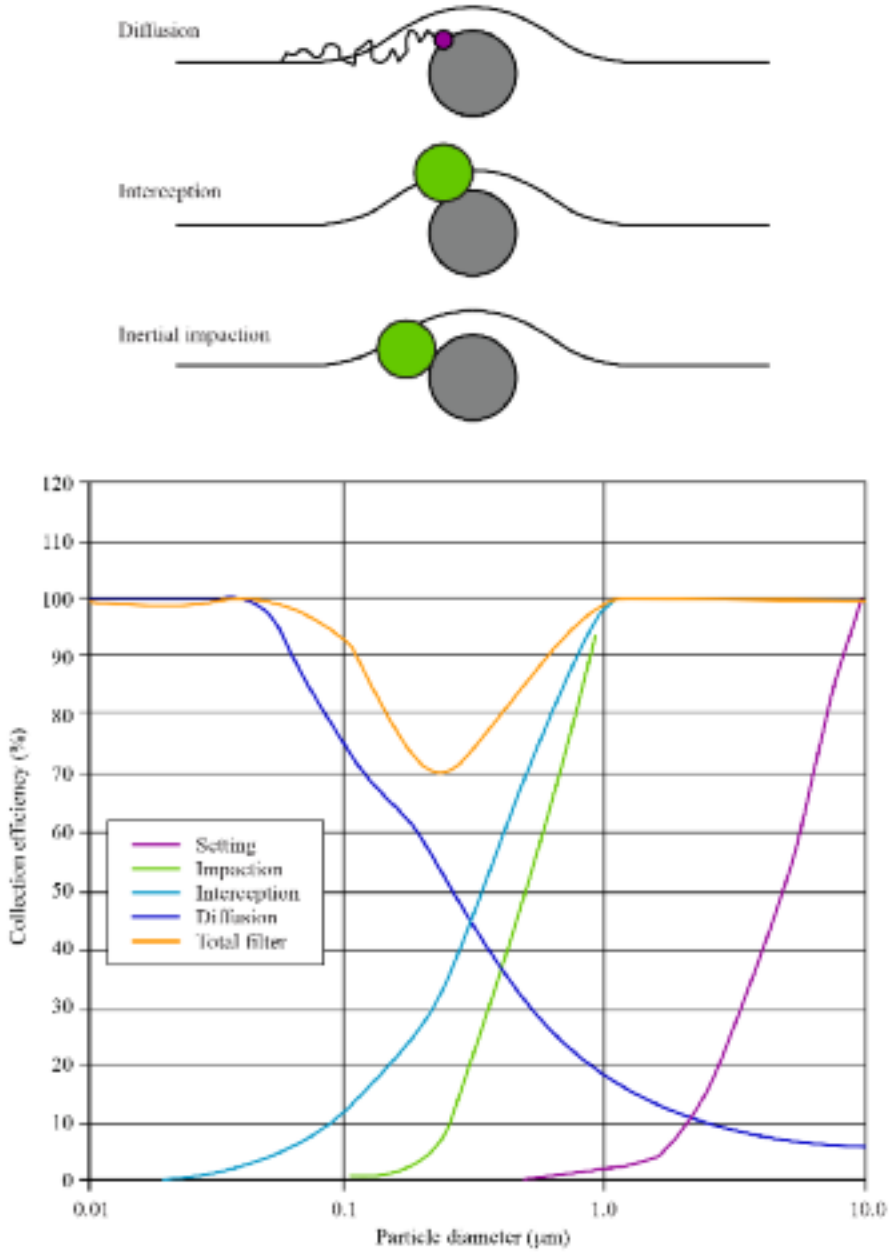

FIGURE 9.7. The four filtration mechanisms that impact filter efficiency.

mechanism which Fuchs (1964) described. In accelerating flow, particles will not follow the flow precisely. The deviation between gas path and particle path is a function of gas acceleration and the particle's size and density. We may use the Stokes number *St* to characterize particle behavior.

$$St = \frac{\rho_p d_p^2 U}{18\mu \cdot 2L} \qquad L - s \cdot \sin(\beta_b - \beta_1) \tag{1}$$

Larger particles, with a larger Stokes number, will deviate more from the gas path than smaller particles, and will consequently impact more frequently on the compressor blade's pressure side. The capture rate *E* of particles therefore increases with Stokes number (Tarabrin *et al*., 1998):

$$E = 0.08855 \cdot St - 0.0055 \tag{2}$$

Particles may also impact a compressor blade's leading edge's suction side (Figure 9.2). However, Tarabrin *et al*. (1998) or Song *et al*. (2003, 2004) did not consider particle impact on the suction side. Tarabrin *et al*. (1998) developed the method and Song *et al*. (2003, 2004) extended it. The method considers how particles reach the compressor blade pressure side and the compressor casing, and the compressor blade suction side immediately downstream of the leading edge. However, it does not model the process by which particles deposit themselves on the compressor blade suction side. When one studies in-service compressor blades, the observable fouling patterns indicate that sub-micron particles are responsible for fouling on the compressor blade suction side. The mechanism responsible for deposition for these small particles is not inertia and interception, as is the case for larger particles, but rather diffusion. This diffusion occurs in proportion to small particle concentration Brownian motion (Levine, 1998). Consequently, turbulent mixing and diffusion enhance particle transport to the surface.

Siegel (2002) studied heat exchanger tube fouling, which is subject to similar fouling mechanisms as compressor airfoils. Siegel's findings (2002) are applicable to the discussion which we present in this chapter as the involved Reynolds numbers are similar, and we may regard a heat exchanger tube as an approximation for the compressor blade's leading edge:

- deposition rates are sensitive to the level of turbulence in the flow;
- impaction of particles is an important factor at the leading edges;
- Brownian motion does not significantly contribute to deposition rates due to the very short residence times — the flow velocity is very large compared to the particle movement;
- particle interception does not significantly add to particle deposition;
- the motion of particles due to the shear force gradient in the boundary layer does not result in significant deposits except for very large particles;

- while wet particles and droplets have a very high rate of adhesion to the surface, most dry particles will bounce off the surface; and
- the particle size most responsible for fouling is 1 to 5 µm, although higher velocities shift the average particle size downward.

Siegel's findings (2002) include an observation that deposition rates are dependent on turbulence levels. Deposition rate dependency on turbulence level indicates that diffusion is important. Of the fouling mechanisms that we listed earlier, only diffusion is sensitive to the turbulence level. Impaction can only explain deposition at the leading edge, but not on a convex surface. Particle interception also is not a major factor. Of the remaining mechanisms, we can also exclude settling because the particles would have to be much larger. Electrostatic forces may also be excluded, because the compressor blades and casings are good electrical conductors. Therefore, when we consider Siegel's findings (2002), we may conclude that diffusion is the primary mechanism that results in the presence of small particles on the compression blades' suction surface.

We associate particle deposition by diffusion with low flow velocities, significantly lower than the free stream velocities in a compressor (Fuchs, 1964). We associate the blade boundary layer with significantly lower velocities than the free stream velocity close to the blade surface. Consequently, fouling can occur within a compressor as a consequence of the diffusion mechanism. We may characterize particle diffusion in laminar flow in a tube of radius R using the equation:

$$n / n_0 = 1 - 2.56 \cdot \left(\frac{Dx}{R^2 U} \right)^{2/3} + 1.2 \cdot \left(\frac{Dx}{R^2 U} \right) + 0.0177 \left(\frac{Dx}{R^2 U} \right)^{4/3} \tag{3}$$

where n is the number of particles out of an initial n_0 particles that the tube walls do not capture after traveling the distance x along the tube (Fuchs, 1964). The tube serves as a proxy for the flow through a compressor blade row. Fuchs (1964) derived similar equations to describe the diffusion for flows in channels with parallel walls. In Equation 3, D is the diffusion coefficient, which is a function of particle size and flow velocity. We know that diffusion in a turbulent flow is orders of magnitude larger than in laminar flow (Prandtl *et al*., 1990). We may conceptualize turbulent flow as a combination of eddies of various sizes. The eddy size in turbulent flow follows a power law distribution, with correspondingly more small eddies than large eddies and consequently, the small particle diffusion rate will be larger than for larger particles (Prandtl *et al*., 1990).

Fuchs (1964) presents experimental data for air flow in a tube, indicating that the particle flux I, the flow of particles per surface area and time to the tube walls, is:

$$\frac{I}{N_0} = \frac{D^{\frac{3}{4}} \, \mathrm{Re}_f^{\frac{7}{8}} \, v^{\frac{1}{4}}}{90 \cdot r_{particle}} = \frac{D^{\frac{3}{4}} U_f^{\frac{7}{8}} v^{\frac{5}{8}}}{90 \cdot \left(r_{particle} / L^{\frac{7}{8}} \right)} \tag{4}$$

This above equation suggests that for a constant quantity N_0 of particles, increasing flow velocity and reducing relative particle size both lead to increased deposition rates. This combination results in deposition rates increasing as the blade length L increases compared to particle size. The result is that larger compressors have a higher particle accumulation for a given particle size distribution than smaller compressors. Fuchs' results (1964) also indicate that only in a turbulent boundary layer is the diffusion coefficient $D = D_1 + D_t$ large enough to result in appreciable particle deposition.

Casing fouling occurs as a consequence of centrifuge forces on the flow through a compressor. Larger particles impact the casing in earlier compressor stages and more frequently, while smaller particles will come into contact with the casing in later compressor stages. Tabakoff *et al*.'s (1991) study conclusions corroborate the primary importance of centrifugal action, noting that a small percentage of particles 2.5 μm and smaller come into contact with the casing, while a large portion of particles of 15 μm will come into contact with the casing.

Consideration of blade aerodynamics

Compressor aerodynamics play a determining role in particle transportation and deposition through a compressor. To better understand how compressor aerodynamics drive compressor fouling, it is helpful to consider both two-dimensional compressor blade flow and three-dimensional compressor blade-to-blade passage flows.

The first stages of gas turbine compressors are typically transonic, while later stages are typically subsonic. In either case, the incidence angle of air onto the compressor blade is a function of the compressor's operating point. In transonic blades, where an oblique shock exists at or upstream of the leading edge, particles will not follow the air flow through the shock without deviation from the air flow's path. Particles whose path deviates can impact on the blade suction side near the leading edge. When particles pass through an oblique shock, they accelerate to a higher velocity than the surrounding air, and consequently any model of particle drag must adapt to take the effect of the oblique shock on particles into account (Kurz, 1991).

Jacobs *et al*. (2012) have developed a computer simulation of particle dispersion as a result of oblique shocks, identifying the shock–particle interaction as a mechanism for creating a particle velocity component perpendicular to the main flow. In subsonic compressor blades the incidence angle increases for low flows and decreases for high flows (Boelcs and Suter, 1986). No shock will form, but the airflow's streamlines are curved and particles may deviate from the streamlines.

When we consider the boundary layer that forms between free stream and blade surface, it will initially be laminar and the transition to turbulent. In a laminar boundary layer, particle transport perpendicular to the streamlines is possible by means of diffusion. At typical gas turbine compressor velocities, diffusion processes are negligible, although in a laminar boundary layer where flow velocities are lower,

diffusion processes can become significant. In contrast to laminar flow, we may conceptualize turbulent flow as a large number of varying-sized eddies (Deutsch and Zierke, 1986). Particle transport perpendicular to the streamlines increases in turbulent flow, providing a mechanism to transport small particles to the blade's surface.

When considering the significance of boundary layer flow for the fouling process, there is a second feature that researchers have identified as important (Deutsch and Zierke, 1986; Kurz, 1991). Depending on the state of the boundary layer, the shear stress between the air and the blade surface varies significantly. The consequence of this variation in shear stress is that particles which reach areas of high shear stresses have a high probability of being swept downstream. Areas with high shear stress are also areas with a high friction factor (Figure 9.8).

The observation that a variation in shear stress results in particles reaching the flow's high shear stress areas and being swept downstream is based on a two-dimensional analysis of the compressor flow field. When we consider the compressor flow as a three-dimensional flow field the significance of secondary flow features becomes apparent. Blade tip-to-casing clearance and corner vortex flow drives the compressor's secondary flow, and the resultant blade passage static pressure field. The blade passage static pressure field in turn impacts on boundary layer development through the blade passage (Figure 9.9). A consequence of the blade passage secondary flow structure is that particles driven by this three-dimensional flow field may deposit in unpredicted locations if we used a purely two-dimensional analysis.

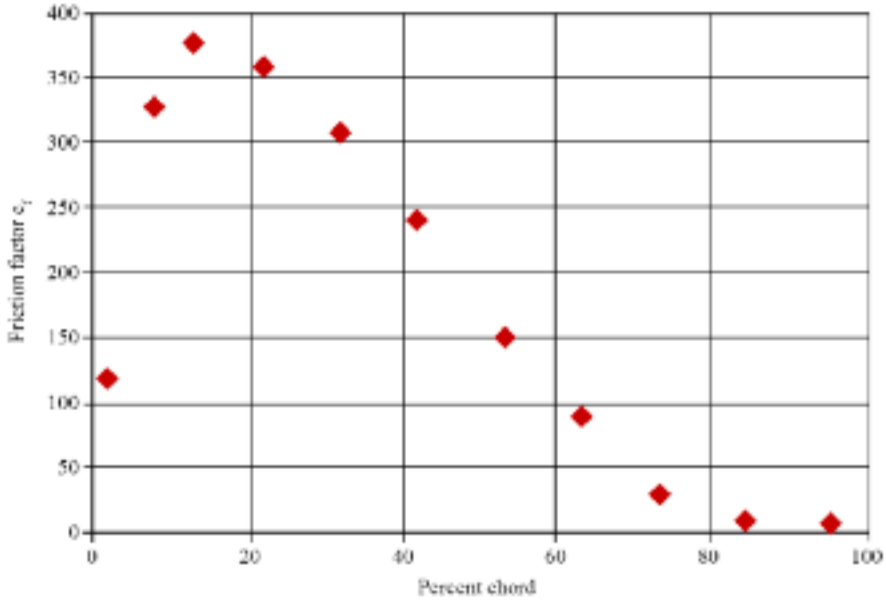

FIGURE 9.8. Friction factor on the compressor blade's suction side, from Deutsch and Zierke (1986).

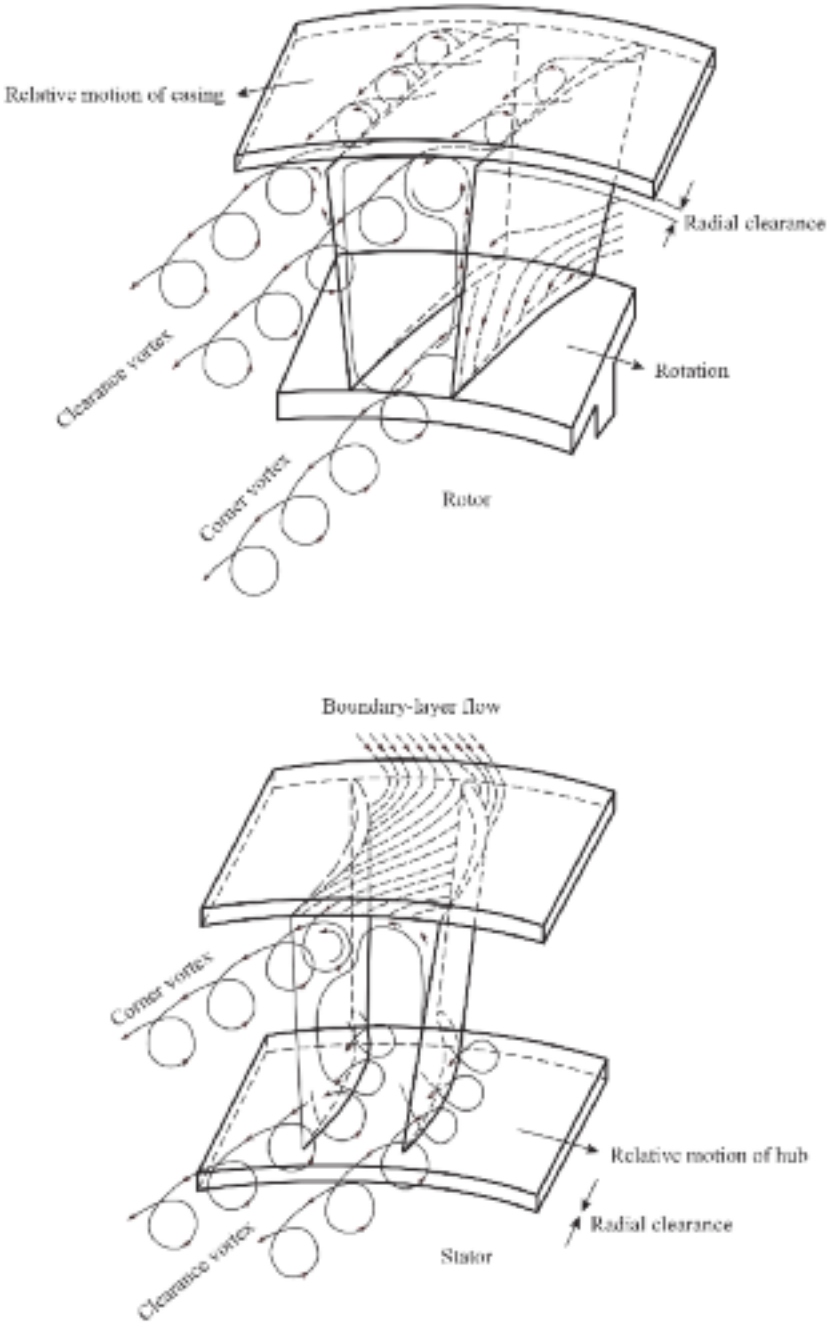

FIGURE 9.9. Secondary flow regions in the axial flow compressor's rotor and stator, from Fottner (1989).

Beacher *et al*. (1982) describe a third mechanism that enables larger particles to reach the blade suction side, at least the part close to the leading edge. Particles bouncing off the previous blade's surface will show a large velocity and flow direction discrepancy relative to the main flow, and thus can reach at least the front part of the airfoil's suction side. However, for compressor blades, with their smaller curvature, particles may reach the suction surface's rear parts. Whether the particles that reach the suction surface actually stick there depends on the particle's consistency.

Liquid droplets hitting the blade's leading edge can transport themselves along the blade surface both on the suction side and the pressure side as a consequence of the shear stress in the boundary layers. If these liquids contain solid contaminants and the liquids evaporate, the contaminants will remain on the blade surface. For this mechanism, droplet size is not important, because even larger particles will hit the blade leading edges.

Engineers often assume that particles enter a compressor with homogeneously distributed particle sizes. This is generally not the case as large particles may collect on the previous blade's pressure side without sticking to it. Consequently, the larger particles enter the next compressor stage's inlet with lower momentum. The compressor's centrifuge effect on particles will result in larger particles centrifuging outward and consequently, having a higher concentration at the blade tip and a lower concentration at the hub. The particles' centrifugal migrations towards the blade tip may make larger tip-to-hub ratio compressors less susceptible to fouling. In larger tip-to-hub ratio compressors a smaller blade portion is subjected to the large particles.

In cases where one introduces bearing oil at the rotor hub, the oil enters the air stream in the hub boundary layer. As the oil enters into a boundary layer region, we can describe its movement by considering the three-dimensional compressor blade passage flow field. The blade rows' secondary flow structure will drive the oil transport. Oil deposits on the blade surface have two consequences: like any other deposit, they change the surface of the blade, and additionally they provide a sticky surface that allows particle to adhere to the blade surface. Table 9.1 summarizes the discussion of entrainment mechanisms and their relevance for particle deposition on compressor blades.

Sticking mechanisms

If particles come into contact with the blade surface, the mechanism by which they attach themselves to the surface depends on two factors: the "stickiness" of the surface relative to the particle and the shear forces in the boundary layer (Sreedharan and Tafti, 2010). The stickiness of the surface increases if the surface is wet, but the ability of particles to stick is also a function of particle size. Particles above about 10 μm in diameter tend not to stick irrespective of the stickiness of the surface. Fine particles adhere to rotating blades due to their stickiness that is sufficient to hold the particles when centrifugal forces are high (Levine, 1998). Additionally, the angle of impact of particles onto the surface influences their probability of sticking to the surface. The more acute the angle of impact, the less likely a particle is to stick irrespec-

tive of the surface's stickiness. Shear forces in boundary layers are particularly low in areas where the flow separates or transitions from laminar to turbulent flow. Therefore, we routinely find particle deposits in areas where flow separates or transitions.

Fuchs (1964) concluded that wet walls increase the entrainment efficiency significantly. Fuchs (1964) noted that it is virtually impossible to blow particles with a diameter of 1 to 2 μm from deposits on clean plates, even at a velocity of 200 m/s. The particles seem to lodge into surface pits and crevices, and thus are only dislodged by the blade vibrating. Solid particle adhesion with diameters 2 to 10 μm only occurs if an adhesive film formed from grease or oil is present. The grease or oil film thickness and viscosity impact the probability of a particle sticking to the surface. One of Fuchs' (1964) conclusions was that a layer thickness of 0.5 to 1 μm is the most effective. Thinner layers do not retain particles over 2 μm diameter.

Liquid particles behave differently to solid particles. The higher a liquid droplet's impact velocity, the higher is the probability of the liquid remaining on the surface. Surfaces covered in grease or oil increase the probability of liquid particles bouncing off the surface. Researchers have studied in detail the process by which fly ash particles stick to surfaces in boilers and a gas turbines' high-pressure turbine vanes and blades. The mechanisms which cause particles to stick include van der Waals, capillary and electrostatic forces, plus re-entrainment (Sreedharan and Tafti, 2010). The forces that we associate with each of the aforementioned mechanisms become more dominant for smaller particles. If the compressor is wet, capillary forces tend to dominate. The probability of a particle sticking to a surface increases the lower the particle's viscosity becomes and, therefore, we may conclude that dry particles have to be very small to stick, whereas larger particles or wet particles are more likely to stick.

Compressor performance deterioration mechanisms

The primary effect of fouling on compressor blades is to increase blade surface roughness. An increase in surface roughness affects the blade boundary layer's formation. We associate compressor airfoils with adverse pressure gradients. Adverse pressure gradients affect boundary layer development on the blade suction side more so than on the blade pressure side and hence, the impact of increased roughness is more significant on the blade suction than pressure side.

Morini *et al*. (2011) studied a compressor stage's performance with smooth and increased blade surface roughness. They observed a significant deterioration in compressor performance when surface roughness increased to $k_s/c = 0.714 \times 10^{-3}$, with k_s = 40 μm. Morini *et al.* (2011) concluded that we could attribute almost entirely compressor performance degradation to an increase in blade suction surface roughness.

If the fouling mechanism is impacted as a consequence of high enough inertial forces on larger particles that they cannot follow the flow streamlines, then blade fouling would predominantly occur on the blade pressure side. If the blades or the particles are wet, then larger particles would stick, and they would cover the pressure side more or less uniformly. When conditions through the compressor are dry, small

particles would follow the flow streamlines through the compressor blading and consequently, stick to the compressor blades primarily towards the blade trailing edge. An exception would be dry particles entrained in blade passage secondary flow, which could transport themselves to those areas of the blade suction side that the secondary flow impacts.

If the fouling mechanism is diffusion, then small particles may migrate to both the blade suction and pressure side. One would expect to find more particles deposited in high turbulence areas due to the higher diffusion rates in turbulent flows. One also would expect to be able to identify boundary layer transition areas that occur with either laminar to turbulent boundary layer transition or flow separation. In both cases, the low shear stress at the transition points results in the deposited particles forming contamination patterns similar to those which Parker and Lee (1972) observed (Figure 9.4).

Syverud *et al*. (2007) found that the surface roughness on a compressor blade's suction side was significantly lower than on the pressure side after spraying atomized salt water into the gas turbine inlet. For the industrial gas turbine that we studied, the suction side roughness was 6 μm while the pressure side was up to 110 μm. The difference in roughness between the suction and pressure surface supports our assertion that only smaller particles can reach the compressor airfoil's suction side.

Syverud *et al*. (2007) observed that the suction side increase in surface roughness was 6 μm; however, Parker and Lee (1972) observed that only very fine particles in the 0.13 to 0.19 μm range were able to reach the suction side. It is not clear how very fine particles in the 0.13 to 0.19 μm range can cause a 6 μm increase in surface roughness. Bammert and Woelk (1979), Milsch (1971) and Morini *et al*. (2010) all studied the effect of increased surface roughness on compressor performance. In each case the size of the necessary roughness increase to cause a measureable reduction in compressor performance was significantly larger than the particles' size that can transport to the blade suction side. Only increasing roughness to the point where it impacts the boundary layer development can result in reduced compressor performance. As such, we must conclude that sub-micron particles are able to cause an increase in suction side surface roughness more than an order of magnitude greater than the particle size.

Susceptibility correlations

Some researchers (Seddigh and Saravanamuttoo, 1991; Tarabrin *et al*., 1998; Song *et al*., 2003, 2004; Meher-Homji *et al*., 2009) have developed correlations that derive the susceptibility and sensitivity to fouling of a specific gas turbine from readily available data. Based on available gas turbine geometry and performance data, the correlations characterize the gas turbine's susceptibility and sensitivity to performance deterioration as a consequence of fouling. The index then acts as a comparator for performance deterioration due to fouling. If we compare two gas turbines with one having a higher index than the other, the gas turbine with the higher index should show a faster performance deterioration under a given contaminant load.

Tarabrin *et al*. (1998) postulate that a relationship for fouling exists that combines the gas turbine compressor's geometric and aero-thermal characteristics. They named the relationship the Index of Sensitivity to Fouling (ISF). They derived the ISF from considering a cylinder's inertial deposition entrainment efficiency corrected to the inertial deposition entrainment efficiency of a row of airfoils:

$$ISF = \frac{Wc_p \Delta T_{stage}}{(1 - r_h^2) D_c^3} \cdot 10^{-6} \tag{5}$$

The susceptibility of a given gas turbine to particles of a given size d_p is then:

$$\lambda = ISF \cdot \frac{\rho_p \cdot d_p^2}{\eta_f} \tag{6}$$

which leads to a conclusion that larger, heavier particles have a higher probability than small particles of colliding with the blade surface. In so doing, the model predicts a higher susceptibility of smaller gas turbines to fouling, with some impact of higher stage loading. Song *et al*. (2003, 2004) extended Tarabrin *et al*.'s (1998) method and concluded:

- Fouling is closely related to the geometric and compressor stage's flow characteristics. Particle adhesion to blades (defined as the cascade collection efficiency) increases with a decrease of chord length and an increase of solidity. Furthermore, fouling increases with reduced flow rates, which are closely related to the incoming air velocities.
- Large particles increase the cascade collection efficiency. Large particle deposition in front stages makes fouling dominant in front stages. However, small particles pass through the front stages and influence downstream compressor stages.
- Particle size distribution is an important parameter that influences the extent of fouling.

Neither Tarabrin *et al*. (1998) nor Song *et al*. (2003, 2004) consider how the blade surface retains particles. However, the mechanism by which the blade surface retains particles is important as if the contamination mechanism is due to inertial impact, then most contamination would be on the pressure side. If the blades or the particle are wet, then larger particles would stick, and they would cover the pressure side more or less uniformly. Otherwise, for dry particles, mostly small particles would stick and because they are more readily able to follow the flow streamlines they would mostly stick towards the trailing edge. The exception is particles entrained in the blade passage vortex, which could migrate to the blade suction side.

Surface shear stresses on a compressor blade's pressure side are high enough to prevent significant dust build-up. At relatively low build-up levels the shear stresses

and the particles' capability to adhere to the surface reach equilibrium and consequently, no further build-up occurs. The result in service is that the maximum fouling on the compressor blades' pressure surface occurs after relatively few operating hours. In contrast, gas turbine performance deterioration that we observed in service occurs over many hundreds of operating hours. If we accept that pressure side blade fouling stabilizes relatively quickly when compared to the time scales that occur with performance degradation, then we must also accept that compressor blade pressure side fouling is not the dominant mechanism responsible for gas turbine performance deterioration.

If we accept that compressor blade pressure side fouling does not explain the observed in service gas turbine performance deterioration, then compressor blade suction side fouling must be responsible. Particle size and flow velocity inversely affect the compressor blade suction side particle collection efficiency and consequently, the smaller the particle and the slower the airflow, the higher the deposition rate. Fuchs (1964) studied collection efficiency for the diffusion process. For a compressor blade of length L, Fuchs (1964) characterized collection efficiency as:

$$\lambda = 3\frac{\left(\frac{8hDR}{3\bar{U}}\right)^{2/3}}{2h^2} = 2.884\frac{\left(\frac{DR}{\bar{U}}\right)^{2/3}}{h^{4/3}} \tag{7}$$

with $\bar{U}$ the free stream flow velocity, D the diffusion coefficient, R the maximum blade thickness and h the blade to blade distance. The impact of wider spaced blades with larger blade-to-blade distance h and higher flow velocity U is lower collection efficiency. Collection efficiency also depends on the diffusion coefficient D. Turbulent eddies drive turbulent diffusion and is several orders of magnitude larger than laminar diffusion. As such, if the majority of diffusion is turbulent diffusion then the turbulence rate in the flow determines the diffusion rate.

Seddigh and Saravanamuttoo (1991) propose a relationship for the fouling index (FI):

$$FI = \frac{P_{GT}}{Wc_p\Delta T} \approx \frac{P_{GT}}{P_{compr}} \tag{8}$$

In so doing, they postulate that the higher the compressor efficiency, the higher the compressor's susceptibility to fouling.

Meher-Homji *et al*. (2009) studied 92 gas turbines in an effort to evaluate gas turbine sensitivity to an imposed level of fouling. The research indicated that a gas turbine's net work ratio (NWR) is a good predictor of both the gas turbine's susceptibility to foul and its sensitivity to fouling effects. Low NWR gas turbines, where the compressor consumes a higher portion of the total turbine work, tend to be both more susceptible and sensitive to axial compressor fouling (Meher-Homji *et al*., 2009). The reason for the higher susceptibility and sensitivity to fouling is that for a

given loss of compressor efficiency, the impact of compressor fouling on power output is larger for low NWR gas turbines:

$$\frac{W'_{out}}{W'_{out}} = \frac{W_t - W'_c}{W_t - W_c} = \frac{W_t - \frac{\eta'_c}{\eta_c} W_c}{W_t - W_c} = \frac{\frac{W_{out}}{NWR} - \frac{\eta_c}{\eta'_c} W_{out} \left(\frac{1}{NWR} - 1 \right)}{W_{out}} \tag{9}$$

Meher-Homji *et al*. (2009) concluded that NWR is a good predictor of both the gas turbine's susceptibility to foul and its sensitivity to the effects of fouling. This implies that a gas turbine's design parameters may impact the fouling rate and therefore the performance degradation rate in service. Figure 9.10 compares the degradation rate data for five gas turbines of different sizes and design. Neither gas turbine size nor type has a significant influence on the degradation rate. Consequently, it is not possible to generalize the importance of any individual gas turbine design parameters from the available data on degradation rate.

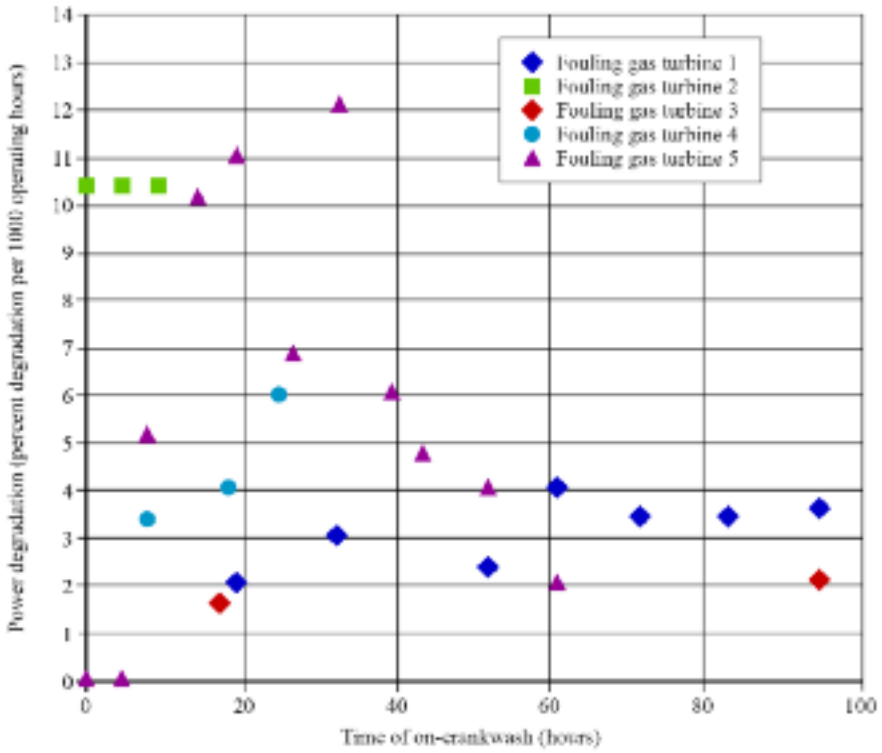

FIGURE 9.10. Fouling rates (power degradation) for different gas turbines. Gas turbines 2 (Haub and Hauhe, 1990), 3 (Veer *et al*., 2004) and 4 (Schneider *et al*., 2010) are all larger than gas turbines 1 and 5 (data by the authors). Gas turbines 1, 2, 4 and 5 are single-shaft. Gas turbine 3 is two-shaft.

SUMMARY

Taking a theoretical approach, complemented by the observation of fouled gas turbine compressor blades and the observed degradation rates of actual gas turbines due to fouling, some insight into the fouling process is possible. We emphasize that our conclusions only pertain to gas turbine fouling and not to gas turbine degradation due to erosion or corrosion. We do not cover mechanisms that drive both erosion and corrosion in this chapter. Considering a gas turbine compressor's sensitivity to fouling:

- Particle sizes of 10 μm and below cause fouling. Industrial gas turbine air filtration systems are effective for particle sizes of approximately 5 μm and above, but depending on the types of filter systems, allow ingestion of some smaller particles. In typical operating environments, a range of particle sizes are present, including sub-micron sized particles.
- The capability of particles to stay at a surface is dependent on both particle size and the wetness of the particle or surface. Larger particles will probably not stay attached to a surface unless the particle or the surface is wet.
- Particles that can only reach a surface through inertial impact will not reach the blade's suction surface except for the region next to the leading edge. Such particles will reach the pressure surface, as well as the compressor casing.
- Mechanisms that can bring particles to the blades' suction side occur with small and sub-micron particles.
- To influence the blade or wall casing boundary layer, the particles that stay on the surface must increase surface roughness.

When considering a gas turbine's susceptibility to fouling, we can make two additional observations:

- The quality of the air filtration system is the dominant driver of gas turbine compressor fouling. The air filtration system determines particle size, particle count and the presence of wet particles.
- High humidity ambient conditions are also a dominant driver of gas turbine compressor fouling as the presence of moisture increases the probability of particles sticking to a compressor blade or casing.

In this chapter we considered whether gas turbine design measurably affects the gas turbine's susceptibility and sensitivity to fouling. We evaluated the assumptions underpinning commonly used correlations for gas turbine fouling rates, concluding that it is not the gas turbine design, but the air filtration system design that has the greatest impact on performance deterioration due to fouling.

REFERENCES

Bammert, K., and Woelk, G.U. (1979), "The Influence of the Blading Surface Roughness on the Aerodynamic Behavior and Characteristic of an Axial Compressor", *Proceedings of the 24th American Society of Mechanical Engineers Gas Turbine and Aeroengine Congress,* San Diego, USA, 11–15 March, Paper No. 79-GT-102.

Beacher, B., Tabakov, W., and Hamid, A. (1982), "Improved Particle Trajectory Calculations through Turbomachinery Affected by Ash Particles", *Transactions of the ASME, Journal of Engineering for Power*, vol. 104, pp. 64–8.

Boelcs, A., and Suter, P. (1986), *Transsonische Turbomaschinen*, G. Braun, Karlsruhe, Germany.

Brekke, O., and Bakken, L.E. (2010), "Performance Deterioration of Intake Air Filters for Gas Turbines in Offshore Installations", *Proceedings of the 55th American Society of Mechanical Engineers Turbine and Aeroengine Congress*, Glasgow, UK, 14–18 June, Paper No. GT2010-22454.

Deutsch, S., and Zierke, W.C. (1986), "The Measurement of Boundary Layers on a Compressor Blade in Cascade at High Positive Incidence Angle", NASA Report CR-179491.

Elrod, C.E., and Bettner, J.L. (1983), "Experimental Verification of an End-wall Boundary Layer Prediction Method", Report No. AGRAD CP-351.

Fottner, L. (1989), "Review of Turbomachinery Blading Design Problems", Report No. AGARD-LS-167.

Fuchs, N.A. (1964), *The Mechanics of Aerosols,* Pergamon, Oxford, UK.

Haub, G.L., and Hauhe, W.E. (1990), "Field Evaluation of On-Line Compressor Cleaning in Heavy Duty Industrial Gas Turbines", *Proceedings of the 35th American Society of Mechanical Engineers Gas Turbine and Aeroengine Congress,* Brussels, Belgium, 11–14 June, Paper No. 90-GT-107.

Jacobs, G.B., Don, W.S., and Dittmann, T. (2012), "High-Order Resolution Eulerian-Lagrangian Simulations of Particle Dispersion in the Accelerated Flow Behind a Moving Shock", *Theoretical Computational Fluid Dynamics*, vol. 25, pp. 37–50.

Kurz, R. (1991), "Experimentelle und theoretische Untersuchungen an gleichfoermig und ungleichfoermig geteilten Turbinengittern", Dissertation, UBwH, Hamburg, Germany.

Kurz, R., and Brun, K. (2009), "Degradation Effects on Industrial Gas Turbines", *Transactions of the ASME, Journal of Engineering for Gas Turbines and Power*, vol. 131, pp. 1–7.

Lefebvre, M., and Arts, T. (1997), "Numerical Aero-Thermal Prediction of Laminar/Turbulent Flows in a Two-Dimensional High Pressure Turbine Linear Cascade", *Proceedings of the 2nd European Conference on Turbomachinery, Fluid Dynamics & Thermodynamics,* Antwerpen, Belguim, 5–7 March, pp. 401–10.

Levine, P. (1998), "Axial Compressor Performance Maintenance Guide", EPRI, Palo Alto, USA, Report No. TR-111038.

Meher-Homji, C.B., Chaker, M., and Bromley, A.F. (2009), "The Fouling of Axial Flow Compressors — Causes, Effects, Susceptibility and Sensitivity", *Proceedings of the 54th American Society of Mechanical Engineers Gas Turbine and Aeroengine Congress,* Orlando, USA, 8–12 June, Paper No. GT2009-59239.

Milsch, R. (1971), "Systematische Untersuchung ueber den Einfluss derRauhigkeit von Verdichterschaufeln auf den Gitterwirkungsgrad", Dissertation, Technische Hochschule Hannover, Germany.

Morini, M., Pinelli, M., Spina, P.R., and Venturini, M. (2010), "CFD Simulation of Fouling on Axial Compressor Stages", *Transactions of the ASME, Journal of Engineering for Gas Turbines and Power*, vol. 132, pp. 1–10.

Morini, M., Pinelli, M., Spina, P.R., and Venturini, M. (2011), "Numerical Analysis of the Effects of Non-uniform Surface Roughness on Compressor Stage Performance", *Transactions of the ASME, Journal of Engineering for Gas Turbines and Power*, vol. 133, pp. 1–8.

Parker, G.J., and Lee, P. (1972), "Studies of the Deposition of Sub Micron particles on Turbine Blades", *Proceedings of the Institute of Mechanical Engineers,* Series Article v186, pp. 519–26.

Poon, W., Gessner, M., and MacDonald, R. (2010), "Eliminating Turbine Compressor Fouling With HEPA Membrane Composite Air Intake Filters", *Proceedings of the 39th Turbomachinery Symposium,* Houston, USA, 4–7 October.

Prandtl, L., Oswatitsch, K., and Wieghard, K. (1990), *Fuehrer durch die Stroemungslehre*, 9th edn, Vieweg, Braunschweig, Germany.

Schneider, E., Demircioglu, S., Franco, S., and Therkorn, D. (2010), "Analysis of Compressor On-Line Washing to Optimize Gas Turbine Power Plant Performance", *Transactions of the ASME, Journal of Engineering for Gas Turbines and Power*, vol. 132, pp. 1–7.

Schroth, T., Rothmann, A., and Schmitt, D. (2007), "Nutzwert eines dreistufigen Luftfiltersystems mit innovativer Technoloie fuer stationaere Gasturbinen", *VGB Powertech*, vol. 87, pp. 48–51.

Seddigh, F., and Saravanamuttoo, H.I.H. (1991), "A Proposed Method for Assessing the Susceptibility of Axial Compressors to Fouling", *Transactions of the ASME, Journal of Engineering for Gas Turbines and Power*, vol. 113, pp. 595–601.

Siegel, J.A. (2002), "Particulate Fouling of HVAC Heat Exchangers", Ph.D. Thesis, University of California Berkeley, Berkeley, USA.

Song, T.W., Sohn, J.L., Kim, T.S., Kim, J.H., and Ro, S.T. (2003), "An Improved Analytic Model to Predict Fouling Phenomena in the Axial Flow Compressor of Gas Turbine Engines", *Proceedings of the International Gas Turbine Congress*, Tokyo, Japan, 2–7 November, Paper No. TS-095.

Song, T.W., Sohn, J.L., Kim, T.S., Kim, J.H., and Ro, S.T. (2004), "An Analytical Approach to Predicting Particle Deposit by Fouling in the Axial Compressor of the Industrial Gas Turbine", *Proceedings of the Institute of Mechanical Engineers*, Part A, vol. 219, p. A06304.

Sreedharan, S.S., and Tafti, D.K. (2010), "Composition Dependent Model for the Prediction of Syngas Ash Deposition with Application to a Leading Edge Turbine Vane", *Proceedings of the 55th American Society of Mechanical Engineers Turbine and Aeroengine Congress*, Glasgow, UK, 14–18 June, Paper No. GT2010-23655.

Syverud, E., Brakke, O., and Bakken, L.E. (2007), "Axial Compressor Deterioration Caused by Saltwater Ingestion", *Transactions of the ASME, Journal of Turbomachinery,* vol. 129, pp. 119–27.

Tabakoff, W., Hamed, A., and Metwally, M. (1991), "Effect of Particle Size Distribution on Particle Dynamics and Blade Erosion in Axial Flow Turbines", *Transactions of the ASME, Journal of Engineering for Gas Turbines and Power*, vol. 113, pp. 607–15.

Tarabrin, A.P., Schurovsky, V.A., Bodrov, A.I., and Stalder, J.-P. (1998), "An Analysis of Axial Compressor Fouling and a Blade Cleaning Method", *Transactions of the ASME, Journal of Turbomachinery*, vol. 120, pp. 256–61.

Veer, T., Haglerod, K.K., and Bolland, O. (2004), "Measured Data Correction for Improved Fouling and Degradation Analysis of Offshore Gas Turbines", *Proceedings of the 49th American Society of Mechanical Engineers Gas Turbine and Aeroengine Congress*, Vienna, Austria, 14–17 June, Paper No. GT2004-53760.

Vigueras Zuniga, M.O. (2007), "Analysis of Gas turbine Compressor Fouling and Washing on Line", Ph.D. Thesis, Cranfield University, UK.

Wilcox, M., Baldwin, R., Garcia-Hernandez, A., and Brun, K. (2010), *Guideline for Gas Turbine Inlet Air Filtration Systems,* Gas Machinery Research Council, Dallas, USA.

Chapter 10

Solid Particle Surface Impact Behavior in Turbomachines to Assess Blade Erosion

K. Brun, M. Nored and R. Kurz

ABSTRACT

Solid particle admission is one of the principal damage mechanisms responsible for gas turbine and centrifugal compressor in-service failure. Consequently, there is interest within the turbomachinery community to better predict and improve the durability of machines that operate in environments where one cannot avoid ingestion of sand, dust and dirt. This chapter describes the development of a mixed computational fluid dynamics and empirical software tool that utilizes a probabilistic analysis of the kinematic and impact behavior of solid particulates in the near-field of turbomachinery blade and impeller surfaces. Researchers have successfully employed the method to predict the surface wear characteristics and fouling rates in ground-based gas turbines and centrifugal compressor applications. The tool employs a commercially available computational fluid dynamics solver to calculate the gas turbine or centrifugal compressor steady-state flow field. It then uses the output to determine the non-dimensional coefficients in a set of empirical functions. One can then use the empirical functions to predict statistically the impact probability of a given weight, size and distribution of solid particles on a specified rotating or stationary surface. The tools' output provides design engineers with a basis to optimize inlet air filter selection and gas turbine or centrifugal compressor maintenance practice.

This chapter is a revised and extended version of Brun, K., Nored, M., and Kurz, R. (2012), "Analysis of Solid Particle Surface Impact Behavior in Turbomachines to Assess Blade Erosion and Fouling", *Proceedings of the 41st Turbomachinery Symposium,* Houston, USA, 24–27 September.

NOMENCLATURE

A, B, C, D, E, F	velocity vector impact coefficients
L	characteristic length in Stokes number
R	mean radius of particle
St	Stokes number
U	absolute velocity in Stokes number
V	velocity vector
m	particle mass
r	radius of curvature of streamline
t	time
v	velocity component
Γ	non-dimensional coefficient for particle behavior (turbulent)
γ	non-dimensional coefficient for particle behavior (laminar)
μ	viscosity
ρ	density
τ	particle stopping time in Stokes number

Subscripts

C	centrifugal
f	flow
I	inertial mass acceleration
O	Coriolis
p	particle
t	tangential

INTRODUCTION

Gas turbine and centrifugal compressors must regularly operate in hostile environments where significant amounts of sand, gravel or biological matter are ingested. The result is blade erosion which occurs when particles come in contact with rotating and stationary surfaces. There is ongoing interest within the oil, gas and power generation industries in better predicting gas turbine and centrifugal compressor erosion rates, and their durability and performance degradation in hostile environments.

Gas turbine and centrifugal compressor degradation rates and ultimately failure mechanisms are a function of the ingested particle size. The kinetic energy of particles smaller than 10 μm is too low to result in blade erosion (Kurz and Brun, 2009). However, they can cause fouling if they stick to blade surfaces. Particles larger than 10 μm are less prone to sticking to a surface, but do have sufficient kinetic energy to cause erosion.

Centrifugal compressors in the natural gas compression system application may ingest various sized solid and liquid particles. When operating near upstream wellheads in oil and gas applications, centrifugal compressors frequently ingest sand and

other solid matter from the gas production site. Sand travels from the gas well, through the pipe and into the compressor. Filtration in these applications is difficult, and consequently, the compressors can be subject to significant blade erosion.

Jeske and Sandstede (1985) investigated the impact of erosive particles in fluid catalytic cracking process expanders. Despite the use of multiple stages of dust separation, there are still significant amounts of catalyst particles in the hot gas stream that can cause erosion in the hot gas expander. Jeske and Sandstede (1985) found a relationship between particle size, blade speed and expected blade life. They found main erosion damage at the leading and trailing edges near the blade tip. They also considered the effectiveness of anti-erosion features, concluding that although some anti-erosion features provide some benefit, they do not eliminate erosion in erosive regimes.

For industrial gas turbines, inlet air filtration systems can control larger particles (Wilcox *et al*., 2011). However, low-grade liquid fuels or syngas may cause ash formation as part of the combustion process. Despite advances in gas cleanup procedures, syngas produced from coal gasification contains traces of fly-ash particles with diameters ranging from 1 μm to 10 μm that can result in erosion downstream of the combustor.

It is not possible to fit aircraft gas turbines with the large, heavy air filtration systems which industrial gas turbines utilize. Researchers within the aerospace industry have studied the erosive effects of sand and ash ingestion into aircraft gas turbines. However, they have conducted relatively little research into the effects of erosive particles on ground-based gas turbines. In most ground-based gas turbine applications design engineers can utilize air filtration systems to eliminate larger particles to avoid blade erosion. Even the best air filtration systems are not able to eliminate the smaller particles and consequently, fouling remains an issue for ground-based gas turbines.

In recent years there has been renewed interest in the prediction of solid particle behavior in an on-going effort to provide design engineers with the necessary tools to select air inlet filter material and size appropriate to the application. Selecting air inlet filter material and size requires an understanding of the effects of particle size, type and weight on both erosion and fouling of gas turbine and centrifugal compressor blades, rotating and stationary surfaces. Additionally, when using low-grade fuels or coal-derived syngas in a gas turbine, ash particles created in the combustor can result in fouling and erosion of turbine blades, rotating and stationary surfaces (Lawson and Thole, 2010).

In the gas turbine's compressor, damage that occurs as a consequence of particle ingestion primarily occurs with fouling due to solid matter build-up on the blades and the erosive removal of metal from the blades' leading and trailing edges (Figure 10.1). The net consequence of the above is a reduction of compressor pressure ratio and gas turbine efficiency. Cleaning the blades can reverse some of the effects of fouling; however, losses that occur with erosion are typically irrecoverable.

In the combustor, the local flame temperature can reach 2500°C. At this temperature sand will become a liquid silica oxide that will deposit on the combustor injector and liner walls. These deposits can lead to plugging of cooling holes on the combustor liner. Plugging of cooling holes leads to premature combustor liner metal failure.

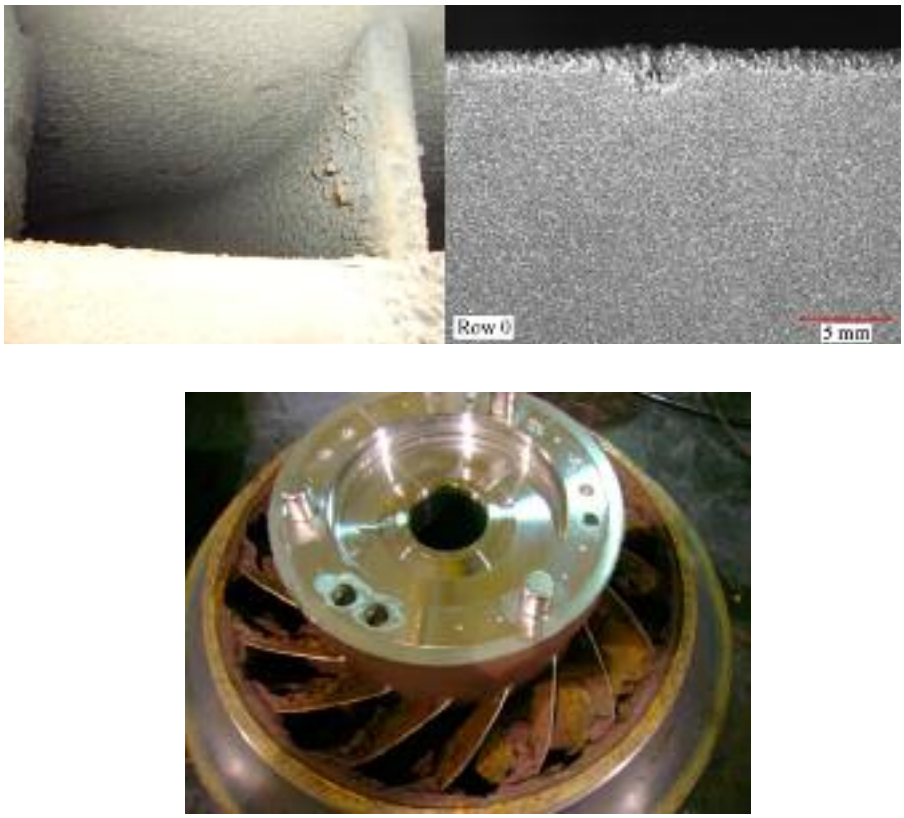

FIGURE 10.1. Result of particle admission: (top left) fouled compressor inlet guide vanes, (top right) first stage compressor blade leading edge erosion and (bottom) heavily fouled centrifugal compressor impeller.

Downstream of the combustor in the gas turbine's high-pressure turbine, sand and dirt particles result in two issues. First, solid particles can plug film cooling holes and slots and prevent the blade's secondary air system from cooling the blade. Second, hot sand exhausting the combustor and entering the high-pressure turbine nozzle guide vanes can result in silica deposits on the vanes. The sand particles' high temperature results in the silica melting. This liquid silica forms a solid layer on the vanes' surfaces. This layer decreases heat transfer from the vane to the film-cooling air and therefore results in an increase in vane temperature.

A final issue for gas turbines is the cooling air that one bleeds at compressor discharge and uses in a secondary air system to cool turbine vanes and blades. Particles that travel through the secondary air system deposit within either the secondary air system itself or vane and blade cooling passages. The result will be a reduction in cooling air flow, and correspondingly higher vane and blade metal temperatures.

We may conceptualize the phenomenon of particulate ingestion damage in terms of an analysis of solid particle kinematic behavior in a high-velocity rotating

fluid. A solid particle of a given density and size that the compressor or turbine flow carries would follow the flow streamlines if it had no mass and, therefore, would never impact blades, rotating or stationary surfaces. However, the particles do have mass and consequently, centrifugal and Coriolis forces on the particle act on them resulting in particles deviating from the flow streamlines. As particles deviate from the flow streamlines they are able to impact on blades, rotating or stationary surfaces. The larger the particle, the greater the particle mass, the greater the effect of centrifugal and Coriolis forces on the particle and, therefore, the greater the particles' deviation from flow streamlines.

We may characterize the suspended particles' behavior in a fluid flow using the Stokes number (Fuchs, 1964). We define the Stokes number (*St*) as the ratio of a particle's stopping distance to a characteristic dimension of the obstacle:

$$St = \frac{\rho_p d_p^2 U}{18\mu \cdot 2L} \tag{1}$$

with L as the characteristic dimension that within a turomachinery context would typically be blade chord, blade pitch or impeller diameter. A fluid with a high viscosity μ will lower the Stokes number, while large particle density ρ_p, particle diameter d_p or high flow velocities will increase the Stokes number. If we define L as blade chord length, L/U becomes the time a particle requires to pass through the blade row (Dring *et al*., 1979).

Corsini *et al.* (2012) have studied the probability of particles impacting on blades, rotating and stationary surfaces in axial flow fans and Corsini *et al.* (2013) studied this in centrifugal fans using a particle cloud tracking model. Corsini *et al.* (forthcoming) were able to use the probability of particles impacting to predict erosion rate, the performance of eroded blades and consequently, blade life in an erosive environment.

For a given gas path geometry, we can evaluate the probable particle impact regions, forces and likely surface damage through a consideration of the forces that affect particle motion in a moving fluid (Figure 10.2). This chapter describes a set of application tools that model the forces that affect particle motion, based on a computational fluid dynamics and a semi-empirical particle transport model to predict gas path particle erosion and fouling. We verified the model using data which we gathered during a high-speed centrifugal compressor sand test with laser particle image velocimetry. We used the tool to predict the characteristic behavior and particles' impact forces in an axial air compressor for a refinery compression application.

One can apply this set of application tools to centrifugal compressors, ground based or aircraft gas turbine compressors that are subjected to solid particle ingestion. The tool predicts:

1. The size and density of particles primarily responsible for damage, erosion and degradation in the turbomachine. Using the results, one can optimize filter size and design.

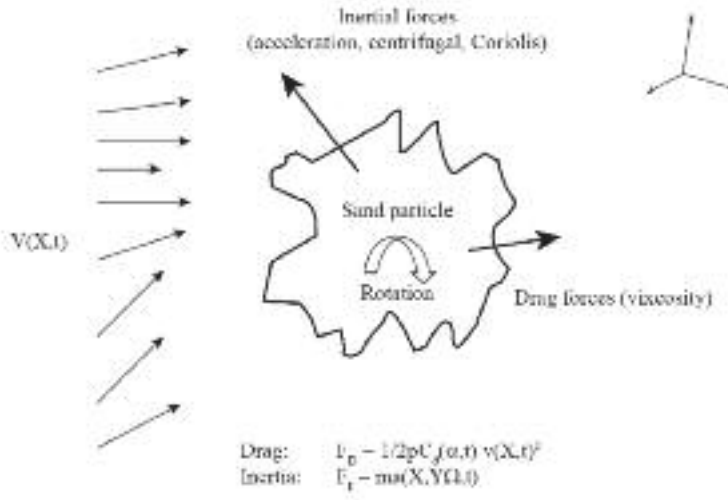

FIGURE 10.2. Forces acting on a particle transported by a fluid in motion: drag and inertia.

2. The local impact force of sand particles on the turbomachine's blades, vanes, rotating and static surfaces. Using these results, one can predict coating life, metal abrasion and wear to optimize the turbomachine's maintenance schedule.
3. The most likely areas within the gas path for fouling and cooling flow interruptions. Using these results, a maintenance team can focus on high-risk areas for closer and more frequent inspection.

Using the above results in combination, one can develop a strategy to "harden" a centrifugal or gas turbine compressor's gas path locally against the effects of sand ingestion and develop better maintenance techniques. Local strengthening or surface coating becomes possible in those areas with the highest probability of particle impact. Additionally, analysis results show that only specific size and weight particles ingested into the gas path are responsible for the majority of damage. Knowing particle size and weight can assist design engineers when optimizing air inlet filter specification to target these particles.

In this chapter we report research aimed at developing a software tool to analyze the sand and other particulates' kinematic behavior inside industrial, aircraft and centrifugal compressors. Using the tool's output, we realized improved inlet air filtering techniques, gas turbine maintenance and component designs. In parallel with the tool's development, we injected particles into a full-scale high-speed centrifugal compressor to verify, optimize and fine-tune the tool's particle transport model. The result is a generally applicable tool to predict the motion and impact probability of sand and other solid particles on a turbomachine's internal gas path structures.

PROBLEM STATEMENT

Particle ingestion damages turbomachinery gas path components. We may conceptualize the particle's behavior in terms of particle-flow transport in a non-uniform fluid. A solid particle of a given density and size carried by the flow would follow the flow streamline if it had no mass, and therefore would not impact blade, rotating or stationary surfaces. As the particles do have mass, centrifugal and Coriolis forces result in particles deviating from the flow streamlines and consequently, impact on blades, rotating or stationary surfaces. For a given gas path geometry, we can calculate the blade-to-blade flow field and also the resultant force imbalance on particles within the flow field (Figure 10.3). We can use particle lag transport theory and computational fluid dynamics to identify the probable particle impact regions and resultant erosive surface damage.

The flow field through turbomachinery blading is non-uniform as a consequence of secondary flow features. Particle transport calculation within a non-uniform flow using computational fluid dynamics is computationally intensive. Maxey (1983) characterized a single sphere's motion within an incompressible flow:

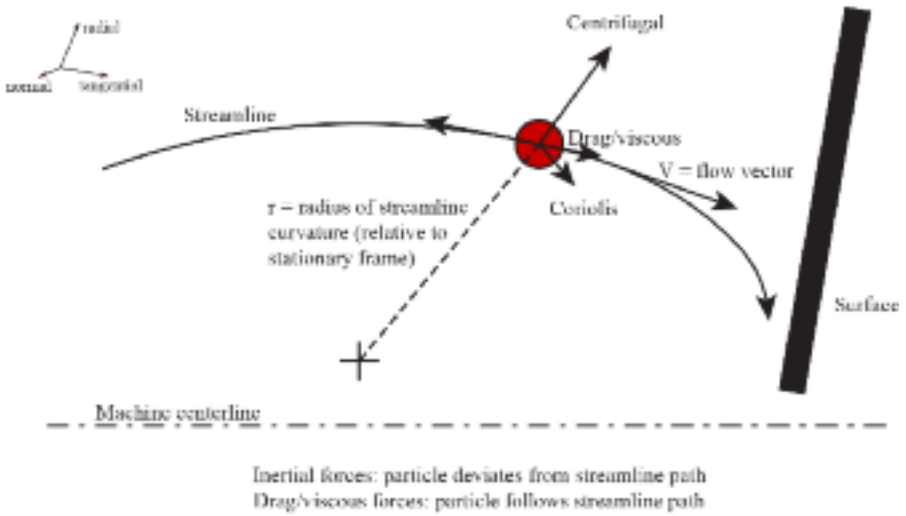

FIGURE 10.3. Particles deviating from streamlines and impacting on surfaces in the blade path.

$$m_\rho \frac{dV_i}{dt} = (m_\rho - m_F) g_i = m_F \frac{Du_i}{Dt}\Big|_{Y(t)} - \frac{1}{2} m_F \frac{d}{dt}\left\{ V_i(t) - u_i[Y(t),t] - \frac{1}{10} a^2 \nabla^2 u_i \Big|_{Y(t)} \right\} \quad (2)$$

$$-6\pi a\mu \left\{ V_i(t) - u_i[Y(t),t] - \frac{1}{6} a^2 \nabla^2 u_i \Big|_{r(t)} \right\}$$

$$-6\pi a^2 \mu \int_0^t dr \left(\frac{d/d\tau \left\{ V_i(\Gamma) - u_i[Y(t),t] - \frac{1}{6} a^2 \nabla^2 u_i \Big|_{Y(\Gamma)} \right\}}{[\pi \nu (t-\tau)]^{1/2}} \right)$$

Solving the equation requires a conjugate computational fluid dynamics and particle transport analysis that is both complex and computationally demanding. Corsini *et al.* (2012) considered the practical difficulties that occur with predicting the individual particles' trajectories and concluded that a cloud tracking approach was more practical. Therefore, when considering particle tracking we may summarize the current state-of-the-art as:

1. One can obtain numerical solutions to the Navier-Stokes equations with reasonable accuracy using commercially available computational fluid dynamic codes.
2. These codes predict the fluid flow field only; they are not capable of solving transient particle transport kinematics problems.
3. Some commercial computational fluid dynamic codes offer particle transport modules or "tracer" visualization techniques, but these are essentially a form of flow streamline visualization. They do not predict how a particle would behave and are only valid for very low Stokes number particles at low seeding densities.
4. Recently, researchers have attempted to develop transient computational fluid dynamics models to predict particle behavior. These models are computationally intensive and researchers have not fully validated them. They do not account for particle interaction or particles bouncing from surfaces. They can only model a single rotating stage.

The current state-of-the-art in particle tracking requires the design engineer to use less rigorous, but more computationally efficient methods to determine probable particle impact locations. These methods should avoid unsteady analysis, relying instead on steady computational fluid dynamics with an associated model to predict particle trajectory. In the program of work in this chapter, we developed a model to predict particle trajectory for the solid particles that enter centrifugal, industrial and aircraft gas turbine compressors.

SOLUTION APPROACH

The purpose of the reported research in this chapter was to model:

1. various size and specific gravity solid particles that can enter the gas path depending on the application;
2. the turbomachinery fluid flow which is non-uniform and unsteady; and
3. Coriolis and centrifugal forces on particles, to enable particle deviation from the predicted flow streamlines.

The proposed approach to the modeling was:

1. to use commercially available computational fluid dynamic codes to determine the steady-state flow field in a single rotating stage without the influence of solid particles in the flow;
2. to refine the mesh only near critical blade, rotating and stationary gas path surfaces; and
3. to utilize the resultant flow field prediction to determine the probability of particles impacting blade, rotating and stationary gas path surfaces using non-dimensional coefficients which we derived from the ratio of inertial to drag forces on the particles.

We based the proposed approach on an assumption that the particles of concern are larger than the Kolmogorov length scale, the smallest scale in turbulent flow, and interact with fluid primarily through Stokes viscous drag. Consequently, we propose that:

1. the relevant inertial forces are centrifugal and Coriolis;
2. the surface near-field aerodynamics dominates the behavior of those solid particles which impact blade, rotating and static surfaces;
3. particle distribution is homogenous in both space and time and Gaussian in size; and
4. a steady-state computational fluid dynamics model and stage-by-stage approach is adequate to determine particle impact locations.

To develop a model to predict particle trajectory for the solid particles that enter centrifugal, industrial and aircraft gas turbine compressors, we concluded that it was necessary to determine the steady-state turbomachinery flow field and then utilize non-dimensional physical parameters related to solid particle lag to predict impact locations using a probabilistic analysis. Development of the model required a particle transport kinematics analysis and experimental verification. The particle transport kinematics analysis required:

1. derivation of transient particle transport equations and their numerical modeling;
2. implementation of the transport equations in a numerical model and the development of a computational fluid dynamics code interface;
3. development of a semi-empirical model to predict particle behavior;
4. benchmarking of the developed numerical model against a simplified geometry;
5. numerical model calibration against experimental test data; and
6. application of the numerical model to a centrifugal compressor's first stage.

The experimental verification required:

1. particulate flow behavior testing in a wind tunnel's non-rotating flow using particle image velocimetry;
2. particulate flow behavior benchmark testing in a centrifugal compressor's rotating flow; and
3. the numerical model's computational fluid dynamic validation using experimental results.

We undertook verification in an experimental facility which was able to measure particle trajectory using particle image velocimetry. The use of an abrasive paint complemented the particle image velocimetry measurements, and in so doing enabled us to determine particle impact density. We undertook particle transport kinematics analysis using the commercial computational fluid dynamics package CFDesign.

LITERATURE REVIEW

Researchers have evaluated erosion effects on submerged pumps (Hadiiyannis *et al*., 2009), but there is little literature reporting the effect of either erosion or fouling on centrifugal compressor performance. An exception is Haq *et al*.'s (1998) publication on process gas compressor fouling. Known erosion issues affecting centrifugal compressors include severe cases of almost complete impeller vane removal. In many applications, one does not plan or anticipate solid particle ingestion. One often only detects erosion effects by monitoring the compressor's performance degradation, or by observing the onset of vibration issues.

Solid particles may enter a gas turbine through the compressor as airborne ash, sand, dust or ice. The gas turbine combustor can also produce solid and molten particles when burning heavy oil or synthetic fuels. The path particles take through a compressor, and the effects of particle impact or deposition, are dependent on particle type, size and distribution. Previous research has centered on modeling, design mitigation and prediction of four degradation effects:

1. compressor and turbine blade erosion;
2. deposition in the combustor and turbine leading to corrosion;
3. impingement and deposition on gas turbine blades leading to blockage of cooling passages; and
4. reduction of compressor efficiency and surge margin as a consequence of an increase in blade tip-to-casing clearance.

Hamed *et al*. (2006) developed surface coatings intended to reduce erosion in erosive environments and reviewed coating technology development from its inception in the 1960s. Tabakoff *et al*. (1974) studied erosion in a wind tunnel with the objective of determining coating erosion rates and thermal barrier coating life reduction due to particle impact. Tabakoff *et al*. (1974) performed tests over a range of temperatures from 871°C to 1093°C. They undertook these elevated temperature tests to identify the increase in erosion rate with increasing temperature.

Grant and Tabakoff (1975) studied the erosive process and observed that sand particles blunted the compressor blades' leading edges. This reduced blade chord and increased surface roughness. Grant and Tabakoff's experimental work (1975) indicated that the higher the velocity of particles, the higher the erosion rate. At lower particle velocities the erosion rate became a weaker velocity function.

Richardson *et al*. (1979) observed that high-pressure compressor blade erosion occurs primarily over the outer 50 percent of blade span. Towards the blade tip both blade chord and blade thickness reduction became aerodynamically significant. Richardson *et al*. (1979) also concluded that there was a limit on erosion-induced surface roughness, after which continued particle impact and mass removal from the blade no longer resulted in increased surface roughness.

More recently, those scholars studying erosion have focused on the importance of the interaction between particles when they rebound from a blade, stationary or rotating surface. When particles rebound from a surface their trajectory relative to other surfaces can be high, and consequently particles that rebound from one surface can have a highly erosive effect on the next surface that they impact. Tabakoff and Sugiyama's (1980) laser Doppler velocimetry measures on fly-ash particles demonstrated that impact angle is the primary factor affecting a particle's restitution ratio. Restitution ratio is the ratio of the particle's velocity after an impact divided by its velocity before an impact. A lower restitution ratio signifies a greater reduction in velocity due to the impact.

Cowan *et al*. (2010) studied sand particle ingestion using a fan array test facility. They also conducted numerical simulations that demonstrated that erosion rates were a function of a particle's Stokes number. A smaller Stokes number for a particle resulted in the highest deposition rate and least number of surface impacts, possibly as a consequence of a faster time to deposit and less resulting rebound impacts.

Deposits in a gas turbine's combustor and turbine occur as a consequence of particles that enter the combustor through the fuel system. The particles may be either solid or liquid, with liquid particles vaporizing in the combustor and then condensing on cooler surfaces in the turbine's latter stages. Diffusion may transport ex-

tremely small solid particles that also tend to collect on a cooler surface (Hamed *et al*., 2006). Larger solid particles collect in specific locations through the combustor and turbine as a consequence of inertial impact.

Dunn *et al*. (1996) studied the effect of volcanic ash on gas turbines and described the "St Elmo's glow" that appears around a gas turbine inlet as a consequence of ash particles. The ash particles strike the gas turbine fan's tip region that heats and then glows. This produces the characteristic ring of light. The ash particles pass through the gas turbine compressor and into the turbine. Dunn *et al*. (1996) reported that the particles must reach in excess of 1100°C if they are to deposit in either the combustor or turbine. Today's gas turbines operate at combustion and turbine entry temperatures above 1100°C, with the result that both combustor and turbine components suffer both deposition and erosion when they ingest volcanic ash.

Haase and Bons (2010) studied turbine film cooling-hole blockage as a consequence of impurities within synthetic fuel. Flow visualization techniques enabled Haase and Bons (2010) to identify that large impurity deposits in the front rows of film cooling-holes impeded cavity and coolant airflow. Walsh *et al*. (2006) studied film cooling-hole blockage that occurs as a consequence of sand ingestion over a range of sand particle sizes. Walsh *et al*. (2006) concluded that increased coolant velocity and pressure ratio across the cooling-holes aided the passage of particles through the holes. However, the most significant factor affecting particle deposition was metal temperature. Sand melts above 1000°C, resulting in rapid cooling-hole blockage.

Combustor and turbine inlet temperatures are well above 1000°C in the current generation of gas turbines, and consequently sand ingestion routinely results in cooling-hole blockage. In an attempt to reduce cooling-hole blockage, Land *et al*. (2010) studied double-walled cooling geometries with both impingement and film cooling. Land *et al*. (2010) suspected that impingement cooling could result in the break-up of larger particles that could then more easily pass through film cooling-holes. This minimized film cooling-hole blockage. Land *et al*. (2010) concluded that a staggered film cooling arrangement in combination with impingement cooling did aid in breaking down larger particles and in so doing minimized film cooling-hole blockage.

When studying ground-based gas turbines in desert locations, Musgrove *et al*. (2009) evaluated the effectiveness of a novel sand filter which incorporated multiple arrays of louvers. Musgrove *et al*. (2009) optimized the filter design. They used the louvers to generate a vortex that centrifuged sand away from the gas turbine inlet. This minimized sand ingestion.

Cardwell *et al*. (2009) studied particle motion within the internal ribbed passages that form the cooling passages within combustor liners, turbine vanes and blades. Cardwell *et al*. (2009) observed "particle bouncing" in the cooling passages and noted that larger particles were more prone to bouncing than smaller particles. Cardwell *et al*. (2009) concluded that particle bouncing was independent of rib spacing, with the phenomenon occurring with three conditions:

1. a particle must impact an upstream rib face at a relatively high velocity;
2. a particle must have a sufficiently high Stokes number if it is to follow a ballistic path across the passage; and

3. a particle must impact another rib face at a high enough velocity for the process to repeat.

Dunn *et al*. (1996) reported that erosion could increase blade tip-to-casing clearance by three times the initial build clearance. This effectively eliminated compressor surge margin. Schmuecker and Schaffler (1994) reported that erosion leading to a 1 percent increase in compressor blade tip-to-casing clearance resulted in a 7.5 percent reduction in surge margin and a 2 percent loss in efficiency.

Ghenaiet *et al*. (2005) studied the effect of sand ingestion on compressor performance and utilized Lagrangian methods to track sand particles up to 1000 μm diameter. Ghenaiet *et al*. (2005) concluded that blade chord reduction that occurred as a consequence of erosion resulted in a significantly greater loss of compressor performance than erosion-induced increases in blade tip-to-casing clearance. Ghenaiet *et al*. (2005) defined a 10 percent reduction in compressor efficiency as 100 percent of the gas turbine's service life. They concluded that the time taken to reduce compressor efficiency by 10 percent decreased exponentially with linearly increasing sand concentration. When sand concentration increased beyond 100 mg/m^3, gas turbine life fell to only 100 hours.

Predicting fouling and erosion rates requires both an understanding of the involved physical mechanisms and a method of predicting the particles' trajectories. Reliable particle trajectory prediction provides a design engineer with data on where particles will impact blade, stationary and rotating surfaces. Hussein and Tabakoff (1973) developed the first particle trajectory simulation using experimentally obtained restitution ratios to simulate particle trajectory. Hussein and Tabakoff's (1973) work illustrated that blade surface impacts increase with increasing particle diameter and increased velocities at the compressor inlet. Following Hussein and Tabakoff's pioneering work (1973), other researchers have incorporated three-dimensional flow effects and viscous forces into particle Eulerian-Lagrangian models.

Predicting the motion of particles in a fluid

The equations that govern the three-dimensional, transient fluid flow in a blade's rotating frame of reference are the Navier-Stokes equations. The Navier-Stokes equations are named after Claude-Louis Navier and George Gabriel Stokes and describe the motion of substances that can flow. These equations arise from applying Newton's second law to fluid motion, together with the assumption that the fluid stress is the sum of a diffusing viscous term (proportional to the velocity's gradient), plus a pressure term. Like all Newtonian conservation-based equations, they consist of mass continuity, force balance and energy balance equations. They comprise a set of higher order, coupled, non-linear and non-homogenous partial differential equations for which scholars can only obtain a closed form analytical solution for a limited set of basic problems.

We may derive numerical solutions to the Navier-Stokes equations with reasonable accuracy using commercially available computational fluid dynamics codes.

However, as these codes are intended to predict the fluid flow field only, they are generally not capable of solving transient particle transport kinematics problems. Some computational fluid dynamic codes offer simple single particle transport modules or "tracer" visualization techniques. However, these are essentially flow streamline visualizations and do not predict how a particle would behave.

To analyze particle movements within an unsteady fluid flow, it is first necessary to determine the transient flow field using a computational fluid dynamics code. It is then necessary to apply time-dependent particle transport equations to model individual particle kinematics within the three-dimensional flow field. One must perform the analysis in a three-dimensional flow field with small time-steps if one is to accurately characterize the flow field. Consequently, the analysis is computationally intensive. To compound matters, there is little experimental data available in the public domain against which researchers may compare analytical predictions.

Proposed analysis approach

For the research in this chapter, we utilized a commercially available computational fluid dynamics code in combination with a semi-empirical approach to determine particle behavior. We based our approach on a commercially available computational fluid dynamics code that we utilized to predict the steady-state flow field. We then used the steady-state flow field as input to a semi-empirical model to determine particle impact locations and velocities. Our approach was to determine particle motion using a simple model that balances the inertial forces acceleration, centrifugal plus Coriolis against drag forces on the particle:

$$m\frac{d\overline{V}}{dt} + F_{Centrifugal} + F_{Coriolis} = \overline{F}_{Drag} \tag{3}$$

We augmented the above equation with experimentally derived velocity vector impact coefficients. The resultant analytical technique predicts particle motion around a stationary airfoil with reasonable accuracy. A Buckingham-Pi analysis enabled us to derive the non-dimensional parameters that governed particle behavior in unsteady flow (Table 10.1).

Table 10.1. *Non-dimensional parameters governing the particle behavior in unsteady flow.*

	Acceleration	Centrifugal	Coriolis
Inertial viscous	$\gamma_1 = \frac{R^2\rho_p\dot{V}_p}{\mu_f\Delta V}$	$\gamma_C = \frac{R^2\rho_p V_i^2}{\mu_f r\Delta V}$	$\gamma_O = \frac{R^2\rho_p V_r V_i}{\mu_f r\Delta V}$
Inertial drag	$\Gamma_1 = \frac{R\rho_p\dot{V}_p}{\rho_f\Delta V^2}$	$\Gamma_C = \frac{R\rho_p V_i^2}{\rho_f r\Delta V^2}$	$\Gamma_O = \frac{R\rho_p V_r V_i}{\rho_f r\Delta V^2}$

These non-dimensional parameters are solely related to the particle inertial forces. The denominator is either viscous fluid force or drag force on the particle. The numerator is inertial forces. Viscous drag forces carry the particle on the streamline. Inertial forces cause the particle to deviate from the streamline. Intuitively, we propose that:

1. if γ and Γ are small, particles follow the streamline; and
2. if γ and Γ are large, particles deviate from the streamline.

If one accepts the above proposal, one can form the following hypothesis. A solid particle's ability to follow a streamline vector V is related to the non-dimensional parameters and some undefined velocity vector impact coefficients, A, B, C, D, E and F, based on the following functional form for the particle's velocity vector:

$$V = A\gamma_1 + B\gamma_C + C\gamma_O + D\Gamma_1 + E\Gamma_C + F\Gamma_O \tag{4}$$

where V is a normalized velocity vector in the surface's boundary layer flow. The velocity vector impact coefficients A, B and C correspond to laminar (viscous force) dominated flow, while D, E and F correspond to turbulence (high Reynolds number) dominated flow. Since the flow in gas turbines is highly turbulent, it is logical to utilize the turbulence velocity vector impact coefficients D, E, F and neglect A, B and C.

Departure of particles from the flow streamlines occurs as a consequence of the centrifugal and Coriolis forces acting on a particle. We may characterize these forces using the Stokes number. We define the Stokes number for particle flow as:

$$St = \frac{Particle\ stopping\ length}{Characteristic\ length} = \frac{\tau \cdot U}{L} \tag{5}$$

For a Stokes number very much less than one, particles follow the streamline and are not significantly affected by the Coriolis or centrifugal forces. For a Stokes number very much greater than one, the particles deviate from the streamline. We indirectly derive τ from measurement or analysis as we may not derive τ directly from either flow field or force parameters that we can obtain from commercially available computational fluid dynamic codes. Booker (1998) did derive a Stokes number equation for aerosol transport in curved ducts:

$$St = \frac{R^2 \cdot \rho \cdot U}{\mu r} \tag{6}$$

which is similar to the inertial (γ_I and Γ_1) terms in Equation 4. In the program of work in this chapter, the flow vector is functionally related to the individual velocity vector impact coefficients, as Figure 10.4 schematically illustrates, as do the non-dimensional parameters contained within Equation 3.

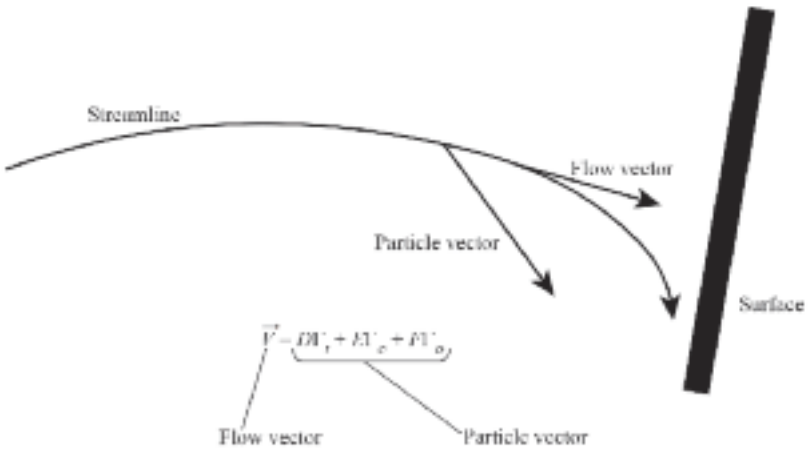

FIGURE 10.4. Functional description of particle vector with D, E and F velocity vector impact coefficients.

We must determine the individual velocity vector impact coefficients (D, E and F) radially, tangentially and normally from a steady-state computational fluid dynamic analysis of the flow field. Relative to the stationary frame, these velocity vector impact coefficients respectively approximate to acceleration, centrifugal and Coriolis forces. However, to determine the velocity vector impact coefficients accurately, it is necessary to perform a coordinate transformation. The three required coefficients for a coordinate transformation are:

Acceleration:

$$\Gamma_1 = \frac{F\rho_p \dot{V}_p}{\rho_f \Delta V^2} \tag{7}$$

Centrifugal:

$$\Gamma_C = \frac{R\rho_p V_t^2}{\rho_f r \Delta V^2} \tag{8}$$

Coriolis:

$$\Gamma_O = \frac{R\rho_p V_r V_t}{\rho_f r \Delta V^2} \tag{9}$$

The analysis approach is:

1. Calculate velocity vector impact coefficients (D, E and F) for each direction individually:
   - D for ΓI (velocity vector impact coefficient: acceleration)
   - E for ΓC (velocity vector impact coefficient: centrifugal)
   - F for ΓO (velocity vector impact coefficient: Coriolis)
2. Calculated values of D, E and F near the surface provide an indication of the likelihood that a particle will impact on a blade, rotating off a stationary surface.
3. Impact velocity derived by assuming that the particle velocity will correspond to the average flow velocity immediately upstream of the surface boundary layer.

For small values of D, E and F, we expected particles to deviate from the streamline path and impact blades, rotating and stationary surfaces. The analytical sequence which we utilized for a given flow path geometry is:

1. calculate the three-dimensional flow field around a given rotating or stationary geometry using a commercially available computational fluid dynamics code;
2. determine the aerodynamic flow field near surfaces and normalize flow vectors using the mean passage flow;
3. determine non-dimensional coefficients, ΓI ΓO ΓC, corresponding to acceleration, Coriolis and centrifugal forces divided by drag force;
4. calculate velocity vector impact coefficients D, E and F for each flow direction;
5. overlay results of D, E and F as a surface contour on blade, rotating and stationary surface geometry to identify the highest probability particle impact regions;
6. values of D, E and F less than unity indicate that the non-drag forces dominate the particles' trajectories and therefore that they will likely impact;
7. for the highest probability regions with velocity vector impact coefficients less than 0.5, calculate impact velocities from computational fluid dynamic code results using local velocity vectors stream-wise upstream of the impact locations.

The particle impact density behaves linearly with the velocity vector impact coefficients. The reader should note that the impact velocity is a vector and that one must individually evaluate the non-dimensional coefficients for each direction: x, y, z in the stationary frame. In the rotating frame the impact velocity vector must be evaluated in the normal, bi-normal and tangential directions. Additionally, as a consequence of our assumption that equations could be linearized, the velocity vector V and velocity vector impact coefficients are valid only for the immediate vicinity around a blade, rotating or stationary surface.

The assumption that equations could be linearized resulted in our focusing on the immediate forces that were acting on a particle near the impact surface and not on secondary fluid dynamic effects which tend to complicate the flow field's computational analysis. Our objective was to simplify flow field analysis and reduce the necessary computational effort to predict the particle deviation from the flow streamlines. We considered the consequence of equation linearization and concluded that it did not significantly reduce accuracy of the particle impact simulation. As such, we accepted equation linearization as a reasonable approach to particle impact density prediction within the constraints of available computational resources. To determine particle impact velocity, we assumed that the particle velocity corresponds to the average flow velocity just upstream from the particle location. This assumption is conservative as it will result in over predicting impact velocities. Therefore, we considered it acceptable.

PARTICLE ANALYSIS IN NON-ROTATING FLOW

Prior to performing experimental measurements and computational analysis on particulate behavior in the rotating frame, we undertook an experimental campaign in the stationary frame. The geometry which we selected for analysis was a NACA-0009 airfoil. The gas turbine industry routinely uses the NACA-0009 airfoil geometry for stationary flow elements. We analyzed sand behavior around the airfoil using both a commercially available computational fluid dynamics code and experimental flow visualization.

Case study 1: sand impacting airfoil in non-rotational flow field

To analyze how various sizes and specific density sands behaved around a NACA-0009 airfoil, we mounted an airfoil in a small wind tunnel fitted with a particle image velocimetry system. The non-rotating flow experiment comprised:

1. a NACA-0009 airfoil mounted in a small subsonic wind tunnel;
2. a particle image velocimetry system consisting of a 300 mW argon-ion laser, a mirror mounted on a 20,000 rpm high-speed direct current motor and a 35 mm camera;
3. a slow exposure photograph of this light scatter allowing single particle movement to be traced at fixed intervals. The time between fixed intervals corresponds to the laser beam's rotational speed in the light sheet;
4. velocity vectors for the two-dimensional light sheet which we determined from a slow exposure photograph;
5. three different sand grain sizes and three angles of attack:
   (a) coarse: 0.5 mm average particle size
   (b) medium: 0.2 mm average particle size
   (c) fine: 0.05 mm average particle size
   at 0, 5 and 10 degrees angle of attack;

6. a comparison of experimentally measured velocity vectors with computationally derived velocity vector impact coefficient.

Results of particle behavior in stationary frame

The wind tunnel we used in the reported research program utilized an open loop centrifugal air compressor capable of producing test section flows up to a Mach number of 0.95. The wind tunnel also included an optical window and upstream particle seeder (Figure 10.5). Figure 10.6 shows typical particle image velocimetry results.

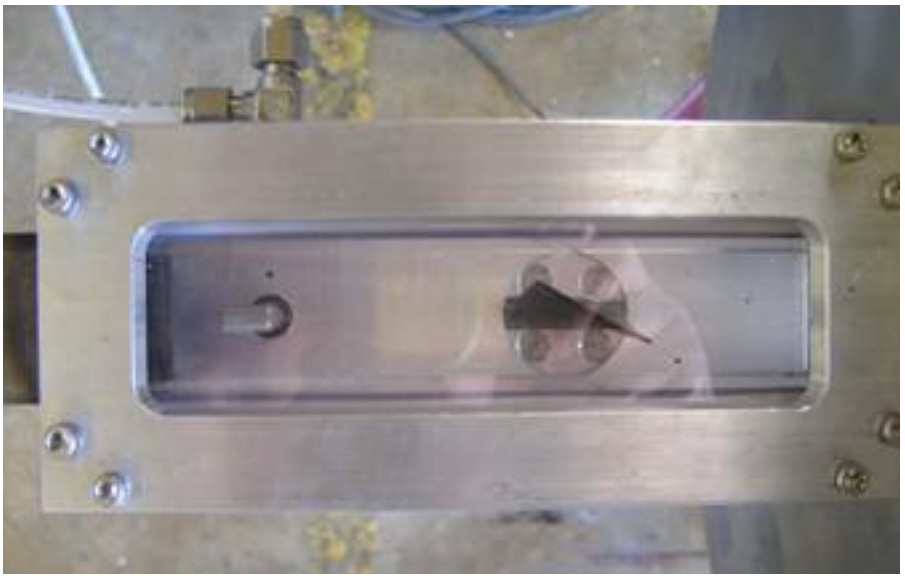

FIGURE 10.5. Wind tunnel optical window.

FIGURE 10.6. Typical particle image velocimetry results for stationary frame measurements.

Comparison of experimental and computational results

In parallel to the experimental work, we employed a two-dimensional commercially available computational fluid dynamics code to model the flow field streamlines around the NACA-0009 airfoil (Figure 10.7). Using the computational fluid dynamics code results, we determined the velocity vector impact coefficient. Table 10.2 gives typical results for 0.2 mm diameter sand particles. The results were within 20 percent of those which we obtained experimentally using particle image velocimetry. This was good considering our assumptions in the computational modeling and the measurement uncertainty. The computational results indicate that the

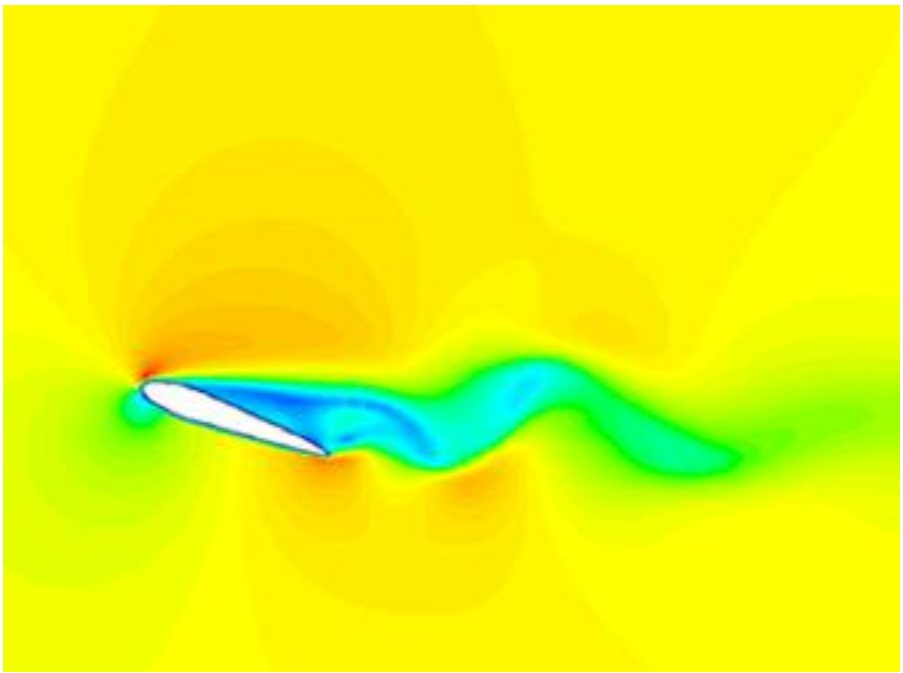

FIGURE 10.7. Computational fluid dynamic model of NACA-0009 airfoil flow.

Table 10.2. *Velocity vector impact (VVI) coefficients for 0.2 mm diameter sand particle motion on a NACA-009 airfoil. Equations 6, 7 and 8 give a complete description of D-VVI, E-VVI and F-VVI as velocity vector impact coefficients.*

Velocity vector impact (VVI) coefficients				
Location (mm)	D-VVI (Acceleration term)	E-VVI (Centrifugal term)	F-VVI (Coriolis term)	Sum VVI
0.0 (center line)	0.1	0.5	0.0	0.6
0.1	0.4	0.7	0.0	1.1
0.2	0.8	0.6	0.0	1.4

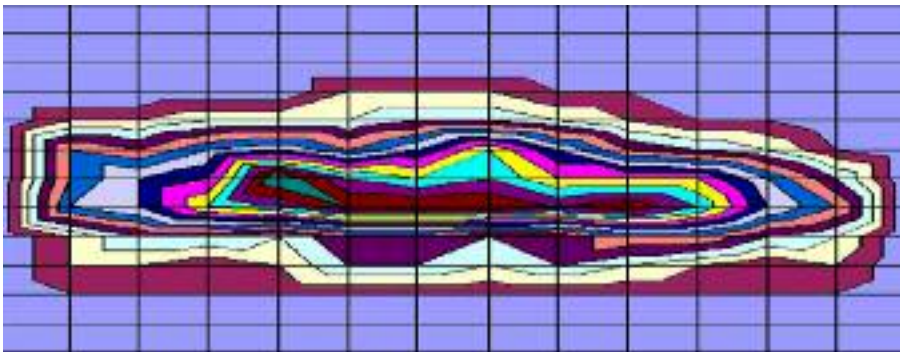

FIGURE 10.8. Velocity vector impact coefficients total sum indicating probability of particle impacts on a NACA-0009 airfoil leading edge.

highest impact velocities and highest impact probability were at the airfoil's leading edge (Figure 10.8). Note that the F velocity vector impact coefficient term was zero for all cases. This term corresponds to Coriolis forces, which do not act in a stationary flow field.

PARTICLE ANALYSIS IN ROTATING FLOW

Case study 2: sand ingestion into a centrifugal compressor

When extending the model to the rotating frame, one must model centrifugal and Coriolis forces as they affect particle motion. To assist in the development of a rotating frame model, we performed experimental sand injection experiments in a high-speed compressor at the Southwest Research Institute. These compressor tests provided experimental data that we could then correlate with computational fluid dynamics results and facilitate the derivation of velocity vector impact coefficients. Calibration of the computational model using experimental results in turn facilitated the derivation of a generalized sand transport model.

Computational fluid dynamics modeling approach

We performed a flow field computational fluid dynamic analysis and compared the results with their experimental results. Input to the computational analysis was a Southwest Research Institute high-speed centrifugal compressor three-dimensional solid model. We only modeled the first stage of the two-stage compressor as the first stage was the experimental work's focus (Figure 10.9).

We imported the three-dimensional solid model into a commercially available computational fluid dynamics code. Using experimentally derived flow velocities

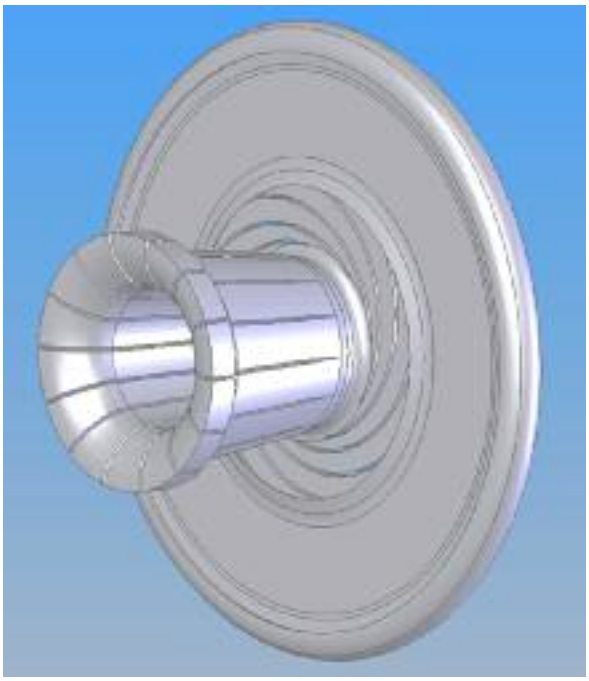

FIGURE 10.9. Single-stage impeller solid model, which we meshed and incorporated into the computational fluid dynamic model.

and impact angles, we conducted a series of computational fluid dynamic simulations to determine flow field characteristics at the compressor blades' leading edges. We then took velocity components from the computational fluid dynamic analysis and computed non-dimensional flow and velocity vector impact coefficient parameters. We went on to analyze a series of computational models using permutations of mesh density, boundary conditions and turbulence models. Figure 10.10 presents results from a representative computational simulation.

The reader should note that the images in Figure 10.10 represent the fluid volumes' geometry and not the compressor's solid components. The computational fluid dynamics software that we used allowed for the determination of flow characteristics at specific locations within the compressor. An area of particular interest was the impeller blade's leading edge. The velocity vector plot in Figure 10.10 therefore focuses on the blade's leading edge region.

We calculated non-dimensional parameters using the computational fluid dynamic analysis results. We utilized the non-dimensional methodology that forms the basis of the research reported in this chapter. To ascertain the properties of sand, we analyzed desert sand from Qatar. We used various sand grain diameters, weights, volumes and distributions to calculate average density and radius values. We used this average value as input to the computational simulations. We repeated the computational fluid dynamic analysis for a range of particle sizes and densities over a range of compressor flow and head conditions.

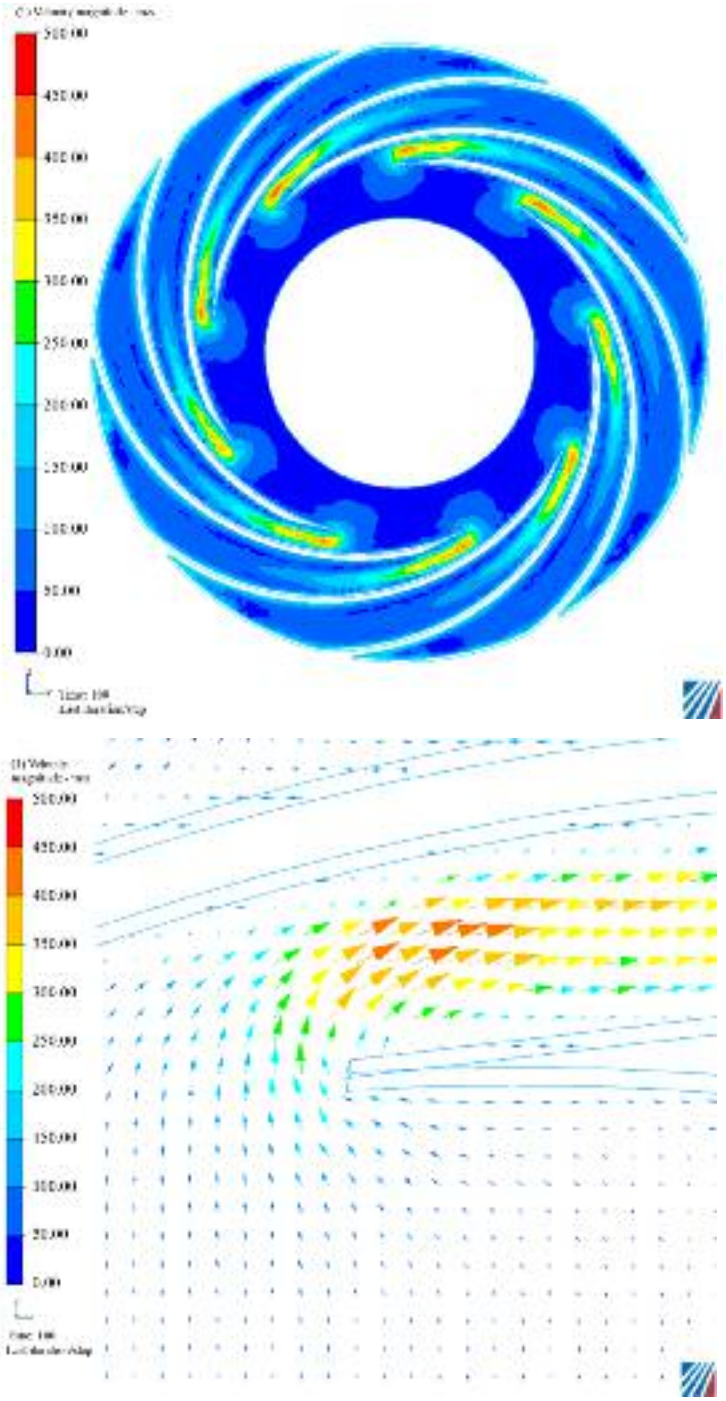

FIGURE 10.10. Computational fluid dynamic results — velocity magnitude plot and vector plot near the leading edge.

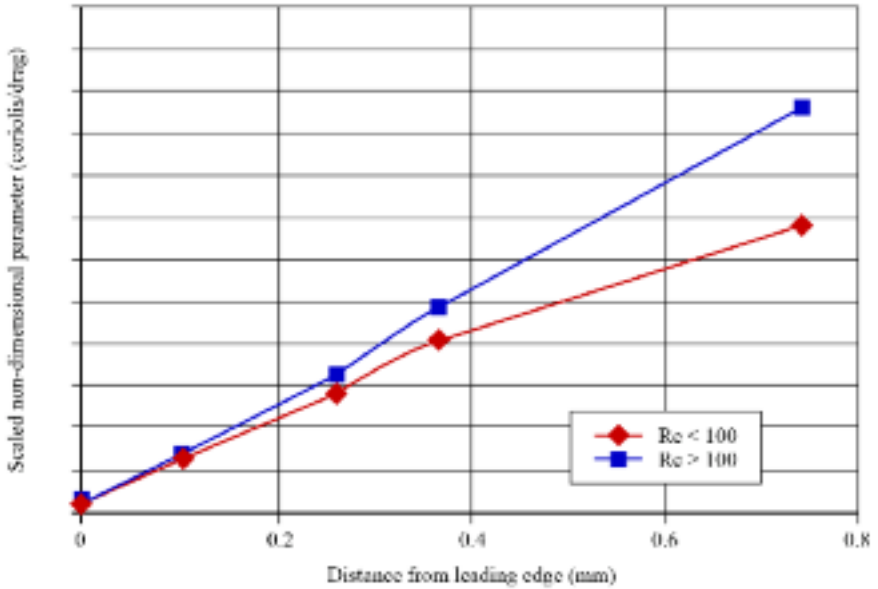

FIGURE 10.11. Coriolis velocity vector impact coefficient terms as a function of radial distance from the leading edge.

We also performed a computational fluid dynamic parametric analysis to assist in the development of a qualitative understanding of the relative physical influences of each of the velocity vector impact coefficients. We used results of the computational analysis to demonstrate that centrifugal and Coriolis terms dominated the inertial terms. While the centrifugal parameters did not vary significantly at small distances from the compressor blades' leading edges, the Coriolis term showed a significant dependence on position relative to the compressor blades' leading edges (Figure 10.11).

Particle testing in the compressor

We performed experiments using the Southwest Research Institute's high-speed centrifugal compressor. Using a variable speed drive and electric motor, we were able to drive the compressor to speeds up to 10,000 rpm, while injecting sand into the compressor. The test stand consisted of a 700 hp variable speed drive, driving a Clark two-stage compressor capable of running in open or closed loop mode through a gearbox capable of variable speeds up to 14,000 rpm (Figure 10.12).

We used the experimental results to determine where sand impacted the compressor blades. We painted the compressor blade surfaces that were exposed to the airflow through the compressor with an abradable paint prior to each test run. We inspected the impeller after each test run to determine where sand impacted the blades.

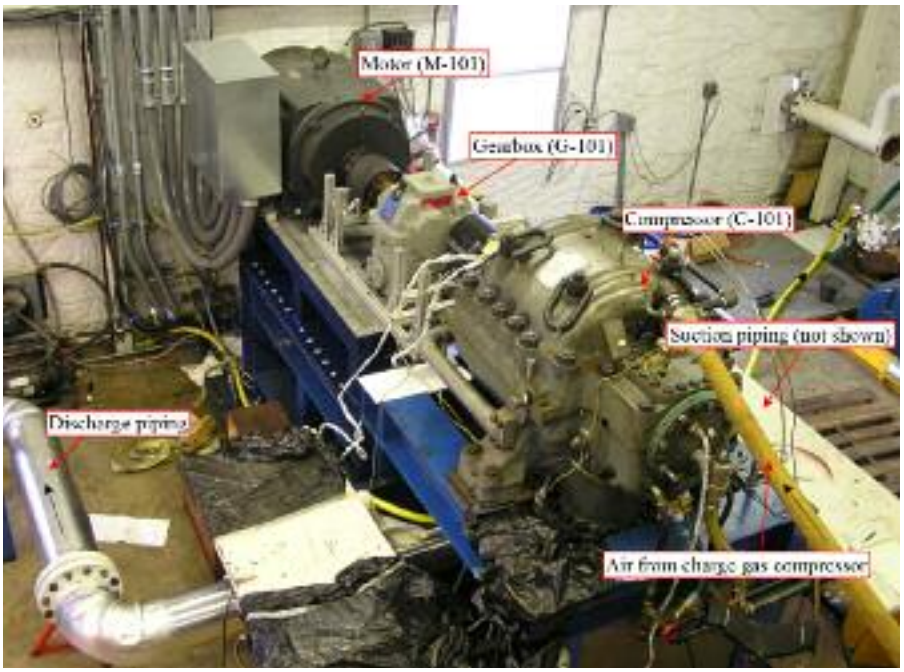

FIGURE 10.12. Centrifugal compressor test stand.

We injected measured quantities of sand into the duct work upstream of the compressor and mixed it using a pre-swirler. Because the compressor operates in an open-loop arrangement, the sand particulates passed only once through the compressor. This open-loop arrangement facilitated control of both the consistency and quantity of sand passing through the compressor. After a test we disassembled the compressor and visually inspected it for paint abrasion. From the visual inspection, we were able to measure the primary particle impact locations and infer the impact density (Figure 10.13). In all, we performed three separate test runs:

1. fine sand (D = 0.05 mm, ρ = 1.694 g/mL) at 10,000 rpm;
2. fine sand (D = 0.05 mm, ρ = 1.694 g/mL) at 5000 rpm;
3. diatomaceous earth (D = 0.002 mm, ρ = 0.325 g/mL) at 5000 rpm.

Experimental results

An analysis of the experimental results facilitated a comparison of computationally predicted velocity vector impact coefficients with measured particle impact distribution. For each test we documented abrasion locations inside the impeller and kept records of the location, size and paint removal. We then compared these experimentally identified abrasion locations and sizes to computationally identified

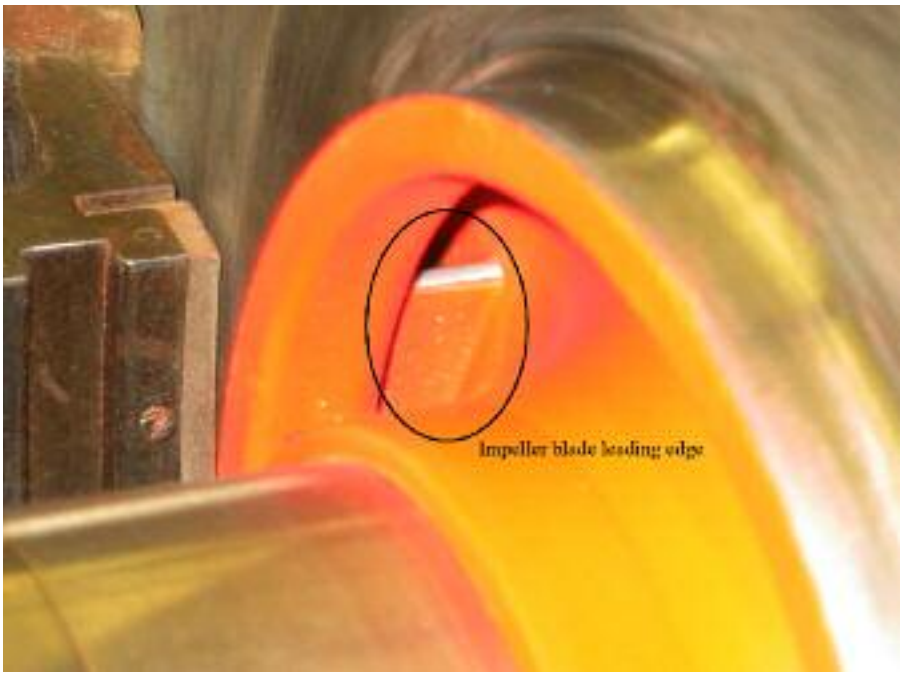

FIGURE 10.13. Leading edge visual inspection of the impeller blades after fine sand ingestion.

locations. We identified computational locations by summing velocity vector impact coefficients and individual velocity vector impact direction coefficients for each directional component.

We overlaid the experimental and computational results to determine the accuracy with which the computational results predicted the experimentally observed regions of highest erosion. We also overlaid the computationally derived velocity vector impact coefficients map on a compressor photograph (Figure 10.14).The photograph was taken after the compressor had been tested, with the overlay assisting us in determining the accuracy with which the computational results predict the primary sand impact locations. We judged the agreement to be good between velocity vector impact coefficients and local abrasion. We performed a similar analysis for all test results for the impeller sand ingestion testing. For each location that we identified in the test as showing significant sand abrasion, we overlapped and compared the computational results. In each case, we judged the agreement as good.

Results of rotating frame analysis

We found good agreement between the predicted highest probability impact locations from the computationally derived velocity vector impact coefficients and the experimentally observed results for all tests. It is difficult to derive measurement

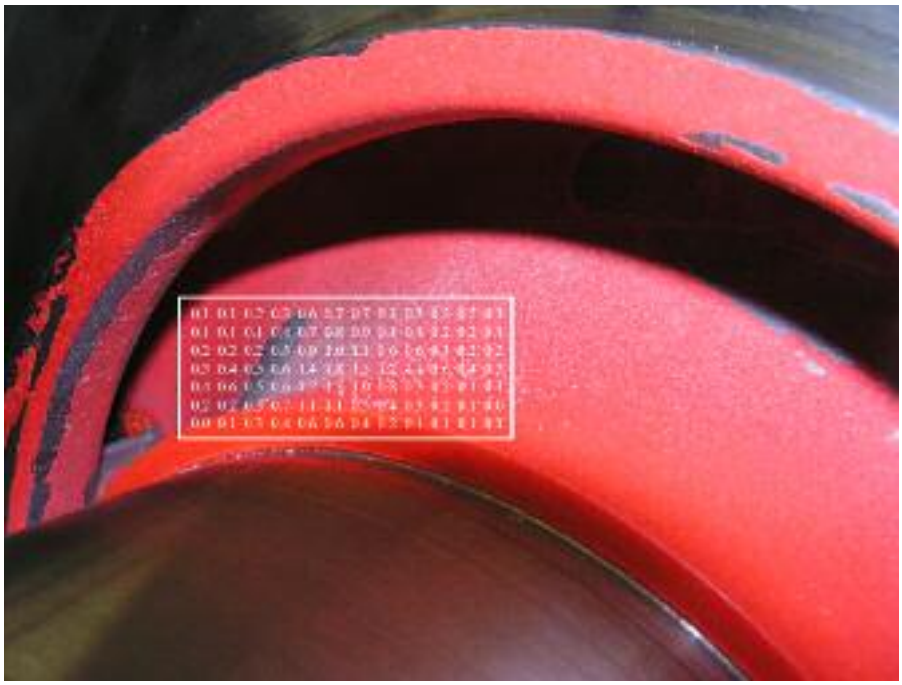

FIGURE 10.14. Sand abrasion in centrifugal impeller with local velocity vector impact coefficients.

uncertainty, as the experimental method depended on visual inspection and interpretation of the extent to which the sand particles had removed the abradable paint during a test. However, results indicated good agreement between computational and experimental results. When analyzing the experimental results, we observed that when any of the individual velocity vector impact coefficients normal to the surface were below 0.5, or the sum of the velocity vector impact coefficients normal to the surface were below 0.8, a measurable particle impact area existed in all test cases. Consequently, we concluded that one may use the computational results to predict areas of sand abrasion with good reliability.

Despite the success of the computational method to predict sand abrasion locations, we did not predict approximately 20 percent of experimentally observed particle impact locations. This was probably a consequence of the sand's uneven particle flow into the compressor. We also considered that particles may be bouncing off the compressor blades, an effect that Beacher *et al*. (1982) reported.

SUMMARY

The research program that we report in this chapter presents development of a software tool that utilizes a semi-empirical model to predict sand, dirt and dust

particle behavior in gas turbine and centrifugal compressors. The adopted approach utilizes a commercially available computational fluid dynamics code to determine the flow field without the particle influence. We then use the code's steady three-dimensional velocity flow field results as input to the semi-empirical model to determine probable particle impact locations and surface impact velocities. We based the analysis method on:

1. a derivation of the particle transport kinematic equation non-dimensional parameters in a rotating fluid;
2. analysis of a numerical solution of these equations based on a given velocity vector field; and
3. interfacing of the semi-empirical model with a commercially available computational fluid dynamic code.

Comparative sand flow tests in a wind tunnel around a NACA-0009 airfoil and sand flow inside a high-speed centrifugal compressor results showed good agreement with computational fluid dynamic and semi-empirical model predictions. The semi-empirical model predicted likely particle impact locations well, with a "miss rate" of approximately 20 percent. The combined computational fluid dynamic and semi-empirical model approach provides a practical method for predicting likely solid particle impact locations. The approach avoids the need for computationally demanding transient particle transport calculations.

The developed computational method provides design engineers with a tool that they can use to develop a "hardening" strategy for gas turbine and centrifugal compressors. Design engineers can identify those locations most prone to erosion and then locally reinforce or coat them against the effect of ingested particles. By identifying those locations most prone to damage, the design engineer can develop a more focused inspection and replacement strategy and in so doing minimize compressor inspection and repair times.

REFERENCES

Beacher, B., Tabakov, W., and Hamid, A. (1982), "Improved Particle Trajectory Calculations through Turbomachinery Affected by Ash Particles", *Transactions of the ASME, Journal of Engineering for Power*, vol. 104, pp. 64–8.

Booker, D.R. (1998), *Aerosol Sampling Guideline,* Cambridge University Press, London, UK.

Cardwell, N.C., Vlachos, P.P., and Thole, K.A. (2009), "A Method for Identifying and Visualizing Foreign Particle Motion Using Time Resolved Particle Tracking Velocimetry", *Proceedings of the 54th American Society of Mechanical Engineers Gas Turbine and Aeroengine Congress,* Orlando, USA, 8–12 June, Paper No. GT2009-60273.

Corsini, A., Marchegiani, A., Rispoli, F., Sheard, A.G., and Venturini, P. (2012), "Predicting Blade Leading Edge Erosion in an Axial Induced Draft Fan", *Transactions of the ASME, Journal of Engineering for Gas Turbines & Power*, vol. 134, Paper No. 042601, pp. 1–9.

Corsini, A., Delibra, G., Rispoli, F., Sheard, A.G., and Venturini, P. (2013), "Simulation of the Particle-Laden Flows in a Large Centrifugal Fan", *Proceedings of the 58th American Society of Mechanical Engineers Gas Turbine and Aeroengine Congress,* San Antonio, USA, 3–7 June, Paper No. GT2013-94982.

Corsini, A., Rispoli, F., Sheard, A.G., and Venturini, P. (forthcoming), "The Impact of Blade Erosion on the Induced-Draft Boiler Fan Aerodynamic Performance and Stall Margin Ventilation", Accepted for publication in *Transactions of the ASME, Journal of Fluids Engineering*, Manuscript No. FE-12-1425.

Cowan, J.B., Tafti, D.K., and Kohli, A. (2010), "Investigation of Sand Particle Deposition and Erosion within a Short Pin Fin Array", *Proceedings of the 55th American Society of Mechanical Engineers Turbine and Aeroengine Congress,* Glasgow, UK, 14–18 June, Paper No. GT2010-22362.

Dring, R.P., Caspar, J.R., and Suo, M. (1979), "Particle Trajectories in Turbine Cascades", *Transactions of the AIAA, Journal of Energy*, vol. 3, pp. 161–6.

Dunn, M.G., Baran, A.J., and Miatech, J. (1996), "Operation of Gas Turbine Engines in Volcanic Ash Clouds", *Transactions of the ASMA, Journal of Engineering for Gas Turbines and Power*, vol. 118, pp. 724–31.

Fuchs, N.A. (1964), *The Mechanics of Aerosols,* Pergammon Press, Oxford, UK.

Ghenaiet, A., Tan, S.C., and Elder, R.L. (2005), "Prediction of an Axial Turbomachine Performance Degradation due to Sand Ingestion", *Proceedings of IMechE, Journal of Power and Energy*, vol. 219, pp. 273–87.

Grant, G., and Tabakoff, W. (1975), "Erosion Prediction in Turbomachinery Resulting from Environmental Particles", *Journal of Aircraft*, vol. 12, pp. 471–8.

Haase, K., and Bons, J.P. (2010), "Velocity Measurements around Film Cooling Holes with Deposition", *Proceedings of the 55th American Society of Mechanical Engineers Turbine and Aeroengine Congress,* Glasgow, UK, 14–18 June, Paper No. GT2010-22358.

Hadiiyannis, S., Charalambous, N., Tourlidakis, A., and Michaelides, K. (2009), "An Experimental and Computational Study of the Erosion in Submersible Pumps and the Development of a Methodology for Selecting Appropriate Protective Coatings", *Proceedings of the 54th American Society of Mechanical Engineers Gas Turbine and Aeroengine Congress,* Orlando, USA, 8–12 June, Paper No. GT2009-60090.

Hamed, A., Tabakoff, W., and Wenglarz, R. (2006), "Erosion and Deposition in Turbomachinery", *Journal of Propulsion and Power*, vol. 22, pp. 350–60.

Haq, I.U., Bu-Hazza, A.L., and Al-Baz, K. (1998), "Multistage Centrifugal Compressor Fouling Evaluation at High Power Settings", *Proceedings of the 43rd American Society of Mechanical Engineers Gas Turbine and Aeroengine Congress,* Stockholm, Sweden, 1–4 June, Paper No. 98-GT-53.

Hussein, M.F., and Tabakoff, W. (1973), "Dynamic Behavior of Solid Particles Suspended by Polluted Flow in a Turbine Stage", *Journal of Aircraft*, vol. 10, pp. 434–40.

Jeske, H.O., and Sandstede, H. (1985), "Turbine Blade Behaviour [sic] in Gas Streams Containing High Dust Loads", *Forschung im Ingenieurwesen*, vol. 51, pp. 52–62.

Kurz, R., and Brun, K. (2009), "Gas Turbine Tutorial: Maintenance and Operating Practices Effects on Degradation and Life", *Proceedings of the Turbomachinery Symposium,* Houston, USA, 14–17 September.

Land, C.C., Joe, C., and Thole, K.A. (2010), "Considerations of a Double-Wall Cooling Design to Reduce Sand Blockage", *Transactions of the ASMA, Journal of Turbomachinery*, vol. 132, pp. 1–8.

Lawson, F.A., and Thole, K. (2010), "Simulations of Multi-Phase Particle Deposition on Endwall Film-Cooling", *Proceedings of the 55th American Society of Mechanical Engineers Turbine and Aeroengine Congress*, Glasgow, UK, 14–18 June, Paper No. GT2010-22376.

Maxey, M.R. (1983), "Equation of Motion for a Small Rigid Sphere in Non-uniform Flow", *Journal of Physics of Fluids*, vol. 26, pp. 883–9.

Musgrove, G.O., Barringer, M.D., Thole, K.A., Grover, E., and Barker J. (2009), "Computational Design of a Louver Particle Separator for Gas Turbine Engines", *Proceedings of the 54th American Society of Mechanical Engineers Gas Turbine and Aeroengine Congress,* Orlando, USA, 8–12 June, Paper No. GT2009-60199.

Richardson, J.H., Sallee, G.P., and Smakula, F.K. (1979), "Causes of High Pressure Compressor Deterioration in Service", *Proceedings of AIAA, SAE and ASME Joint Propulsion Conference*, Las Vegas, USA, 15–18 June, Paper No. 79-1234.

Schmuecker, J., and Schaffler A. (1994), "Performance Deterioration of Axial Compressors due to Blade Defects", *Proceedings of the Propulsion and Energetic Panel (PEP) Symposium,* Rotterdam, The Netherlands, 25–28 April, Paper No. 16.

Tabakoff, W., and Sugiyama, Y. (1980), "Experimental Methods of Determining Particle Restitution Coefficients", *Proceedings of the Symposium on Polyphase Flow and Transport Technology,* San Francisco, USA, 13–15 August, pp. 203–10.

Tabakoff, W., Grant, G., and Ball, R. (1974), "An Experimental Investigation of Certain Aerodynamic Effects on Erosion", *Proceedings of the AIAA 8th Aerodynamic Testing Conference*, Bethesda, USA, 8–10 July, Paper No. 74-639.

Walsh, W.S., Thole, K.A., and Joe, C. (2006), "Effects of Sand Ingestion on the Blockage of Film-Cooling Holes", *Proceedings of the 51st American Society of Mechanical Engineers Gas Turbine and Aeroengine Congress,* Barcelona, Spain, 8–11 May, Paper No. GT2006-90067.

Wilcox, M., Brun, K., and Kurz, R. (2011), "Successful Selection and Operation of Gas Turbine Inlet Filtration Systems", *Proceedings of the Turbomachinery Symposium,* Houston, USA, 12–15 September.

Chapter 11

Industrial Gas Turbine Performance Degradation

R. Kurz, K. Brun and M. Wollie

ABSTRACT

This chapter presents the mechanisms by which degradation develops and affects gas turbine performance. A gas turbine's performance is the result of its constituent components' collective performance, and therefore the emphasis of this chapter is on the performance of a gas turbine's components as a system. We clarify component interaction through the use of a model which we used to isolate the impact on gas turbine performance of the different types of degradation experienced in-service. We use the model to isolate the impact of three aspects of degradation on gas turbine performance: the impact of component degradation on the gas turbine compressor's operating point, the impact of component degradation on full and part load performance characteristics, and the impact of component degradation on measurable operating parameters. We validate the model through a comparison with experimental data. The chapter concludes by linking the change in measureable operating parameters to the level of degradation, and provides compression system operators with the necessary guidance to define condition monitoring best practice.

This chapter is a revised and extended version of Kurz, R., Brun, K., and Wollie, M (2009), "Degradation Effects on Industrial Gas Turbines", *Transactions of the ASME, Journal of Engineering for Gas Turbines and Power*, vol. 131, pp. 1–7. This paper won the International Gas Turbine Institute Oil & Gas Application Committee 2008 best paper award.

INTRODUCTION

Any prime mover exhibits the effects of wear over time. Because the performance of a gas turbine is the result of the collective performance of its components, this chapter emphasizes the gas turbine as a system rather than the performance of its components. Treating the gas turbine as a system provides insight into the effects of degradation on the match of the components. In this chapter we consider the impact of degradation on both single-shaft and two-shaft gas turbines. A key difference between single- and two-shaft gas turbines is that a two-shaft gas turbine's turbine speed varies with load. In contrast, a single-shaft gas turbine speed remains constant with varying loads. The chapter considers the implications of component degradation for both single- and two-shaft gas turbines and presents the implication for praxis.

Six mechanisms result in gas turbine degradation. Adherence of particles to airfoils and annulus surfaces causes *fouling*. *Hot corrosion* is the loss or deterioration of material from components that are exposed to combustion gases, caused by chemical reactions between the component and contaminants. Inlet air contaminants, fuel and combustion derived contaminants cause *corrosion*. *Erosion* is the abrasive removal of material from the flow path by hard or incompressible particles impinging on flow surfaces. *Abrasion* occurs when a rotating surface rubs on a stationary surface. *Foreign objects* striking the flow path components may also cause damage. While cleaning or washing the gas turbine can reverse some of these effects, others require adjustment, repair or component replacement.

The dominant degradation mechanisms for aircraft gas turbines and industrial gas turbines are different. Aircraft gas turbines operate without inlet air filtration, and therefore erosion, especially of the compressor, is a key contributor to degradation. Industrial gas turbines, assuming that they have an appropriate air filtration system, are subject to fouling caused by smaller particles and corrosion. The exception may be gas turbines subject to water injection in the compressor inlet (Brun *et al*., 2005), where an incorrectly sized water injection system can generate sufficient sized water droplets to cause blade erosion.

DEGRADATION OF COMPONENTS

Three primary effects determine the performance deterioration of a gas turbine's compressor: increased tip clearances, changes in airfoil geometry and changes in airfoil surface roughness. While the first two effects typically lead to non-recoverable degradation, we can, at least, partially reverse the latter effect by washing the compressor (Stalder, 1998). Stage degradation also has a cumulative effect. A degraded compressor stage will create different exit conditions than a new stage, and each subsequent stage will operate further from its design point. When new, all stages work at their optimum efficiency point. Degradation will result in all stages after the first working at reduced efficiency. Operating the latter compressor stages off-design not only reduces overall gas turbine efficiency, but also the achievable compressor pressure ratio and consequently, gas turbine operating range. Further-

more, increased tip clearances will reduce the compressor's flow capacity, further limiting operating range. One can re-adjust variable geometry, where available, to counteract some of the mismatching degradation effects, but not completely eliminate the reduction in either compressor efficiency or gas turbine operating range.

A degraded compressor also will have a reduced surge margin (Spakovszky *et al*., 1999; Brun *et al*., 2005). Graf *et al*. (1998) presented data for an axial compressor, where increased clearances reduced surge margin and efficiency. Graf *et al*. (1998) demonstrated that as tip clearance increased from 2.9 percent (design value) to 4.3 percent, the surge flow coefficient increased 20 percent, design pressure coefficient reduced 12 percent and design point efficiency reduced 2.5 percent. Smith and Cumpsty (1984) reported similar results where an increase in tip clearance from 1.0 percent to 3.5 percent reduced the pressure coefficient by 9 percent. Frith (1992) tested a helicopter gas turbine with compressor blades cropped to simulate increased tip clearances. A 3.0 percent crop on the compressor stages reduced flow by 4.6 percent and pressure ratio by 3.0 percent. The compressor discharge temperature remained unchanged, which indicates a reduction in compressor efficiency of approximately 2.5 percent.

Wear of compressor bleed air valves constitutes a form of compressor degradation and can result in significant performance deterioration. Many gas turbines bleed air from the compressor discharge directly into the exhaust, either for surge avoidance during start-up or for emission control purposes. Leakage in these bleed valves constitutes a direct loss of gas turbine efficiency. Although potentially significant, leaking bleed valves are relatively easy to detect and repair as they are typically external to the gas turbine. As such, we will not consider further the effect of bleed air valve leakage.

Gas turbine combustion system degrading does not directly result in performance deterioration. Combustion efficiency does not decrease, except in severe cases of combustor distress. However, combustor degrading may lead to a variation in the combustor exit temperature profile. A distorted exit temperature distribution may cause the turbine to degrade in three ways. Local temperature peaks can damage the turbine and reduce turbine life. The altered temperature profile will increase secondary flow development and reduce turbine efficiency. The change in circumferential temperature profile will result in the gas turbine's over- or under-firing, respectively, resulting in either reduced turbine life or power. The over- or under-firing occurs as a consequence of deriving the combustor control temperature from temperature measurement made at discrete circumferential points at the combustor exit. A change in circumferential temperature profile will result in an average of these measured temperatures not being a true combustor exit temperature, with the consequence that the gas turbine control system will then either over- or under-fire the gas turbine.

As with a gas turbine's compressor, the turbine is subject to degradation as a consequence of increased tip clearances, changes in airfoil geometry and changes in airfoil surface roughness. Maintaining design tip clearances is a particular problem in the turbine as a consequence of the extreme changes in temperature that occur as a gas turbine accelerates from cold start-up to full load. The stationary turbine com-

ponents expand at a different rate than rotating components as a consequence of their different thermal inertia and the effect of centrifugal force on rotating components.

Turbine designs incorporate abradable seals to enable tip clearance to fall to zero at some point through the turbine operating cycle. This minimizes tip clearance. Minimum clearance classically occurs over a turbine's blades after a hot restart. The relatively thick turbine discs remain hot, while the relatively thin casings have cooled. The result is that the gap between turbine blades and casings falls to zero, and thus sets the clearance that is in practice achieved at every other point through the gas turbine's operating cycle. Radtke and Dibelius (1980) reported a reduction in efficiency of a multistage turbine by 0.6 percent when they increased the tip clearances from 0.5 percent of the blade height over the rotors and 0.4 percent of the blade height over the stators to 0.8 percent over both rotors and stators. The negative impact on gas turbine performance associated with increasing turbine tip clearance is significant. In response, industrial gas turbine manufacturers now fit active clearance control systems to industrial gas turbines to minimize turbine blade tip clearance at the gas turbine's operating point to maximize turbine efficiency (Sheard, 2012).

Corrosion alters the flow path in two ways. It increases the surface roughness, but it also removes material, in particular, at the turbine blade's leading and trailing edges. The turbine nozzles, operating at or near choked conditions, are especially sensitive to changes in the flow area. Furthermore, changes in the turbine's flow capacity will subsequently alter the operating points for the gas turbine compressor. Increased surface roughness results in thicker boundary layers on the blades and sidewalls, and thus may reduce the flow capacity, especially near choking conditions. Boyle (1994) found for a two-stage turbine efficiency losses of 2.5 percent for a 10.2 μm surface roughness when compared with smooth blades. He also found that the most pronounced differences appear at the turbine's optimum operating point. In contrast, the off-design efficiency was almost identical for rough and smooth blades. Note that aerodynamic losses associated with tip clearance effects were the same order of magnitude as profile losses.

If turbine corrosion leads to material removal in the nozzle area, the consequence is an increase in flow capacity. Because the throat area limits the flow capacity of any nozzle, erosion of the nozzle trailing edge causes the exit flow angle to become more axial. This results in a reduction of turning in the stator and the rotor, which will lead to reduced work extraction for this stage and to an increased flow capacity. Since the turbine nozzles constitute a flow restriction, any change in the turbine's flow capacity will also impact the gas turbine compressor's operating points.

AIR FILTRATION SYSTEM

Fouling of inlet filters occurs progressively over time. This leads to an increased pressure drop in the inlet system and, as a result, reduced gas turbine power and efficiency. Figure 11.1 shows the relative impact of the pressure loss in the inlet system on power and efficiency. Self-cleaning filters, where appropriate, or changing of filter pads or cartridges can reverse this pressure loss. Note that air filtration systems

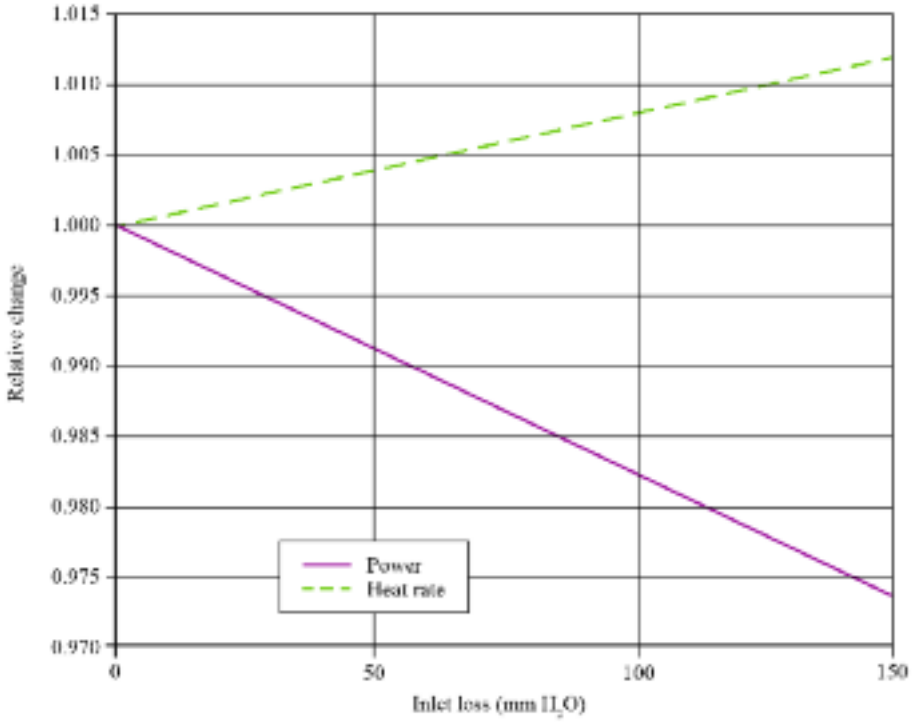

FIGURE 11.1. Impact of inlet pressure loss on gas turbine power and heat rate.

are always a compromise between filtration effectiveness, pressure loss and size or cost of the system. Also, the filtration system has to be appropriate for the type of expected contamination. Some types of filters are very effective for small particle sizes, some are specifically designed for high dust loads and others are effective in keeping droplets with potentially dissolved contaminants out of the gas turbine.

EFFECT OF DEGRADATION ON THE GAS TURBINE

Degradation of components has a compounded effect on gas turbine performance, because the change in component performance characteristics leads to a mismatch of these components at the gas turbine level. The gas turbine's control system and control modes also influence the impact of individual component degradation. Single-shaft gas turbines operating at constant speed will show a different degradation behavior than two-shaft gas turbines. The impact of degradation on two-shaft gas turbines depends on the control mode that one uses, specifically whether the gas turbine speed or firing temperature is the limiting factor.

In the following comparisons, we used a gas turbine performance model to separate effects that occur together. For example, compressor degradation will impact

pressure ratio, efficiency and flow capacity, albeit to various degrees depending on the type of degradation. The models therefore allow us to study in isolation the impact of reduced compressor efficiency (predominantly due to fouling), reduced compressor flow capacity (opening of clearances and fouling), altered gas turbine flow capacity (corrosion, erosion, fouling) and reduced gas turbine efficiency (fouling, erosion) as isolated events. Note that, if we state a change in efficiency, we assume that the component loses that amount of efficiency over its entire operating map. Since in many instances the operating point on the map is different between the new and the degraded gas turbines, the actual efficiency in the cycle calculation is the result of degradation and movement of the operating point.

Do not confuse the reduced flow capacity associated with compressor blockage that we used in this chapter with the observed reduction in flow through a degraded gas turbine. The observed reduction in flow is a result of the compressor's higher power consumption and is generally related to a deteriorated compressor or the turbine's reduced flow capacity. Frith (1992) cropped a two-shaft turboprop gas turbine's compressor blades, thus simulating the blade tip rubs' effects. This crop reduced both flow and compressor efficiency, and also compressor pressure ratio. This indicates that the compressor's increased power consumption leads to a reduced pressure ratio. In turn, since Frith (1992) did not change the turbine's flow capacity, cropping the compressor blades caused a flow reduction.

We will present the results that we obtained using the model as a series of figures that we should consider within the context of a typical gas turbine compressor map (Figure 11.2). The compressor map defines the relationship between compressor flow and discharge pressures. The available power to drive the compressor determines the compressor's actual operating point.

REDUCED COMPRESSOR EFFICIENCY

Compressor degradation will have a different effect on overall performance for single- and two-shaft gas turbines. Due to the fixed speed of single-shaft gas turbines in combination with a usually choked turbine nozzle, compressor efficiency loss will primarily affect the compressor pressure ratio, but only to a limited degree the flow through the gas turbine. A two-shaft gas turbine with a compressor with reduced efficiency will exhibit significant changes in flow and pressure ratio (Figure 11.3). Researchers have observed the reduction in flow (Millsaps *et al*., 2004; Syverrud *et al*., 2005). For a fixed operating point, the gas turbine will have to run faster and the compressor will consume more power once it deteriorates.

The impact of reduced compressor efficiency on full load power and heat rate of a two-shaft gas turbine depends on the ambient temperature and appears more severe at warm ambient temperatures (Figures 11.4 and 11.5). For a temperature limited two-shaft gas turbine, speed reduces with reduced compressor efficiency. This speed reduction occurs because for a given pressure and flow, the compressor now consumes more power. For single-shaft gas turbines, where the compressor speed remains

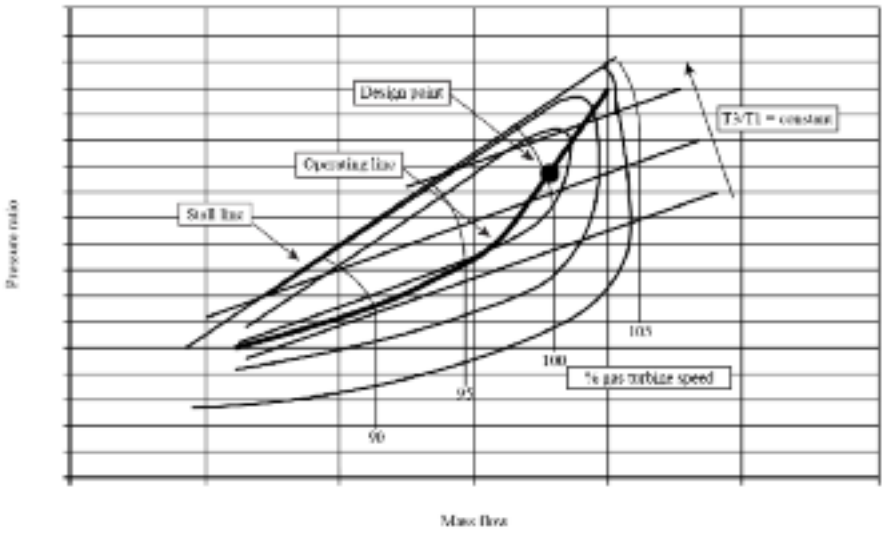

FIGURE 11.2. Schematic compressor map for a two-shaft gas turbine (Cohen *et al*., 1996).

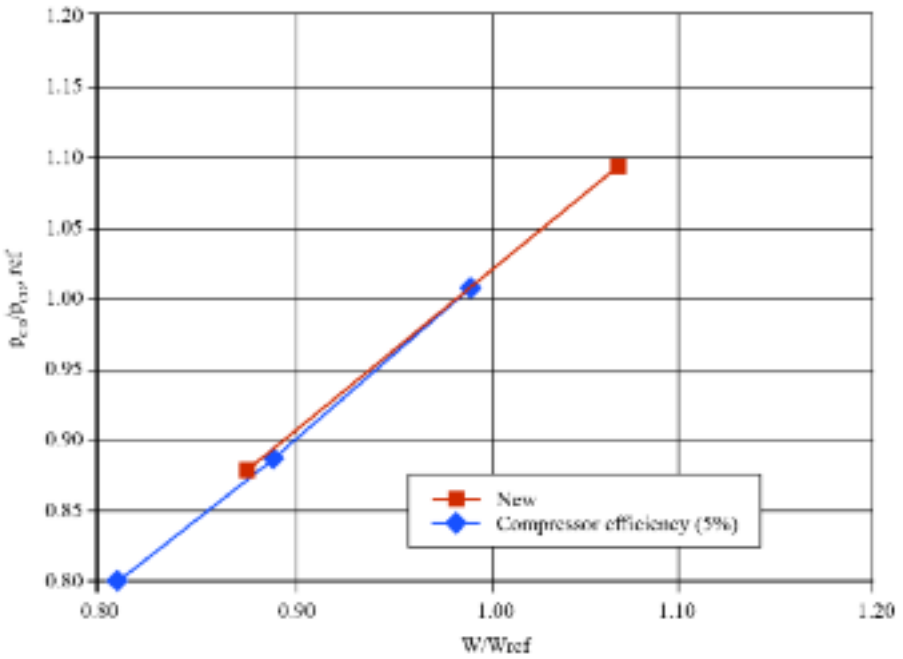

FIGURE 11.3. Compressor discharge pressure as a function of compressor flow for a new compressor and a compressor with 5 percent reduced efficiency.

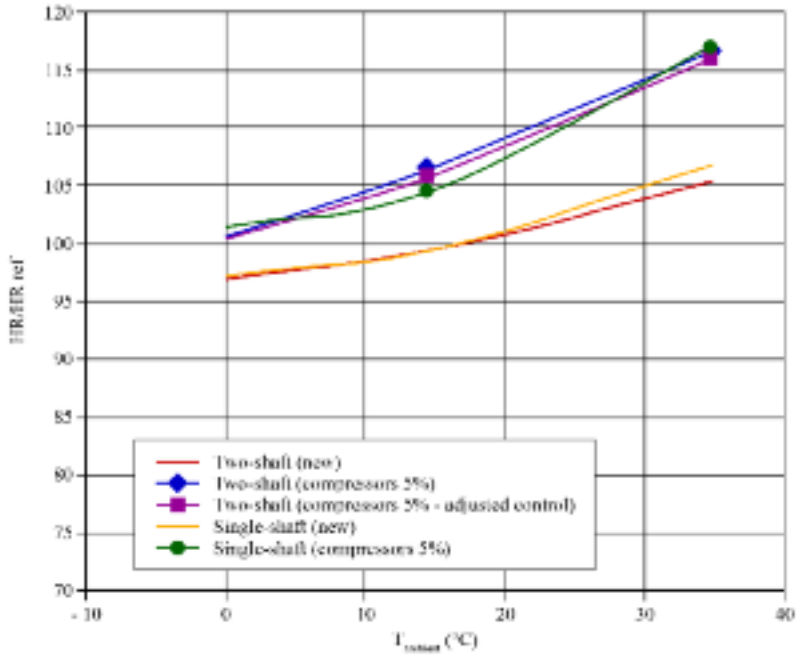

FIGURE 11.4. Impact of reduced compressor efficiency (reduction of 5 percent) on the full load heat rate of a single-shaft and a two-shaft gas turbine for a range of ambient temperatures.

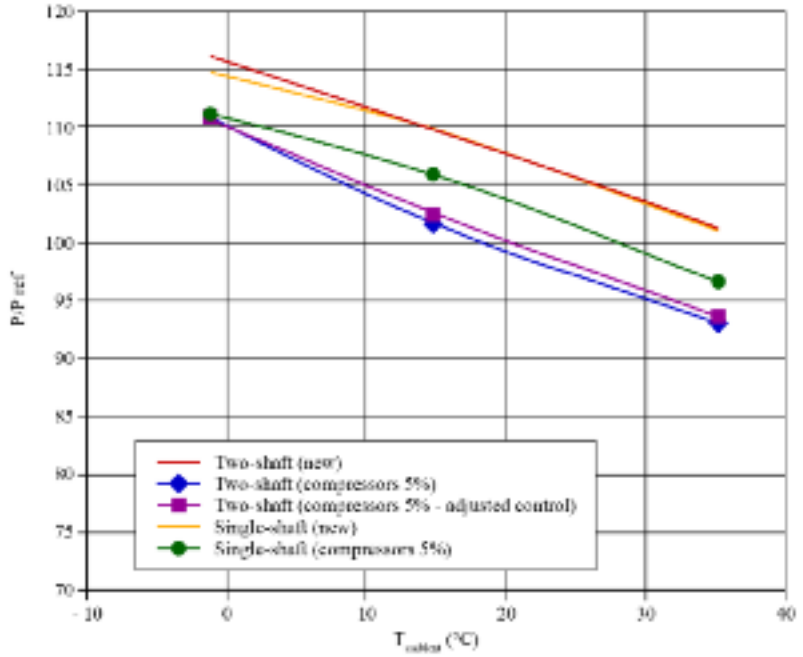

FIGURE 11.5. Impact of reduced compressor efficiency (reduction of 5 percent) on the full load power of a single-shaft and a two-shaft gas turbine for a range of ambient temperatures.

constant, the impact on power and heat rate is almost identical at all ambient conditions. Additionally, the reduction in performance is less pronounced than for a two-shaft gas turbine. We may reduce some of the degradation impact for two-shaft gas turbines by re-adjusting its control system to allow the gas turbine to reach full firing temperature.

Both Tarabrin *et al*. (1998) and Meher-Homji and Bromley (2004) found that twin-shaft and three-shaft gas turbines are particularly susceptible to performance deterioration. For both twin- and three-shaft gas turbines, the relative degradation in power is more pronounced than the degradation in heat rate for a single-shaft gas turbine.

The model illustrates that for a gas turbine with a standard combustion system, at constant load, a reduction in compressor efficiency will cause the gas turbine speed to drop (Figure 11.6). The compressor discharge pressure and the flow also drop with a reduction in compressor efficiency. Reduced compressor efficiency will also result in the firing temperature increasing to maintain the required power output and heat rate.

Syverrud and co-workers (Syverrud and Bakken, 2005, 2006; Syverrud *et al*., 2005) performed tests on a J-85 gas turbine. They deteriorated the compressor performance by spraying salt water into the gas turbine inlet. The deposits caused an increase in surface roughness on the compressor airfoils. They found that the majority of deposits occur on the first stage and become insignificant after the fourth stage.

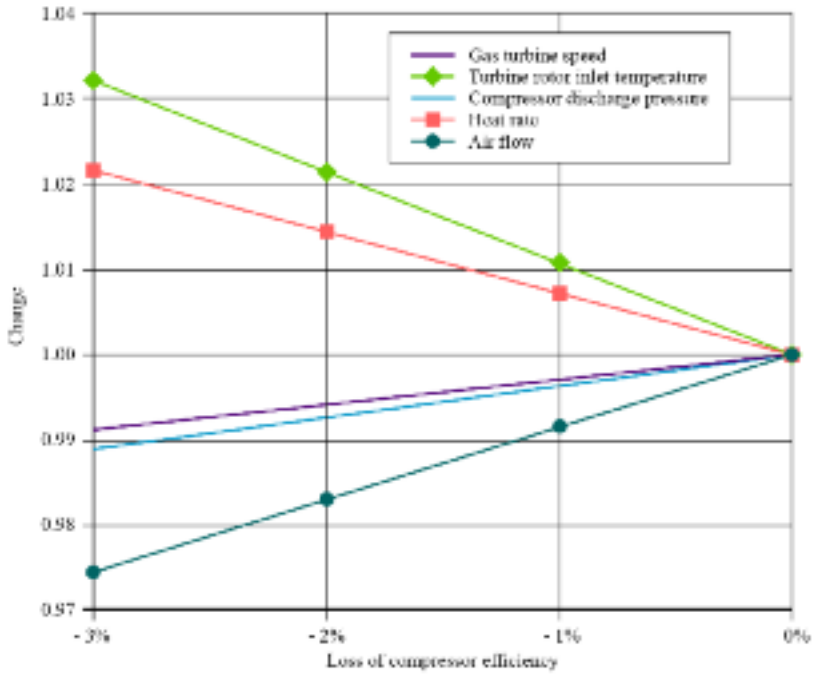

FIGURE 11.6. Impact of reduced compressor efficiency (at constant gas turbine power) on gas turbine speed, turbine rotor inlet temperature, compressor discharge pressure, heat rate and flow for a two-shaft gas turbine.

Syverrud *et al*.'s (2005) data illustrate that the degradation not only leads to reduced stage performance, but also to additional losses because individual stages no longer operate at their design flow coefficients. The deteriorated gas turbine's operating points were consistently at lower flow coefficients than for the clean gas turbine. The reduction of flow coefficients also leads to additional efficiency reductions due to the stage operating points' movement away from the stage design point.

REDUCED COMPRESSOR FLOW CAPACITY

Reduced compressor flow capacity can occur as a result of fouling or increased tip clearance. Spakovszky *et al*. (1999) and MacLeod *et al*. (1991) related increased tip clearance to an increase in flow blockage, thus reducing compressor flow capacity. Khalid *et al*. (1998) investigated the effect of component deterioration on overall gas turbine performance on a single-shaft turboprop gas turbine operating at a constant speed. Besides the expected loss in overall gas turbine efficiency, they found a significant reduction in compressor flow capacity with increased compressor blade tip clearances, but no significant change in compressor efficiency.

The model predicts that the same level of compressor flow blockage leads to more power degradation in a two-shaft gas turbine than in a single-shaft gas turbine (Figure 11.7). For both single-shaft and for two-shaft gas turbines the compressor flow blockage results in a small increase in heat rate at higher ambient temperatures.

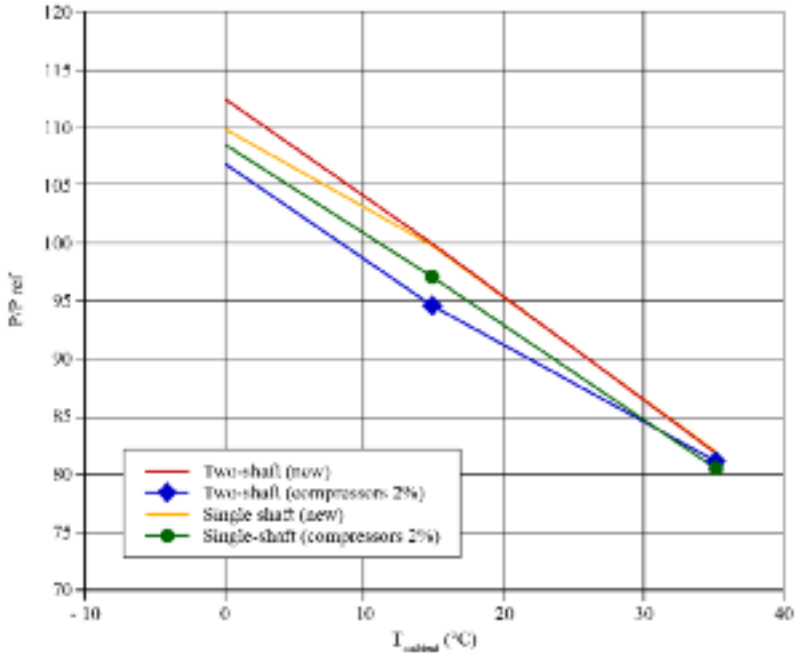

FIGURE 11.7. Impact of reduced compressor flow capacity (reduction by 2 percent) on full load power for a single-shaft and a two-shaft gas turbine at varying ambient temperatures.

The model illustrates that the loss in available power is more pronounced at low ambient temperatures (Figure 11.7). This is probably due to higher Mach numbers at low ambient temperatures, which make the compressor more sensitive to changes in flow capacity. Compressor deterioration in isolation will cause higher power than heat rate losses, because a higher compressor exit temperature (due to lower efficiency) at a fixed firing temperature will reduce the possible fuel flow. One can maintain an operating point at part load with a degraded gas turbine, albeit at a lower firing temperature and a higher gas turbine speed than for the new condition. The relative loss in efficiency is significantly lower than for a gas turbine at full load for the same level of degradation. Compressor flow and discharge pressure change little.

CHANGES IN TURBINE FLOW CAPACITY

Degradation effects on the gas turbine's high-pressure turbine flow capacity can either increase or reduce the flow capacity. The reduction in the available flow path is either due to added surface roughness or eroded leading edges, both leading to thicker boundary layers and thus a reduced effective throat area (Kurz, 1995). The throat area increases when the nozzle trailing edges erode, thus increasing the turbine's flow capacity.

The model illustrates that for single- and two-shaft gas turbines, changes in gas turbine flow capacity lead to a pronounced change in the compressor's operating points (Figure 11.8). Increased gas turbine flow capacity moves the compressor op-

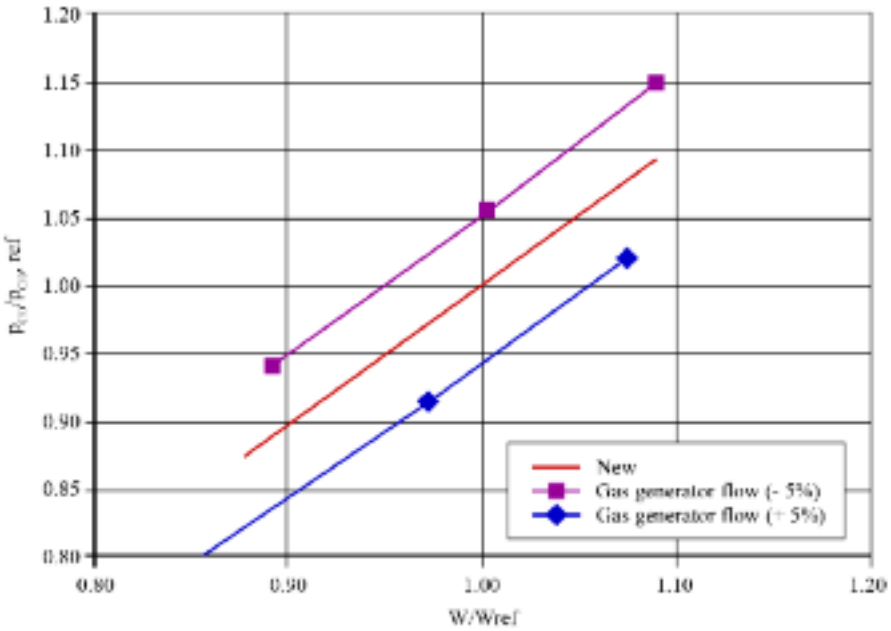

FIGURE 11.8. Impact of changed gas turbine flow capacity (increased by 5 percent and decreased by 5 percent, respectively) on the operating lines of the compressor in a two-shaft gas turbine.

erating points further into the choked region and thus leads to lower compressor efficiency. In contrast, a reduced flow area has the opposite effect (Figure 11.9). The model illustrates that opening the turbine throat area has a more detrimental effect than a reduction in flow area. This is, at least partially, because that increased flow area moves the compressor operating points further into the choked region and thus leads to lower compressor efficiency.

For a single-shaft gas turbine operating at a constant speed, an increase in turbine flow capacity will lead to a drop in compressor discharge pressure. The compressor gains in surge margin, while flow remains constant. A loss in power and efficiency accompanies this effect. A reduction in flow area has a more significant impact at low ambient temperatures. In a two-shaft gas turbine, the reduced flow capacity will cause the speed to increase, which may be beneficial at higher ambient temperatures. Depending on the gas turbine's operating point relative to its design point, the lower flow area can reduce the heat rate at higher ambient temperatures. At lower ambient temperatures, the speed may already be at its maximum, thus causing higher losses in power and efficiency.

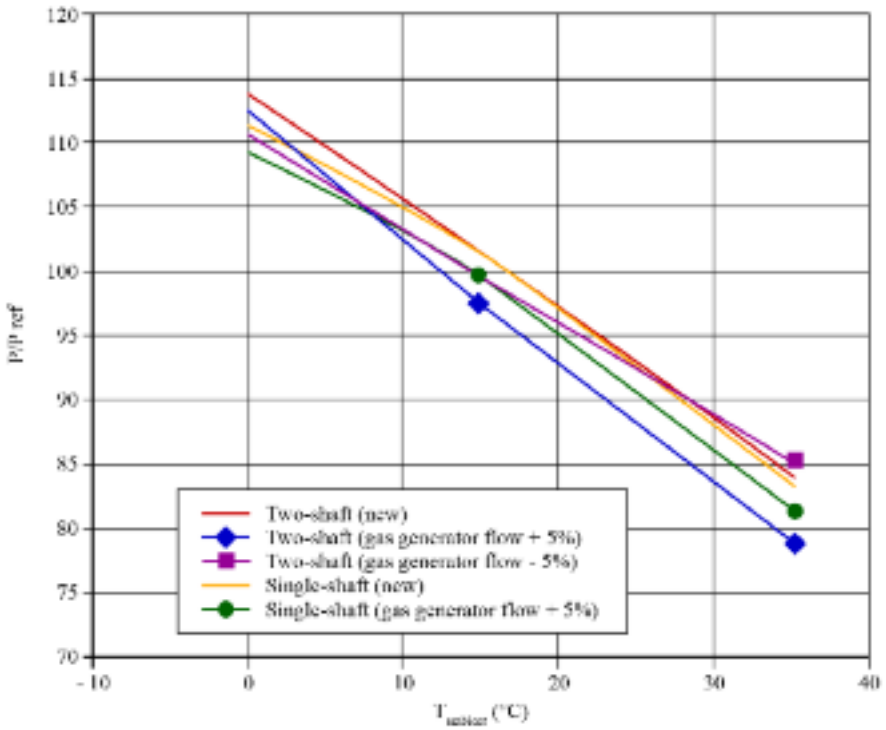

FIGURE 11.9. Impact of reduced and increased gas turbine flow capacities (by 5 percent, respectively) on full load power at varying ambient temperatures.

REDUCED TURBINE EFFICIENCY

The removal of material from the gas turbine's high-pressure turbine vanes as a consequence of erosion or corrosion results in the turbine efficiency dropping (Kurz, 1995), while the turbine's flow capacity increases. The model illustrates that both full load power and heat rate deteriorate (Figure 11.10), but the loss in power is more pronounced than the increase in heat rate. The model also illustrates that the deterioration in performance is more pronounced at high ambient temperatures.

At a constant load, the model illustrates that reducing gas turbine efficiency results in a reduction in flow, speed and compressor discharge pressure (Figure 11.11). At the same time, the heat rate and firing temperature increase. The decrease in flow and compressor discharge pressure occur at different rates, and thus the compressor's operating line moves closer to its surge line.

A change in a gas turbine's high-pressure turbine efficiency or flow capacity has a pronounced effect on the gas turbine output and a smaller effect on its efficiency. The model illustrates that a reduction in turbine efficiency or an increase in flow capacity will lead to the under-firing of a two-shaft gas turbine where the firing temperature is indirectly controlled via the power turbine inlet temperature (Figure 11.11). This is one of the positive side effects of this control mode: it does not drive the gas turbine into a more damaging over-firing situation.

Degradation also affects the optimum power turbine speed (Figure 11.11), albeit not substantially. If a lower compressor pressure ratio or deterioration of the turbine itself leads to a lower turbine pressure ratio, then the actual flow through the power turbine will increase slightly, thus increasing the optimum speed. However,

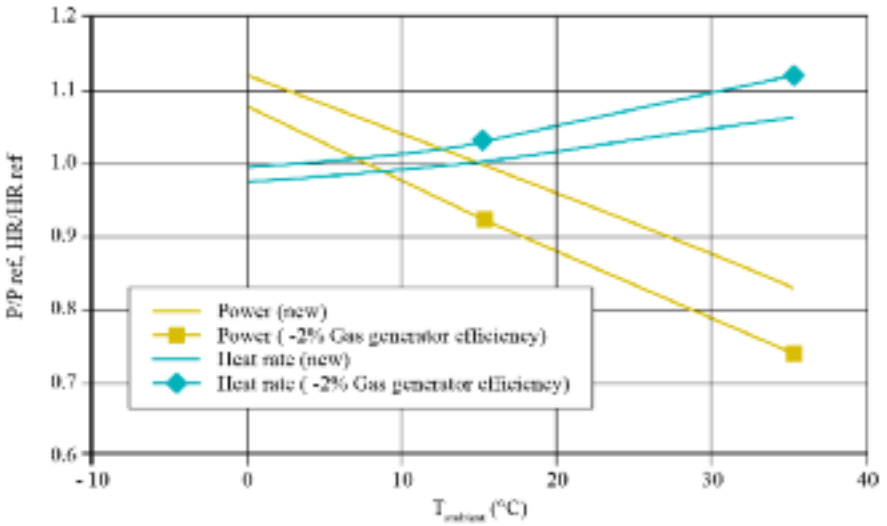

FIGURE 11.10. Impact of a gas turbine's reduced turbine efficiency (by 2 percent) on full load power and heat rate for a two-shaft gas turbine.

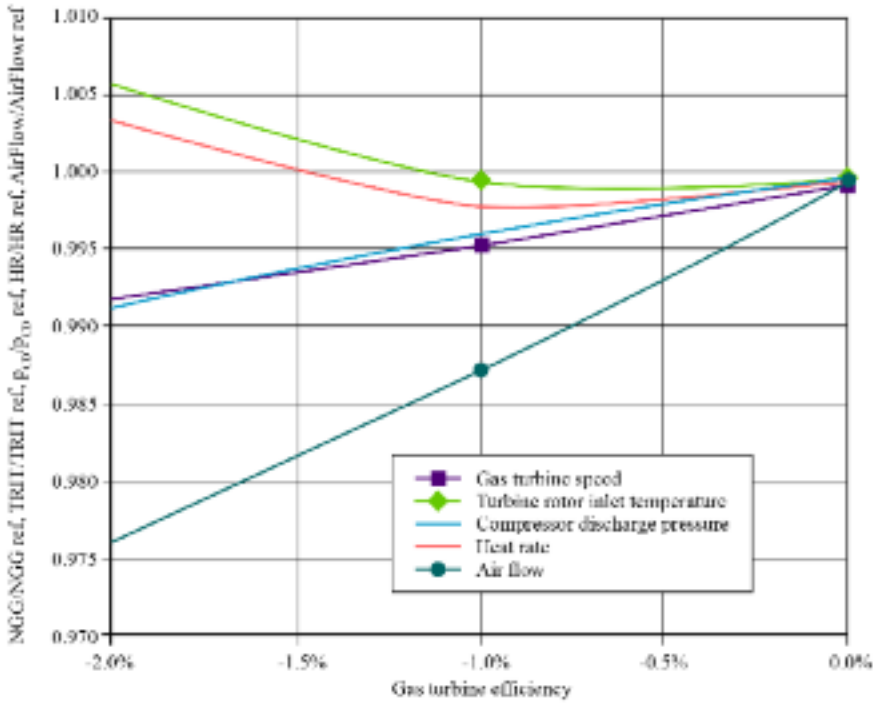

FIGURE 11.11. Impact of a gas turbine's reduced turbine efficiency, speed, firing temperature, compressor discharge pressure, heat rate and flow for a two-shaft gas turbine at constant load.

the effect on the gas turbine output at fixed power turbine speed is less than 0.1 percent for power turbines with a relatively wide operating range.

COMBINED EFFECTS

The model results in Figures 11.3 to 11.11 assume a reduction in compressor efficiency as a cause of gas turbine degradation. However, we may characterize many industrial gas turbines returning for overhaul after 30,000 to 40,000 hours in-service by reduced compressor flow and reduced turbine efficiency, but only with little deterioration in compressor efficiency. This is particularly true for gas turbines that have been subjected to regular condition-based water or detergent washing combined with good air filtration and clean fuel. Reduced compressor flow and reduced turbine efficiency lead to a change in the compressor's operating line, as well as a reduction in firing temperature when the gas turbine is controlled by exhaust temperature or power turbine inlet temperature. The test data that we used to create the model enabled individual degradation effects associated with compressor flow reduction, a reduction in compressor efficiency and a reduction in turbine efficiency to be isolated (Figure 11.12).

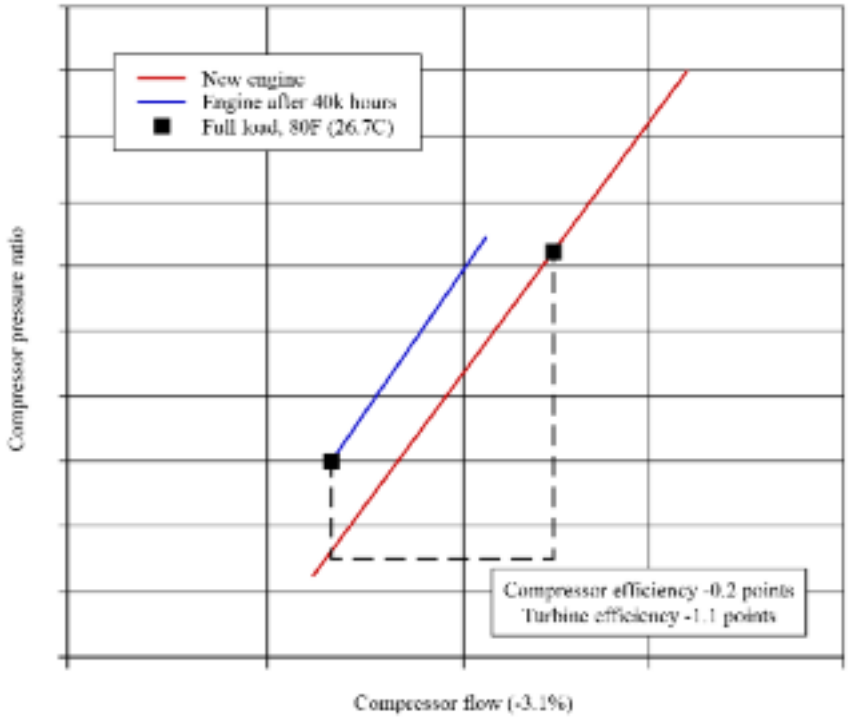

FIGURE 11.12. Compressor operating line for a gas turbine after 40,000 actual operating hours.

Kurz and Brun (2001) reported results for an industrial gas turbine that a facility operated for 3500 hours without a detergent wash. Gas turbine exhaust fumes and salt-laden air contaminated the environment. Borescope inspections had shown deposits on the compressor and turbine. Kurz and Brun (2001) recommended a detergent wash. We recorded control system data at full load before and after detergent washing. We took the data with the ambient temperature below the design ambient temperature.

The improvement in compressor pressure ratio, efficiency, power and heat rate were as we expected. The gas turbine was also under-fired, because one of the effects of degradation is the reduction in the TRIT/T5 ratio. These improvements explain the 9.7 percent increase in output power. After washing and given the test uncertainties, this gas turbine appeared to be performing essentially as new. The model predicts this behavior. If we use a 2.1 percent loss in compressor efficiency, a 5.0 percent reduction in flow and pressure ratio and a 0.5 percent reduction in the gas turbine's high-pressure turbine efficiency, we see a reduction in power of 8.6 percent. The efficiency drops by 3.5 percent, while the gas turbine speed stays almost constant and T3 drops due to a reduction in TRIT/T5 ratio.

While Tarabrin *et al*. (1998) indicated that smaller gas turbines may be more susceptible to degradation, Aker and Saravanamuttoo's (1988) study reaches exactly

the opposite conclusion. We suspect that the interactions that define the amount of degradation as a function of level of ingested material, or of amount of material removal, are gas turbine specific and do not lend themselves to generalization. Comparison of emission controlled gas turbines with lean premix combustion systems with standard combustion gas turbines reveals different degraded part load behavior. The behavior of emission controlled gas turbines is usually less linear, as the control algorithm tries to control the temperature conditions in the combustor.

INSIGHTS

While the models indicate that the gas turbine flow tends to react more to some degraded components than, for example, compressor discharge pressure (Figures 11.6 and 11.11), we still believe that monitoring compressor discharge pressure (against a reference) is the correct way to monitor degradation. This is for the practical reason that it is not as easy to monitor gas turbine flow at site as it is to monitor compressor discharge pressure. Haq and Saravanamuttoo (1991) came to a similar conclusion based on their tests on a two-shaft industrial gas turbine at high ambient temperature conditions.

A consideration of the relative impact of component degradation on a two-shaft gas turbine provides an insight into the relative severity of component degradation (Table 11.1). When we study the impact of component degradation we may conclude that:

1. the amount of power or efficiency lost for a given amount of component degradation differs for different ambient conditions. It is therefore not possible to establish a universal gas turbine degradation model that is valid for any condition;
2. the impact of any component degradation is more severe on full load power output than on gas turbine full load efficiency or heat rate;
3. except for a reduction in compressor flow capacity or a reduction in turbine flow, all other component degradations have a larger impact on gas turbine performance at higher ambient temperatures than at lower temperatures; and
4. degradation has the largest impact on turbine and compressor efficiency.

Degrading a component will always lead to observable changes in gas turbine parameters due to the impact of altered operating points, not only at the degraded component, but also for all other gas turbine components. In a reverse sense, we also can use this finding for diagnostic purposes, because different types of degradation on different components will alter the gas turbine in a different way (Lambiris *et al.*, 1991). For example, compressor efficiency deterioration will not change the compressor operating line, but a loss in turbine efficiency will. Conversely, at a given load in a two-shaft gas turbine, the reduction in compressor flow capacity will not change the gas turbine flow, while a reduction in turbine efficiency will lead to a significant change plus a more distinct change in compressor discharge pressure.

Table 11.1: *Relative impact of component degradation on a two-shaft gas turbine at two different ambient temperatures, normalized to power degradation at 15°C that would result from the degradation of compressor efficiency by 1 percent. For example, if a new gas turbine produces 10,000 kW at 15°C and 8500 kW at 35°C, the power at 15°C may be reduced by 5 percent (500 kW) due to a reduction in compressor efficiency of 1 percent. The table predicts that, for this engine, a reduction of the compressor flow by 1 percent would cause a reduction in power output of (0.77 × 5 percent) = 3.85 percent, or 385 kW at 15°C, and of (0.25 × 5 percent) = 1.25 percent, or 106.25 kW at 35°C.*

	Power 15°C	Power 35°C	Heat rate 15°C	Heat rate 35°C
Compressor efficiency	1.00	1.71	0.49	0.66
Compressor flow	0.77	0.25	0.08	–0.007
GG turbine efficiency	1.30	2.04	0.46	0.88
GG turbine flow increase	0.27	0.42	0.08	0.02
GG turbine flow reduction	0.13	–0.01	–0.02	–0.01

PROTECTION AGAINST DEGRADATION

While one cannot entirely avoid gas turbine degradation, there are precautions that can slow the effects. These precautions include the appropriate selection and maintenance of air filtration equipment and the effective treatment of fuel, steam or water that inject into the combustion process. It is also helpful to observe the manufacturer's recommendations regarding shutdown and restarting procedures. One needs to consider the site location and environment conditions, which dictate airborne contaminants, their size, concentration and composition in the selection of air filtration. Atmospheric conditions including humidity, smog, precipitation, mist, fog, dust, oil fumes and industrial exhausts will affect the gas turbine. Fuel quality will have an impact on the degradation rate of the high-pressure turbine.

Given the above variables, degradation rate is difficult to predict accurately. While frequent online washing can slow the deterioration rate, thorough on-crank washing can yield a more significant recovery (Byington *et al.*, 2003). Online washing will clean usually only the first few stages of the compressor because the increase in air temperature during compression will evaporate the washing fluid. The online washing process therefore can transport contaminants from the compressor's front stages to the rear stages or through the combustor and into the turbine. No matter how good the washing, the compressor's rear stages will not get cleaned. If one can access the compressor blades with moderate effort, for example, when the compressor casing is horizontally split, hand cleaning the blades can be very effective.

SUMMARY

This chapter covered degradation mechanisms and the impact of component degradation on overall gas turbine performance. We have attempted to clarify the

impact of component interaction by clarifying how components interact and affect overall gas turbine performance. An understanding of component interaction is also important in understanding and applying other studies which typically only address individual components. One must understand that the apparent change in a component's efficiency is both due to its deterioration and a change in its operating point as a result of component interactions. In particular, we have highlighted the change in the compressor operating point as a result of compressor and turbine degradation, both in terms of flow and efficiency. This study also shows the impact of a given component degradation on gas turbine power and heat rate. It further indicates the resulting changes in parameters that operators use as inputs to a gas turbine's condition monitoring system.

Appropriate design and selection of air filtration and fuel treatment systems, together with maintenance and good operating practices, can significantly reduce the performance degradation rate and thus time between gas turbine repairs or overhauls. We have avoided presenting data focused on the degradation rate, because degradation rate is subject to a variety of operational and design factors that compression system design engineers typically cannot control. Design engineers ultimately base maintenance and overhaul decisions on economic and safety considerations. Understanding performance degradation, as well as factors that influence degradation, can help when making these decisions.

REFERENCES

Aker, G.F., and Saravanamuttoo, H.I.H. (1988), "Predicting the Gas Turbine Performance Degradation Due to Compressor Fouling Using Computer Simulation Techniques", *Proceedings of the 33rd American Society of Mechanical Engineers Gas Turbine and Aeroengine Congress*, Amsterdam, The Netherlands, 6–9 June, Paper No. 88-GT-206.

Boyle, R.J. (1994), "Prediction of Surface Roughness and Incidence Effects on Turbine Performance", *Transactions of the ASME, Journal of Turbomachinery*, vol. 116, pp. 745–51.

Brun, K., Kurz, R., and Simmons, H. (2005), "Aerodynamic Instability and Life Limiting Effects of Inlet and Inter-stage Water Injection into Gas Turbines", *Proceedings of the 50th American Society of Mechanical Engineers Gas Turbine and Aeroengine Congress,* Reno, USA, 6–9 June, Paper No. GT2005-68007.

Byington, C.S., Watson, M., Roemer, M.J., Golie, T.R., McGroarty, J.J., and Savage, C. (2003), "Prognostic Enhancements to Gas Turbine Diagnostic Systems", *IEEE*, vol. 7, p. 3247.

Cohen, H., Rogers, G.F.C., and Saravanamuttoo, H.I.H. (1996), *Gas Turbine Theory*, Addison-Wesley, Reading, USA.

Frith, P.C. (1992), "The Effect of Compressor Rotor Tip Crops on Turbo-shaft Engine Performance", *Proceedings of the 37th American Society of Mechanical Engineers Gas Turbine and Aeroengine Congress,* Cologne, Germany, 1–4 June, Paper No. 92-GT-83.

Graf, M.B., Wong, T.S., Greitzer, E.M., Marble, F.E., Tan, C.S., Shin, H.-W., and Wisler, D.C. (1998), "Effects of Nonaxisymmetric Tip Clearance on Axial Compressor Performance and Stability", *Transactions of the ASME, Journal of Turbomachinery*, vol. 120, pp. 648–61.

Haq, I., and Saravanamuttoo, H.I.H. (1991), "Detection of Axial Compressor Fouling in High Ambient Temperature Conditions", *Proceedings of the 36th American Society of Me-*

chanical Engineers Gas Turbine and Aeroengine Congress, Orlando, USA, 3–6 June, Paper No. 91-GT-67.

Khalid, S.A., Khalsa, A.S., Waitz, I.A., Tan, S.C., Greitzer, E.M., Cumpsty, N.A., Adamczyk, J.J., and Marble, F.E. (1998), "Endwall Blockage in Axial Compressors", *Proceedings of the 43rd American Society of Mechanical Engineers Gas Turbine and Aeroengine Congress*, Stockholm, Sweden, 1–4 June, Paper No. 98-GT-188.

Kurz, R. (1995), "Effects of Non-uniform Blade Pitch on the Flow Through an Annular Turbine Nozzle", *International Journal of Rotating Machinery*, vol. 2, pp. 59–65.

Kurz, R., and Brun, K. (2001), "Degradation in Gas Turbine Systems", *Transactions of the ASME, Journal of Engineering for Gas Turbines and Power*, vol. 123, pp. 70–77.

Lambiris, B., Mathioudakis, K., Stamatis, A., and Papalliou, K. (1991), "Adaptive Modeling of Jet Engine Performance With Application to Condition Monitoring", *Proceedings of the International Society for Air Breathing Engines (ISABE) 10th International Symposium on Air Breathing Engines,* Nottingham, UK, 1–6 September, pp. 573–9.

MacLeod, J.D., Taylor, V., and Laflamme, J.C.G. (1991), "Implanted Component Faults and Their Effects on Gas Turbine Engine Performance", *Proceedings of the 36th American Society of Mechanical Engineers Gas Turbine and Aeroengine Congress,* Orlando, USA, 3–6 June, Paper No. 91-GT-41.

Meher-Homji, C.B., and Bromley, A. (2004), "Gas Turbine Axial Compressor Fouling and Washing", *Proceedings of the 33rd Turbomachinery Symposium*, Houston, USA, 21–23 September, pp. 163–91.

Millsaps, K.T., Baker, J., and Patterson, J.S. (2004), "Detection and Localization of Fouling in a Gas Turbine Compressor from Aero-thermodynamic Measurements", *Proceedings of the 49th American Society of Mechanical Engineers Gas Turbine and Aeroengine Congress*, Vienna, Austria, 14–17 June, Paper No. GT2004-54173.

Radtke, F., and Dibelius, G. (1980), "Reynoldszahleinfluss bei hochbelasteten axialen Turbinenbeschaufelungen", VDI-Berichte Nr. 361.

Sheard, A.G. (Ed.) (2012), *Tip Clearance Measurement in Aero and Industrial Turbomachinery,* Sigel Press, Cambridge, UK.

Smith, G.D.J., and Cumpsty, N.A. (1984), "Flow Phenomena in Compressor Casing Treatment", *Transactions of the ASME, Journal of Engineering for Gas Turbines and Power*, vol. 106, pp. 532–41.

Spakovszky, Z.S., Gertz, J., Sharma, O.P., Paduano, J.D., Epstein, A.H., and Greitzer, E.M. (1999), "Influence of Compressor Deterioration on Engine Dynamic Behavior and Transient Stall Margin", *Proceedings of the 44th American Society of Mechanical Engineers Gas Turbine and Aeroengine Congress*, Indianapolis, USA, 7–10 June, Paper No. 99-GT-439.

Stalder, J.P. (1998), "Gas Turbine Compressor Washing State of the Art Field Experiences", *Proceedings of the 43rd American Society of Mechanical Engineers Gas Turbine and Aeroengine Congress*, Stockholm, Sweden, 1–4 June, Paper No. 98-GT-420.

Syverrud, E., and Bakken, L.E. (2005), "Online Water Wash Tests of GE J85-13", *Proceedings of the 50th American Society of Mechanical Engineers Gas Turbine and Aeroengine Congress*, Reno, USA, 6–9 June, Paper No. GT2005-68702.

Syvverrud, E., and Bakken, L.E. (2006), "The Impact of Surface Roughness on Axial Compressor Deterioration", *Proceedings of the 51st American Society of Mechanical Engineers Gas Turbine and Aeroengine Congress*, Barcelona, Spain, 8–11 May, Paper No. GT2006-90004.

Syverrud, E., Brekke, O., and Bakken, L.E. (2005), "Axial Compressor Deterioration", *Proceedings of the 50th American Society of Mechanical Engineers Gas Turbine and Aeroengine Congress*, Reno, USA, 6–9 June, Paper No. GT2005-68701.

Tarabrin, A.P., Schurovsky, V.A., Bodrov, A.I., and Stalder, J.P. (1998), "Influence of Axial Compressor Fouling on Gas Turbine Unit Performance Based on Different Schemes and With Different Initial Parameters", *Proceedings of the 43rd American Society of Mechanical Engineers Gas Turbine and Aeroengine Congress*, Stockholm, Sweden, 1–4 June, Paper No. 98-GT-416.